Study of Underground Coal Gasification and Carbon Storage in the Residual Cavity

by

Md Moniruzzaman Khan

A thesis submitted in partial fulfillment of the requirements for the degree of

Doctor of Philosophy

in

CHEMICAL ENGINEERING

Department of Chemical and Materials Engineering
University of Alberta

Abstract

Underground coal gasification (UCG) is a process of 'in-situ' conversion of coal into gaseous products with usable heating value through combustion with oxygen/air and gasification with steam. From the economic and environmental point of view, UCG is a highly promising clean energy technology which has a potential to meet the increasing energy demands in several countries. Moreover, the voids created in deep underground following gasification generate the intriguing possibility of storing carbon dioxide. Since, in-situ UCG is a complex process, laboratory-scale experiments on coal blocks/packed beds can provide significant insight into UCG process. In this study, several laboratory scale experiments have been carried out to observe the effect of feed flow rate, steam injection, initial combustion etc. on product gas compositions. Results and limitations of the experiments are discussed in detail.

In general, post-gasification sites consist of a tear-drop shape cavity with ash and rubble left at the bottom. The residual coal seam can be broadly classified as the partially-gasified char layer, the pyrolyzed char layers, and the raw coal layer. A series of carbon dioxide adsorption experiments have been carried out to assess the carbon dioxide capture and storage capacity (CCS) of the coal and pyrolyzed/gasified chars. The results from this study suggested that UCG-CCS process is feasible.

Preface

This thesis comprises lab-scale UCG experiments and several carbon dioxide adsorption experiments on coal/coal char. The contributions of the author on each experiment are described below:

- Ex-situ Experiments: The author built a lab-scale Ex-situ experimental set-up to mimic the UCG process. The effect of various coal seams and the operating parameters on the gas compositions were studied through a number of experiments to understand the performance of the UCG process in terms of syn gas production.
- Adsorption Experiments: The adsorption behaviour of CO_2 on virgin coal, pyrolyzed coal and gasified coal was studied to assess the UCG-CCS option. Four sets of experiments were conducted. The Author worked as a co-researcher in each of the experimental sets conducted. The author was a part of the initial team with Dr. S. Ramasamy and Tian S. to build the experimental set-up and the methodology of the adsorption process. However, the setup was slightly modified by Pramod Sripada and later by Sara Zabihi according to the needs of the nature of the experiments. The author was also involved in the team of conducting the first two sets of experiments and data analysis. The pyrolyzed coal samples were obtained from the M.Sc work of Tian S. However, in the 4^{th} set of experiments, the author was more involved in supervising the adsorption experiments. The experiments were conducted by Sara Zabihi using the gasified coal samples collected from the ex-situ UCG experiment conducted by the author.

The followings are the publications/presentations from the above works:

Articles Published in Referred Journals:

- **Khan, M.M**.; Mmbaga, J.P.; Shirazi, A.S.; Trivedi, J.; Liu, Q.; Gupta, R.., Modelling Underground Coal Gasification—A Review, Energies 2015, 8, 12603–12668
- Ramasamy, S.; Sripada, P.P.; **Khan, M.M**.; Tian, S.; Trivedi, J.; Gupta, R., Adsorption behavior of CO_2 in coal and coal char. Energy and Fuels 2014, 28(8), 5241-5251
- Sripada, P.P.; **Khan, M.M**.; Ramasamy, S.; Trivedi, J.; Gupta, R., Influence of Coal Properties on the CO_2 Adsorption Capacity of Coal, Energy Science and Engineering, 2018, 1-15

Articles Published in Book Chapters:

- Sripada, P.P.; **Khan, M. M.**; Ramasamy, S.; Kanneganti, V. T., Gupta, R., "Comparison of CO_2 Storage Potential in Pyrolysed Coal Char of different Coal Ranks," in *Gas Injection for Disposal and Enhanced Recovery*, Y. Wu, , J. J. Carroll, , and Q. Li, Eds., ed: John Wiley & Sons, Inc., 2014, pp. 293-304

Articles Presented in Conferences:

- **Khan, M.M.**; Trivedi, J.; Liu, Q.; Gupta, R.., Laboratory studies on gasification of subbituminous coal in an Underground Coal Gasification (UCG) reactor, 67 Canadian Chemical Engineering Conference. 2017, October 22-25, Edmonton, AB, Canada
- **Khan, M.M.**; Trivedi, J.; Liu, Q.; Gupta, R., Laboratory Studies on Cavity Formation and Product Compositions during Gasification of Subbituminous Coal in Underground

Coal Gasification (UCG) Reactor, The 41st International Technical Conference on Clean Coal & Fuel Systems June 5 to 9, 2016, Sheraton Sand Key, Clearwater, Florida, USA

- Ramasamy, S.; Tian, S.; **Khan, M.M.**; Trivedi, J.; Gupta, R., Assessing CO_2 Storage Potential in Coal Chars for UCG-CCS System. IEA 2nd underground coal gasification network workshop, Banff, AB, Canada, 2012.

Acknowledgements

I would like to express my deep gratitude to Dr. Rajender Gupta for giving me an opportunity to work under his supervision and endless guidance throughout the period of this study. His inspiration, encouragement, instruction and support contributed remarkably towards the completion of this dissertation.

I would also like express my gratitude to my co-supervisor, Dr. Qingxia Liu for his enthusiastic guidance, valuable suggestion and cooperation.

It is my great pleasure to express my gratefulness to Dr. Bob Hayes as he kindly agreed to be in my guiding committee. I would like to express my gratitude to Dr. Nikrityuk for his active support, time, guidance.

Appreciation goes to Dr. Japan Trivedi for his support and generosity for letting me build the experimental setups in his lab and use the facilities in the School of Petroleum Engineering. I would like to thank Yogesh Dalsania, Tarang Jain and Daimeng from the research group of Dr. Trivedi for their help in attending the laboratory during the experiment. I would also take the opportunity to thank Todd Kinnee at the school of Petroleum Engineering for his valuable comments and suggestions during troubleshooting and helping me in preparing experimental accessories.

I would also like to express my gratitude to Dr. Joe Mmbaga for his countless hours with me in discussing topics related to underground coal gasification during this study.

I had the opportunity to work with some colleagues who contributed generously toward the completions of the research works. I would like to take the opportunity to express my sincere appreciation to Dr. Shan Ramasamy and Pramod Sripada more a younger brother than a colleague for continuous support and inspiration during their presence. I received full support from them in developing the experimental setups and conducting the preliminary experiments. I am also thankful to Dr. Moshfiqur Rahman and Dr. Deepak Pudasainee for helping me in preparing the standard operating procedure and risk assessment and making the course of my experiments hazard free and safe. I would like to extend my gratitude to Deepak Pudasainee to become the first person in providing his time to review the dissertation.

I would also like to mention the friendly environment of Dr. Gupta's research team. In particular, Vinoj Kurian, Sara Zabihi, Nirlipt Mahapatra, Dr. Shayan Karimipour, Sania Basher, Wan Keji, Ananthan Santhanakrishnan, Komal Dhankhar Kalyan, Madhumita Patel, Mehdi Alipour, Ahad Shirazi, Nisarg Tripathi and Su Tian offered unparalleled support whenever needed.

I would also like to thank Mr. Walter Boddez for his technical help for my research.

A final acknowledgement is made to the Canadian Centre for Clean Coal/Carbon and Mineral Processing Technologies (C5MPT) for the funding of this study.

Table of Contents

List of Tables

List of Figures

Nomenclature

		Unit
a_{ij}, a_{kj}	Stoichiometric matrix	
C	Molar concentration of gas species	mol/(m^{2}s)
C_i	Molar concentration of species i (gas)	mol/(m^{2}s)
C_w	Molar concentration of water	mol/(m^{2}s)
C_2	Inertial resistance factor	1/m
C_{p_g}	Specific heat of gas	J/(mol K)
C_{p_s}	Specific heat of solid	J/(mol K)
C_{p_w}	Specific heat of water	J/(mol K)
$C_{1\varepsilon}, C_{2\varepsilon}$	Constant for turbulence model	
D	Solid thermal Conductivity	W/(m K)
D_i	Diffusion coefficient of gas species	m^2/s
D^{eff}	Effective diffusivity	m^2/s
d	Pipe diameter	M
e	Specific internal energy of flowing gas	J/mol
e_s	Solid specific energy	J/mol
E	Activation Energy	J/mol
G	Number of gas species	
Gr	Grashof number	
G_{k_t}, G_b	Source terms for turbulence model	kg/m-s^3
h	Specific enthalpy of flowing gas	J/mol
h_i	Specific enthalpy of gas species i	J/mol
h_k	Specific enthalpy of solid species k	J/mol
h_T	Convective heat transfer coefficient	W/m^{2}K
H_1, H_2	Coal seam length and height respectively	M
H_i	Heat of combustion of gas species i	W/m^3
ΔH_i	Heat of reaction of species i	W/m^3
ΔH_v	Heat of evaporation of water	J/mole
j_i	Total flux of gas species i	mol/m^{2}s
$\bar{J}$	Gas diffusion flux vector	kg/m^{2}s
K	Number of solid/condensed species	
k	Rate constant	
k_o	Frequency factor	
k_t	Turbulent kinetic energy	J/m^{3}s
k_{eff}	Effective thermal conductivity calculated from thermal	W/K

	conductivity of solid and gas	
k_y	Mass transfer coefficient	mol/m^{3}s
L_e	Entrance length	M
$\dot{m}$	Mass flow rate	kg/s
M	Moisture content of coal	
M_k	Molecular weight of solid species k	kg/mole
M_w	Molecular weight of water	kg/mole
p	Pressure	Pa
p_∞	Pressure in blast region outside of cavity boundary layer	Pa
P	Total pressure	Pa
p_w	Vapor pressure of water	Pa
Q_g	Energy release in gas due to chemical reactions	J/m^{3}s
Q_s	Solid energy source rate	J/m^{3}s
r	Radius in cylindrical coordinates	M
R_j	Jth reaction rate	mol/(m^{3}s)
R_{c-ij}	Rate of reaction of carbon with O_2, CO_2, H_2O and H_2	mol/(m^{3}s)
R_T	Total chemical rate of reaction	mol/(m^{3}s)
R_c	Effective chemical rate of reaction	mol/(m^{3}s)
R_m	Mass transfer rate associated with reaction	mol/(m^{3}s)
R	Gas constant	J/(mol K)
$rate_i$	Reaction rate	kg/(m^3 s)
Re	Reynolds number	
S_m	Gas phase mass source due to chemical reactions	kg/m^3-s
S	Specific surface area	1/m
Sc	Schmidt number	
Sh	Sherwood number	
S_s	Solid species mass source per unit volume of bed	kg/m^3-s
S_ϕ	Source term due to heterogeneous chemical reactions	kg/m^3-s
S_φ	Source term for porosity, calculated based on reactions in coal	
s	Upstream end velocity	cm/min
s_b	Downstream end velocity	cm/min
T	Gas temperature	K
T_s	Solid temperature	K
x, y	Space coordinate	
$X\ (y,t)$	Burn front location	M
x_{rz}	Total length of the reaction zone	M

X	Char conversion	
Y_i	mass fraction of species in gas phase	
Y_{s_i}	Mass fraction of solid component	
Y_m	Source term for kinetic energy	kg/m-s^3
y_i	Mole fraction of species in gas phase	
y_w	Mole fraction of water	
y_l	Limiting reactant	
u	Superficial velocity (gas)	m/s
u_w	Mobile water velocity	m/s
U	Velocity of uniform stream	m/s
$\overline{v}$	Velocity vector (gas)	m/s
$\|v\|$	Velocity (scalar) of gas	m/s
$\overline{v_s}$	Superficial solid velocity	m/s
v_c	Burn front velocity	m/s
VM	Volatile matter at any moment	
VM^*	Volatile matter content from proximate analysis	
w_k	Mass fraction of solid species k	
w_c	Weight fraction of carbon in charcoal	
$\dot{w}_{k_t}, \dot{w}_\varepsilon$	User defined source terms	

Greek Symbols

ρ	Blast density	kg/m^3
ρ_g	Density of gas	kg/m^3
ρ_s	Density of solid	kg/m^3
ρ_k	Density of k^{th} solid species	kg/m^3
ρ_w	Density of liquid water	kg/m^3
ρ_{w^o}	Uniform initial moisture density	kg/m^3
φ	porosity	
φ_{lim}	Upper limit of porosity	
φ_e	Bed porosity external to particles	
Ψ	Stream function	
μ_g	Viscosity of gas	Pa.s
μ_t	Turbulent viscosity	Pa.s
ε	Rate of dissipation of turbulent kinetic energy	m^2/s^3
α	permeability	m^2

α_o	Initial permeability	m^2
η_r	Resistance parameter	
ξ	Dimensionless position variable in horizontal direction	
β	Weighing coefficient	
σ	Experimental parameter in permeability-porosity equation	
$\sigma_\varepsilon, \sigma_{k_t}$	Prandtl number for the turbulent kinetic energy and its rate of dissipation, respectively	
ϕ	User defined scalar	
ϕ_v	Velocity potential	
θ	Angle between x axis and radius in cavity	
κ	Radiation extinction coefficient	1/m
Γ	Diffusion coefficient	

CHAPTER ONE: INTRODUCTION

1.1 Scope of Underground Coal Gasification and Carbon Capture & Storage

Coal is the most abundant and widespread type of fossil fuel, with reserves of economically recoverable coal estimated to be about 900 gigatons, 64% of the major fossil fuels [1]. However, the total amount of coal potential including the economically non-recoverable part is reported to be 18 terratons [2], most of which are too deep or too costly to be mined by traditional methods. With the current trends of energy consumption, and the rise of developing countries, the total fossil fuel reserve is expected to be the same while the total energy consumption is increasing around the world. To increase the recoverable fossil fuel reserve, it is important to find appropriate technology to extract the non-recoverable part of the reserves economically. Early studies suggest that the use of UCG could potentially increase the world's coal reserves by as much as 600 gigatons [3], which represents a 70% increase [2]. The UCG product gas, called synthesis gas (syngas), is mainly a mixture of CO, H_2, CH_4, and CO_2 with trace amounts of ethane and other components. However, UCG is not a step towards low carbon future until carbon capture and storage (CCS) is considered with it. The development of the UCG technique is paving the way to access deep coal seams and simultaneously providing a scope of using the post-burn site as a geological sink for storing CO_2.

1.2 Aspect of UCG

A comparison of UCG with conventional mining and subsequent gasification in terms of environmental issues and capital requirements indicates that UCG offers a unique means of recovering energy from coal without the necessity of mining [4]. The technology of coal mining

and the use of coal have been affected by the pollution caused by its transport, storage, and combustion [5]. In addition, coal-fired power plants have higher greenhouse gas (GHG) emission per generated energy due to lower efficiency of the process and a higher carbon-to-hydrogen ratio of coal. However, the most alarming issue is the worldwide fatalities and injuries per year in the coal mining industries. It has been reported that there were a total 36,910 deaths in a six-year period, from 2000 to 2005, in the coal mining industries of China alone [6]. On the other hand, the USA has reduced its fatalities after ensuring safe work environments in the current century; however, the death fatalities of the USA have still numbered more than 300 since 2003 [7]. Considering the fatalities alone, UCG is the safest energy harness process. Moreover, UCG has several advantages over the conventional gasification process. Examples of such benefits include [4, 8, 9]:

- Elimination of coal mining and thus avoids a dangerous practice with the current equipment and safety regulations.
- Lower capital investment due to the elimination of surface gasification units.
- Elimination of ash handling operations by keeping the ash underground.
- Lower water consumption.
- Generation of possible sites for CO_2 sequestration.

From the economic and environmental point of view for large-scale gas production, UCG is a highly promising technology [8, 10]; however, UCG introduces some challenges that should be addressed before the process can be adopted on a large scale. Some of the main challenges are process stability, aquifer contamination, and subsidence [11]. However, the potential risks of subsidence and aquifer contamination can be avoided through careful site selection and adoption of best management practices for operations [4, 8, 11, 12].

1.3 Process Description of UCG and Aspect of CCS

The UCG process involves four main steps, namely drilling, linking, ignition, and gasification. The basic layout of the process requires one borehole for the injection of gases and one for production; however, over the years three standard configurations of wells have evolved. They are:

- Linked vertical wells (LVW);
- Controlled retraction injection point (CRIP);
- Steeply dipping seams (SDS).

From the historical reviews of UCG technology [13, 14] the method of UCG can be classified as shaft method and shaftless method. However, soon after few field trials of using shaft method (namely, chamber, borehole producer, and stream method) in former USSR, Russian scientists concluded that shaft gasification methods offered no economic or labor advantages over conventional deep mining [14]. Shaftless methods, on the contrary, require no underground labor. Considering this fact, the direction of UCG process in the latter phase continued to develop shaftless method. The seam preparation using shaftless method either follows the artificial breakdown of the seam or creation of narrow channel inside the seam to connect two boreholes. The former method more nearly resembles the operation of a packed chemical reactor where small passages in permeable media provide intimate contact between the gas and the solid, and also provide a large surface area for gasification reactions. The latter method, known as channel method permits high gas flow at low pressure drops and provide more control of the process.

Figure 1-1shows a sketch of linked vertical wells arrangements for the channel gasification process. In the first step, injection and production wells apart from each other are drilled at some specified distance from the surface into the coal seam. In the following step, a permeable channel (link) is created between two wells, which allows enough flow of gases in a large-scale operation. It is necessary to ignite the coal initially to raise the coal temperature using combustible gas and oxygen mixture with the help of a suitable ignition source. The duration of this combustion stage depends on the seam properties as well as the operating conditions. After this stage, the mixture of air/oxygen and steam are injected into the seam to gasify the coal. The main product of gasification, syngas, is then recovered from the production well. As the coal is being consumed, ash falls down and a void space is created, which is referred to as a cavity. When the cavity reaches the production well, there will be less contact between the injection gases and the virgin coal; thus, the quality of produced gases drops significantly. Therefore, fresh coal should be made available by moving the location of the injection gases for further continuation of the process. After the completion of gasification, steam and/or water are usually flushed to the cavity to remove the pollutants from the coal seam to prevent them from diffusing into surrounding aquifers.

Unlike surface gasification, underground coal seams are not completely subjected to gasification. Different layers of the coal seams apart from the origin of combustion are exposed to different temperature levels. As a result, the boundary layers of the void created due to UCG process are exposed as different layers, such as, gasified coal char, pyrolyzed coal char followed by dried coal and raw coal layers (see Figure 1-1). The properties of the coal and char vary from layer to

layer. That is why, it is also essential to know coal properties subsequent to gasification in a deep un-minable coal layers to evaluate the effects of coal properties on CO_2 storage potential.

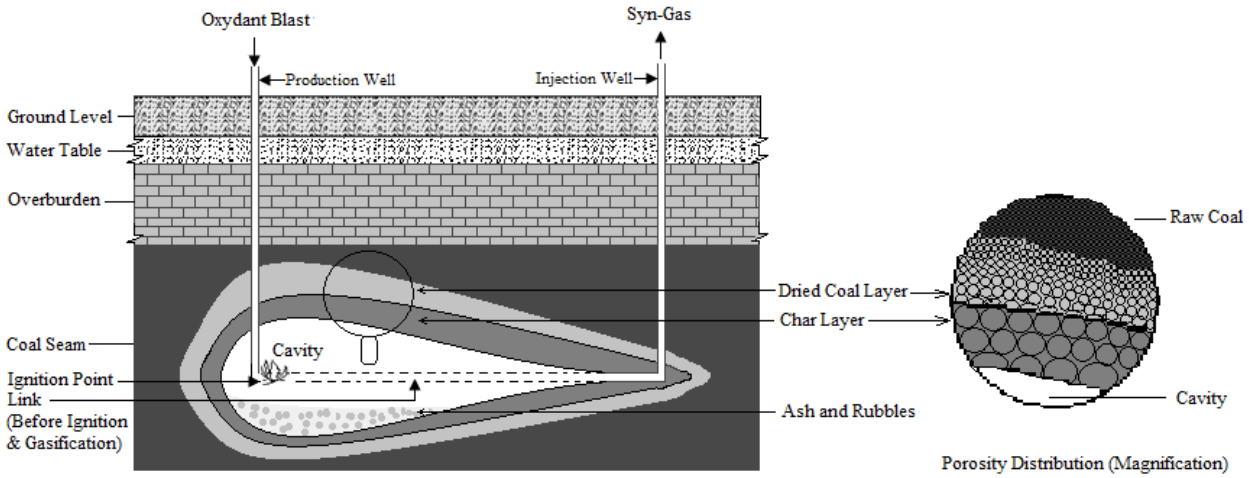

Figure 1-1 Schematic (not to scale) of the UCG process for linked vertical wells (Modified from Ramasamy et al., 2014[15]).

1.4 Motivation and Objectives

1.4.1 Motivation

Canada is midsized coal-producing country, nevertheless coal was accounted around 6% only in 2014 to meet the country's primary energy demands [16] and the future direction is downwards due to environmental protection, mainly directed towards reducing carbon emissions. However, a successful UCG-CCS facility can trigger the possibility of increasing the use of coal, especially subbituminous coal which is known as a thermal coal and abundant in Canada.

As mentioned earlier UCG is site specific. The site selection is perhaps the single most important factor that determines the technical and economic feasibility of coal gasification [17]. Quality of the seam is considered one of the important variables that cannot be changed after the selection

of a site. In this investigation, sub-bituminous coal was chosen due to its abundance in Canada; however, the coal seam was prepared in various ways. For a selected coal seam, establishment of a link between injection and production boreholes is necessary to create a path of enhanced permeability (low resistance). Similarly, the linkage was also established in various ways which resembles to a drilled channel (channel gasification) or fractured coal seam (packed bed gasification).

1.4.2 Objectives

The main objective of this research was to investigate the performance of the Canadian sub-bituminous coal to be used in UCG process and to determine the influence of coal/char properties in the implementation of carbon storage facility in post-burn UCG sites. To achieve the main objective, the objectives of this research are threefold:

1. Reviewing the relevant preceding field/lab-scale experiments and developed models on UCG to acquire adequate knowledge on UCG process.
2. Investigating the performance of the UCG process of different modes by conducting laboratory scale UCG experiment at atmospheric pressure.
3. Finally, studying the adsorption behaviour of coal/char to assess the CO_2 storage potential, in specific, to determine the influence of coal properties in the implementation of CCS in UCG sites.

1.5 Organization of this Research

This thesis is divided into four chapters. Chapter 1 introduces the thesis and its layout. This chapter also provide brief description of UCG process, objectives, scope and the methodology to meet the objectives in this dissertation.

Chapter 2 starts with a description of historical evolution of UCG practice. Subsequently, overviews of important field trials as well as laboratory tests on UCG in some details are also presented. This chapter also provide a detail review of relevant models, CFD tools and model parameters.

Chapter 3 deals with UCG lab-scale experiments as well as CO_2 adsorption experiments. The findings and experience obtained in each experiment are presented in this chapter. This chapter also includes a description of the experimental equipment and procedure used.

The final chapter includes the general conclusion and the recommended future work.

CHAPTER TWO: LITERATURE REVIEW

This chapter presents a brief description of UCG process and a review of literature relevant to the field/lab-scale UCG experiments and UCG models. The chapter begins with a chemical process of UCG followed by historical developments of the UCG process. The performances of UCG from field tests and lab-scale experiments are reviewed in Section 2.3. A review of UCG models is presented in Section 2.4. The consideration of model parameters is discussed in the subsequent sections. The concept of UCG-CCS is described in section 2.6. The details of the sections from 2.4 to 2.6 can be found in a review paper published by the author [18]. The chapter ends with conclusions in Section 2.7.

2.1 Chemical Reactions in UCG

The UCG process occurs in three different zones: drying, pyrolysis, and combustion and gasification of solid char. In the drying zone, wet coal is heated and converted into dry coal by removing moisture associated to it. Upon further heating of the coal, the pyrolysis reactions begin at temperatures around 350–400 °C [19] and coal loses its weight, generating volatile matters and the solid known as char. Finally, the char reacts with the injected/pyrolyzed gases to produce the syngas. After devolatilization, the two essential types of char layer reactions which govern the UCG product gas composition are: oxidation and reduction. Many reactions occur during this process but the most important reactions, which are considered in most of the models, are summarized in Table 2-1.

Table 2-1 Major reactions in the gasification process [16].

Reaction	Reaction No.	Representation	Heat of Reaction (kJ/mol)
Drying	1	Coal → Dry Coal+ H_2O	+40
Pyrolysis	2	Dry Coal → Char + Volatiles	0
Coal combustion	3	C (Char) + O_2 → CO_2	−393
CO_2 gasification	4	C (Char) + CO_2 → 2CO	+172
Steam gasification	5	C(Char) + H_2O → CO+ H_2	+131
Methanation	6	C(Char) + 2H_2 → CH_4	−75
Water-gas shift	7	CO + H_2O↔ CO_2+ H_2	−41
	8	CO + 0.5O_2 → CO_2	−111
Gas phase oxidations	9	H_2 + 0.5O_2 → H_2O	−242
	10	CH_4+2O_2→ CO_2+2H_2O	−802

The reactivity of the char to O_2, H_2O, CO_2, and H_2 determines the rates at which the desired products are formed [9]. Reactions 3, 5, and 8 are the main chemical reactions considered for both shallow and deep coal gasification processes. The methanation (reaction 6) is favourable at a high hydrogen pressure. In the UCG, at low pressure, this reaction is not significant. Reactions 3–6 take place on the wall of coal seams, while reactions 7 and 8 occur at the gaseous stage [20]. Different reactions are favourable at different temperature ranges. Figure 2-1 shows the equilibrium constants as a function of temperature for some of the important reactions in the gasification process. As the equilibrium constants for all the reactions shown in Figure 2-1 are at unity at approximately 1000 K, the temperature becomes the key factor in determining the shift of chemical equilibria towards the product or reactions by deciding whether it is an endothermic or exothermic reaction. For example, at temperatures above 1000 K, the formations of H_2 and CO are favourable since reaction 4 and reaction 5 are endothermic [17]. Similarly, other reactions seem to be favoured at temperatures below 1000 K. Reactions involved in UCG are not fundamentally different from the reactions of coal and char in the surface gasifiers.

In gasification reactions, the combustion of coal and volatiles provides the necessary heat for endothermic gasification reactions.

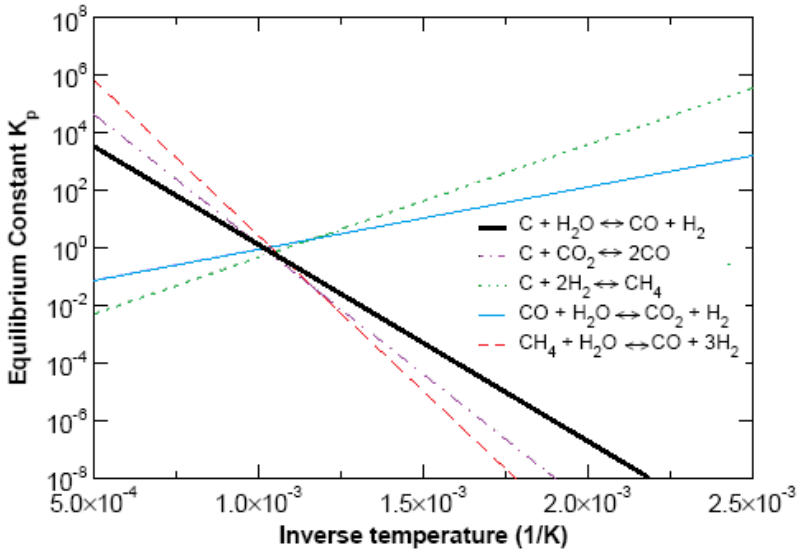

Figure 2-1 Equilibrium constant "Kp" as a function of temperature for some reactions in coal gasification [17].

2.2 Brief History of UCG Practices

The idea of the UCG was first mentioned by Sir William Siemens of Great Britain in 1868 [21-23] and the idea was consolidated (1988–1899) independently by the famous Russian chemist Dmitri I. Mendeleev, who also pointed out the economic benefit of UCG over conventional mining [21]. A Major credit goes to an American chemist, A.G. Betts, due to his detailed technical contents and engineering drawing on the UCG method that closely resemble modern approaches presented in his three UCG patents received during 1909–1910 [21, 22]. In 1912, famous British chemist Sir William Ramsay expanded the ideas of Betts and proposed gasifying coal underground as a way to avoid air pollution and as a solution for the mining worker [21]. His strong advocacy for the development of this technology created an international

surge of interest that eventually helped him to culminate the first ever UCG experiment being carried out at Hett Hill near Tursdale Colliery in County Durham, North East England, in 1912 [21, 23]. Unfortunately, the experiments did not proceed due to the outbreak of World War I in 1914 and Ramsay's death in 1916. A detailed description of early ideas in UCG and their evolution is given in the excellent historic review of UCG by Klimenko [21].

In the former USSR, the gas generator No 1 of Gorlovskaya Podzemgaz station known as the first underground gas generator was prepared in 1934 where the seam was opened by a shaft and pit [13]. However, this open up method was not without the aid of mining methods. Beside the investigation of its economic aspect, Soviet works also aimed to reduce human labor in coal mines and introduce an improved working conditions in the coal industry to obtain a solution of important social problems [13]. Finally, in 1956, a shaftless method of gasification of coal seam was developed at underground gas generator No. 2 of Yuzhno-Abinskaya station where no mining work was required [13]. The former USSR was the first country to operate UCG successfully and they gained extensive knowledge in the UCG process through a number of successful UCG field trails until the discovery of large gas field in Siberia in 1960s [21, 24]. However, their knowledge was scarcely available until the 1960s. Most of the information on Russian tests was available in the Russian literature. As a result, most of the field trials conducted by other countries before the 1960s, without the benefit of detailed data on Soviet field tests, did little to advance the process and left an impression that UCG was not a viable process [14]. Later on, many Russian articles on UCG were translated into English. As a result, the volumes of works on UCG carried out by the former USSR were exposed to the rest of the world. After getting a complete picture of the Soviet UCG experience with the large-scale

translation of Russian technical literature, Gregg and Edger [14] concluded that “the amount of effort expended and degree of success achieved by the Soviets (having constructed and operated several commercial plants) far exceeds the summation of efforts by other nations”. Translations of a Russian book and summaries of the translations of Russian articles and specific experiences on UCG can be found in several references: Skafa[13], Gregg et al. [25], Derbin et al. [26].

After successful operations of UCG throughout the 1930s and 1960s, the process was left out mostly because of the low prices of gas and oil. During the politically induced energy crisis in 1973, USA renewed the interest on UCG and after gaining knowledge from Soviets' field practices, an extensive theoretical and laboratory works on UCG were performed by USA. Subsequently, to improve control and efficiency, extensive field trials were performed in the USA and large-scale pilots proved the basic feasibility of UCG [27]. Earlier, the field tests were limited to shallow depth, following the Soviet practice, but over time, with the improvements in drilling technology, the depth of UCG operations has increased markedly as can be observed in most of the European field trials [11]. Because of the continuous technological advancement and the modeling effort, UCG works after 1995 have extended in some new countries, such as Australia, South Africa, Canada, India etc. Recent works has been focused on increasing the resource recovery and reduce its environmental impact on underground and surface conditions [28].

The underground preparation of the seam and gasification are performed using drilled holes. Earlier, LVW and steeply dipping seams (SDS) were the most popular drilling configurations for horizontal and steeply dipping seams, respectively. However, recently, the controlled retraction

injection point (CRIP) invented in the Centralia series of UCG trials in the 1980s has gained considerable attraction due to its greater control and improved overall efficiency [2, 10]. Establishing a highly permeable path between the injection and production holes is considered as the single most important task prior to gasification because a highly permeable narrow channel can control gas leakage, water intrusion, liquid condensation, phenol contamination, and oxidant bypass during UCG operation [14]. Directional drilling, reverse combustion, and hydrofracturing are the popular linking methods currently used [2, 14]. After the invention of reverse combustion linking (RCL) in 1941 by former Soviet researchers [29], the technique was widely used by many countries in UCG field trials, including the former USSR. Reverse combustion linking (RCL) is the opposite of forward combustion linking (FCL) where the coal is ignited at the base of the injection well and the flame propagates towards the production well, i.e., in the direction opposite to the gas flow within the channel [29, 30]. As compared to FCL, RCL is the preferable linking option in terms of channel dimension, consumption of coal per unit of the link, linking speed, operational stability, and controllability [29]. However, FCL can also be used for widening the hydraulic links between the wells which exist naturally or have been preliminarily established using, for example, hydrofracturing [29]. Hydrofracturing is employed to establish a linking channel in coal seam of low permeability where RCL alone is not a suitable option initially due to in-situ coal properties and the fact that directional drilling is too sophisticated for that situation. The effectiveness of hydrofracturing is independent of both the electrical properties and the natural permeability of the coal. However, the lack of control limits its use primarily for steeply dipping beds where it is not essential to ensure that the cracks formed at the bottom of the seam or that they formed parallel or perpendicular to the bedding planes [14]. Directional drilling is one technique that is relatively independent of the coal properties. The in-

seam drilling of coal seams has been part of coal exploitation since at least the 1940s in Soviet plants [14]. Due to continuous and significant advances in the techniques used for directional drilling, this method is being currently considered as the most reliable way of establishing the link between wells.

2.3 Review of UCG Tests

2.3.1 Field-scale trials

UCG field tests have been carried in different coal seams worldwide, using different techniques to evaluate the effects of various factors of overall UCG performance. Some significant field trials worldwide are summarised in Table 2-2. A quick look at Table 2-2 indicates a significant increased heating value of the product gas for an injection gas of oxygen/steam mixture over air. Moreover, the overall performance is largely affected by coal properties (i.e., ranks and chemical composition), coal seam geology (i.e., depth, thickness), and drilling configurations. The dependence of coal properties, coal seam geology, and overburden properties (geology and hydrology) indicates that the performance of UCG is site-specific.

From Table 2-2, it can be observed that the field trials were conducted in different coal seams with different depths and thicknesses at different geographical areas. However, from the general observation of all the previous field trials, qualitatively it can also be concluded that increasing the depth is proportional to increasing drilling costs and operating pressure. Similarly, thicker seam is proportional to higher potential resources per unit projected surface area and lower costs. Figure 2-2 summarizes all the UCG field trials performed worldwide in term of their depth and thickness of the coal seam.

Table 2-2 Summary of significant UCG field trials worldwide [2, 17, 31-33].

Country	Site	Start-up Year	Coal Rank	Well Configuration	Injected Gas	Seam Depth (m)	Seam Thickness (m)	Gas Calorific Value (MJ/m^3)
USA	Hanna II	1975	B	LVW	Air	85	9	4.2
	Hoe Creek I	1976	B	LVW	Air	40	8	3.6
	Hoe Creek IIB	1977	B	LVW	O_2/H_2O	40	8	9.0
	Price town 1	1979	B	LVW	Air	270	2	6.1
	Rawlins IA	1979	SB	SDS	Air	105	18	5.6
	Rawlins IIB	1979	SB	SDS	O_2/H_2O	105	18	8.1
	Centralia A	1984	SB	CRIP	O_2/H_2O	75	6	9.7
	Centralia B	1984	SB	LVW	O_2/H_2O	75	6	8.4
	Rocky Mount. IA	1987	SB	CRIP	O_2/H_2O	110	7	9.5
	Rocky Mount. IB	1987	SB	LVW	O_2/H_2O	110	7	8.8
	Alaska SHR	2012	L/SB		Air	50-650	1-12	3.3-5
Belgium	Thulin	1986	A	LVW	Air	860	6	7.0
Spain	El Tremedal	1997	SB	CRIP	O_2/H_2O	580	2	6.6
Australia	Chinchilla	2000	SB	LVW	Air	140	10	6.6
	Bloodwood	2011		CRIP	Air	200	8-10	6.4
China	Suncan	2002	B	Tunnel	Air	80	2	8.5
S. Africa	Majuba	2007	B	LVW	Air	285	3.5-4.5	6.2

B= Bituminous, SB= subbituminous, A=anthracite

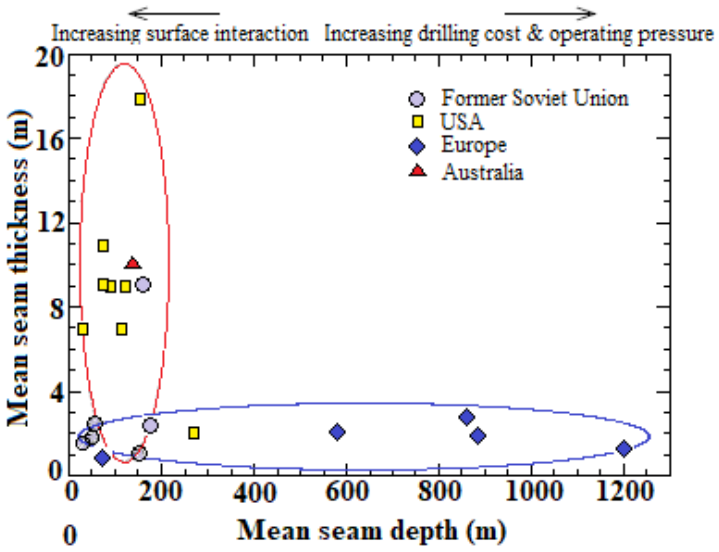

Figure 2-2 Thickness vs. depth of the field trials conducted worldwide (Modified from Perkins [17]).

From the Figure 2-2, it can also be observed that most of the European trials were conducted under high depth and thin seam whereas USA concentrated on shallow depth and thick seam. Most of the field trials of the former Soviet Union were conducted on shallow depth having thin seam.

2.3.1.1 Former Soviet Union

As mentioned before, although USSR was the pioneer in the field trials of UCG, the earlier trials followed shaft gasification method which required mining work and mining labour. However, after continuous efforts towards reducing mining work and labour they developed shaftless gasification method that completely eliminated mining work. The first shaftless method was conducted in 1956 at gas at underground gas generator No. 2 of Yuzhno-Abinskaya station [13].

The initial success for shafless gasification was obtained from steeply dipping coal seam. Figure 2-3 and Figure 2-4 show a single channel and multiple channel gas generators in steeply dipping coal seam, respectively.

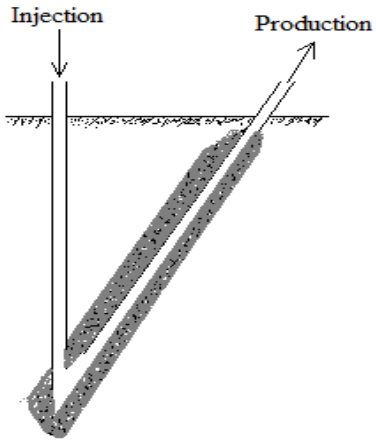

Figure 2-3 Single-channel underground gas generator in a steeply dipping coal seam in the plane of the seam's strike (modified from Skafa [13]).

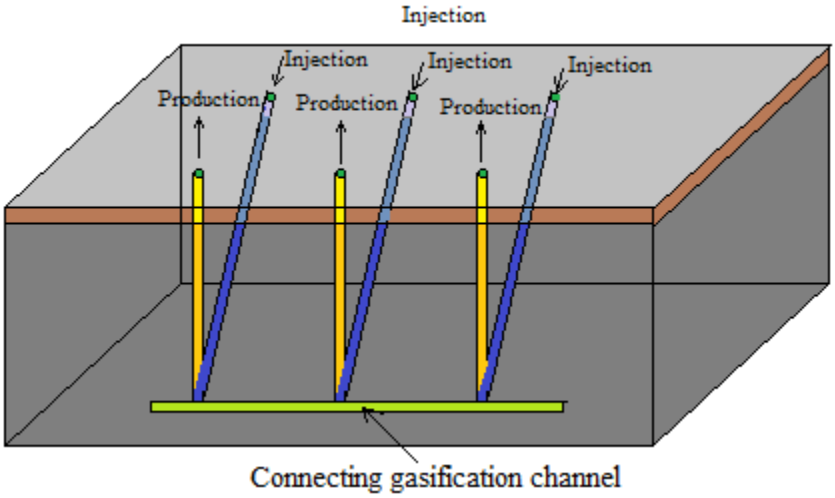

Figure 2-4 Multiple-channel underground gas generator in a steeply dipping coal seam in the plane of the seam's strike (modified from Skafa [13]).

In the horizontal coal seam, they also introduced multiple channel gasifier to intensify the gas production. Figure 2-5 shows a typical plan view of the Soviet experience in processing

horizontal coal seams. The dotted lines indicate the location of the underground linkage channels formed in the coal by countercurrent combustion step in preparation for gasification. The production phase of gasification is carried out by cocurrent combustion in the channel (row 2 and row 1). However, in practice, the Soviets conducted the gasification in both directions; the choice is critically dependent on the nature of the roof subsidence [14, 25].

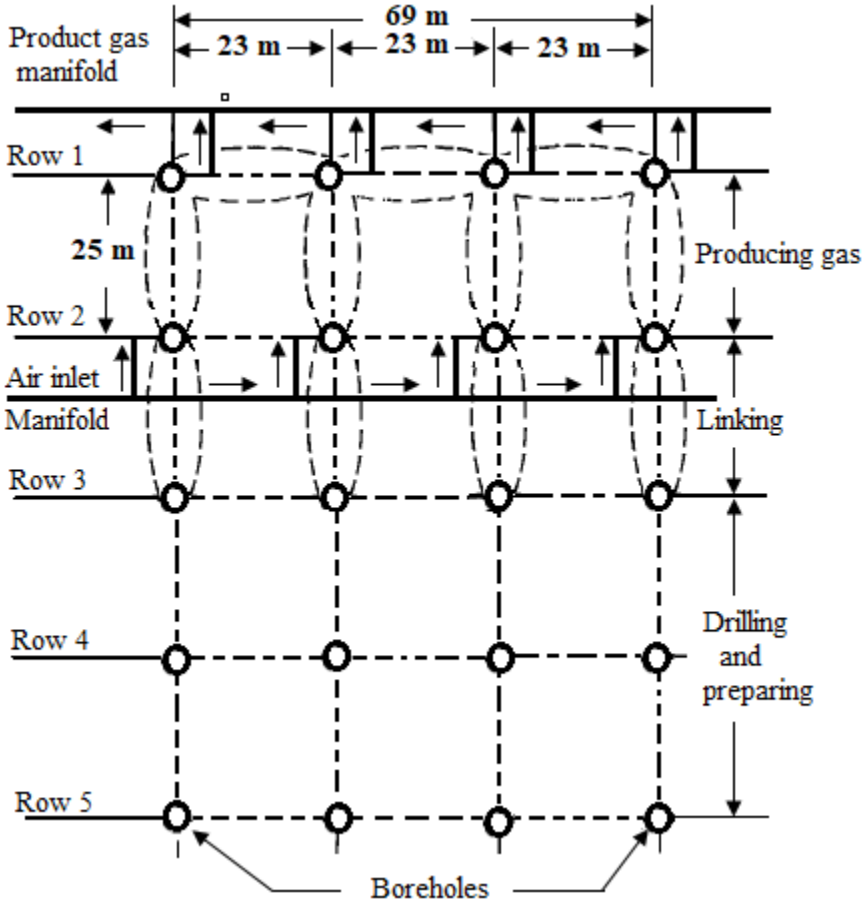

Figure 2-5 Plan view of a shaftless gas generator for a plant in Former Soviet Union (redrawn from Gregg and Edger [14]).

Most of the field trial operations were performed in shallow and thin coal seam depth <100 m and thickness of 0.6-2.1 m nearly at atmospheric pressure. Due to the shallow depth of the coal seam extensive gas leakage was reported. As soon as the cavity grew towards upward and the roof rock was exposed to hot blast and gas, three types of change in the state of the roof rock were distinguished [13].

The first type (Figure 2-6) is represented by a sagging of the roof rocks without any substantial break in continuity. In this type the characteristics of the blast and gas flow remains constant.

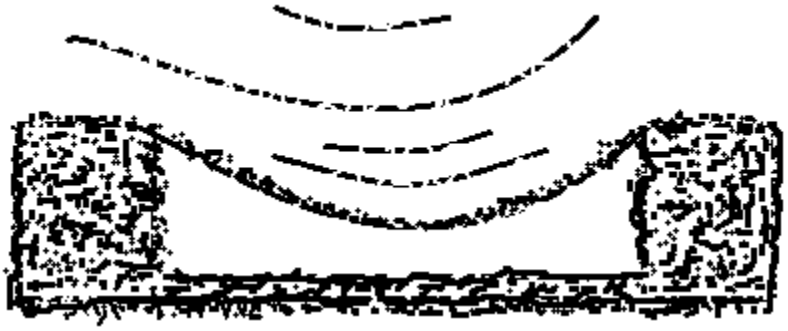

Figure 2-6 Character of the filling of the gasification space due to sagging of the roof rocks (redrawn from Skafa [13]).

The second type (Figure 2-7) is represented by developing a cavity partially filled with thermally affected rocks due to the fragmentation and/or swelling the roof with a minimal void at top. The layer of fallen rock rubbles alters the gasification path which in turns yields a favorable effect on the course of the gasification process.

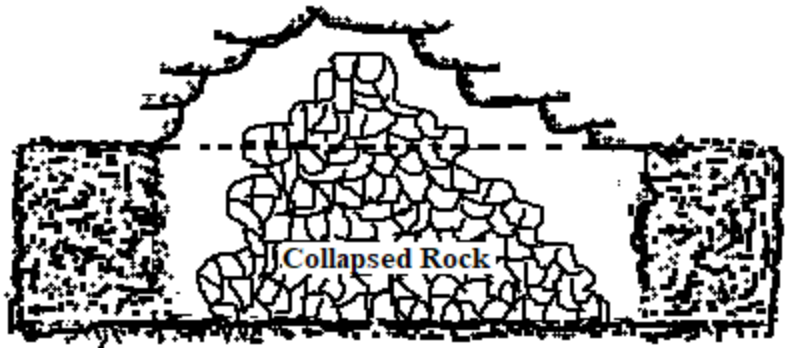

Figure 2-7 Character of the filling of the gasified space by collapse of the roof rocks (redrawn from Skafa [13]).

The third type (Figure 2-8) is represented by a collapse of the roof rocks in the case of which the specific reaction surface of the coal in the gasification channel is not kept nearly at constant value. As a result, as soon as the larger surface area of overburden is exposed to the hot gas, bypass channels for blast and gas becomes dominant.

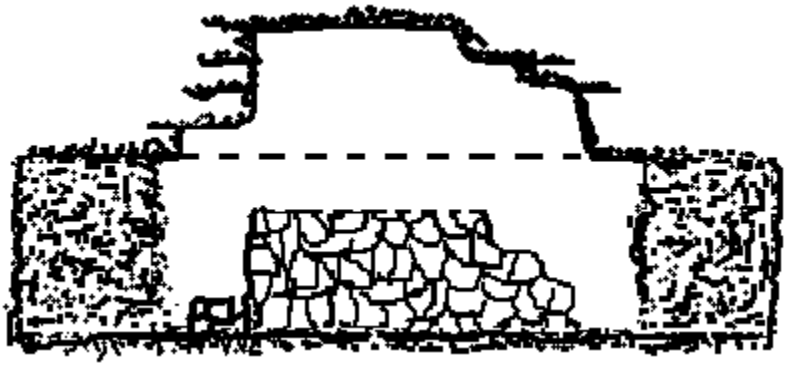

Figure 2-8 Scheme of the collapse of the roof rocks into the gasified space without considerable breakdown of these rocks (redrawn from Skafa [13]).

The effort of UCG in Soviet Union was dramatically decreased at around early 1970s, probably due to the discovery of large natural gas resources. However, in harmony with the new wave of

worldwide interest to UCG studies, Ukraine, Russia and Uzbekistan have started new research activities on UCG. A detailed investigation of USSR trials is given elsewhere [13, 25, 34].

Among the former Soviet field trials, there is only one is still operating today – the Yerostigaz UCG plant in Uzbekistan that feeds syngas to the 480 MW Angren electricity station. Currently this is known as the only one commercial UCG plant in the world [35].

2.3.1.2 European Union

The earliest most significant effort occurred in England (1949 – 1959) at a depth of 300 m; however, because of lack of information from successful trials of the former Soviet Union, they could only produce gas with very low heating value and experienced excessive water leakage, oxygen bypassing and recycling of gas in the cavity. Failure to establish a successful gasification channel was considered as one of the causes of the poor UCG results. After obtaining information from previous field data, several UCG field trials are conducted in Belgium, France and most recently in Spain in deeper coal seam.

France conducted a number of UCG trials (1979-85). However, the trials were suffered to establish a successful linking in an anthracite coal seam at great depth. Hydrofacturing and electro-linkage process or even reverse combustion did not work well to establish a successful gasification channel. Later, the early stage of Thulin trials in Belgium (a joint German-Belgium project, 1982-84) also showed that the reverse combustion is not a viable method of linking in a semi anthracite coal seam and at a great depth. Only the drilling method of linking was found successful for that coal seam. These unsuccessful trials led to the conclusion that reverse

combustion, hydro-fracturing, and electro-linking are not suitable for establishing a link between injection and production wells in an anthracite/semi-anthracite coal seam due to very low porosity.

An advanced deviated (directional) drilling technique was used in El Tremedal trials in Spain (1989-98) at an intermediate depth in subbituminous coal seam. This is considered as the first to fully test the in-line CRIP method of control and ignition with oxygen at a depth of 550 m [28]. It produced an average gas composition of over 10MJ/Nm^3. However, 50% water volume in the product gas led to the conclusion that there could be a breached aquifer that resulted water influx. Unfortunately, in the late 90s the trial was terminated when a malfunction caused a build up of methane, resulting in an explosion. Despite this problem, El Trededal trials is considered as the most successful project in Europe that inspired European Union to move more large-scale experiment before going to commercialization.

2.3.1.3 USA

The Department of Energy (DOE) has sponsored a number of field projects to determine the feasibility of UCG process between 1973 and 1989. These tests covered a range of coal seams (flat subbituminous, deep flat bituminous, and steeply dipping subbituminous). Those are well-documented, and results have been published in different reports and articles. The followings are the test programs at [2]:

- Hanna, WY, run by the Laramie Energy Technology Center;
- Hoe Creek, WY, run by the LLL;
- Pricetown, WV, run by the Morgantown Energy Technology Center in West Virginia;

- Centralia, Washington state, run by the LLL;
- Rawlins, WY, in a steeply dipping seam run by the US DOE and Gulf Oil;
- Rocky Mountain 1 which took place very close to the Hanna site, and was run by an industry.

A very brief description of important field trials is provided here. However, the details of each trials can be found in recent references: Camp [36]; Burton et al. [11].

2.3.1.3.1 Hanna (I-IV)

The Laramie Energy Technology Center, with assistance from Sandia National Laboratories, conducted the Hanna experiments at a gasification site located in South Central Wyoming. The first phase of Hanna, for Hanna I sixteen wells were drilled to assess the feasibility of UCG using air in sub-bituminous coal following LVW configuration. Because of the very low air acceptance rate, permeability was increased in some wells by introducing hydraulic fracturing. In the latter phase, reverse combustion linking was initiated with air injection to increase the permeability. Excavation indicated that only the top part of the coal seam was consumed. This was related to the placement of the wells near the top of the coal seam.

Hanna II was carried out in the Hanna No. I coal seam at a depth of 84 meter below the surface. After establishing the link by RCL, forward gasification took place with a cavity growth towards upward and along the centerline by taking a teardrop shape.

The third phase of the Hanna trials, Hanna III, was primarily designed to assess the environmental consequences of UCG. Results indicated that beyond gasification cavity, there is no sign of contaminant movement. Solubilized pyrolysis products were mostly found in cavities.

The Hanna IV site was located approximately midway between the Hanna I and II areas. The depth to the top of the coal seam was about 100 meters and process wells were spaced at > 30 meters which resulted significant problem in developing the RCL's because of the presence of the fractures perpendicular to the centre line. Unsuccessful operation of Hanna IV demonstrated that reverse combustion should not be used to establish linking over long distances.

2.3.1.3.2 Hoe Creek (I-III)

In parallel to the Hanna UCG series, a series of UCG trials were also conducted by Lawrence Livermore National Laboratory (LLNL) at Hoe Creek located in Northeastern Wyoming from 1976 to 1979 and tested three different linking methods:

- explosive fracture;
- reverse combustion;
- directional drilling.

Explosive fracture was used in Hoe Creek I; however, from the forward gasification results, the explosive fracture was not found to be viable method for developing a controlled region of high permeability for this shallow site.

Reverse combustion linking method was used in Hoe Creek II. The gasification lasted 43 days; however, excessive water influx in this trial lowered the gas quality. To resist the water inflow,

the operating pressure was increased; however, this resulted a significant gas loss (approximately 20%) into the rock formation.

Directional drilling with a combination of reverse combustion linking method was used in Hoe Creek III for establishing the link near the bottom of the coal seam for a well spacing of 17-30 m. As the burn zone moved into the upper coal seam, a significant gas loss of about 17% was resulted. Post-burn coring exhibited a tear-drop cavity shape. Cavity was filled with thermally affected rocks with a void at the top. Directional drilling was found to be an effective method for controlling the forward gasification. It was concluded that establishing the link at the bottom part of seam would improve quality of syngas by 15% [37].

Due to shallow depth and weak roof of seam, Hoe Creek II and III tests resulted in the propagation of subsidence of the surface. However, the serious concern was the contamination of the local aquifers from the toxic volatiles and semi-volatiles originated from the gasification process identified in the latter phase of Hoe Creek II gasification. The subsidence and collapse of the cavity roof exacerbated the situation by establishing a connection of the hydrostratigraphic zone [2, 11]. The tests are considered very important as these gave rise to the first recognition of possible groundwater hazards and triggered to develop a technique for better control over the collation of the reactions.

2.3.1.3.3 Pricetown

The Morgantown Energy Technology Center conducted a UCG experiment at a site near Pricetown, West Virginia. The swelling bituminous coal is located 270 meters below the surface

with an average thickness less than 1.8 meters. The module used a directionally drilled horizontal borehole as the link between the injection and production wells and the link length was 20 m. However, the gasification lasted only 8-10 days due to reducing rate of gasification reactions. It was reported that the agglomerating property of the coal apparently sealed the walls and inhibited the propagation of the cavity. This trial was an evidence of the coal agglomeration of swelling coal on gasification process.

2.3.1.3.4 Rawlins

The Gulf Research & Development Company supported by DOE conducted two field tests in inclined subbituminous coal seam with dipping angle of 60° located at Rawlins in Wyoming. These tests exhibited a thermal efficiency of more than 80% [38]. Test with oxygen (with a steam-oxygen ratio of 5:1) exhibited a higher gasification rate (more than 3 times) and higher heating value (nearly 3 times) as compared to the air blown test. In terms of operational control, product gas composition and thermal values, these trials were considered very successful ones as compared to UCG in horizontal strata.

2.3.1.3.5 Centralia

Based on the Hoe Creek results, to avoid the upward development of the cavity and mitigate the environmental concern, LLNL conducted a number of large coal block experiments by adopting a Russian experience in UCG of movable injection point at the Widco mine, Centralia, Washington [2, 39]. The CRIP system permitted horizontal retraction of the injection point within the coal seam to expose fresh coal to the UCG process [40].

Figure 2-9 shows a basic well configuration for Linear CRIP. The details of CRIP well configuration can be found elsewhere [2, 41]. Because of greater control of gasification process, this process received popularity and applied in different field trials later one.

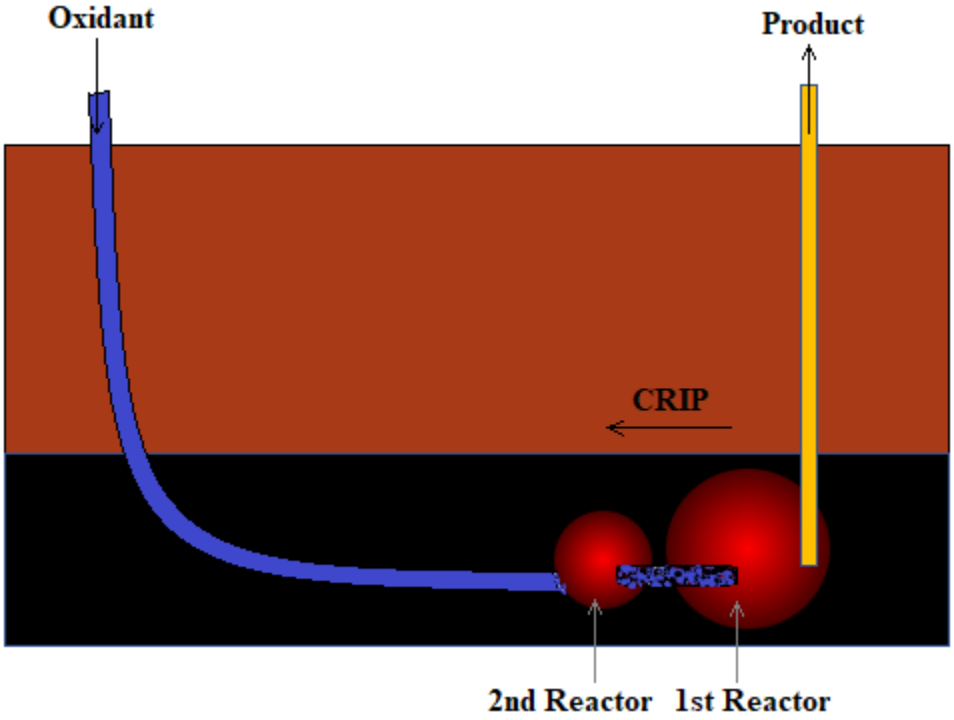

Figure 2-9 Linear CRIP (modified from Beath et al. [41]).

2.3.1.3.6 Rocky Mountain

Trials at Rocky Mountains were performed i) to compare extended LVW and the CRIP using the parallel in-seam boreholes method (see Figure 2-10) and ii) to develop methods to reduce and mitigate environmental impacts to groundwater from UCG operations. Table 2-3 summarizes the data from these tests. In-seam drilling was established at this trial and the CRIP manoeuvre was successfully performed three times. CRIP technique resulted in 10-15% improvement in syngas quality. A detailed procedure for CRIP operation as a result of this trial can be found in references: Couch [2], Dennis [42].

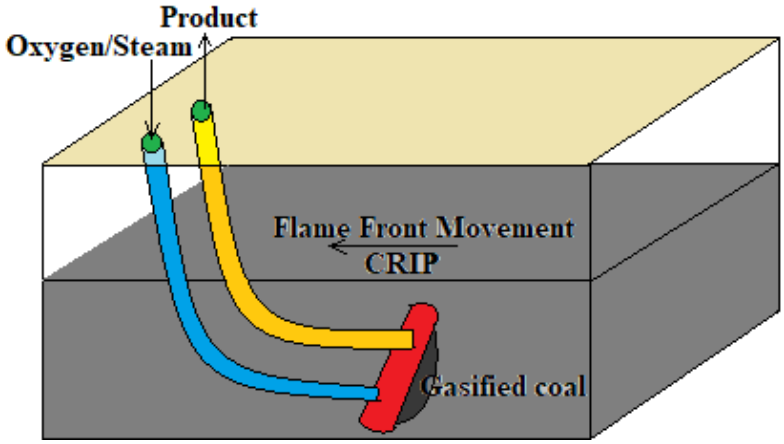

Figure 2-10 Parallel CRIP (modified from Beath et al. [41]).

Table 2-3 Results of LVW and CRIP methods in Rocky Mountain trial (data extracted from Couch [2]).

Well Configuration	LVW	CRIP
Process Duration (Days)	65	90
Coal Consumption rate (Tons/Day)	60-90	60-180
Higher Heating Value of syngas (MJ/m^3)	8	9-10

2.3.1.4 Australia

The most recent pilot plants are found in Australia. Linc Energy Ltd. conducted a series of trials from 1999 to 2002 at Chinchilla, Queensland, Australia. The UCG technology developed in Uzbekistan was used in the Chinchilla. The details of the trials can be found in references: Perkins et al.[43], Couch [2]. The years of experience of design and successful operation of this demonstration facility yielded confidence toward enlarging the UCG project and the lead companies, i.e. Cougar Energy, Carbon Energy and Linc Energy were working together to carry out several UCG large scale plants toward commercialization. Although in terms of gas production, coal consume and energy extraction, these plants were comparatively ahead of any

of the earlier UCG trials, these trials are now halted due to allegation on environmental issue. Because of these allegations, the commercialization of these plants is not very optimistic until the environmental issues are addressed with prime importance in future trials. In April 2016, the Queensland Government permanently banned UCG in response to major groundwater and soil contamination resulting from one of Linc Energy's trials [35].

2.3.1.5 Other countries

The recent research activities, field/lab-scale tests of UCG show that some other countries such as China, South Africa, Canada, New Zealand, India, Japan are also interested in UCG.

Considering the volume of works (research activities including patents, field and lab-scale tests, it is believed that China is very active toward developing the UCG. The primary focus of their study is the production of hydrogen-rich syngas from abandoned shallow coal mines. However, the detail information about their field trial activities is very scarce.

Eskom's Majuba UCG pilot plant in Mpumalanga, South Africa, began operations in 2007 and shut down in 2015 [35]. Eskom used εUCG technology licensed from Ergo Exergy Inc. Coal seam was 250-380 m deep and 1.8-4.5 m thick. A demonstration plant led to the production of 3-5000 m^3/hr syngas which was used to generate 100 kWh electricity.

In 2009, Swan Hill conducted a single pair UCG trial using linear CRIP linking method in Alberta, Canada. This trial is considered as the deepest (1400 m) trial in the history of UCG field

trials. However, mechanical difficulties and an injection well over-pressurization, resulted in limited output and duration [28].

A small scale UCG trial was operated in 1994 in the Huntly Coal Basin, New Zealand. The test was carried out over a period of 13 days and approximately 80 tonnes of coal were consumed during linking of five vertical wells by reverse combustion; however, the forward gasification was not successful [8].

India and Pakistan also carried out initial tests and identified sites for exploitation.

2.3.2 Small/Laboratory-scale tests

Due to smaller economic investments and site-specific nature of UCG, several laboratory-scale coal block experiments have been reported [44, 45]. Table 2-4 represents major laboratory studies on UCG. Feed temperature, feed flow rate, steam-to-oxygen ratio, operating pressure, combustion time, total operation time, and distance between wells are varied to observe their effects on the product gas composition and flow rate and gas outlet temperature. As well, the temperature distribution in the coal seam during gasification, the final cavity dimension and the rate of recession of the coal surface due to reaction are also observed and, finally, the optimum operating conditions for the expected UCG performance are determined.

Table 2-4 Major UCG experiments on coal blocks [18, 33].

Researchers	Coal Types	Dimension of Seam	Major Observations
Thorsness et al. [46]	Sub-bituminous	1.5 m × 0.15 m dia	Product gas composition
Yeary and Riggs [47]	Lignite	25 cm × 5 cm × 25 cm	Lateral cavity growth
Yang [48]	Gas fat	4.45m × 1.5 m × 0.5 m (65°)	Product gas composition
Daggupati et al.[49, 50]	Lignite	30-38 cm × 20cm × 25cm	Cavity growth and shape
Stańczyk et al. [51, 52]	Lignite, Hard coal	2.5m × 0.7m × 0.7m	Two-phase UCG in lignite

Almost all the lab-experiments except very few were conducted using channel mode. The major observation of all the lab-scale experiment following channel was the lateral cavity growth. However, on the other hand, the major observation of packed bed or fixed bed gasifier was product gas composition.

The concept of packed bed UCG process involves fracturing thick, deep, coal seam to get a high-permeability zone. To prove the benefit of packed bed, Thorsness et al.[46] under LLNL's research program conducted a lab-scale packed bed experiment using a 1.5 m long and 0.15 m diameter reactor filled with 19 kg crushed coals of 1 cm size. They carried out the experiment under 4.8 atm pressure with a very high steam-to-oxygen ratio (6:1) to observe the thermal-front propagation and product gas composition. Considering the packed bed gasification, production gas was found high in hydrogen (≈ 45%) and carbon monoxide (≈ 18%). Although they did not provide a details description of their experiment, details of their input parameters and outlet gas concentration can be found in Table 2-7 and Table 2-8. This packed bed lab-scale experiment was used by them and others to verify packed bed model.

Beside the packed bed UCG experiment, LLNL's research program also carried out a number of small-scale experiments in channel mode to evaluate the cavity growth and shape of different coals. Under LLNL's research program Thorsness and Hill [53] conducted a series of barrel test following the channel gasification process on three different coals (Widco, Hanna, and Wyodak) and observed different cavity formation for different coals, i.e., a teardrop-shaped cavity for Widco and Wyodak coals whereas a circular shape for Hanna coal. However, LLNL barrel tests for Widco and Wyodak coals, exhibited some major cracks perpendicular to the bedding plane and a preferential propagation of the cavity in the direction of the cracks [54].

Parallel to the work of LLNL, a series of lab-scale tests were carried out under the supervision of Park and Edger at the University of Texas, Austin. Mai et al.[55] reported an experimental set-up for lignite coal similar to the work of LLNL's tests. Their observation was almost similar as observed by Thorsness and Hill [53] in case of lignite coal experiment. They also reported a cavity shape of teardrop, presence of ash layer and major cracks in the direction perpendicular to the bedding plane and many fine cracks in the direction parallel to the bedding plane. The cavity growth was found to be propagated through the major cracks as the reactant gases could penetrate into the large cracks. Finally, their results indicated that shrinkage of coal due to pyrolysis and drying plays a dominant role in crack growth perpendicular to the bedding plane.

Yeary and Riggs [47] conducted a small-scale UCG experiment to evaluate the lateral cavity growth for lignite and sub-bituminous coal. However, instead of ignition inside the coal block, they ignited the oxidant and fuel in a water-jacketed chamber and allowed the high-temperature gases to enter the reaction cavity to expose directly to the side wall or cavity roof depending on

the orientation of the bedding plane. From the increase of surface recession rate due to the increase of gas temperature and gas flow rate they speculated that the surface recession process was heat transfer-controlled gasification. Their result exhibited no structural failure for the side wall; however, significant structural failure for the roof in case of lignite coal only. The downward growth of the cavity was limited by the presence of rubble pile due to high spalling rate and ash layer for lignite coal. That's why they recommended having ash removal mechanism to formulate a feasible lateral growth. The cause of structural failure of lignite coal was probably due to the presence of clay stringers in the lignite samples.

Yang et al. [48] conducted a UCG lab-experiment to study the effect of oxygen, oxygen-steam and moving point gasification methods using a gasifier of a dimension of 4.45 m × 1.5 m × 0.5 m with a dip angle of about 65°. They used big natural gas-fat coal chunks; however, the crevices were filled with small coal chunks and spatulated with a mixture of a small quantity of cement and coal powder to retain the natural state of coal seams as much as possible. A gasification channel was created that connected the injection and the production lines. There were a number of auxiliary holes along axial length of the reactor to accommodate the shift of injection hole if needed. The moving point oxygen-steam gasification method is actually a change of the injection hole from the original to an auxiliary hole in the forward direction near the vicinity of a gasification working face. In this, as soon as the temperature and the outlet gas volume decrease followed by the decline of syngas volume fraction are observed, the injection hole is shifted. Experiments showed that shifting gas feed from pure oxygen to oxygen and steam (2:1 ratio) almost double the volume fraction of hydrogen and carbon monoxide in the product. A steam/oxygen ratio of 2 was found to give the stable syngas product gas composition and heating

value. Using multiple injection points increased the duration of the gasification stage, while shortened the oxidation phase.

Daggupati et al.[49] conducted a series of experiments to evaluate the cavity growth, shape and product gas composition with respect to feed flow rate, gasification channel length and operating time. They used a 30 cm × 20 cm × 25 coal lignite coal blocks with a 3 mm-diameter gasification channel connected the injection and production wells. They reported a very short ignition phase of 5 minutes when LPG was used as a fuel with oxygen. The first series of their experiment was to study the evolution of cavity for 8 hours combustion phase with different injection rates and well distance. However, all the experiments resulted a similar teardrop cavity shape as observed in earlier experiments for lignite coal [53, 55]. They measured the linear, vertical growth rate of 1.1 cm/h (obtained using the measured cavity heights at different times, with the other operating conditions being the same). Increasing feed flow rate resulted in linear increase in cavity volume in all dimensions. The increase flow rate was considered to reduce the external mass transfer resistance due to the ash layer from the bulk gas to the solid surface and thus increase the combustion rate which in turns increased the growth of the cavity. The forward and backward growth and volume of the cavity was found to decrease with increasing the distance between the wells, while cavity width and height were found to increase. As soon as the cavity reaches the production well, considerable bypass of oxygen terminated the process.

In the latter phase of their experiment, Daggupati et al.[50] studied steam gasification and observed a decline in temperature after injection of steam. To keep a desired cavity temperature (> 700 °C), they suggested preheating and introducing sufficiently high temperature (400 – 600

°C) steam in a cyclic manner of 10 minutes interval. The best syngas heating value was achieved by a steam/oxygen ratio of 2.5. Spalling was found to be active during coal gasification only. Cavity shape was observed to be the same but larger in case of steam/oxygen injection.

Stańczyk et al.[51, 52] carried out several UCG experiments to investigate the atmospheric gasification behaviour of lignite and hard coal seams using oxygen, air and oxygen enriched air as gasifying agents. Experiments were conducted in a 2.5×0.7×0.7 m coal block with a gasification channel. Three distinct stages for the UCG process were observable in the experiments: ignition, combustion, and gasification with steam. As steam was not injected separately, strata moisture content as a steam source. The gasification stage was further divided into three phases where in the first phase only oxygen was introduced. In the second phase, only air was introduced and in the third phase oxygen enriched air was introduced. The ignition phase was continued until a temperature reached 400 °C. It took two hours for lignite coal and one hour for hard coal to reach this temperature. During oxygen gasification phase, oxygen flow rate was kept sufficiently high to accumulate sufficient amount of thermal energy for the development of gasification process. However, replacing oxygen with air was unfeasible due to sharp decline in temperature that termination gasification process. Thus, oxygen-rich air was used and optimum oxygen/air ratios for lignite and hard coal UCG were proposed accordingly. Shorter ignition and combustion periods, higher temperatures and lower oxygen/air ratios were found to be attainable for hard coal due to its higher carbon content compared to lignite. In their latter phase of experiment, Stańczyk et al. (2012) extended the oxygen gasification following a process known as two-stage gasification where steam was supplied separately in a cyclic manner. The process is

followed to maintain a suitable gasification temperature as observed in the latter phase of experiment of Daggupati et al. [50]. This process improved the overall efficiency.

2.3.3 Summary of UCG tests

From a number of trials and experiments, it can be summarized that:

- UCG is very site specific.
- Deeper coal seam is preferable to resist surface leak.
- The location should be away from aquifer.
- Coking coal is not very suitable for UCG.
- Lower rank coal is preferable due to its non-swelling property.
- Higher operating pressure than the hydrostatic pressure must be applied to resist control water influx and leak in to surrounding aquifer.
- From economic consideration, oxygen rich air is preferable to achieve higher heating value syn gas.
- Directional drilling is getting popular to achieve a control gasification channel
- CRIP technology generally provides higher heating value gas.
- An appropriate risk assessment should be conducted before any trial and the trial should be terminated if any concerns of environmental pollutions are detected.

2.4 Review on Relevant Models on UCG

Although a number of UCG field trials have been performed, the information on the detailed UCG process is very limited because of the high cost of extracting data as well as the difficulty in controlling the operating variables. In addition, there is a limited scope of adjusting parameters due to the site-specific nature of the performance of UCG. The generalizing data from the lab-

scale experiments should still be done with extreme care since the whole process may not be properly represented in lab-scale experiments. It may not be possible to represent the entire phenomenon in laboratory-scale experiments [53, 56]. The coal seam is a three-dimensional reactor without specific geometry and the flow pattern inside the UCG cavity is highly non-ideal. The complexity increases further because of several other complex physical and chemical processes occurring simultaneously, such as chemical reactions and kinetics, transport phenomena (i.e., heat and mass), water intrusion from surrounding strata, thermo-mechanical processes related to the structure of the seam, and other geological aspects. Both field tests and lab-scale experiments are not sufficient to provide a detailed quantitative description due to the demand of extensive instrumentation and trials. The difficulties encountered in controlling and operating the UCG process serve to be the incentive to develop quantitative models to predict the effects of various physical and operating parameters on the performance of the process and to extrapolate the understanding to other operating conditions and coals. Prior to 1975, the development of UCG models was very limited, and focused only isolated cases, such as heat transfer, mass transfer, combustion rate, etc. However, after gaining a better understanding of the UCG process, the intensity of developing a global model increased significantly. A full UCG model that describes the complete mechanisms would typically include a number of the following sub-models:

Injection/production linkage sub-model.

- UCG reactor sub-model.
- Ground water hydrology.
- Ground subsidence model.
- Surface facility models.

Combining all these sub-models would theoretically give an exact description of the process; however, building such a model is not a trivial task. Therefore, all previous models have focused on studying these aspects separately through several simplifying assumptions. There are lots of models developed thus far; however, a successful model should be able to:

- Compute transient temperature profiles along the coal seam during gasification.
- Determine the rate of gas and coal consumption.
- Determine the effect of coal shrinkage or swelling on UCG performance.
- Predict the pressure and velocity of the produced gas in a coal seam of known porosity and permeability.
- Predict the progressive configuration of the combustion front during gasification.
- Predict the cavity formation and dimension with time.
- Predict the effect of operating pressure, feed inlet temperature, feed rate, feed mixture ratio, and well spacing and configuration for the gas production rate, composition, and its heating value as well as cavity dimension.
- Predict the effect of coal bed thickness, ash content, moisture content for the gas production rate, composition, and its heating value as well as cavity dimension.

In this chapter, a brief overview of the UCG reactor sub-model of forward gasification is particularly discussed due to its direct impacts on coal resource recovery, cavity growth, energy efficiency and, consequently, economic feasibility.

Over the years, several approaches have been developed for the modeling of the UCG process; however, the two main approaches are:

- Packed bed model.
- Channel model.

Since there are a number of mathematical/numerical models in the literature, it is most instructive to indicate the significant features and limitations of these models. Most of the earlier models were one-dimensional (1D); however, with the advancement of computational power, two-dimensional (2D) and even a few three-dimensional (3D) models were developed. In the following section, the primary modeling approaches are discussed.

2.4.1 Packed bed models

The earliest models of UCG in literature include models that describe the process as a packed bed reactor. The consideration of the "in-situ" coal seam as a packed bed primarily originated from the concept of Higgins [57] considering the creation of a permeable zone between two boreholes either by reverse combustion linking (RCL) or by fracturing the coal seam using pressurized air or chemical explosives [58, 59]. The resultant coal seam resembles a packed bed where coal particles are filled in the reactor. This concept is similar to the major Soviet approach to seam preparation where they included extensive drying of the seam and reverse combustion to obtain a region of enhanced permeability between the boreholes [60]. On the other hand, according to Gunn and Whitman [61], the coal seam consists of lignite or subbituminous coal can be gasified without establishing any linkage path due to their high permeability, also known as the percolation or filtration method which more closely resembles the operation of a packed bed chemical reactor. The packed bed model assumes that coal gasification occurs in highly permeable porous media with a stationary coal bed which is consumed over time [62]. Table 2-5

and Table 2-6 represent a glimpse of a list of packed bed models discussed here with their essential features and reaction rate control mechanisms of the main reactions in the gasification process, respectively.

Table 2-5 Some essential features of reported packed bed models [18].

Researchers	Dimension & Time Dependence	Heat Transfer			Mass Diffusion	Fluid Flow	Thermo Mechanical Failure	Water Influx	Heat Loss
		Conduction	Convection	Radiation					
Winslow [63]	1D & T	√	√			D			
Thorsness et al. [46]									
Thorsness and Rozsa [58]	1D & T	√	√			D			
Khadse et al. [62]	1D & PS	√	√			D			
Uppal et al [59]	1D & PS	√	√			D			
Thorsness and Kang [64]	1D & T	√	√		√	D	√		
Gunn and Whitman [61]	1D & PS	√			√			√	
Abdel-Hadi and Hsu [4]	1D & T	√	√		√				

1D= One dimensional, D = Darcy flow, PS = Pseudo-steady state, T= Transient.

Initially, around 1976, several 1D transient packed bed models [46, 58, 63] with the finite-difference approach were developed in parallel, supported by the Lawrence Livermore National Laboratory (LLNL) program. However, there is no basic difference between the models developed by Thorsness et al. [46] and Thorsness and Rozsa [58]. Thorsness and Rozsa [58] provided a detailed description of the lab-scale gasification experiment whereas Thorsness et al. [46] provided a detailed description of the development of the physical and chemical model where they made many simplifying physical and chemical assumptions, based on experimental and theoretical comparisons and correlations, which include:

- the gas permeability.
- the effective thermal conductivity.
- the interphase heat-transfer coefficient.
- the chemical reaction rates.
- the various thermodynamic properties of each species, and.
- the stoichiometric coefficients.

Table 2-6 Reaction rate control mechanisms of the main reactions in the gasification process [18].

Researchers	Drying	Pyrolysis	Char Reaction				Water Gas Shift Reaction	Gas Phase Reaction		
			$C + O_2 \rightarrow CO_2$	$C + CO_2 \rightarrow 2CO$	$C + H_2O \rightarrow CO + H_2$	$C + 2H_2 \rightarrow CH_4$	$CO + H_2O \leftrightarrow CO_2 + H_2$	$CO + 0.5O_2 \rightarrow CO_2$	$H_2 + 0.5O_2 \rightarrow H_2O$	$CH_4 + 2O_2 \rightarrow CO_2 + 2H_2O$
Winslow [63]	D	P	K	K	K	K	K			
Thorsness et al. [46]	D	P	K	K	K	K	K	I	I	I
Thorsness and Rozsa [58]	D	P	K	K	K	K	K	I	I	I
Khadse et al. [62]		P	K	K	K	K	K			
Uppal et al [59]		P	K	K	K	K	K	I	I	I
Thorsness and Kang [64]			K	K	K	K	K	I	I	I
Gunn and Whitman [61]		EC	P		P					
Abdel-Hadi and Hsu [4]	D	P	P	P	P	P	E			

D = Diffusion limited, I = Infinite rate, K = Kinetic (power law) and bulk diffusion, P = Power law kinetics, EC= Experimental correlations

In their model, to avoid complexity, they neglected tar condensation and plugging, gas losses to surroundings, water intrusion from surroundings, heat losses, and coal bed movement due to shrinking or swelling during drying and pyrolysis.

Winslow [63] also followed their work, except using a different numerical solution scheme. Thorsness et al. [46] considered all the main reactions for gasification (reaction 1 to reaction 10); however, for homogeneous reactions, only the water-gas shift reaction was considered by Winslow [63]. Although, for convenience, most of the researchers represent char as a molecule containing one carbon, they considered the chemical formula of char and dry coal as $CH_{a1}O_{b1}$ and $CH_{a2}O_{b2}$, respectively, where the composition parameters a1, b1, a2, b2 depend on the type of coal (usually obtained from the ultimate analysis). Beside the moisture content for drying, they also considered mobile condensed water which undergoes evaporation and condensation upon the removal of heating. However, for the simplicity of the calculation, they assumed a fixed velocity of mobile water. Their model considered fitted kinetic models for pyrolysis data developed by Campbell [65]. The controlling mechanisms of reaction rates that they considered are listed in Table 2-6. Eight gas species (N_2, O_2, H_2O, H_2, CH_4, CO, CO_2, tar) and five solid/condensed species (coal, char, mobile liquid water, fixed liquid water, and ash) were considered, upon which the balances were written. The reaction rates of the heterogeneous reactions (char-gas reactions) were considered to be influenced by three mechanisms: mass-transport limitation from the bulk gas to the solid surface, mass-transport limitations in any internal particle porosity, and kinetic limitations at the solid surface. This reaction mechanism was also considered for the water-gas shift reaction due to the influence of a catalyst that might be present in the coal bed. Because of the high reactivity of char as compared to pure carbon, the mass transfer limitation was considered important. However, in their model, one effective chemical rate expression (R_c) was assumed to account for the internal transport and surface kinetics. As a result, the total rate (RT) was considered as a kinetic internal-diffusion rate and expressed as follows:

$$\frac{1}{R_T} = \frac{1}{R_C} + \frac{1}{R_m} \quad \textit{(Eq. 2.1)}$$

where R_c is linearly dependant on the mole fraction of the limiting reactant (y_l) in the bulk phase and the parameter R_m is the mass transfer rate of a limiting reaction defined by:

$$R_m = k_y y_i \quad \textit{(Eq. 2.2)}$$

where k_y is the mass transfer coefficient.

In their models, the fluid flow was described by the Darcy equation, in which permeability was set to change with the extent of the reactions. From the experimental data of drying and pyrolysis of subbituminous Wyodak coal, they formulated a functional relationship relating permeability to porosity that was used later by a number of researchers [12, 63, 64] who developed their model using subbituminous coal. The relationship is as follows:

$$\alpha = \alpha_0 exp[\sigma(\varphi - \varphi_0)] \; for \; \varphi > \varphi_{lim} \quad \textit{(Eq. 2.3)}$$

where α_o is the initial permeability, φ_o is initial porosity of coal, and φ_{lim} is the upper limit of porosity above which the permeability was assumed to be constant. Based on the experiment, the calculated value of the parameter σ was approximately 12. In their report, they considered φ_{lim} = 0.25 so that the particle size decreases with increasing porosity (φ < 0.25). As a result, the permeability was assumed to reach a constant value for porosity larger than 0.25.

Thorsness et al. [46] incorporated a quasi-steady approximation for changes associated with the gas phase that allowed them to use ordinary differential equations for gas phase mass and energy balances. The governing equations were as follows:

Mass balance:

$$Gas: \frac{duC_i}{dx} = \sum_j a_{ij} R_j \; (i = 1,2, \ldots . G) \quad \textit{(Eq. 2.4)}$$

where *G* is the number of gas species.

It is noted that gas phase diffusion, which had been considered an important factor in the channel and coal slab model development, was neglected.

$$\textit{Solid: } \frac{\partial \rho_k}{\partial t} = M_k \sum_j a_{kj} R_j \ (k = 1,2,3 \ldots . K) \qquad \textit{(Eq. 2.5)}$$

where *K* is the number of solid/condensed species.

$$\textit{Mobile water: } \frac{\partial \rho_w}{\partial t} = -u_w \frac{\partial \rho_w}{\partial x} + M_w \sum_j a_{kj} R_j \ (k = 1, i.e., only\ water) \qquad \textit{(Eq. 2.6)}$$

Energy balance:

$$\textit{Gas: } \frac{dT}{dx} = -\frac{1}{u C_{p_g}} [h_T (T - T_s] + Q_g \qquad \textit{(Eq. 2.7)}$$

$$\textit{Solid: } C_{p_s} \frac{\partial T_s}{\partial t} = \frac{\partial}{\partial x}\left[(1-\varphi) D \frac{\partial T_s}{\partial x}\right] + h_T (T - T_s) + Q_s - u_w \rho_w C_w . \frac{\partial T_s}{\partial x} \qquad \textit{(Eq. 2.8)}$$

Momentum balance:

The momentum balance gas phase was replaced by Darcy's law:

$$\frac{\partial p}{\partial x} = -\frac{u}{\alpha} \mu_g \qquad \textit{(Eq. 2.9)}$$

The use of Darcy's law and some theoretical correlations they employed in their model indicate an implicit assumption of the laminar flow process.

On the other hand, Winslow [63] did not approximate any stationary phase for the basic conservation equation, although he followed the physical and chemical model of Thorsness et al. [46]. The following governing equations for mass and energy balance for both the gas and solid phases were used by Winslow [63]:

Overall gas conservation: $\frac{\partial}{\partial t}(\varphi\rho_g) = -\frac{\partial}{\partial x}(\rho_g u) + S_m$ *(Eq. 2.10)*

Conservation of gas species: $\frac{\partial}{\partial t}(\varphi C_i) + \frac{\partial}{\partial x}(C_i u) = \sum_j a_{ij} R_j (i = 1,2, \ldots . G)$ *(Eq. 2.11)*

where *G* is the number of the gas species. Gas diffusion was neglected.

Conservation of condensed species: $\frac{\partial}{\partial t}(1-\varphi)\rho_k = \sum_j a_{kj} R_j (k = 1,2,3 \ldots . K)$ *(Eq. 2.12)*

where *K* is the number of solid/condensed species.

Energy conservation of gas: $\frac{\partial}{\partial t}(\varphi\rho_g e) + \frac{\partial}{\partial x}(h\rho_g u) = -h_T(T - T_s) + Q_g$ *(Eq. 2.13)*

Energy conservation of solid: $\frac{\partial}{\partial t}[(1-\varphi)\rho_s e_s] - \frac{\partial}{\partial x}\left[(1-\varphi)D\frac{\partial T_s}{\partial x}\right] = h_T(T - T_s) + Q_s$ *(Eq. 2.14)*

Using Darcy's law, the gas bulk velocity is given by:

$$u = -\frac{\alpha}{\mu_g}\frac{\partial p}{\partial x}$$ *(Eq. 2.15)*

The primary objective of their preliminary works was to predict and correlate reaction and thermal-front propagation rates and product-gas composition as a function of coal bed properties and process operating conditions, as well as the secondary objective of testing the correctness of the physical and chemical model they developed. Despite the simplifying assumptions as shown in Table 2-7, their results were generally in accordance with steady-state laboratory measurements (Table 2-8). Experimental run 5 was carried out using back heating to eliminate radial heat losses. As a result, model calculations with the assumption of no heat loss were closer to the data of experimental run 5. Although the lab-scale experiment did not represent the field-scale system as the porosity (50%) and the permeability (150 D) were too high and the particle

diameter (1 cm) was too small, the agreement between the model calculations and the lab experiments indicates that the simple physical and chemical models of Thorsness et al. [46] are useful to some extent in the design of the gasification process.

Table 2-7. Input parameters used for model calculation and experimental runs from a 1.6 m reactor [18].

Input Parameters	Calculated (Thorsness and Rozsa [58], Thorsness et al. [46])	Calculated (Winslow [63]	Reactor experiments (Thorsness and Rozsa [58], Thorsness et al. [46])	
			Run 4 (no backheating)	Run 5 (with backheating)
Coal Dimension	L = 150 cm, D =15 cm	L = 150 cm, D =15 cm	L = 150 cm, D =15 cm	L = 150 cm, D = 15 cm
Initial Porosity	50%	44.4%	50%	50%
Initial Permeability	150 Darcy		150 Darcy	150 Darcy
Coal Particle Size	1 cm	1 cm	1 cm	1 cm
Injected Gas Flow Rate	2×10^{-4} gmole/cm^2.s	2.1×10^{-4} gmole/cm^2.s	2×10^{-4} gmole/cm^2.s	2×10^{-4} gmole/cm^2.s
Initial Feed Temperature	450 K	450 K	450 K	450 K
Pressure	4.8 Atm	4.8 Atm	4.8 Atm	4.8 Atm
Injected Gas Composition				
O_2	14.1%	13.4%	13.4%	13.4%
N_2	2.40%	2.2%	2.2%	2.2%
H_2O	83.5%	84.4%	84.4%	84.4%
Steam/O_2 Ratio	6	6	6	6

Table 2-8 Steady-state temperature and major constituents of outlet gas composition [18].

Parameters	Calculated (Thorsness and Rozsa [58], Thorsness et al. [46])	Calculated (Winslow [63])	Measured (average over run) (Thorsness and Rozsa [58], Thorsness et al. [46])	
			Run 4 (no back heating)	Run 5 (with back heating)
Peak Temperature (K)		1250		1200
Speed of burn front	18 cm/h	18 cm/h		18 cm/h
Product Gas Composition (dry basis)				
H_2	43.2%	43.8%	44.9%	44.6%
CH_4	6.6%	4.0%	6.4%	6.9%
CO	22.0%	22.0%	16.5%	19.0%
CO_2	28.2%	30.2%	33.2%	29.5%

Beside the model validation with experimental data, they also illustrated various features of their simulations with time or spatial variations and compared them with the experimental results where possible. The solid and gas temperature distribution along the length in their system at different times indicated the propagation of the reaction and drying/pyrolysis fronts at different speeds (see Figure 2-11).

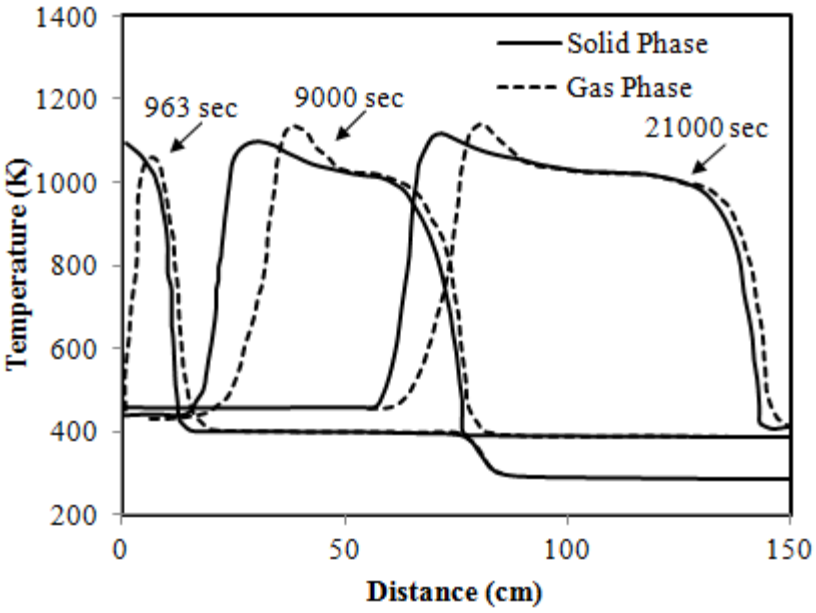

Figure 2-11 Calculated gas and solid temperature at three different times for the 1.5 m reactor simulation [46].

The different fronts that were growing at different speeds associated with the movement of the gasification process were also recognized from the plot of the reaction rate as a function of bed length (Figure 2-12). Those were the coal drying front, then the coal pyrolysis front, followed by the char reaction front considering moving upstream from the outlet. The double-peak of the water-gas shift reaction was due to the changes in equilibrium limits because of changes in temperature (Figure 2-12). The gas concentration along the bed length showed that the inlet gas composition remained unreacted until the reaction front (Figure 2-13). However, after an initial rapid change followed by a more gradual one, a sharp change in gas concentration was observed due to the drying-pyrolysis front. Winslow [63] also observed the same trend.

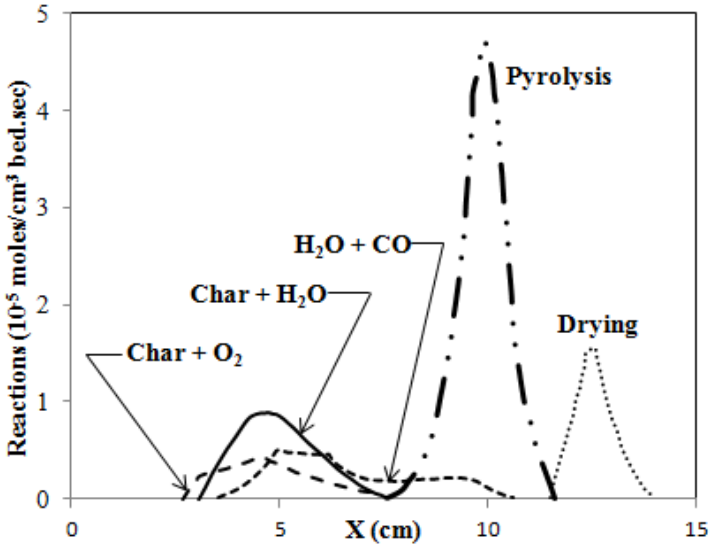

Figure 2-12 Distribution of principal reaction rates at t = 1 h 13 min [46].

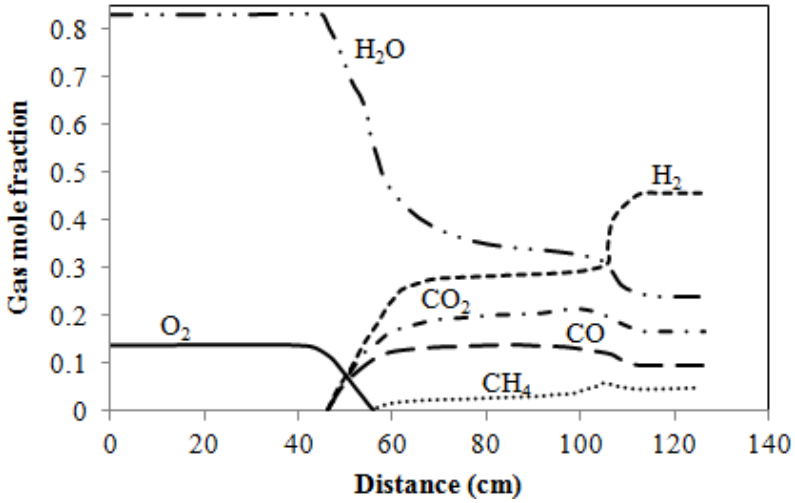

Figure 2-13 Calculated gas phase concentration at time = 1.4 × 104 s for the 1.5 m reactor simulation [46].

A comparison of the position of the calculated reaction and drying front with experimental data showed that the results were in good agreement with the reaction front; however, the predicted drying front movement rate was found higher than the experimental findings (see Figure 2-14). According to them, the latter observation was due to some uncertainty of the product gas mix and the heat losses occurring during the experiment at the drying zone.

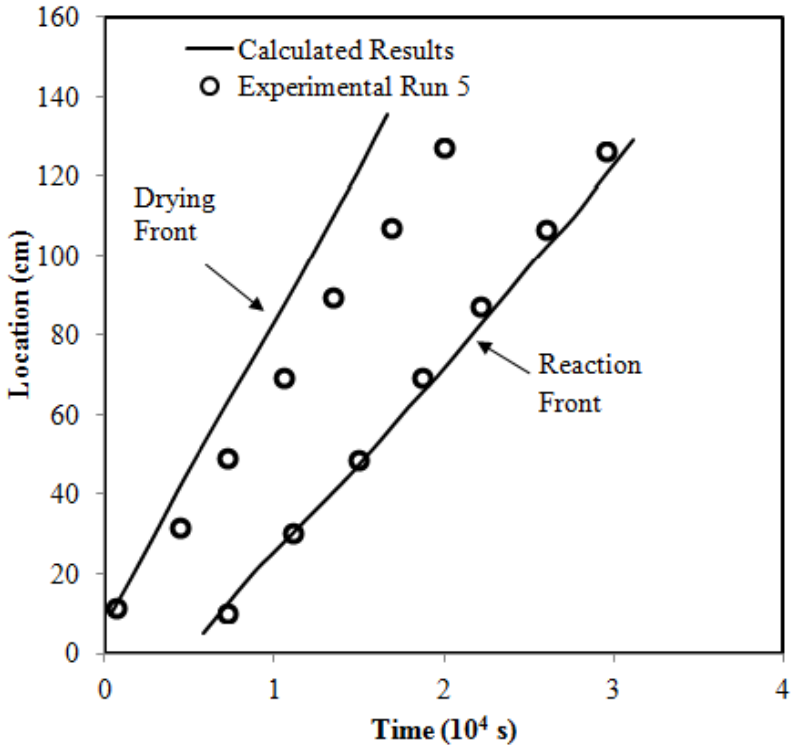

Figure 2-14 Comparison of calculated and experimental reaction and drying front movements [46].

Thorsness et al. [46] extended their works by reporting very limited parametric study. For example, with increasing oxygen concentration in the feed gas (holding a constant gas flow rate), they observed an increased gas/solid temperature and the drying rate of the reaction front moved linearly with oxygen concentration. An increased ratio of CO to CO_2 resulting from the increased temperature generation in the system was also detected. With the increase of total dry gas production, a consistent CO/CO_2 ratio was also noticed with the higher oxygen feed. However, for energy recovery per mole of O_2, they indicated an optimum value of oxygen consumption at a mole fraction of approximately 0.2 (see Figure 2-15). This observation actually sets a limit for the steam-to-oxygen ratio at a value of 4 for maximum energy recovery.

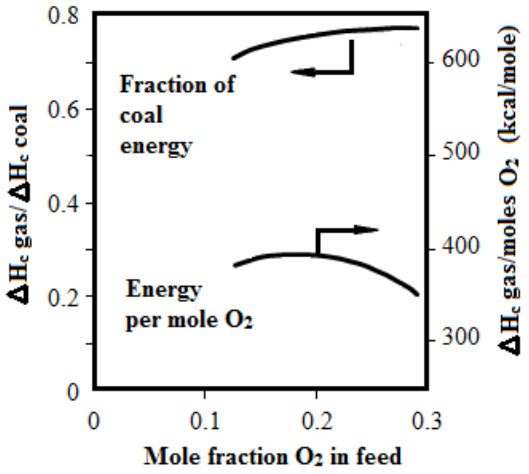

Figure 2-15 Calculated energy recovery for three levels of oxygen feed concentration [46].

There was an attempt by Thorsness et al. [46] to simulate a field-scale system with length equal to 15 m, porosity equal to 0.05, permeability equal to 20 D, outlet pressure equal to 1 atm, and particle diameter equal to 20 cm. However, they could not validate the changes of the process variable except the developing temperature profile that was similar to their lab-scale simulation. Although they showed time and distance changes in the process variable in the principal direction of gas flow, they did not conduct a detailed sensitivity analysis to investigate the effect of coal particle diameter, porosity, permeability, injection gas flow rate, and other parameters in their model despite the fact that the basis of the model formulation was a 1 cm particle diameter. This imposes the use of their model for specific conditions. The applicability of their model to field conditions where the particle diameter is approximately equal to 20 cm is limited because of the lack of sensitivity of the results to particle size and the validation of field trials. The particle size is particularly important because, in their physical and chemical model, the char reaction rates and other transport coefficients such as heat transfer and mass transfer coefficients are directly or indirectly related to the particle sizes. In addition, because of high initial porosity ($\varphi > 0.25$), they considered a constant permeability in their simulation. There apparently was no

use of their formulated functional relationship relating permeability to porosity for considering high initial porosity. The shape of the combustion zone and, hence, the actual gasification volume of the coal could not be determined since the model was only one-dimensional. Because of its transient nature, the model developed by Winslow [63] can be applied for the cases where rapidly changing transient behaviour is important. However, no stark difference between the model outcomes of transient and quasi-steady-state models was observed, and that is probably why some researchers adopted the quasi-steady-state consideration for ease of calculations.

After three decades, in 2006, Khadse et al. [62] developed a simple 1D model following the physical and chemical model as well as the pseudo-steady-state fluid flow model described by Thorsness et al. [46]. However, their model differs from the model developed by Thorsness et al. [46] in that the drying and mobile water evaporation/condensation reactions were not considered and only coal and char were considered as solid phase. Nevertheless, their work gets attention as they analyzed the effects of various operating and model parameters on the temperature and gas phase and solid compositions in UCG that were not completely incorporated in the models discussed above. Their input parameters for the base case were slightly different than that of Thorsness et al. [46] as can be seen from Table 2-9. However, at least for one run, they simulated the experimental conditions of Thorsness et al. [46] to compare their calculated exhaust gas composition with the experimental data (Figure 2-16). However, they could not compare the calculated results of Thorsness et al. [46] that were very close to the experimental results quantitatively, although they followed the development of the model of Thorsness et al. [46]. This is possibly due to considering certain parameters that lack specific information in the literature model and neglecting the drying and mobile water evaporation/condensation reactions

that Thorsness et al. [46] considered. However, their result can be considered only in a qualitative agreement with the experiments of Thorsness et al. [46].

Table 2-9 Comparison of input parameters of Khadse et al. [59] with experimental run 5 of Thorsness et al. [46].

Parameters	Khadse et al. [62] (Base Case)	Experimental Run 5 [48]
Input Parameters		
Coal Dimension	L = 100 cm, D = 15 cm	L = 150 cm, D = 15 cm
Initial Porosity	20%	50%
Coal Particle Size	1 cm	1 cm
Injected Gas Flow Rate	$2 \times 10{-}4$ gmole/cm^2.s	$2.1 \times 10{-}4$ gmole/cm^2.s
Initial Feed Temperature	430 K	450 K
Pressure	4.8 Atm	4.8 Atm
Injection Gas Composition		
O_2	15.4%	13.4%
N_2	7.6%	2.2%
H_2O	77.0%	84.4%
Steam/O_2 Ratio	5	6

The simplicity of the model enabled authors to investigate the effects of various parameters such as O_2 concentration, steam/O_2 ratio, and inlet pressure in their model. They found that increasing oxygen concentration (holding the steam fraction constant) in the feed increases the propagation rate of the reaction front and the temperature in the reaction zone. Similarly, increasing the steam fraction (holding the oxygen concentration constant) increased the propagation rate of the reaction front; however, a decrease in temperature was observed. In the absence of nitrogen, they found an optimum outlet product with a steam/oxygen ratio of 1.5. They also found that input parameters did not influence the pyrolysis reaction.

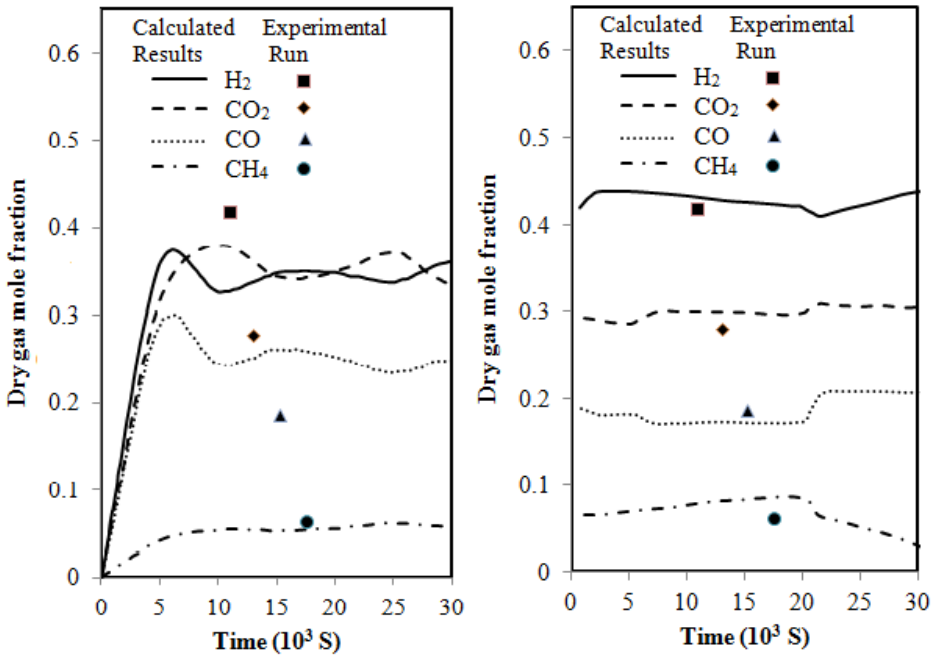

Figure 2-16 Comparison of calculated exhaust gas compositions with experimental results from Thorsness et al. [46]; (a) Khadse et al. [62]; (b) Thorsness et al. [46].

Recently, Uppal et al. [59] also developed another 1D packed bed model adopting the existing model of Thorsness et al. [46] with some modifications in the model structure and solution strategy. To observe their model capability, they considered a bed length of 4.8 m only and observed various features of their simulations with qualitative agreement with the literature. However, for validating their model with the experimental data, they considered the experimental data from their pilot plant which had dimensions of 150 m × 125 m that contained an array (7 × 6) of wells connected by a network of pipes. For comparing with the model calculation, only two consecutive wells that were 25 m apart from each other, were considered. Table 2-10 shows their input parameters, some of which are significantly different from the model that they followed.

Table 2-10 Input parameters for UCG packed bed model developed by Uppal et al. [59].

Parameters	Value
Length of Reactor	25 m
Coal Type	Lignite B
Injected Gas	Air
Injected Gas Flow Rate	2×10^{-4} gmole/cm^2.s (for observation of model capabilities)
Initial Feed Temperature	430 K
Pressure	6 Atm
Initial Coal Density	1.25 g/cm^3

In their pilot plant, the injected gas (air only) flow rate was varied with time (Figure 2-17) and the resultant heating value and the exhaust gas composition were recorded. In their model, they calculated the exit gas heating value and composition utilizing the experimental inlet gas flow rate. In addition, they used a nonlinear optimization technique to compensate the uncertainty in coal and char by optimizing the composition parameters of some pyrolyzed products (H_2, CH_4, and char). The calculated results were in a reasonable agreement with the experimental results (Figure 2-18 a, b). However, according to them, a better prediction can be obtained by increasing the optimization variables. Their model lacks some detailed information such as particle diameter, porosity, permeability, etc., which are considered important for understanding a UCG process. Nevertheless, their model indicates that a control strategy can be employed by manipulating the inlet flow rate to maintain a desired heating value in the presence of disturbances.

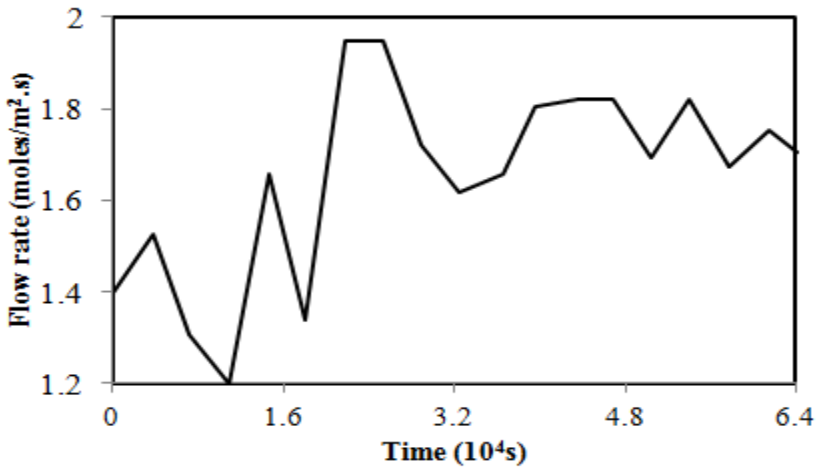

Figure 2-17 Flow rate of the injected air with time [59].

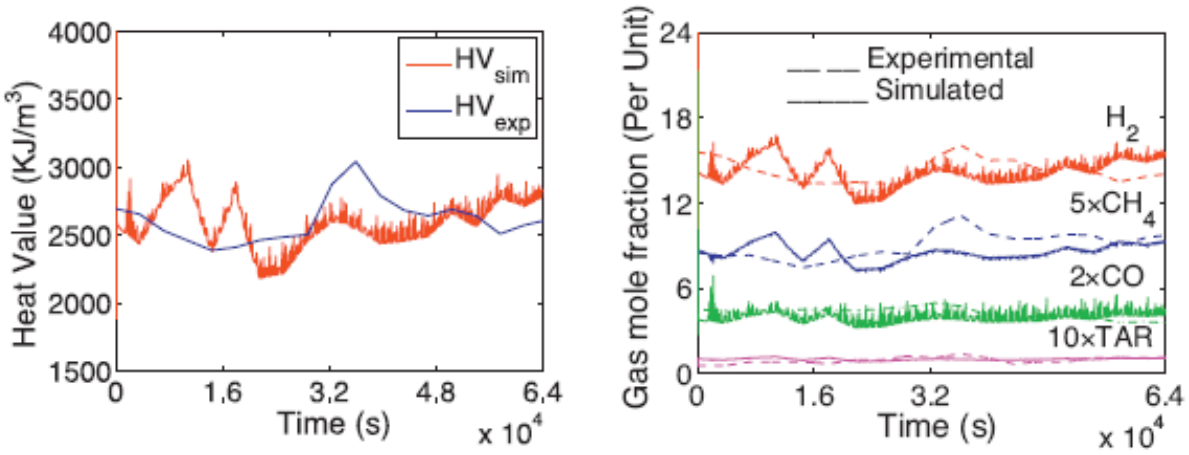

(a) (b)

Figure 2-18 Experimental and simulated (a) heating values and (b) mole fractions of important gases of the product gas mixture with time (reproduced from Uppal et al. [59]).

In 1986, Thorsness and Kang [64] developed a generalized 2D model for describing reacting flows through the packed bed using the following governing equations:

Mass balance:

Overall gas conversion:

$$\frac{\partial(\varphi C)}{\partial t} = -\nabla.(\bar{v}\varphi C) + \sum_j a_{ij} R_j + S_m \ (i = 1,2, \ldots . G) \quad \textit{(Eq. 2.16)}$$

Conservation of gas species:

$$\frac{\partial}{\partial t}(\varphi C_i) = \nabla.(\bar{v}.\varphi C_i) + \nabla.[CD_i \nabla y_i] + \sum_j a_{ij} R_j + S_{m_i} \quad \textit{(Eq. 2.17)}$$

Overall solid conservation:

$$\frac{\partial}{\partial t}[\rho_s(1-\varphi)] = -\nabla.[(1-\varphi)\rho_s \bar{v_s}] + \sum S_{s_k} \quad \textit{(Eq. 2.18)}$$

Solid species conservation:

$$\frac{\partial}{\partial t}\left[\rho_s Y_{s_k}(1-\varphi)\right] = -\nabla.\left[\rho_s \bar{v_s} Y_{s_k}(1-\varphi_e)\right] + S_s \quad \textit{(Eq. 2.19)}$$

Energy balance:

They assumed an identical gas and solid temperature and incorporated one energy equation for the combination of gas and solid as follows:

$$\frac{\partial}{\partial t}\left[\varphi\sum(C_i h_i) + (1-\varphi)\rho_s \sum(Y_{s_k} h_k)\right] = -\nabla.[\sum h_i \bar{J_i})] - \nabla.[\rho_s \bar{v_s} \sum(Y_{s_k} h_k)] + \nabla.\left[k_{eff} \nabla T\right] + \sum rate_i \Delta H_i \quad \textit{(Eq. 2.20)}$$

Considering the negligible difference between the gas and solid temperature obtained by the earlier models [46, 63], the assumption of identical gas and solid temperature seems to be justified.

In their model, they incorporated diffusion effects, wall transport, and also char combustion and water-gas shift reaction rates based on Shell Progressive (SP) and Ash Segregation (AS) reaction

models. In the SP model, a core of unreacted solid was assumed to be surrounded by a shell of ash through which the gas phase reactants diffuse (Figure 2-19 a). On the other hand, the AS model assumed continuous exposure of unreacted material to the gas stream due to the ash segregation (Figure 2-19 b).

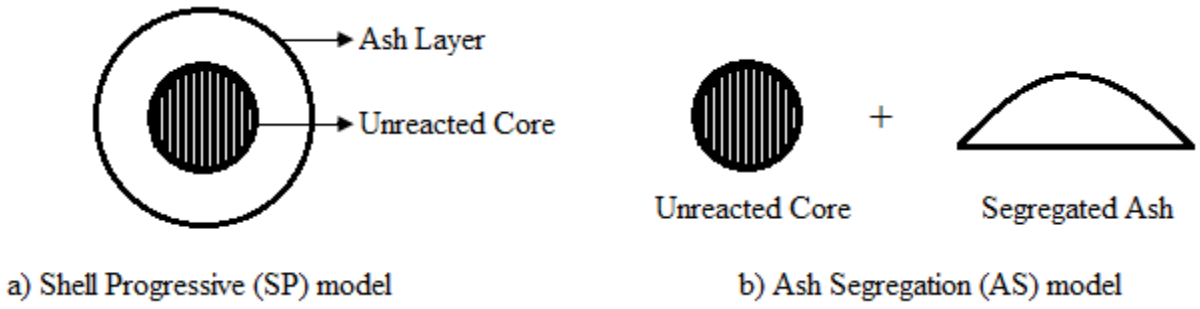

Figure 2-19 Different reaction regimes in packed bed model.

Reaction rates for these two models were as follows:

$$\frac{1}{R_{SP}} = \frac{1}{R_{bulk\ mass\ transfer}} + \frac{1}{R_{ash-layer\ diffusion}} + \frac{1}{R_{diffusion\ into+\ intrincis\ reaction}} \qquad \textit{(Eq. 2.21)}$$

$$\frac{1}{R_{AS}} = \frac{1}{R_{bulk\ mass\ transfer}} + \frac{1}{R_{diffusion\ into\ +\ ntrincis\ reaction}} \qquad \textit{(Eq. 2.22)}$$

Because of the generalized nature of their model, they tested various cases (i.e., transient concentration and thermal wave, steady heat transfer phenomena, etc.) for non-reacting packing materials through the packed bed and compared them favourably with other available studies. Although their generalized model is 2D, only one case (steady heat transfer phenomena) was solved using the 2D model. For all other cases, the 1D model was considered. For validation of a UCG model, they calculated gas composition, temperature, and carbon fraction considering a steady 1D model with very limited gas species and compared the results with the analytical data obtained from literature. They analyzed the following three disparate situations related to the UCG process which were not considered in the earlier models:

- Case 1: Transient water injection into the midpoint of the packed bed during gasification.
- Case 2: Coal wall drying using a hot gas flow.
- Case 3: Wall regression during gasification.

Table 2-11 shows the input parameters for the above situations. For the first case, seven gas species (N_2, O_2, H_2, CO, CO_2, water vapor, and CH_4) and eight reactions (reactions 3–11) were considered. However, drying and pyrolysis reactions were ignored. During gasification process, when the product gases reached a reasonably steady state, water was injected at the midpoint of the bed, slightly downstream of the reaction front, and continued until the mole fraction of CO and CO_2 were observed to approach steady values. However, the liquid water influx was assumed to turn into steam instantly with a flow rate of 8×10^{-4} mol/s. A sudden change in CO and a gradual change in H_2 were noted after the water injection; however, the gases undergoing changes returned to pre-injected conditions as seen in Figure 2-20.

Table 2-11 Input parameters for the three situations considered by Thorsness and Kang [64].

Input Parameters	Case 1	Case 2	Case 3
Packed Bed Dimension	L = 150 cm, D = 5 cm	L = 25 cm, D = 10 cm	L = 1 m, D = 1 m
Initial Gas Temperature	900 K	900 K	900 K
Initial Bed Temperature		300	
Gas Composition			
H_2O	74%	100% (or N_2)	66.6%
O_2	26%		33.3%
Injected Gas Flow Rate	1.5×10^{-3} mole/s	8×10^{-3} mole/s (1 mol/s-m^2 of bed)	6 moles/s

For case 2, a uniformly permeable non-reacting bed with a water-saturated wall at steam temperature was assumed through which hot gas was passed. It was observed that the time to reach steady state increased rapidly with a decreasing flow rate as if the average wall-drying rate

is a function of the injected gas flow (Figure 2-21). However, the wall-drying rate was found to be limited by the available energy for too low injected hot gas due to the insufficiency of the total heat injected.

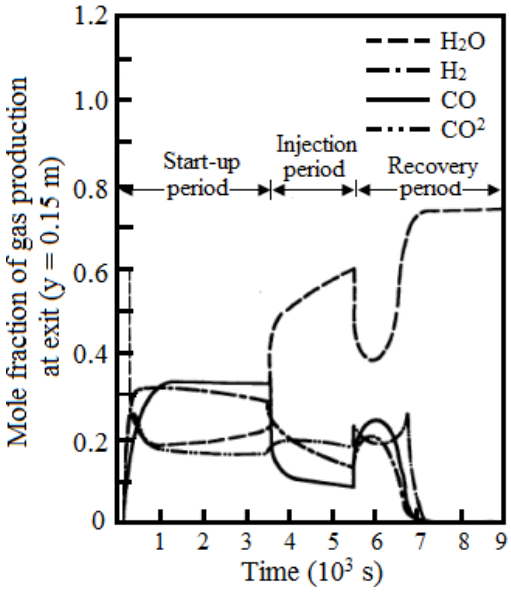

Figure 2-20 Product gas changes during gasification with midpoint water injection [64].

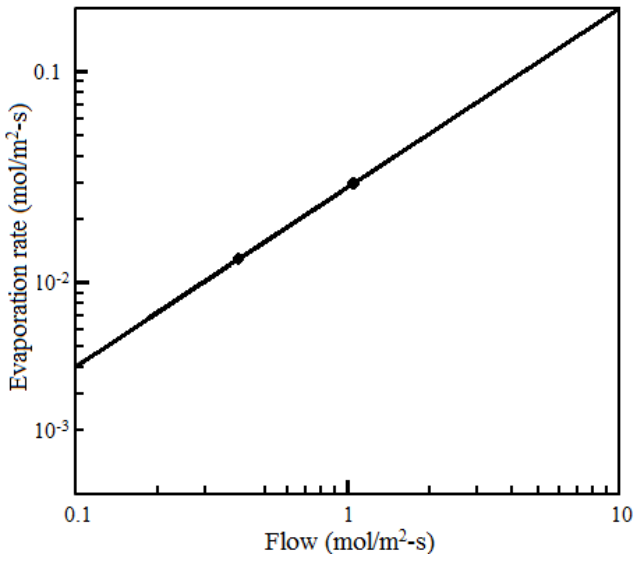

Figure 2-21 Drying rate vs. flow rate (log-log plot, from Thorsness and Kang [64]).

For case 3, the model system was considered to be filled with rubble material consisting of ash in the center and char near the walls and at the top. The walls were considered as coal that can proceed with gasification reactions. The objective of this model system was to determine the thickness of the char bed at the wall that would lead to a self-sustaining system. Calculations were performed using all seven gas species. The computed wall regression rate (i.e., the carbon production rate) was found nearly constant with the increasing char layer thickness, while the carbon consumption varied linearly with the char thickness (Figure 2-22). A wall char bed thickness of 7.5 cm was found close to a self-sustaining system, since the rate of carbon consumption was nearly equal to the carbon production. However, the calculated average wall regression rate of 7.7 × 10−7 m/s (0.07 m/day), when comparing the characteristic field result (~0.5 m/day), indicates that their model is missing some additional physics.

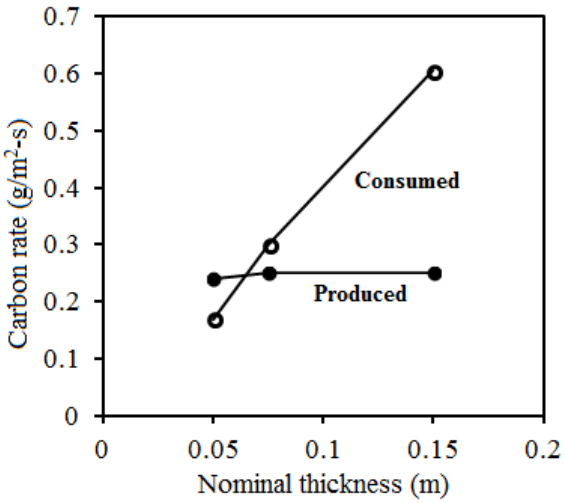

Figure 2-22 Carbon production rate vs. wall char layer thickness [64].

In 1976, in parallel to LLNL, Gunn and Whitman [61] also developed a 1D linear mathematical model separately for UCG. Their work is particularly important as their model is the only packed bed model cited in the literature that was compared with the field trials (Hanna, Wyoming) and exhibited a fairly good agreement with the experimental data (Table 2-12). However, field test

data was considered at a time span when a steady-state condition was observed to conform closely to the assumption of their model. In addition to the gas composition, temperature, and heating value, they also determined the ratio of the gas production rate to the gas injection rate, the effect of reservoir water influx on the heating value of gas, the distribution of thermal energy and thermal efficiency during the gasification process that closely matched the experimental observations and, thus, provided enhanced understanding of the UCG process.

Table 2-12 Comparison of experimental and calculated data for an air injection rate = 1631 Mcf/day [61].

Components	Composition (Mole Percent)	
	Field Test Results	Calculated Data (Average Value)
H_2	18.57	18.60
CH_4	4.10	4.92
N_2 + Ar	47.81	47.13
CO	16.35	15.83
CO_2	12.33	13.29
H_2S	0.04	0.07
Ethan +	0.80	0.14
Gas Production Rate (Mcf/day)	2728	2734
Gas Production Temperature, °F	493 (measured at the surface)	533 (measured at the bottom of the well)
Maximum Temperature, °F	1871	1951
Heating Value, Btu/scf	170.6	164.6
Thermal Efficiency (%)	89.2	87.4

Unlike the above models, the water-gas shift reaction and methanation were not included in their model. Methane was considered to be produced solely through pyrolysis. Only two reactions, water-gas and combustion reactions, were considered. The reaction rate of the water-gas reaction was adopted from the work of Gadsby et al. [66]; however, the constants were determined from the gasification of the pitch coke. For the combustion reaction, the reaction data of Lewis et al.

[67] was used that was obtained from the combustion of metallurgical coke. Even the correlation of the thermal conductivity they used was not intended for subbituminous coal. Drying was not considered in their model. Despite this and the large errors in the reaction rate, they observed only negligible errors in the model predictions.

In their model, water vapor, carbon monoxide, hydrogen, carbon dioxide, oxygen, inert gases (nitrogen and argon), and devolatilized material from the coal were considered. For convenience, the volatile products resulting from the pyrolysis of coal were treated as a single pseudocomponent; however, the pseudocomponent was broken down into individual gases for the purpose of calculating total gas composition. From the proximate and ultimate analysis of the experimental subbituminous coal (from the Hanna field test), they also formulated a correlation between the weight fraction of volatile matters and the temperature with high accuracy. To obtain the composition of devolatilized gas, they considered the experimental devolatilized data of the Hanna I coal seam at 900 °C along with the assumption that the tars (16.2%) and light oil (0.9%) and water (13.3%) in that analyses cracked to the stoichiometric proportion of methane, carbon monoxide, and hydrogen. Their assumption led to the composition for devolatilized products listed in Table 2-13.

Table 2-13 Composition of devolatilized products assumed by Gunn and Whitman [61].

Components	Percent
H_2	42.26
CO	28.53
CO_2	3.79
CH_4	24.36
H_2S	0.37
Ethane +	0.69
Total	100
Average molecular wt.	14.76

Their model transformed the set of partial differential equations into a set of ordinary differential equations by considering the pseudo-steady-state approximation. They considered nine integrated continuity equations (two for overall solid and mass balances and others for individual gas species), a partially integrated energy equation, and a macroscopic material balance equation from which a constant combustion front velocity could be calculated iteratively. The assumption of the constant combustion velocity seems to be valid, according to Figure 2-14, with what was observed by Thorsness et al. [46].

Their model predicted the exhaust dry gas composition and obtained a close agreement with the experimental gas composition history with the exception of methane (Figure 2-23). However, the deviation of methane was believed to be a result of considering a high concentration of methane in the devolatilized products. The only parameter fitted in their model from the field trial was the water influx to get a good prediction for the data that interferes with the water influx rate. Their calculated results were also closely matched with experimental data for ratio of gas production/air injection and gross heating value (Figure 2-24 and Figure 2-25). However, the declination of those quantities with time was believed to be the result of the gradual increase of water flux during field test. They calculated the heating value of gas by changing the ratio of water influx to air injection rate and observed a maximum heating value at a ratio of about 0.15. Usually the maximum heating value at a particular ratio of water intrusion to air injection rate implies the control strategy of closely maintaining the optimum value either by controlling the water intrusion rate by pressure of any other means or by changing the air injection rate.

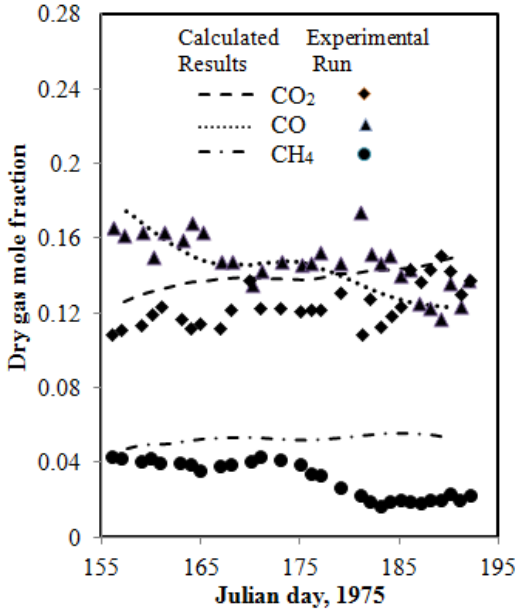

Figure 2-23 Comparison of calculated exhaust gas compositions from Gunn and Whitman [61]. with experimental results from the Hanna field trial.

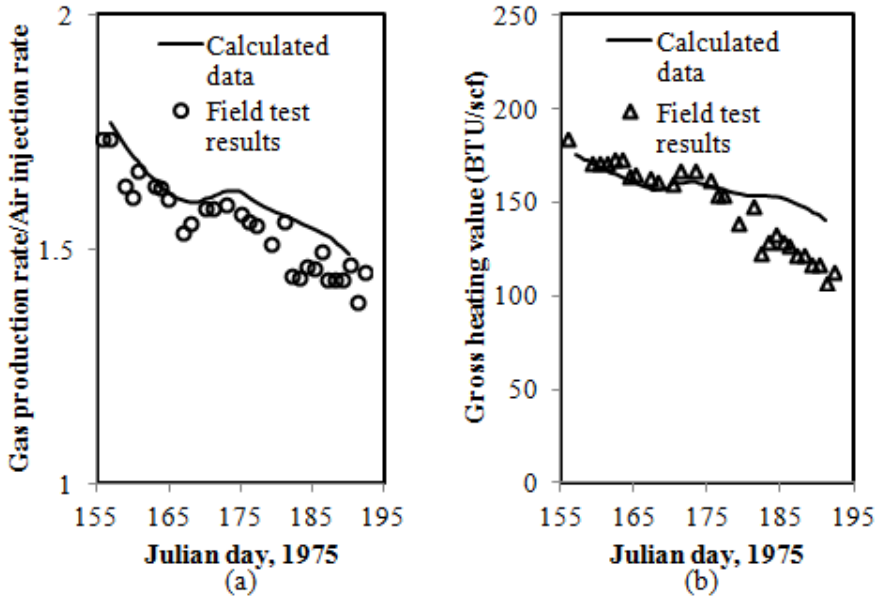

Figure 2-24 Comparison of calculated data and field test: (a) gas production/air injection ratio and (b) gas heating value [61].

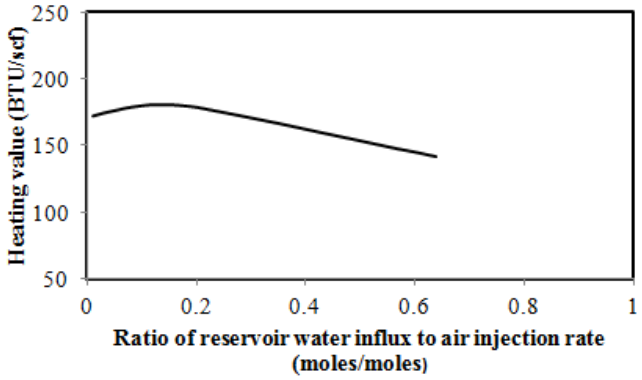

Figure 2-25 Effect of reservoir water influx on heating values of gas [61].

The calculated values of the distribution of thermal energy released by coal combustion were also in good agreement with the experimental values (Table 2-14). From the experimental data, it was observed that only a small amount of energy from a 30-foot coal seam was lost to the overburden and base rock. This implies that neglecting heat losses to the surrounding rocks does not hamper a model outcome too much. The last column of Table 2-14 shows a higher heating value of the product gas when injected air was preheated at 480 °F. To get higher economic value and energy conservation, they suggested using a part of the heat of vaporization of the produced water to heat the inlet gas. They also reported that in all cases, the reaction zone was very narrow, generally two feet or less. This fact was verified by both model calculations and by temperature measurements in the observation wells.

Table 2-14 Distribution of thermal energy from in situ coal combustion [61].

	Calculated, %	Field Test, %	Calculated with Preheating, %
Produced Gas			
Gross heating value	87.4	89.1	91.3
Sensible heat....	5.8	5.2	2.9
Heat of vaporization of water vapor in produced gas	3.4	3.3	2.4
Heat Loss to Surrounding Rock	1.3	3.8	1.3
Heat Loss in Ash	2.1	0.6	2.1
Total	100	100	100

Although they obtained a good agreement with the experimental results for a number of phenomena, they could not quantitatively predict the variation of the temperature and mole fraction along the bed length with the experimental value because of the poor consideration of the thermal conductivity, heat capacities, and the uncertain accuracy of the reaction rates. However, they obtained a qualitative agreement with the experimental values. Despite very close agreement with the experimental data, their model is not sufficient for predicting all aspects of gasification as their model neglected some important phenomena, such as drying, CO_2 gasification, the water-gas shift reaction, gas phase reactions, etc. However, because of the low water/air ratios that were experienced with the Hanna tests, there might be little or no water-gas shift reactions. As a result, the Gunn model was not hampered by neglecting this reaction. In their model, there is also a lack of sensitivity analysis for the kinetic parameters they used. In addition, they included water influx data from a particular field trial. However, water influx is a highly variable phenomenon that depends on coal seam properties and hydrology. All these lacking parameters limit their model for general applicability in the UCG process.

Abdel-Hadi and Hsu [4] extended previous models by developing pseudo-2D geometry with a moving burn front in the axial direction. A rectangular domain with a length of 1.5 m and width of 1 m was used in their model. Their governing equations are nearly similar to the equation considered by Winslow [63] and Thorsness and Kang [64]; however, they included carbon consumption in the reaction zone to track the burn front, and the equation is given by:

$$\rho_s w_c v_c = 12 \int_0^{x_{rz}} \left(\sum_j R_{c-ij}\right) dx \qquad \textit{(Eq. 2.23)}$$

where w_c is the carbon mass fraction, v_c is the velocity of the combustion front, and x_{rz} is the total length of the reaction zone. They also performed an immobilization transformation of coordinates to formulate the irregular front motion as follows:

$$\xi = \frac{x - X(y,t)}{H_1 - X(y,t)} \qquad \textit{(Eq. 2.24)}$$

$$\eta = \frac{y}{H_2} \qquad \textit{(Eq. 2.25)}$$

All other governing equations were transformed to these new coordinates (Figure 2-26). This allowed them to calculate the progressive configuration of the gasified zone at various stages of gasification (Figure 2-27) which, in turn, facilitated the calculation of the rate of coal seam consumption (Figure 2-28). The conversion rate of the coal seam is found fairly constant. To gain confidence for this model, they have compared their model with the laboratory results reported by Thorsness and Rozsa [58] and obtained a good agreement with the experimental data.

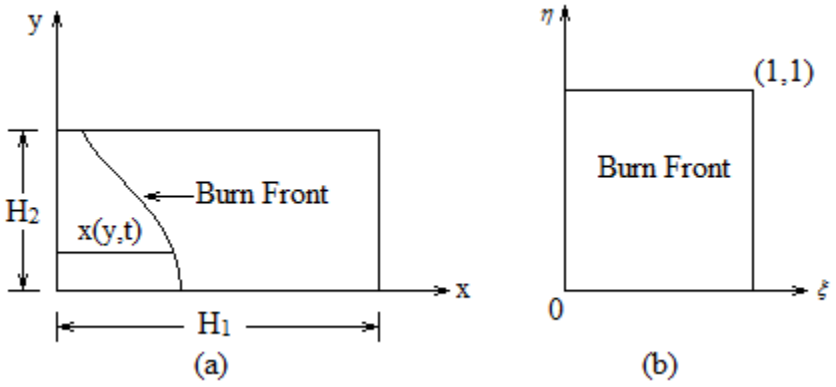

Figure 2-26 Schematic description of the problem: (a) conventional coordinate system; (b) immobilization coordinate system (redrawn from Abdel-Hadi and Hsu [4]).

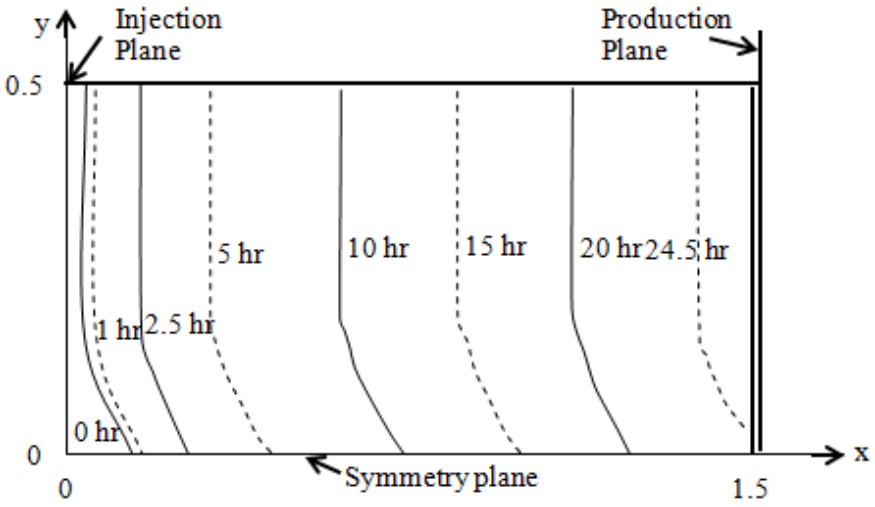

Figure 2-27 Progressive configurations of combustion fronts during gasification [4].

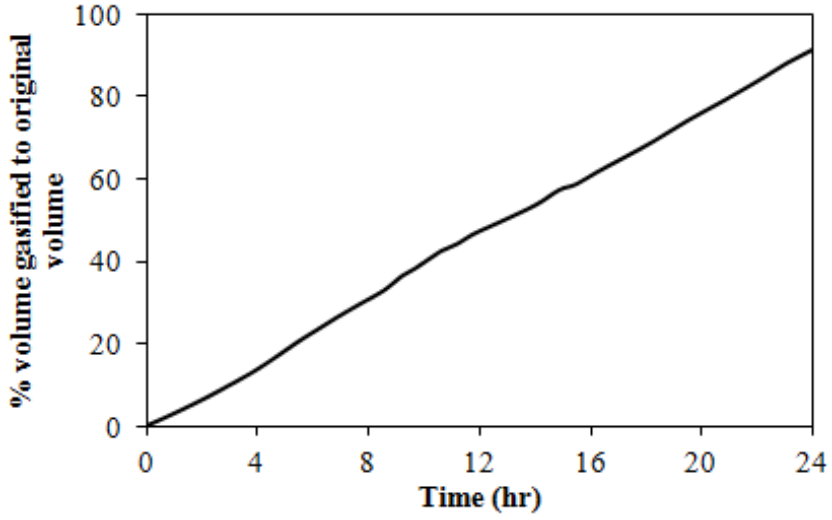

Figure 2-28 Consumption of coal during gasification [4].

The packed bed models have been validated with laboratory experiments to some extent. These models exhibit good agreement for the gas composition. To calculate the heat recovery and gas composition, the model can be very effective. However, the extension of these models to field trials is infeasible, since other cavity growth mechanisms such as thermo-mechanical failure could not be incorporated into the models. Also, as pointed out by Winslow [63], this method requires a fine grid at the vicinity of the reaction front that limits its applicability to three-

dimensional field-scale trials. However, recent advancement of computational power can easily overcome this limitation.

2.4.2 Channel models

Beside packed bed models, a number of channel models have also been developed in the first decades of modeling. The channel model assumes that coal is gasified only at the perimeter of the expanding permeable channel [14]. In this approach, the UCG process is represented by an expanding channel when two distinct zones of rubble/char and open channel exist. This approach is considered due to the observation of the formation of the open channel structure after the gasification phase is terminated in different field tests of coal seams [68, 69]. Figure 2-29 shows the basic concept and physics behind this approach: “Air or oxygen flows down the central channel and is convected by turbulent flow to the boundary layer along the channel wall. The oxygen diffuses through the boundary layer to the solid surface and reacts. The hot combustion gases diffuse back through the boundary layer to the channel” [70]. The channel model is more useful for analyzing sweep efficiency [14].

Table 2-15 and Table 2-16 represent a glimpse of a list of channel models discussed here with their essential features and reaction rate control mechanisms of the main reactions in the gasification process, respectively.

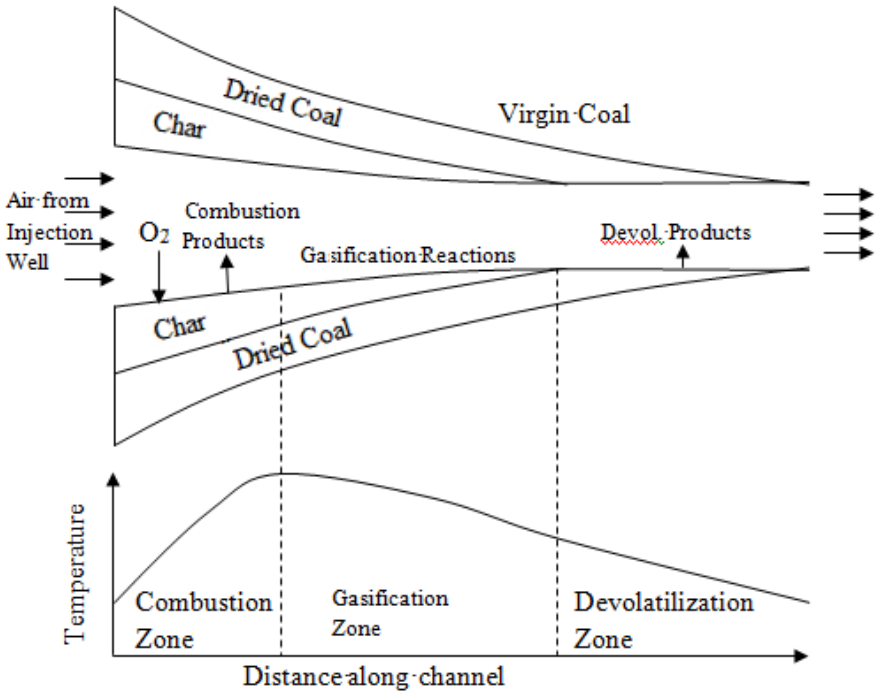

Figure 2-29 Reactions and transport phenomena in channel model (redrawn from Gunn and Krantz [70]).

Table 2-15 Some essential features of reported channel models [18].

Researchers	Dimension & Time Dependence	Heat Transfer			Mass Diffusion	Fluid Flow	Thermo Mechanical Failure	Water Influx	Heat Loss
		Conduction	Convection	Radiation					
Dinsmoor et al. [60]	2D & T	√	√	√		P		√	
Eddy and Schwarz [71]	1D & T	√	√	√	√	M	√	√	√
Luo et al.[72]	2D & T	√	√		√				
Batenburg et al. [68]	1D & SS	√	√	√		D			
Pirlot et al. [73]	2D & S	√	√		√	D		√	
Kuyper [69, 74]	2D & T	√	√	√	√	NS			
Perkins and Sahajwalla [75]	2D & T	√	√	√	√	NS			

D = Darcy flow, P = Plug flow, M = Mixed flow, NS = Navier-Stokes, S = Steady State. SS= Semi-Steady State, PS = Pseudo-Steady State, T= Transient.

Table 2-16 Reaction rate control mechanisms of the main reactions in the gasification process [18].

Researchers	Drying	Pyrolysis	Char Reaction				Water Gas Shift Reaction	Gas Phase Reaction		
			$C + O_2 \rightarrow CO_2$	$C + CO_2 \rightarrow 2CO$	$C + H_2O \rightarrow CO + H_2$	$C + 2H_2 \rightarrow CH_4$	$CO + H_2O \leftrightarrow CO_2 + H_2$	$CO + 0.5O_2 \rightarrow CO_2$	$H_2 + 0.5O_2 \rightarrow H_2O$	$CH_4 + 2O_2 \rightarrow CO_2 + 2H_2O$
Dinsmoor et al. [60]			K	K	K			P	P	
Luo et al. [72]			P	P	P	P	P	P	P	P
Batenburg et al. [68]				E	E	E	E		E	
Pirlot et al.[73]				E	E	E	E	E	E	E
Kuyper [69, 74]				D				M		
Perkins and Sahajwalla [75]				P				M		

D = Diffusion limited, E = Equilibrium, K = Kinetic (power law) and bulk diffusion, M = Turbulent mixing limited, P = Power law kinetics.

Dinsmoor et al. [60] developed a steady-state, 1D channel model by assuming that the gasifier behaves as an expanding cylindrical cavity in the coal seam with reactions taking place at the walls. In their model, for simplicity, no pyrolysis reactions were considered. Heat transfer included conduction for solids only; however, both convection and radiation were included between the wall and gas. Axial heat conduction in the gas phase was neglected. They also considered water influx as evenly distributed along the length of the tube. Char reactions (reactions 3–5) and two gas phase reactions (reactions 9 and 10) were considered in their model. Because of slow channel evolution, they incorporated a pseudo-steady-state assumption for changes associated with the gas phase. They treated a fully developed flow process with the channel despite the initial cylindrical channel diameter (0.3 m) being much smaller than the

channel length (60 m). Considering forced convection as the dominating mechanism of mass transfer, they simulated coal gasification with a forced convection mass transfer correlation. For heterogeneous reaction kinetics, they considered the surface reaction rate constant and wall diffusion resistances. For wall diffusion resistances, the mass transfer coefficients were calculated from a standard correlation for the turbulent flow of gases in tubes. Inlet gas was assumed to be air at 330 K and 6.9 atm with no water added. Their predicted gas compositions and temperature profile showed clear evidence of the presence of a separate oxidation and reduction zone; however, a very high temperature (2400 K) was noted near the inlet (Figure 2-30). According to them, this high temperature was due to neglecting heat loss at the end of the tube and including the radiation heat transfer. However, it appears that apart from their explanations, neglecting the pyrolysis reaction could be another reason for getting high temperature initially, as during ignition, a significant amount of heat is used to create char by the pyrolysis of coal.

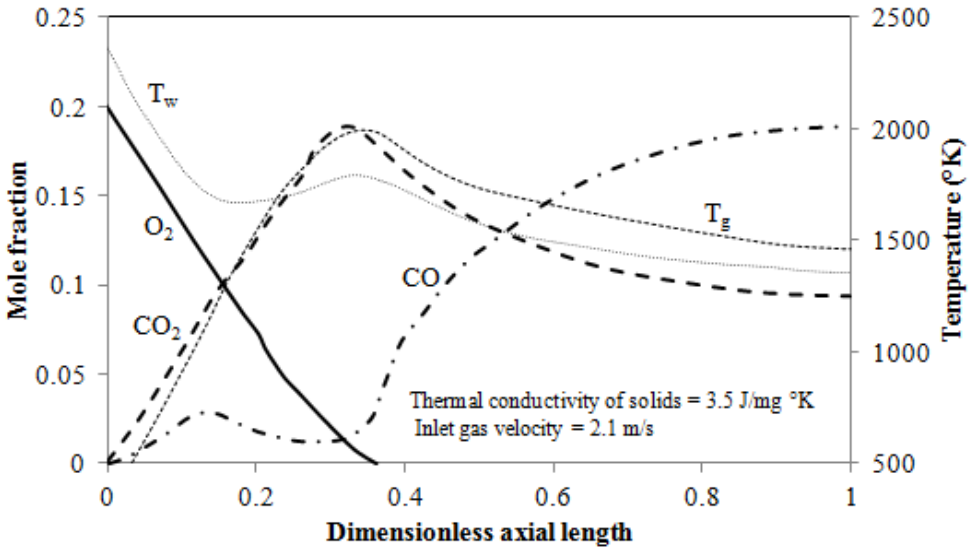

Figure 2-30 Typical channel temperature (gas and wall) and gas composition profiles without water influx [60].

The quality of the predicted product gas observed was inferior to the gas quality usually obtained in the packed bed model for similar situations. For a constant blast velocity, the reaction rates were observed to decrease with the evolution of the channel due to the constant mole fraction of the oxygen. As a result, the oxidation zone became longer which, in turn, was responsible for increased heat losses and the deterioration of gas quality. Compared to the packed bed combustion front (approximately 0.2 m), the oxidation zone (approximately 20 m) was much longer. However, these observations were not supported by any field observations. Apparently, because of the long oxidation and reduction zones, they concluded that "a successful UCG system cannot be operated in the channel regime".

Almost at the same time, the above conclusion was negated by the work of Schwartz et al. [76] as they found an increase of mass transfer by several orders of magnitude when natural convection in channels was considered as the controlling mechanism of mass transfer instead of forced convection alone. The intense mixing of the injected blast with the boundary layer gases depends on the Grashof number (Gr) of the natural convection flow. A good mixing begins when the Grashof number exceeds 108 and becomes intense at about 1010 [77]. However, for dominant natural convection flow, the gases within the boundary layer produce a circulatory flow within the cylinder and a good mixing is obtained. However, Schwartz et al. [76] assumed two different modes of the circulatory pattern based on coal seam thickness as depicted in Figure 2-31. Figure 2-32 shows the difference of cavity growth with and without considering the natural convection. Later, it was established by mathematical correlation that the models assuming forced convection mass transfer as the controlling mechanism for cavity growth were not born out of field trials [17].

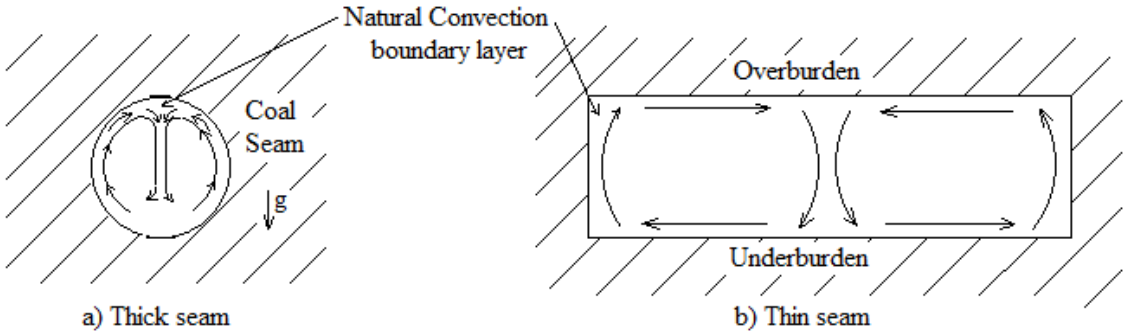

Figure 2-31 Assumed circulation patterns in the thick seam and thin seam configurations (redrawn from Schwartz et al. [76]).

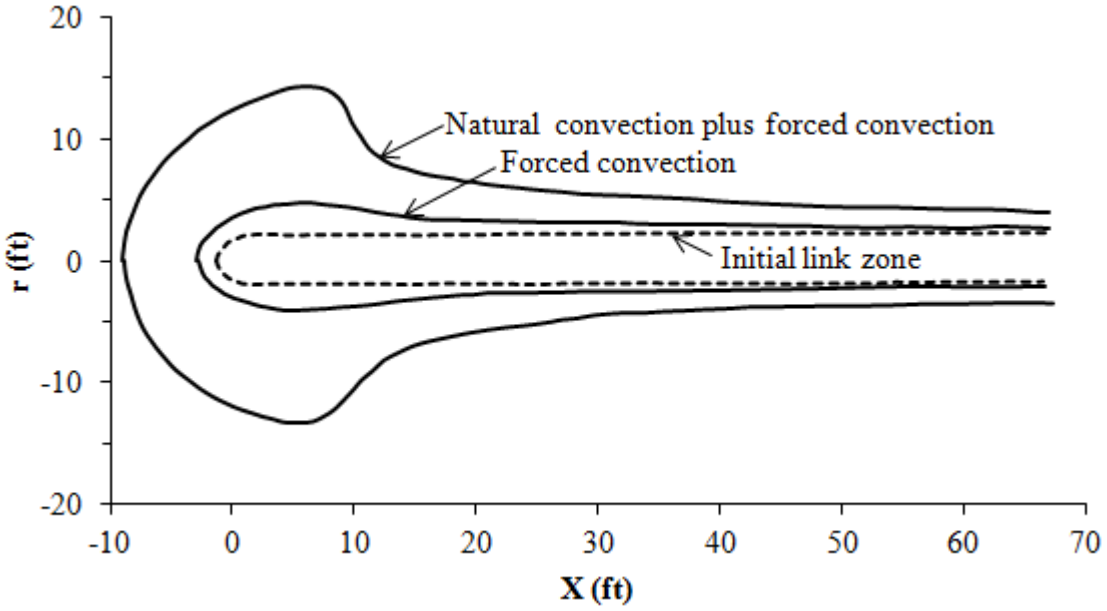

Figure 2-32 A comparison of cavity growth via forced convection and natural convection [76].

Schwartz et al.[76] were the first investigators to consider the natural convection as the controlling mechanism of heat and mass transfer in UCG cavities. In their later paper, Eddy and Schwarz [71] developed a 2D model and described the evolution of the cavity based on the movement of the cavity wall. The blast from the injection well was transported through the reacting walls of a constant temperature via the convection process and ultimately diffused to the

wall and reacted with the coal. The oxygen diffusion rate was calculated by natural and forced convective heat and the mass coefficient. The roof and floor of the cavity were assumed to be non-reacting surfaces. They considered neither subsidence nor rubblization. They included the water-gas shift reaction and two other gas phase oxidations along with three char reactions (reactions 3–5) as considered by Schwartz et al. [76]. To capture the experimentally proven teardrop shape of the cavity formation, they divided the cavity growth into different regions, i.e., a hemispherical region in the vicinity of the injection well and a series of non-equal diameter cylinders (step cylinder) downstream from the injection well, according to the flow process and a cylindrical link zone (Figure 2-33). At any location, the cavity was assumed to be a cylindrical cross-section until the cavity diameter was equal to the seam thickness, which is when the model switches to a rectangular cross-section. It was assumed that all coal volume located in the hemispherical region was consumed in the reaction with oxygen. The volume of char was calculated from the mass of char burned due to the combustion and the density of the char. The half-body volume was then fit to the calculated char volume. Flow was treated as an entrance region of pipe, as the calculated entrance length was much larger than the vertical well distance. The entrance length was calculated using the following equation:

$$\frac{L_e}{d} = 0.0288 Re_d \qquad \textit{(Eq. 2.26)}$$

where Le is the entrance length and d is the pipe diameter. The minimum Reynolds number in the system was 4000, which resulted in an entrance length of 48.8 m. The entrance length was considered to increase with the increase of the cavity diameter. According to them, as fresh blast proceeds down the axis and products of combustion are released at the walls, the forced and natural convection results in a swirling flow that ultimately helps mix the flows and enhance the

flow of oxygen to the vicinity of the wall where boundary layer convective diffusion dominates. The transport of heat and species inside the cavity was considered to be governed by empirical correlations for the turbulent transport phenomena in enclosures. The model was able to reproduce the results of the Hanna II and Pricetown field trials qualitatively.

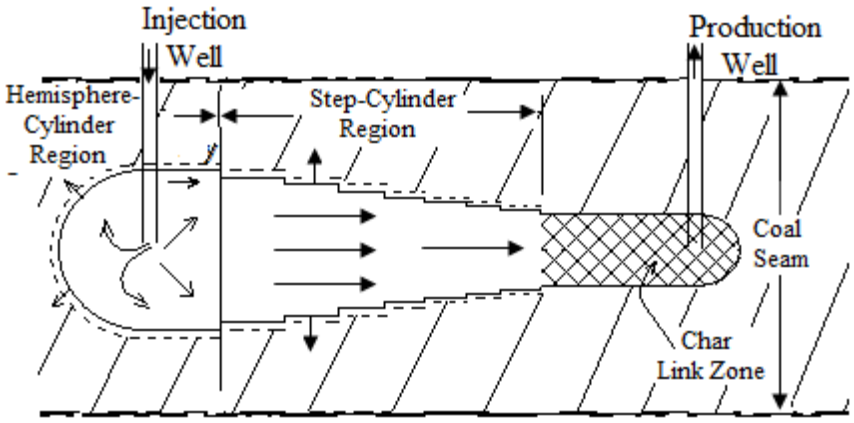

Figure 2-33 Conceptual sketch of the linked vertical well computer model geometry (redrawn from Eddy and Schwarz [71].

At a latter stage, Luo et al. [72] extended the Schwartz et al. [76] model by including heat transfer and more coal wall and gas phase reactions (reactions 3–10). Flow inside the cavity was solved based on irrotational fluid flow inside an enclosure, which describes velocity potential based on geometric features of the enclosure. The geometry is shown in Figure 2-34. The stream function and velocity potential were calculated using the following equations:

Steam function:

$$\Psi = \frac{\dot{m}}{4\pi} cos(\pi - \theta) + \frac{Ur^2}{2} sin^2(\pi - \theta) \qquad \textit{(Eq. 2.27)}$$

Velocity potential:

$$\emptyset_v = \frac{\dot{m}}{4\pi r} + Urcos\,(\pi - \theta) \qquad \textit{(Eq. 2.28)}$$

where U is the velocity of the uniform stream and ṁ is the mass flow rate. Pressure distribution in the cavity was determined using Bernouli's equation:

$$p + \frac{1}{2}\rho u^2 = p_\infty + \frac{1}{2}\rho U^2 \qquad \textit{(Eq. 2.29)}$$

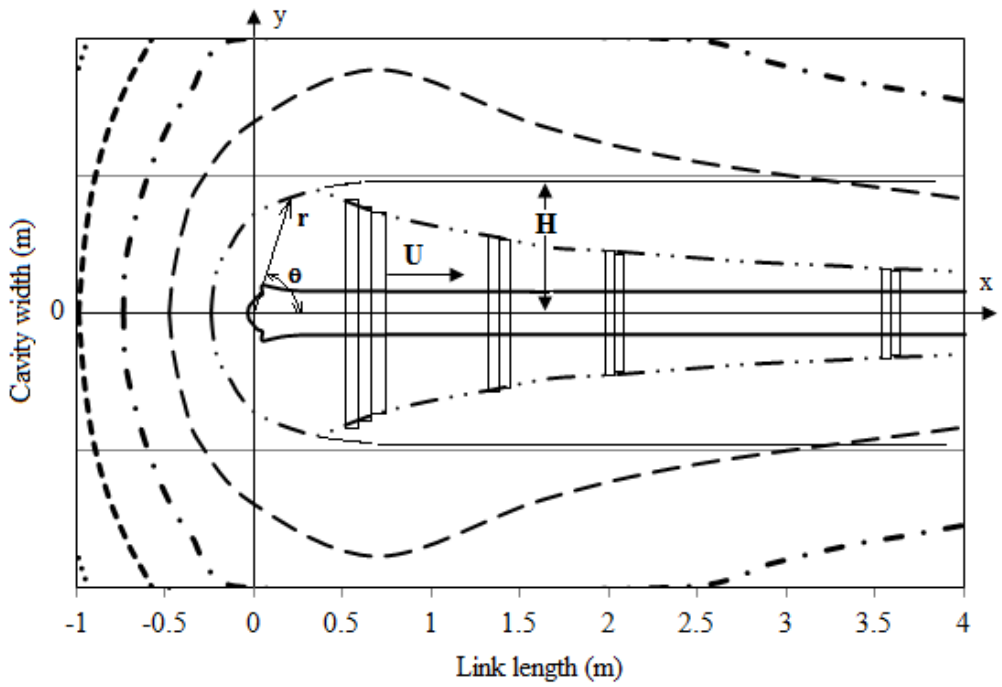

Figure 2-34 UCG cavity defined in the work of Luo et al. [72].

In the Luo model, Fluent was used to predict the cavity shape at different times based on heterogeneous reaction rates at the cavity wall. To quantify the turbulent intensity, they used the standard k-ε model for the turbulent kinetic energy and dissipation. For heterogeneous and homogeneous reactions, they used kinetics/the diffusion control process and a finite rate/eddy dissipation model, respectively. Their model was validated with Chinchilla field trials. The calculated coal consumption closely matched the Chinchilla trial field data (Figure 2-35). For sweep cavity geometry, their model was further validated with the data from the Hanna II and III UCG trials. There is less than 5% error between the results generated with the model (Hanna II:

2436.6 tons of coal gasified in 25 days; Hanna III: 4139.3 tons in 38 days) and reported data (Hanna II: 2500 tons of coal gasified in 25 days; Hanna III: 4200 tons in 38 days). Their model predicts a hemispherical shape for the cavity geometry; however, the model is limited since heat and mass transfer characteristics of the cavity are unknown. Also, the coupling of this model with the mechanical failure of the coal would be cumbersome, since the accumulated rubble in the cavity changes the transport phenomena inside the cavity.

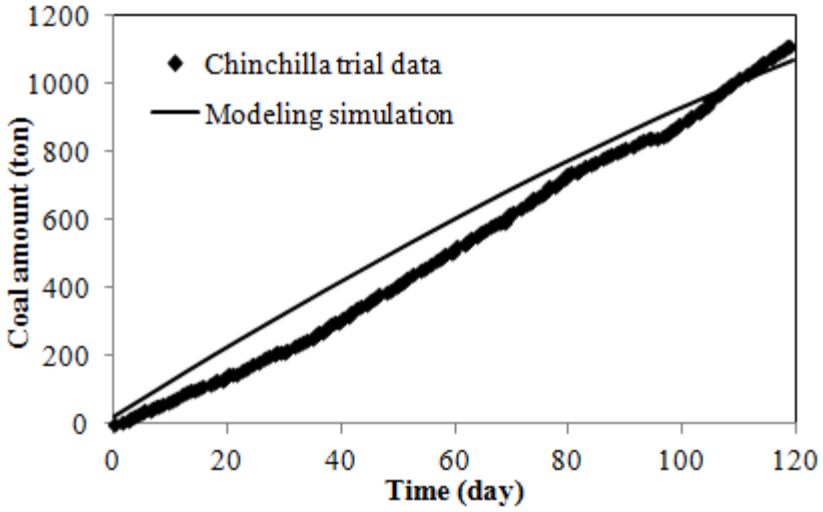

Figure 2-35 Coal consumptions for modeling and Chinchilla trial data [72].

Batenburg et al. [68] developed a semi-steady-state 2D model for UCG in open channels for the developed gasifier only. Unlike other models, they assumed that oxygen instantaneously reacts with the combustible gases present in the channel instead of reacting with the coal surface. Their interest was only to investigate the process within the channel after the injection gas percolates through the inert permeable rubble zone. Reaction rates were calculated based on resistances in the system including boundary layer, pore diffusion, surface phenomena, and chemical kinetics. For laminar and turbulent natural convection along a smooth vertical wall, they used the

Sherwood number (Sh) that is correlated with the Grashof number (Gr) and Schmidt number (Sc) as follows:

$$Sh = 0.59\, Gr^{1/4} Sc^{1/4}, \quad Gr < 10^9 \text{ (laminar)} \qquad \text{(Eq. 2.30)}$$

$$Sh = 0.13\, Gr^{1/3} Sc^{1/3}, \quad Gr > 10^9 \text{ (turbulent)} \qquad \text{(Eq. 2.31)}$$

For forced convection-dominated flow the Sherwood number was expressed in terms of the Reynolds number (Re) as follows:

$$Sh = 0.027\, Re^{4/5} Sc^{1/3} \qquad \text{(Eq. 2.32)}$$

Heat transfer was modeled by radiation between the walls of the channel. They also included the effect of natural convection due to the temperature difference. Their results showed that the effect of pressure on gas composition is negligible (Figure 2-36). Their results also indicated that natural and forced convection transfer coefficients are in the same order of magnitude and both of them are important.

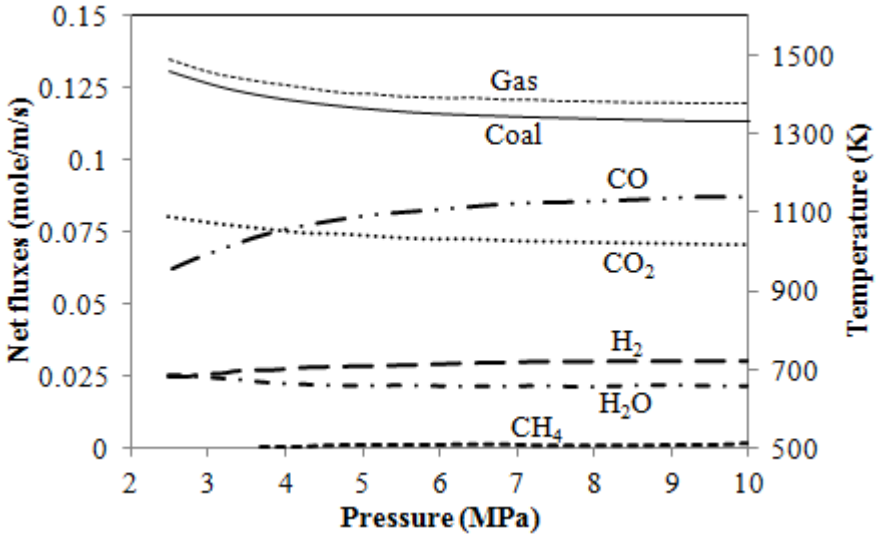

3

Figure 2-36 Net fluxes and temperature as a function of process pressure for oxygen injection rate = 0.1 mol/m/s and water injection rate = 0.05 mol/m/s [65].

Pirlot et al. [73] developed a 2D steady-state model by extending the idea of Batenburg et al. [68] with two distinct zones: a low-permeability rubble and ash around the injection point and a high-permeability peripheral zone along the coal wall (Figure 2-37). After a short transitory starting phase, those two zones were identified by other researchers [78, 79] for a thin seam at great depth. During initial combustion, a cavity was identified partially filled with inert materials near the injection hole [78, 79]. Their simulation for cavity evolution was based on one main parameter, the permeability ratio between the low- and high-permeability zones. The gasifying agent was assumed to pass through the low-permeability zone surrounding the injection point prior to its arrival in the high-permeability zone, where reactions with the coal wall occur. They combined two separate models: (1) a flow model for the calculation of the flow through the low-permeability porous zone using Darcy's law and the continuity equation; and (2) a chemical model for the calculation of the chemical processes occurring between gas and the coal wall in the high-permeability zone using empirical correlations for mass and heat transfer for the packed bed by assuming plug flow in the gas phase. The coal consumption rate was calculated only on the channel wall. Their model did not consider the details of moisture and volatile matter released by drying and pyrolysis. They assumed that volatile matter is released in the form of water and hydrogen in proportion to the consumption rate of carbon. They concluded that the permeability ratio is one of the main parameters for determining the success of UCG because of the observation of the increasing final gasifier area, power, and trial duration with the increase of the permeability ratio. According to them, the cavity growth and shape obtained from their model were in reasonable agreement with the Pricetown field trials.

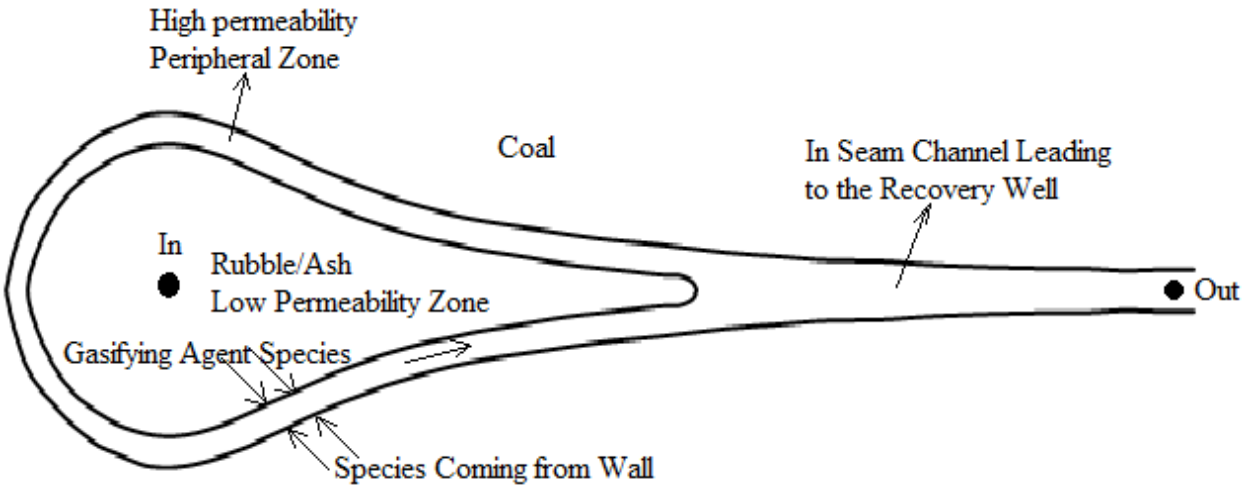

Figure 2-37 Conceptual sketch of the two separate zones and species flow direction (redrawn from Pirlot et al. [73]).

Kuyper [69, 74] developed a 2D model to describe UCG process in a cross-section of an open channel (Figure 2-38) for a typical western European coal layer of thin seams (1–2 m). Field trials of UCG indicated the growth of the cavity upwards and radially outwards around the injection well as gasification proceeds [80]. As a result, at thin seams, the top wall is exposed to rock materials and failure of the overburden is apparently expected. Such a failure would create open channels around the rubble materials deposited on the floor just about the injection hole; as shown in Figure 2-38. Considering this fact, in their model, the top and bottom walls were assumed as impermeable and adiabatic rock materials. However, the main focus of their work was to obtain an insight for heat and mass transfer due to double-diffusive turbulent natural convection in which both the temperature and concentration gradients play a role in the transport process. The justification of using double-diffusive turbulent natural convection was based on the expectation that $Gr/Re^2 >> 1$, considering the Grashoff number (Gr) of the natural convection flow in the process is approximately 1010 while the Reynolds number (Re) of the forced

convection flow is about 104. In this situation, if the forced convection flow is superimposed on the natural convection flow, the heat and mass transport phenomena inside the cavity will be dominated by double-diffusive natural convection and a spiral flow can be expected. The justification for this assumption can be found elsewhere [81]. The Navier-Stokes equation and the k-ε turbulence model were used to describe fluid flow due to large gradients of density and concentration in the channel. Radiation and convection were assumed to be the major heat transfer mechanisms in the channel. Model results showed that oxygen is consumed far from the coal wall by combustible gases. The double-diffusive natural convection in the channel was observed to cause the periodic generation and collapse of CO_2 bubbles (Figure 2-39). Also, mass transfer was reported to be the controlling mechanism (the rate-limiting step) for reduction reactions at the coal wall. They also studied the effect of CO_2 injection into the coal seam and reported that CO_2 injection has a similar effect as adding steam, although to a lesser extent.

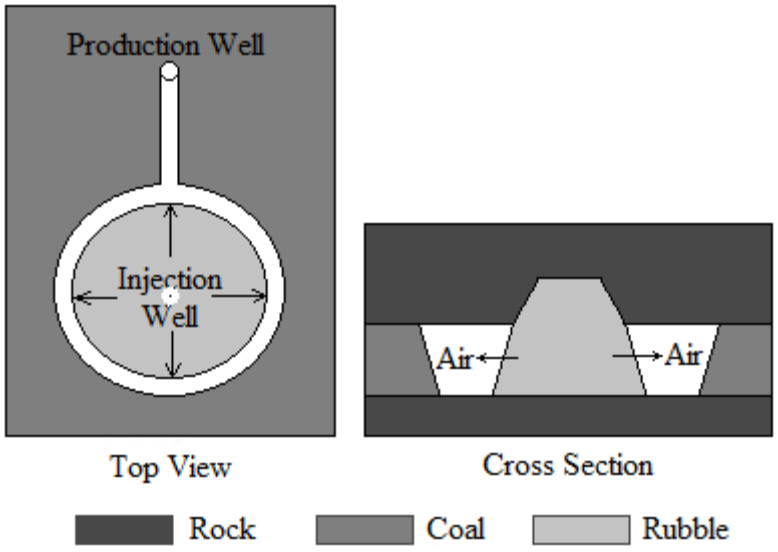

Figure 2-38 Channel formation in thin seams (modified from Kuyper et al. [74]).

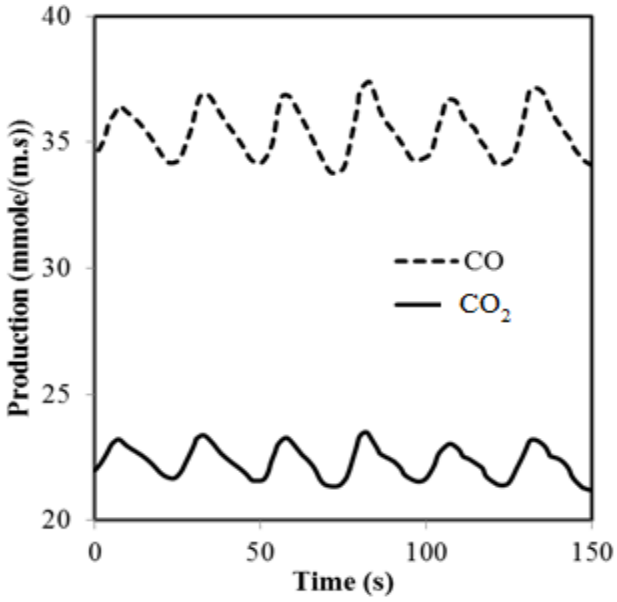

Figure 2-39 Production of CO and CO_2 as function of time for κ = 0.12 m−1 and an oxygen injection rate of 47 mmole $m^{-1}s^{-1}$ [74].

Because of the identification of UCG application in thick coal seams and the presence of a porous bed of ash overlying the injection point and a void space above the UCG cavity based on field trial excavation [40, 80, 82] as depicted in Figure 2-40, Perkins and Sahajwalla [75] considered a thick coal seam and expanded Kuyper's model by including an ash layer at a lower part of the channel (Figure 2-41). They developed a 2D axisymmetric model by using Fluent to investigate double-diffusive natural convection along with relevant reactions in a partially filled cavity. Although the bottom wall was considered to be inert and adiabatic, the side and top walls were considered to be carbon due to the thick coal seam. The temperature of the gas and the porous ash bed were assumed to be in thermal equilibrium. The flow though the porous ash bed was modeled using a laminar approximation; however, the turbulence model is only applied to the void region of the cavity. The low Reynolds number turbulence model of Launder and Sharma [83] was employed for the turbulent model by replacing the constants in the standard k-ε

model with the function of the turbulent Reynolds number to extend the model's applicability to low-turbulence regions that are close to walls. The following turbulent kinetic energy (k_t) and the turbulent dissipation rate (ε) equations were used to account for turbulent intensity:

$$\frac{\partial}{\partial t}(\rho_g k_t) + \nabla.(\rho_g \overline{v} k_t) = \nabla.\left[\left(\mu_g + \frac{\mu_t}{\sigma_{k_t}}\right)\nabla k_t\right] + G_{k_t} + G_b - \rho_g \varepsilon + Y_m + \dot{w}_{k_t} \qquad \textit{(Eq. 2.33)}$$

$$\frac{\partial}{\partial t}(\rho_g \varepsilon) + \nabla.(\rho_g \overline{v} \varepsilon) = \nabla.\left[\left(\mu_g + \frac{\mu_t}{\sigma_\varepsilon}\right)\nabla \varepsilon\right] + C_{1\varepsilon}\frac{\varepsilon}{k_t}(G_k) - C_{2\varepsilon}\rho_g \frac{\varepsilon^2}{k_t} + \dot{w}_\varepsilon \qquad \textit{(Eq. 2.34)}$$

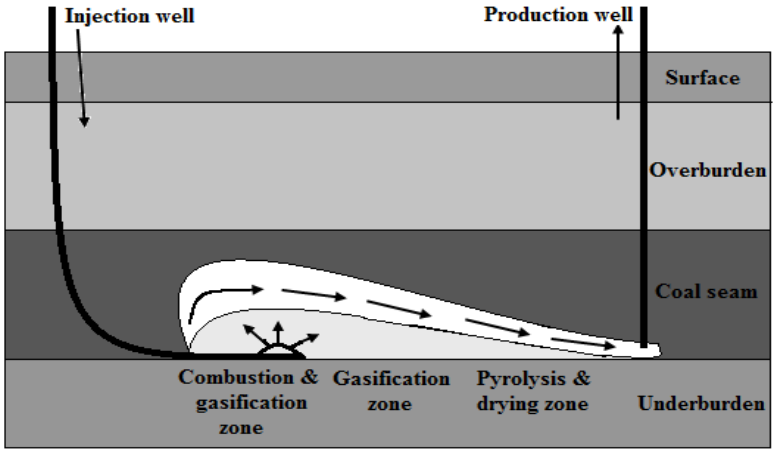

Figure 2-40 Schematic of an underground coal gasification cavity from field observation (redrawn from Perkins and Sahajwalla [75]).

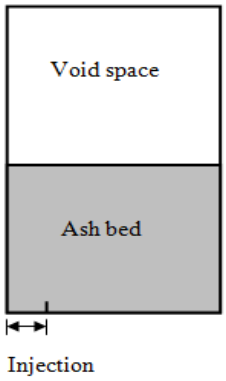

Figure 2-41 Channel geometry in Perkins and Sahajwalla [75].

For other conservation equations for void space, they followed the standard governing equations developed for porous media with the exception of φ (porosity) = 1. For the simplicity of their model, only three chemical reactions (reactions 2, 8, and partial char combustion) were considered. They found that the flow behaviour in the void space is dominated by a single buoyant force due to the temperature gradient resulting from the combustion of oxygen with CO produced from the gasification of CO_2 at the walls. From the observable entity, by changing the injection point, they concluded that oxygen should be injected at the bottom of the channel, otherwise valuable gasification products would be oxidized, leading to a low heating value of the production gas. The model was verified with Biezen's experiments [24] for double-diffusive natural convection in a trapezoidal channel.

Considering the importance of the flame front propagation in the gasification channel for viable operations in UCG, Saulov et al. [84] developed a simplified physical model to describe the primary features of the flame behaviour in a long channel through a coal block. According to their model, a number of factors, such as air flow rate, flame temperature, oxidizer diffusion rate, and radiative heat transport, etc., are the decisive factors to determine if the flame tends to propagate toward the injection point (reverse combustion) or the downstream direction (forward combustion). The flame speed is affected by the air flow rate through the energy balance in the channel. Their model predicts the flame propagation toward the injection point (upstream) for a low air flow rate and toward the downstream direction for a high air flow rate. These predictions from their model are in agreement with qualitative observation by Chernyshv [85]. The flame speed is affected by the air flow rate through the energy balance in the channel. The introduction of oxygen instead of air is found to increase the flame temperature and reactions rates and, as a

result, the flame propagates at a faster rate. They also reported a quantitative comparison with the experimental data reported in the book by Skafa [13]. Figure 2-42 demonstrates two burn velocities, i.e., upstream end velocity, s, and downstream end velocity, s_b, as functions of the injection air speed in the upstream undisturbed section of the channel. It is noted that positive values of the velocity mean that the flame front propagates downstream, while negative values imply that the front moves upstream.

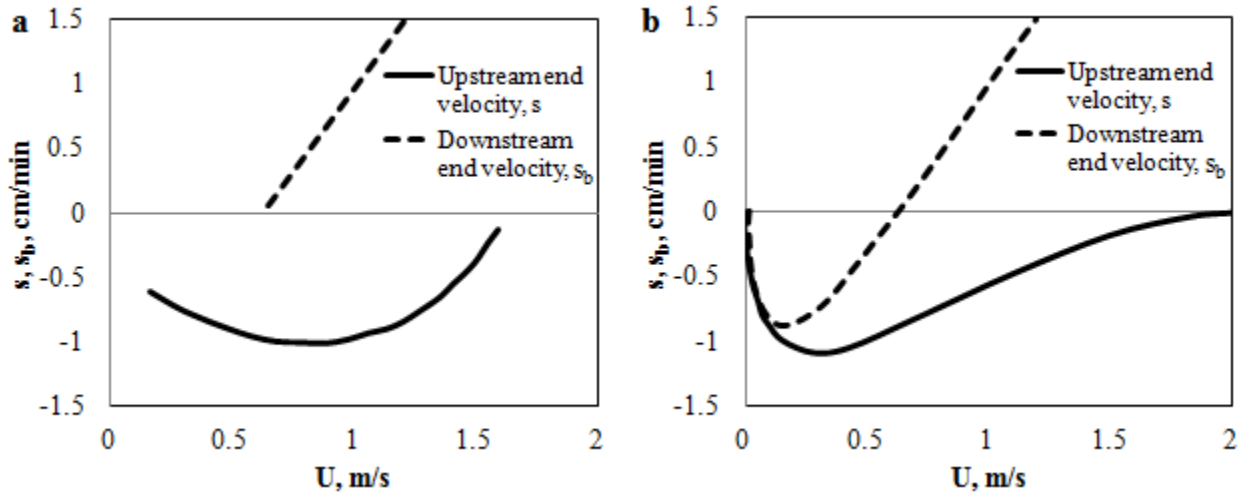

Figure 2-42 Dependence of burn velocity on the air flow rate [72]: (a) experimental data from Skafa [13], and (b) calculated data from Saulov et al. [84].

In the case of very hot and diffusion-controlled flame, Saulov et al. [84] considered the limit of high temperatures, a high activation energy, and a strong air flow. Under these conditions the surface of the channel is considered to have two zones, cold and hot. The temperature is found insufficiently high in the cold zone to initiate reactions, while in the hot zone any oxygen on the surface exhausted quickly due to instant reactions. These zones are separated only by a very small distance due to high activation energy. The overall reaction rate is determined by the rate of diffusion of oxygen to the hot zone, while the oxygen concentration on hot walls is essentially

nil. Under such conditions the flow in the gasification channel is turbulent and the turbulent flame is fully controlled by diffusion. The injection rate is found to have no control over the flame position. On the other hand, if the combustion of coal begins with devolatilization reactions at low temperatures and these reactions play a noticeable role in initiating the rest of the oxidation process or in the overall energy balance, the flame position is affected by the air speed and becomes controllable. On the other hand, if the devolatilization reactions during the combustion of coal begin at low temperatures and play a noticeable role in initiating the rest of the oxidation process or in the overall energy balance, the flame position is affected by the air speed and becomes controllable. In this case, the flame is not very hot and the cooling effect of the air flow is strong.

The consideration of natural convection is found to be one of the main phenomena in the channel model development. Natural convection plays an important role for the mixing of injected blast gas and the gases coming from the channel wall. The channel model is found to better calculate sweep efficiency. However, most of the channel models neglected drying and pyrolysis which are considered very important in the coal block model. To determine cavity shape and size, the channel model is preferred.

2.4.3 Other approaches of UCG models

Some models have attempted to describe the UCG coal seam as a coal slab. These models describe the process by movement of various defined regions in a coal slab perpendicular to the flow of the injected blast gas. However, over the years, there have been developed few UCG

models individually such as, reactor model, process model, probabilistic simulation etc. The details of these models can be found in a model review paper published by the author [18].

2.4.4 Summary of modeling review

The developments of a number of models in different concept imply that UCG is very complex process and the process is still not completely and clearly understood. Because of the complexity, the applicability of the existing model is very limited and specific to an isolated case. Most of the previous models are in 1D or 2D, while the field trials reveal a 3D non-regular shape. However, only very few 3D models have been developed some of which are validated for a specific case only. There are a number of properties and parameter involved in UCG, however, so far there are not any complete model that can address all the properties and parameters in a reasonable manner. There are still lots of scope to improve the modelling part until a complete and reasonably correction information can be achieve from a model.

2.5 Consideration of UCG Modeling Parameters

As mentioned earlier, UCG is site-specific. Controlling UCG is less flexible as compared to surface gasifiers because some important variables such as the thickness, quality of the seam, moisture contents, and other physical and chemical parameters are unique properties of the natural location and cannot be changed. Most of the models indicated the sensitivity of the process to the properties of the seam and the change of these properties with temperature. To obtain the best possible results from governing equations, appropriate solid and gas properties are required. Most of the models discussed above used either constant properties or transient properties obtained from the approximate model or experimental results of others. However, for a realistic model of any specific UCG site, the physical properties of coal and their changes with

temperature and pressure, such as thermal conductivity, specific heat, density, porosity, and permeability, etc., need to be considered. Similarly, properties of gas species and their changes with temperature and pressure, such as density, viscosity, thermal conductivity, diffusivity, and heat capacity, etc., need to be considered as well. Some experiments might be required to formulate these dependencies for the specific seams. To enhance the features of the 3D model and to apply the model in UCG field trials, it is imperative to incorporate the coal properties, the change of properties with temperature, and the coal seam geology of the specific site into the model.

To avoid model complications and to reduce computation time, some models assumed that gas and solids in the porous media are in thermal equilibrium and that is why they used one combined heat transfer equation. However, there is a large difference between the solid and gas characteristic timescale. It is assumed that gas reaches the steady state before any change occurs in the solid [62]. Thus, two separate heat transfer equations for gas and solid, respectively, seem to be more appropriate to incorporate into the model. In some models, the mass conservation of the solid is avoided since drying, pyrolysis and chemical reactions are considered in mass conservation of gas. However, to account for the mass loss of solid as well as ash production, the solid species balance seems to be reasonable for incorporating into the model. The choice of the appropriate use of the reaction rates is always challenging due to the complex situation of UCG operations. As these values are obtained from experiments, a number of experiments were performed to obtain reaction rates. However, obtaining a reaction rate for a specific reaction needs to consider the operating pressure and temperature similar to UCG operational conditions.

There is hardly a UCG site without any water influx from the surrounding strata. Thus, in a UCG site, water influx is unavoidable, and the gasification is performed above the hydrostatics pressure to control the water influx; this allowed the water to be used for steam gasification to utilize the heat of combustion and increase the concentration of CO and H_2 in the product gas. It is imperative to include a water influx formulation that is practicable for a specific site's coal hydrology. Although some investigators claimed a steam/oxygen ratio of 2.5 as optimum for UCG [49, 86], it is also necessary to explore the appropriate steam/oxygen ratio for sites in different geography and coal seams.

2.6 UCG-CCS

Currently, sequestration of CO_2 in a subsurface is becoming popular worldwide because of moving towards a low-carbon future. The un-minable coal seams are currently being considered as carbon dioxide sinks [87, 88]. The accessibility of carbon dioxide to the pores of unworked deep coal seams is limited by the porosity and permeability of coals that tend to decrease with increasing overburden pressure [89]. However, the void created due to gasification and the amount of coal chars left behind after the UCG process triggers the possibility of storing carbon dioxide in that depleted space known as UCG-CCS [15, 90].

Considering the chemistry of gas storage, studies have shown that gas storage in coal occurs in both the adsorbed phase and the free gas phase. At low pressure, the carbon dioxide storage potential in coal seams is mainly a function of its adsorption capacity; however, at high pressure, it is a strong function of the accessibility to CO_2 with respect to pore space for free gas [15, 89-91]. Although the volume of pores in coal is much smaller than in other reservoir rocks, the

storage potential of CO_2 in coal significantly differs from other rocks and exceeds its open pore volume by an order of magnitude predominantly due to the surface adsorption in micropores [91]. Saghafi et al. [91] reported that coal micropore surface area can reach several hundreds of square meters per gram of solid, which makes large areas available for gas adsorption. However, the development of micropores is a function of coal rank, temperature, and coal composition [91].

There are a number of reports concerning CO_2 storage potential in underground coal seams of different ranks [92]; however, there were inadequate reports of CO_2 storage potential in the coal seams subsequent to gasification. Recently, case studies of the feasibility for UCG-CCS storage have been carried out in the Powder River Basin of Wyoming, US [8, 93-95], at a selected site in Bulgaria [93, 96], and at the Williston Basin, North Dakota, US [97]. Roddy and Younger [87] studied the potential of carbon storage and addressed surface subsidence and aquifer contamination as the main challenges for UCG-CCS application. However, in a later paper, Younger [98] studied hydrogeological and geo-mechanical aspects of UCG and proposed an action plan to avoid subsidence and aquifer contamination in the life cycle of UCG-CCS operations. To predict these risks, geo-mechanical and hydrogeological models are required. The models that dealt with surface subsidence and water hydrology in the UCG process can be found in recent references: Yang et al. [99], Sheng et al. [100]. From the studies, it appears that careful planning, appropriate site selection, adequate engineering and modeling, and professional management are the keys to implement UCG-CCS schemes successfully. It was also understood from the literature that the cavity should be located deeper than 800 m, so that CO_2 can be stored in the supercritical state, allowing significantly higher utilization of the pore space [8, 87].

Another interesting feature of UCG-CCS is the cavity temperature during CO_2 injection. As the temperature in the cavity of the UCG process reaches more than 1000 °C, the reactor cool-down process is essential for the preparation of UCG cavities for the subsequent CO_2 storage. The natural cooling of the cavity can be achieved very slowly. However, forced cooling with water flushing can significantly decrease the duration of the cool-down process by a factor of more than three hundred [101]. Most importantly, the implementation of UCG-CCS must be dependent on economic feasibility. Although very few studies are available on the economic assessment for the evaluation of UCG-CCS schemes [100, 102] much remains to be done.

2.7 Chapter Conclusions

This review indicates that the experience of previous field/lab-scale tests and the developed UCG models provides information on specific and isolated cases. So far, there is no model developed that can predict the performance of any UCG process. Considering this fact, to assess the performance of UCG process of Canadian sub-bituminous coal, it is important to acquire adequate insight into the UCG process by conducting lab-scale UCG experiments using Canadian coal.

There is inadequate research on the storage capacity of carbon dioxide on pyrolyzed and gasified coal char. However, to evaluate the applicability of UCG-CCS, a number of adsorption experiments are necessary to estimate the storage capacity of the leftover char (pyrolyzed and gasified) after the UCG trials/experiments.

CHAPTER THREE: EXPERIMENT

This chapter describes the experiments on UCG and carbon storage capacity. Section 3.1 provides the details of UCG experiments to evaluate the performance of subbituminous coal on UCG. On the other hand, Section 3.2 provides the details of adsorption experiments to evaluate the carbon storage capacity.

3.1 UCG Experiment

Most of the lab-scale UCG experiments were conducted under atmospheric pressure; however, the actual UCG is usually performed at elevated pressure. The earlier soviet UCG operations were conducted on shallow depth and the operating pressure was below 2.5 atm pressure [14]. On the contrary, the European UCG trials were conducted on very deep coal seam. The operating pressure is increased with depth to keep in equilibrium with hydrostatic pressure of surrounding that increases with a rate of 0.01 MPa/m depth [33]. High pressure UCG operations yield higher portions of methane and carbon dioxide in the product gas because high pressure favors formation of methane and carbon dioxide [43, 62, 103]. Because of the presence of more methane, high calorific value syngas is produced from high pressure UCG operations from very deep coal seam. However, pressure is found to have less significant on methane-free syngas [104, 105]. This investigation is also supported by the predictions of several models. Khadse et al.[62] varied pressure up to 20 atmospheric pressure in their UCG model; however, they did not find any significant change in the syngas production. Similarly, the UCG model developed by Batenburg at el.[68] also showed a negligible effect of pressure up to 100 bar on product gas compositions.

As the methane-free syngas is not affected by the pressure, Ex-situ experiments are usually chosen to operate under atmospheric pressure to avoid cost for installing high pressure equipment and to avoid dangers associated to high pressure operations inside the laboratory.

In this investigation, an experimental set-up was built in the laboratory to mimic the UCG process under atmospheric pressure (see Figure 3-1). All the experiments were carried out using subbituminous coal (Genesee coal) obtained from a big block of coal. Because of the anisotropic nature of coal, the experimental results may vary if different coal samples are considered.

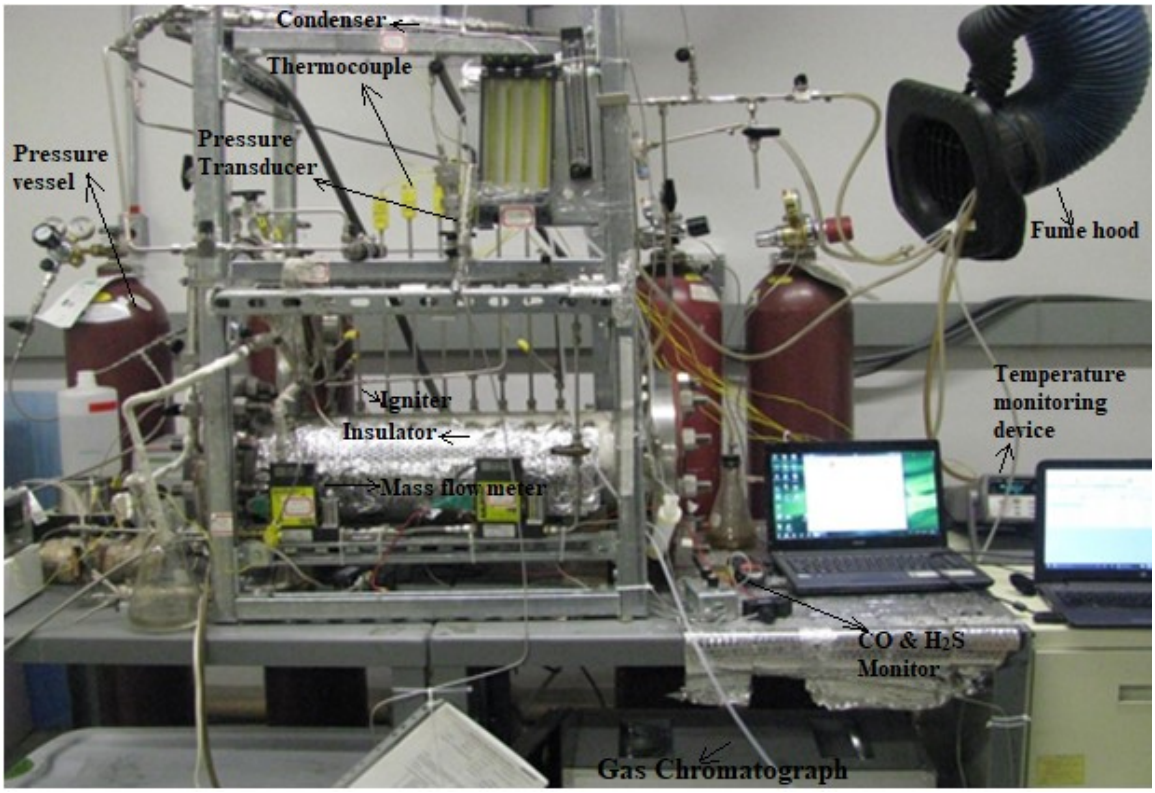

Figure 3-1 Laboratory experimental set-up for atmospheric UCG experiment.

Considering this fact, the coal block of each experiment was simulated from coal particles obtained at different locations within the big coal block to ensure the homogeneity through the

coal block. However, because of very site-specific nature of UCG, this research did not consider sample variability by obtaining big coal blocks from different locations.

3.1.1 Experimental set-up for simulated UCG experiment

The set-up was equipped with feeding system, ex-situ reactor (gasifier), ignition system, product gas collection system (outlet system) and monitoring and controlling system. In addition, a safety precaution system was established to ensure a safe operation inside the laboratory. Figure 3-2 represents schematic diagram that describes the process flow diagram and the control system of the set-up.

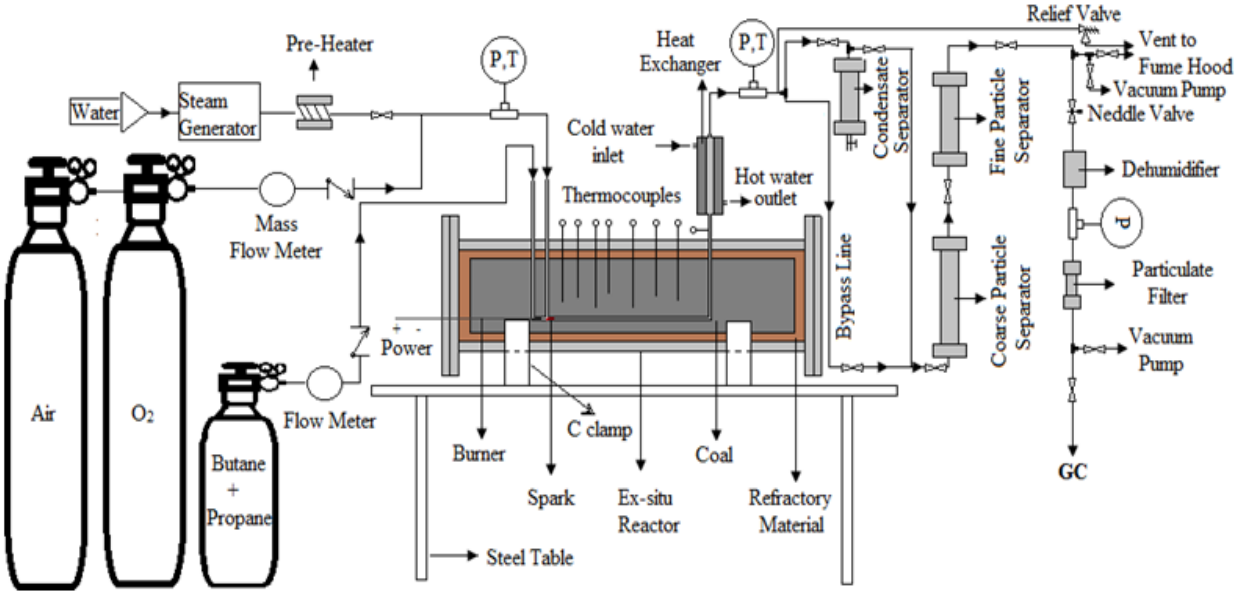

Figure 3-2 Schematic diagram of UCG experimental set-up in the laboratory.

3.1.1.1 Feeding system

The feeding system comprises a supply system of ignition mixture (oxidant and fuel) during the ignition phase and a supply system of gasifying agents (oxidant and steam). In this experiment, oxygen was used as oxidant and propane was used as fuel. Both gases were supplied from the pressure vessels. The ignition phase is considered as the period of time of continuous supply of ignitions gas mixture before a successful ignition. Each injection line was equipped with mass flow meter to control the flow rate.

Oxygen and steam were used as gasifying agent. To facilitate steam gasification, availability of steam in the coal block is often necessary. However, steam acts as an extinguisher for oxidation reaction at lower temperature and that is why Daggupati et al.[50] suggested to heat the steam nearly 400 to 600 °C before introducing into the reactor. Considering this fact, a steam generator assembly was built in the laboratory which could produce and supply steam to the coal block at nearly 400 °C. The assembly includes a metering water pump, a cartridge heater of 1100 W wrapped by 18 inches 1/16" OD Stainless Steel Swagelok tubing (Figure 3-3), temperature controller, thermocouples and heating tape. Injection tube for propane was used for steam injection long after the ignition phase when that tube was not intended to use for propane injection. Figure 3-4 shows the assembly of steam generation and supplying system.

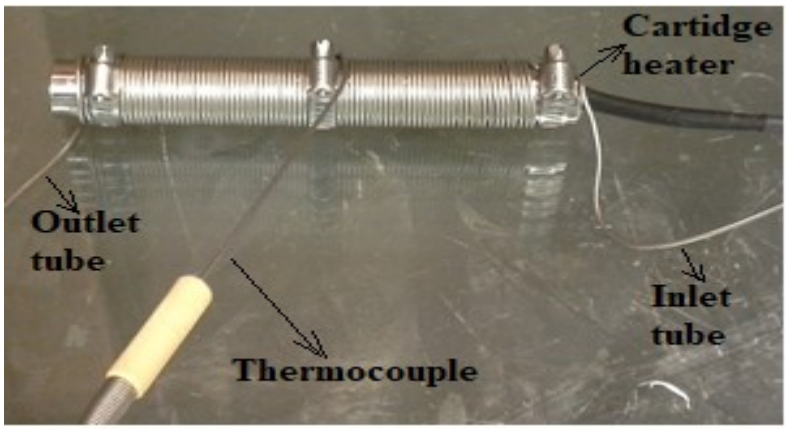

Figure 3-3 Cartridge heater after wrapping.

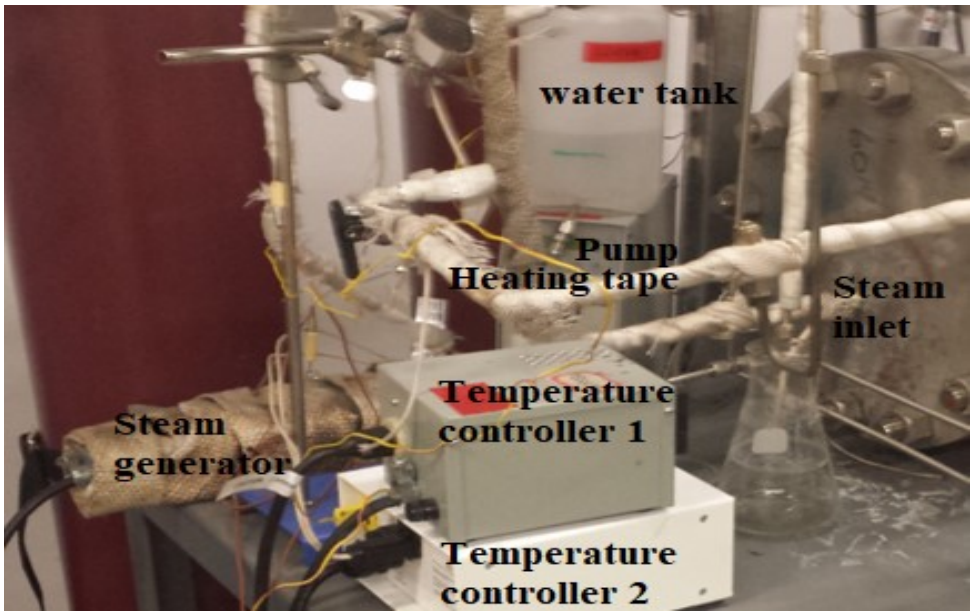

Figure 3-4 Steam production and supply system.

3.1.1.2 Ex-situ reactor

In this investigation, an approximately 17 cm inner diameter by 80 cm long cylindrical and 2.5 cm thick steel vessel was used as ex-situ reactor (Figure 3-5). Although there were 33 holes each of 0.635 cm in 3 rows, only 11 holes in the middle rows were used for injection, production and thermocouples (see Figure 3-6). The holes of other rows were sealed during the experimental

run. After placing the coal/coal block assembly into the reactor, the flanges were tightly bolted using graphite gasket and high temperature silicon gasket. Similarly, Swagelok tube fittings were used in all the holes of the reactor to ensure that there was no leak at the intersection points of inlet and outlet gas lines, spark igniter and the K-type thermocouples connected to the reactor directly. The ex-situ reactor was wrapped with insulator to reduce the heat loss from the reactor.

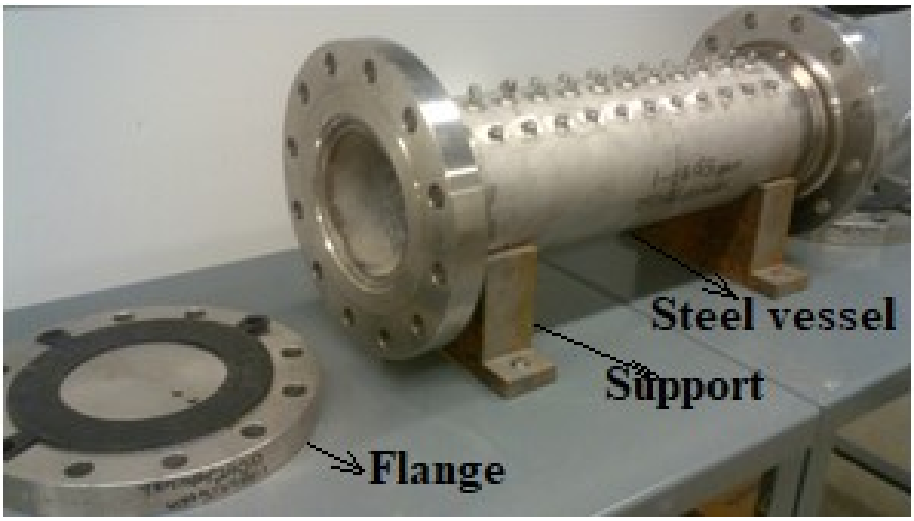

Figure 3-5 Ex-situ reactor with flanges

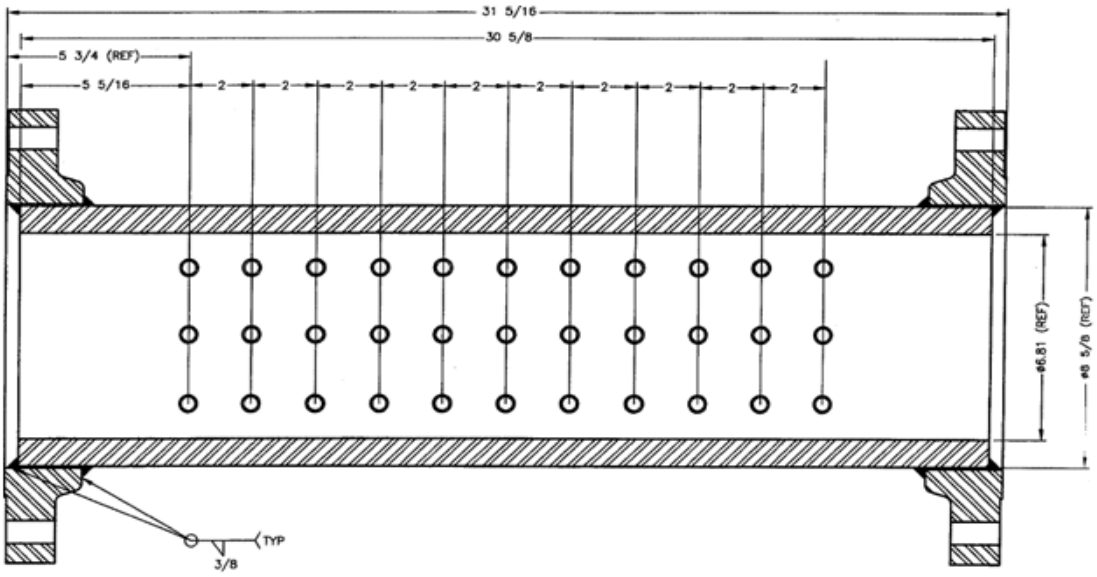

Figure 3-6 Schematic diagram of ex-situ reactor.

3.1.1.3 Ignition system

A special type of spark igniter circuit (Figure 3-7) was constructed by the instrument shop of University of Alberta. The ceramic electrode of the igniter was inserted into a quarter inch Swagelok tube using high temperature resistant adhesive and placed the probe inside the reactor into the coal seam where it came in contact with the ignition gas mixture. To start ignition, an electric spark was generated on the probe of the igniter using the igniter switch located outside the reactor.

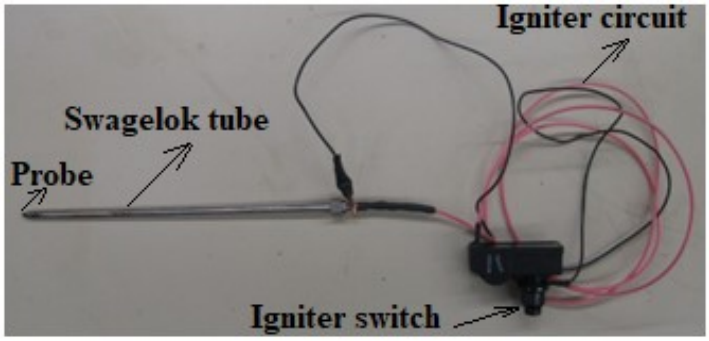

Figure 3-7 Spark igniter circuit.

For each experiment, the first challenge was to establish an ignition which is necessary for any combustion/gasification experiment. Before a fire can occur, two conditions must be satisfied: i) fuel and oxidizer must exist in certain proportion with the spark; ii) the concentration of the fuel must be in between the lower explosive limit (for propane: LEL ≈ 2.3%) and upper explosive limit (for propane: UEL≈ 55%). Stoichiometric calculation shows that five moles of oxygen are required for 1 mole of propane for combustion which indicates a stoichiometric mixture fraction of 3.6. However, to ensure a complete combustion, excess of oxidant is recommended. Initially, the ignition gas mixture with excess oxygen was passed through the injection channel and an electric spark was generated through the ignition circuit. After a number of trials at different

excess oxygen concentration, 20% excess oxygen was found to be effective and used for each of the experiment during the ignition phase. Increase/decrease of oxygen flow rate influenced the flow rate of propane to maintain 20% excess oxygen as long as ignition phase continued.

It should be noted that each ignition trial created a moderate/mild explosion inside the coal block. The fire didn't occur until the block was heated by passing hot air. Because of colder environment inside coal block, some moisture could be deposited, and coal surface could be wet which prohibited any ignition. Passing of hot air for half an hour to one hour could remove the moisture and make a dry environment near the ignition point which could facilitate the ignition.

3.1.1.4 Product gas collection system

The product gas collection system comprises a gas cooling system, solid particles removal system, moisture removal system, dry gas collection and an outlet system.

3.1.1.5 Monitoring and controlling system

During the experiments a wide range of parameters was measured. An automated system was established to measure/monitor the temperature, pressure and composition of the product gas. The data acquisition system includes both pressure (Omega PX409-2.5KGUSB) and temperature (Agilent 34972A LXI) monitoring device. The composition of the gas outlet from the reactor was monitored using micro gas chromatograph (Varian CP 4900). However, the vacuum pump, condenser, water pump, temperature controller, steam generator, mass flow meter etc. were manually controlled.

3.1.1.6 Safety precaution system

Some hazardous gases, such as, H_2S, CO, CH_4, and other light hydrocarbons may be generated during the gasification process. Inhalation of such hazardous gases may lead to dizziness, eye irritation, unconsciousness and even death if exposed at high concentration and prolonged period. A standard helium leak detector was used to ensure the total tubing system of the experimental set-up to be leak proof. A relief valve was placed in the tubing system to vent the gases if for any reason pressure goes more than 300 psi. Before each experiment, the leak was monitored by using high pressure air for couple of hours. Couples of carbon-monoxide and hydrogen sulfide gas monitors were always turn on during the experiment. The experiments were carried out under a fume hood with proper ventilation to avoid any exposure due to the accidental release of hazardous gases. Moreover, due to possible risk of explosion during ignition, the reactor was chosen to have a design pressure of 450 psi at 300 °C for a safe operation.

3.1.2 Coal samples

In this experiment, a big sub-bituminous coal (Genesee coal) block supplied by Sherritt international corporation was used. Table 3-1 shows proximate and ultimate analyses of the coal. This analysis was carried out for different samples that were taken at different locations within the coal block to ensure the homogeneity throughout the coal block. Proximate analysis of coal was carried out according to ASTM D7582 MVA in coal and the ultimate analyses were carried out by a Vario MICRO cube elemental analyzer.

Table 3-1 Proximate and ultimate analyses of raw coal (Genesee coal).

Proximate Analysis (wt.%, A.R)				Ultimate Analysis (wt.%, daf)				
Moisture	F.C	V.M	Ash	C	H	N	S	O
4.4	50.3	29.9	15.4	74.8	4.7	1.3	0.6	18.6

A.R – As Received, daf – dry ash free, F.C – Fixed Carbon, V.M – Volatile Matter

3.1.3 Design and construction of simulated coal bed

Total six simulated UCG experiments in the ex-situ reactors were conducted using two different types of coal beds prepared in two different methods to examine the UCG process at different modes, i.e., i) a channel mode where a link was established inside the simulated coal seam between the injection and production holes and ii) a packed bed mode where the whole coal bed is made up of coal particles.

The coal beds are different in terms of the establishment of the linkage between the injection and the production holes. Links are considered as the most critical step in a successful UCG operation due to its role in the enhancement of the permeability of the coal seam prior to gasification.

3.1.3.1 Coal blocks preparation for channel mode

In the channel mode, four experiments were carried out following the orientation of linked vertical wells (LVW) where the link was established by creating a narrow channel between the injection and the production holes. The methods for preparing coal blocks and the injection of the oxidant and fuel to form ignition mixture for channel mode were not same for all

experiments. Three types of coal beds were prepared to carry on the UCG experiment following channel mode operation.

3.1.3.1.1 Coal block type 1

In the 1st experiment, a 12 cm diameter by 58.50 cm long cylindrical coal block was prepared by tying three cylindrical small coal blocks which were obtained by drilling the raw coal samples using a 5-inch diameter core bit. The gaps between the small blocks were filled with a mixture of cement and fine coals before the whole block was consolidated with concrete to hold the block as well as to resist the heat loss. Injection and production holes and some auxiliary holes (for thermocouples) with 0.7 cm diameters were drilled from the concrete surface to the coal block. Finally, a gasification channels with 0.7 cm diameters were introduced into the coal blocks by drilling holes into the bottom part along the axial direction of the blocks. Figure 3-8 shows the orientation of injection and production holes and the holes used for the k-type thermocouples at different depth. The chronological steps of preparing one of the first type of coal blocks are shown in Figure 3-9.

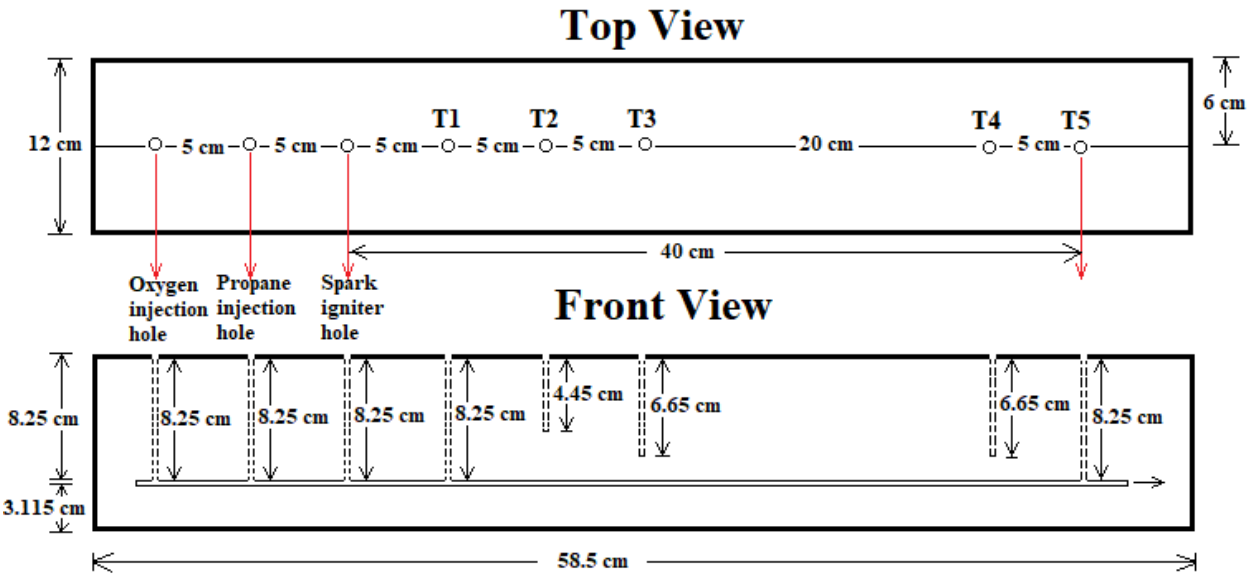

Figure 3-8 The position of injection, production, igniter and thermocouple holes inside the coal block.

Figure 3-9 Preparation of coal block type 1.

3.1.3.1.2 Coal block type 2

In the 2nd experiment, the coal block was made up by filling a concrete tube with 90% coal particles of 1 cm size and 10% coal powder following a standard procedure (ASTM D698-07). The concrete tube having an inner diameter of 12 cm, length 54 cm and a thickness of 2.5 cm was chosen as an insulating material to resist heat loss during the gasification. Each concrete tube was prepared by using the mixture of cement, sand, gravel, silica fume and water with a standard ratio (e.g., a ratio of 14:20:24:2:7) with a curing time of 28 days in a hydration environment. After making a tight bed of coal, the tube was drilled to create holes of 0.7 cm diameter on the top for the injection/production lines and thermocouples. Both sides of the tube were also sealed with concrete and a gasification channel with 0.7 cm diameter were introduced by drilling holes along the lateral direction of the block and following a depth of 3.75 cm from the top of the coal block only (see Figure 3-10). All the thermocouples were placed in the gasification channel from the top.

Figure 3-10 Preparation of coal block type 2.

3.1.3.1.3 Coal block type 3

At a later stage, the coal block was prepared by using a mixture of coal particles of 1 cm size, coal powder and cement with a weight ratio of 8:1:1. Water was added to this mixture to obtain a uniform consistency before pouring the mixture into the concrete tube described in the previous section. After curing the tube, several 7 mm diameter holes were drilled into the tube to accommodate production and injection lines and a maximum of 7 thermocouples to monitor the block temperature during the gasification process. During the filling stage of the mixture, a provision of creating gasification channel and necessary holes for the injection/production lines and thermocouples was kept by introducing some wooden sticks of 7 mm diameter wrapped with wax paper in to the tubes. After filling the tube with coal particle mixture, the block was allowed to dry for several days to solidify the block by driving away the moisture. The wooden sticks were removed after solidification. Figure 3-11shows the chronological steps of preparing the coal block type 3.

Figure 3-11 Preparation of coal block type 3.

For the first 3 experiments, during ignition phase, oxygen and propane were passed separately from the top through the holes to the link inside the coal block so that they can get enough space to mixture properly before exposing to the spark igniter. However, for experiment no. 4, a

colinear tube arrangement through the flange (from the side) was created for this experiment. In this new arrangement, propane was passed through the inner tube and the oxygen was passed through the annular during ignition phase. Figure 3-12 shows the details of the arrangements.

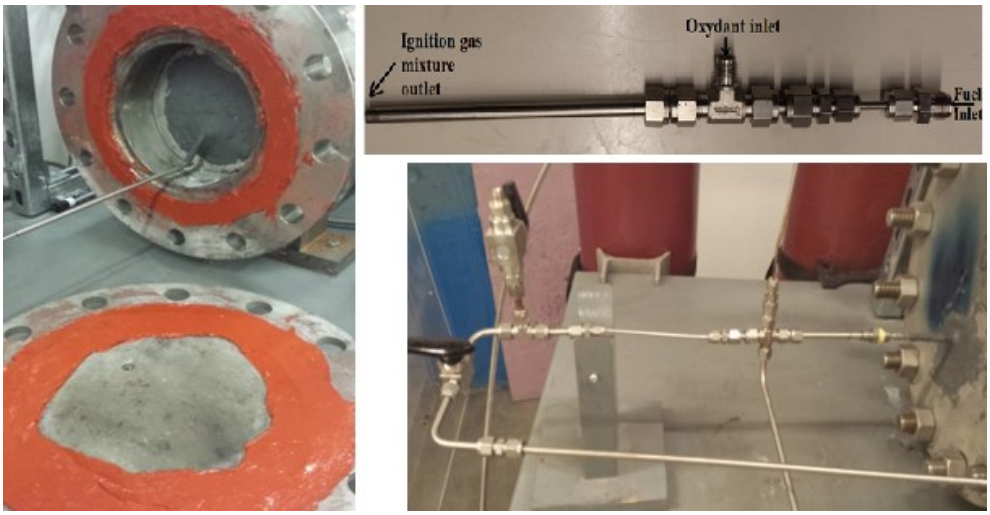

Figure 3-12 Collinear tube arrangement through the flanges to the coal block inside the reactor.

3.1.3.2 Coal blocks for packed bed mode

For the packed bed mode, no concrete tube was used. The reactor was filled with one-centimetre coal particles (see Figure 3-13). Coal particles were used to simulate packed coal seam which allows a less resistant path of the gases to flow from the injection holes to production holes due to high permeability of the packed bed. However, unlike channel mode operation, it is not possible to direct the gas flow to follow a definite path. Due to horizontal orientation of the reactor, two concrete caps (one at the injection side and the other on the production side) were used to restrict the coal particles in the reactor.

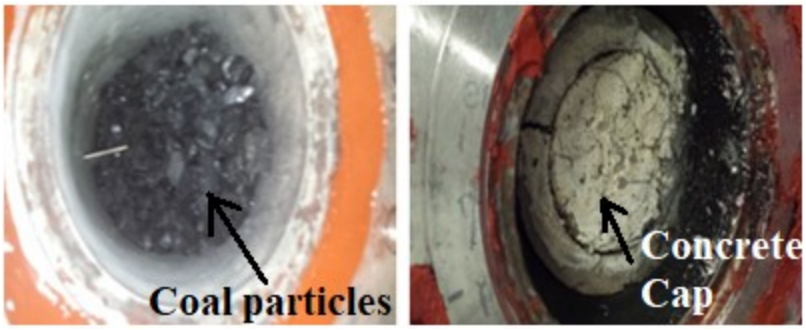

Figure 3-13 Preparation of coal blocks for packed bed mode.

Unlike, the channel mode, the ignition mixture was passed from the side through collinear tubes and released near the spark igniter. The release point of the gases of these co-linear tubes worked as a propane torch after a successful ignition. It is noted that the probe of spark igniter and the gas release point of the collinear tubes were kept very near. A cylindrical empty space of 5 cm diameter was deliberately created around ignition probe and only few big coal particles were placed near the empty space to keep away coal small particles that can block the flow of ignition gas and to facilitate ignition (see Figure 3-14).

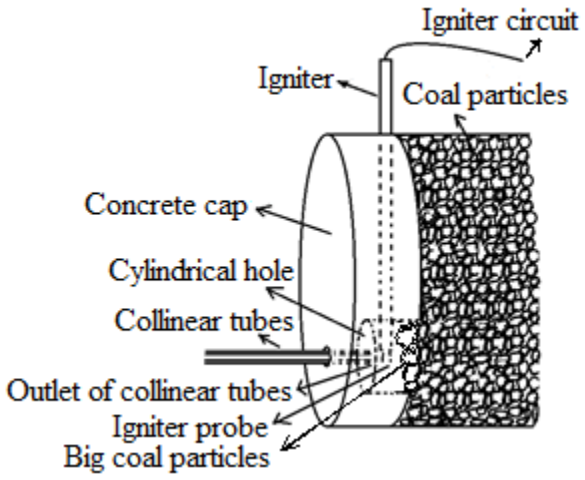

Figure 3-14 Collinear tubes ignition system in packed bed coal.

The details of the coal block type, simulated link and the injection of the ignition/feed gas of each experiment are shown in Table 3-2.

Table 3-2 Coal block types, link type and injection process of gases used in different experiments.

Exp. No:	Coal block type	Link	Injection of ignition/feed gas
1	Original coal block	Directional drilling	From the top, tubes were 5 cm apart
2	Coal particles (90%) + coal powder (10%)	Directional drilling	From the top, tubes were 5 cm apart
3	Coal particles (80%) + coal powder (11%) +cement (9%)	Directional drilling	From the top, tubes were 5 cm apart
4	Coal particles (80%) + coal powder (11%) +cement (9%)	Directional drilling	From the side, Co-linear tubes
5	Coal particles only (packed bed)	Highly permeable packed bed	From the side, Co-linear tubes
6	Coal particles only (packed bed)	Highly permeable packed bed	From the side, Co-linear tubes

Coal particle size: 1 cm

3.1.4 Procedure

With some exceptions, the procedures of each experiment were the same. Once the system was set-up, before carrying out each experiment after heating the block with hot air, the whole system was evacuated using a vacuum pump to reduce air/gases inside the reactor and the tubing systems. To initiate ignition, the ignition mixture (oxygen and propane, using a separate channel or collinear tubes) was passed until the GC shows a constant composition of the ignition mixture. After ignition, the duration of ignition process was controlled on-line by the temperature measurements in the gasification channel. The flow of propane was continued until a minimum temperature of 350 °C was indicated by any of the thermocouples. After reaching the expected

temperature (350 to 400 °C), the ignition process was terminated, and only oxygen was kept continue to flow as a source of combustion/gasification reactions. From preliminary tests, 350 to 400 °C was found to be the sufficient temperature to reach self-ignition temperature of coal. Self-ignition temperature of coal is considered as the minimum temperature at which spontaneous surface reaction (coal combustion only) takes place with the help of oxidant only.

The temperature and pressure at specified locations was continuously recorded. The dry gas compositions of the product gas were also continuously recorded at an interval of 10 minutes through the on-line micro GC. The experiment was continued 30 to 50 hours to consume most of the coal. After few hours (at least after 15 hours of ignition) when the temperature of the block at some point reach a temperature more than 350 °C, steam (ratio of steam to oxygen: 2.5:1) at 350 °C was injected to favor steam gasification reaction.

After the completion of the experiment, the coal block was allowed to cool for approximately 12 hours and after removing the injection and production lines and the thermocouples, the holes were used to take pictures of the cavity using the mini inspection camera (Figure 3-15). Later, after removing and breaking the concrete tube, the condition of leftover coal and ash was examined to estimate the cavity shape and coal consumption rate. In some experiment, the residue was collected for further analysis, such as proximate analysis and adsorption experiment for chars for other project.

Figure 3-15 Wifi wireless 3.9 mm diameter flexible mini inspection.

3.1.5 Results and discussion

The simulated UCG experiments in the ex-situ reactors were conducted with the intent of exploring sub-bituminous coal oxygen/steam gasification process, comparing process results and determining the optimal operational conditions.

The length of the gasification channel is considered an important parameter and has an impact on overall gasification process. From the earlier field gasification study of air gasification, critical length of the link is considered to be five to ten times the seam thickness [14]. Another laboratory study shows a decrease of cavity volume with the increase of the link length [49]. To nullify the effect of the link in gasification process, the length of the gasification channel was kept 35 cm or 40 cm in all experiments.

To capture the whole scenario of the gasification process, beside the common interests on the UGC performance, i.e., product gas composition and the temperature profile, the challenges experienced at different phases of each experiment were also depicted. This could be useful in designing an improved ex-situ reactor design and the experimental arrangements in the future.

3.1.5.1 Experiment 1

This was the only experiment where the coal block (coal block type 1) was closely simulated to underground coal seam. The coal ignition occurred with an oxygen flow rate of 2 L/min and propane flow rate of 333 mL/min.

The temperature profiles within the reactor obtained from experiment 1 are presented in Figure 3-16. The locations of the link and thermocouples can also be seen in the reaction front view from Figure 3-16. The ignition phase was continued nearly 10 hours to obtain a temperature above 623 K to initiate coal combustion without the help of propane. However, for a similar kind of ex-situ reactor with lignite coal, Stańczyk et al. [51] reported to reach a temperature of 673 K in their first couples of thermocouples in only 2 hours when they used propane and butane mixture as a fuel and oxygen enriched air as oxidant. Although, the ignition phase is considered as a period of time when ignition mixture (propane and oxygen) are allowed to pass through the reaction to raise the temperature near ignition zone through the combustion of propane and oxygen only, in reality, the ignition phase cannot be kept limited to only propane and oxygen combustion, coal combustion might be resulted if coal get heated to a self-ignition temperature.

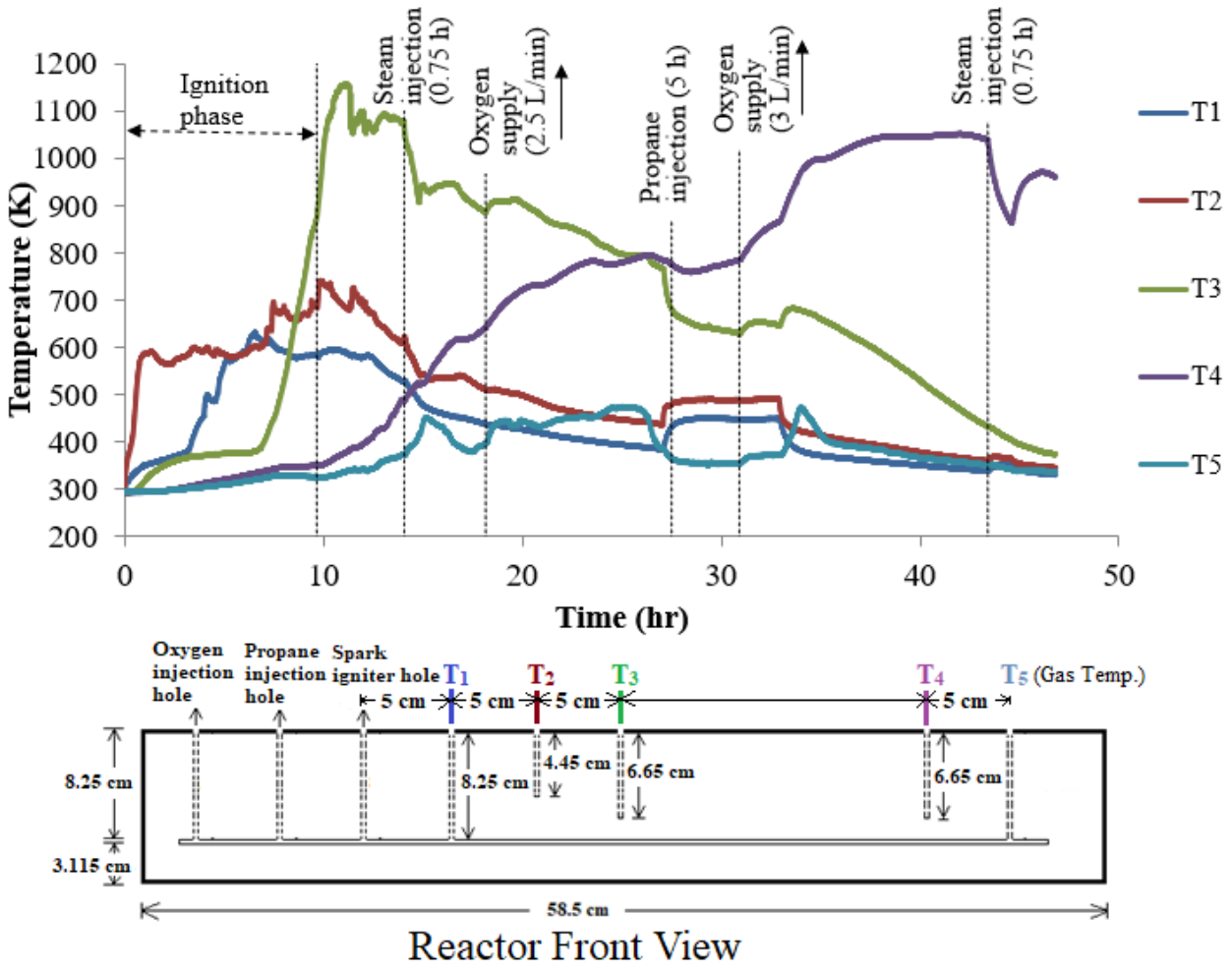

Figure 3-16 Experiment 1: temperature profile in the gasification channel and its surrounding.

The prolong ignition phase for the first experiment could be explained by the facts involved in several ignition trials prior to the gasification experiment to explore a sustained self-ignition temperature of coal. As mentioned earlier, for every ignition trial, a moderate explosion inside the reactor was unavoidable. Due to the explosion, the gasified channel (link) was obstructed by coal debris and ash. High pressure air blast was used to remove the obstacles from the gasification channel. During trial process, the ignition process followed by coal combustion process also consumed some of the fresh coal available surrounding the probe of the igniter. The

combined effect caused a coal deficit space near the thermocouples 1 and 2. As a result, during final ignition, the temperature observed on those thermocouples was less than that could be existed at some radial distant in the same plane from the position of the thermocouples where fresh coal was available.

The position of the thermocouples is also important to analysis temperature profile as all the thermocouples were not at the gasification channel. Thermocouple 1 was in the gasification channel, whereas, thermocouple 2 was 3.8 cm above the gasification channel. However, the temperature observed on thermocouple 2 was marginally above the temperature observed on thermocouple 1. Considering the location of thermocouple 2 and known low heat conductivity of coal, it can be inferred that the actual temperature was much higher in the gasification channel beneath that thermocouple.

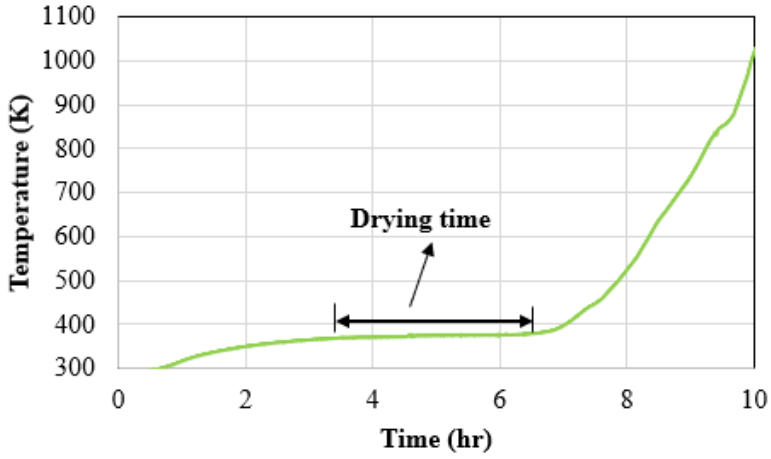

Figure 3-17 Temperature profile observed on thermocouple 3 during ignition phase.

Once the thermal front propagated and exposed to more available coal towards thermocouple 3, the highest temperature (1150 K) was recorded. However, before reaching the highest temperature, a period of nearly constant temperature was noticed (see Figure 3-17). As the

average temperature in that period is around the evaporation temperature of water, the span of time of constant temperature can be considered as the drying time near the zone of thermocouple 3.

Steam injection is a usually applied in most UCG processes, particularly for gasification reactions. After 14 and 44 hours of ignition, steam at 350°C with a steam and oxygen ratio of 2.5:1 was injected twice for a period of 45 mins to enhance the gasification reaction and observe the effect of steam on the temperature. The first injection of steam was found to reduce the temperature recorded on thermocouple 3, however, this negative effect was not observed on thermocouple 4. The second injection of steam also showed the downward trend which was visible from the temperature observed on thermocouple 4.

The drop of temperature upon introduction of steam was also observed by other laboratory gasification studies [50, 51]. Upon injection of steam, some steam readily condenses due to the fall of steam pressure and a temperature reduction is experienced due to evaporation of that steam. As mentioned before, Daggupati et al.[50] considered steam as an act of an extinguisher for oxidation reaction and suggested to inject steam after heating to a sufficiently high temperature (400°C – 600°C), however, production of high temperature steam at atmospheric pressure is considered challenging and expensive. To maintain cavity temperature, gasification process was suggested to carry out in alternate stages of heating up with oxygen/air and steam gasification elsewhere [49, 51, 106]. Daggupati et al. [50] also suggested to increase the initial combustion period so that the combustion reaction could spread in large surface area to provide sufficiently high temperature for subsequent gasification reaction.

After observing a sharp drop and continual decline in temperature recorded in thermocouple 3 due to the injection of steam at first time, the supply rate of oxygen (2.5L/min) was increased to enhance combustion reaction to raise a temperature that favours gasification reactions. The increase of oxygen flow rate did not change the decreasing trend in the temperature observed on thermocouple 3, however, a gradual rise in temperature was observed on thermocouple 4 which also did not reach to enough temperature (>700 °C) to favor gasification reactions. To increase the temperature further, propane (417 mL/min) was injected once again to initiate propane combustion at nearly 28 hours of ignition for a period of 5 hours. Injection of propane increased the temperature to a desirable value observed on thermocouple 4, however, the declining trend of the temperature observed on thermocouple 3 did not change much due to the depletion of the fresh coal near that thermocouple.

The thermal front propagation can be observed from Figure 3-18 by identifying the peak temperature observed on thermocouples 3 and 4 which were located 15 cm and 30 cm from the igniter in an axial direction of the reactor, respectively. In reality, the peak temperature in specific distance from the igniter could be different because of significant temperature difference in the radial direction as observed in different studies [17, 107, 108]. However, due to the same depth location of these two thermocouples, the radial temperature effect can be neglected. Figure 3-18 shows that the peak temperature shifted from thermocouple 3 to thermocouple 4 in about 32 hours which indicates a propagation of thermal front movement of 15 cm in about 32 hours. The thermal front propagation rate during combustion/gasification was found very low; however, those are comparable to the other studies on coal block [51, 107].

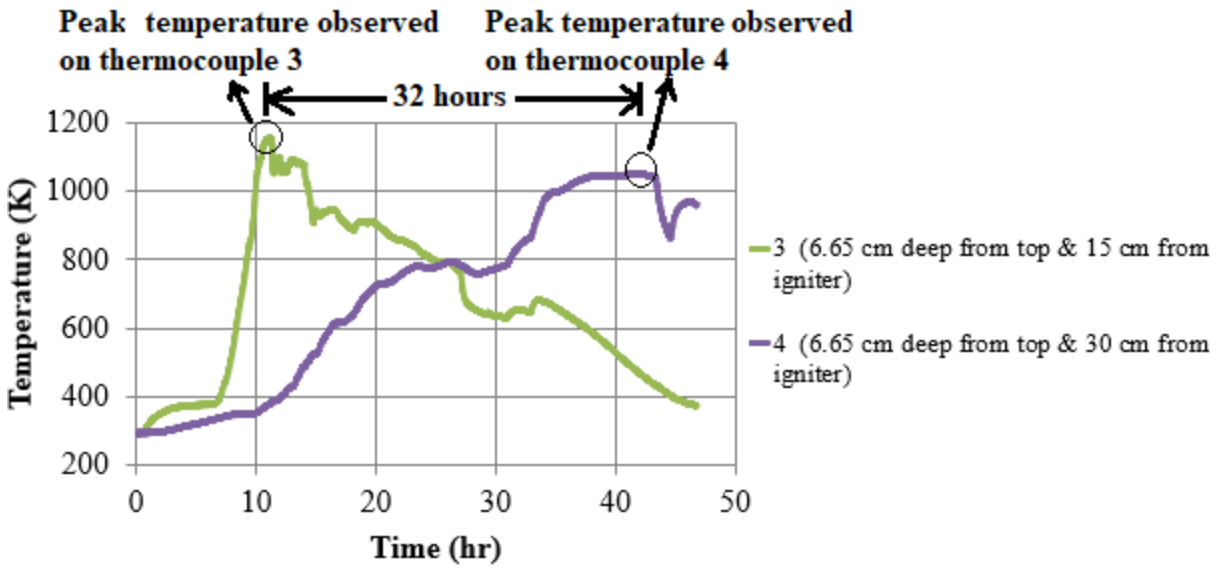

Figure 3-18 Temperature profile 1.6 cm above the gasification channel.

It is noted that although the experiment set up was equipped with water removing arrangement, the moisture condensed in the outlet system after passing the condenser was more than the water handling capacity. As a result, nearly after 7 hours of ignition, some moisture reached the GC line before removing all the water from the exhaust line. Because of the intrusion of water, the GC data recorded after 7 hours was unreliable.

Figure 3-19 shows the percentage composition of the gaseous product mixture for an initial period of ignition phase. As the GC data was spoiled due to the water intrusion, the data recorded after 7 hours of operation was not considered here. Figure 3-19 indicates a gradual decline of the oxygen and an increase of carbon dioxide during the ignition phase, however, an abrupt increase of syngas (CO and H_2) around 7th hour of operation.

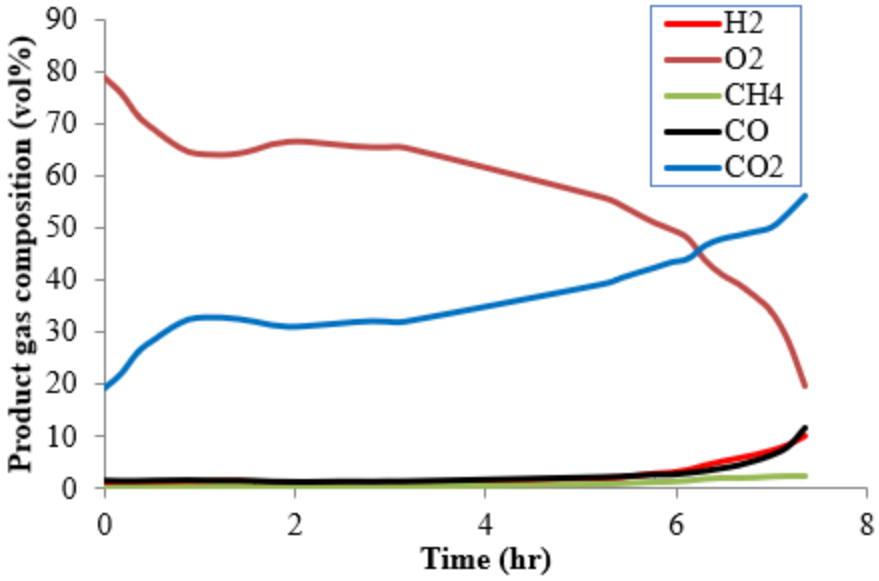

Figure 3-19 Experiment 1: percentage composition of product gas mixture.

There are two plausible reasons of the production of syngas at this earlier stage. It could be due to the effect of devolatilization that released carbon monoxide and hydrogen after evaporation of the moisture at an elevated temperature. The existence of devolatilization can be speculated due to the presence of methane which is considered as a product of devolatilization rather than a product of methanation. Methanation is favored in high pressure; however, the experiment was carried out at an atmospheric pressure. On the other hand, it could be due to the occurrence of gasification reactions rather than partial gas phase combustion. As discussed earlier, it was not possible to record the actual temperature of every space inside the coal. It can be speculated that because of prolong ignition phase, some place inside the coal reached to a temperature favorable for coal combustion and char gasification as well. The enormous water production also indicates that the gas phase combustion was a complete combustion which took place mainly in the gasification channel. Although the presence of high moisture content may reduce the temperature of the gasification channel (as observed by Stańczyk et al.[51]), the presence of moisture favored

steam gasification reaction. Beside steam gasification, the presence of CO_2 in the high temperature also favored CO_2 gasification.

After completion of the experiment, the coal block was examined in-situ by using the mini inspection camera through the injection, production and thermocouples holes. Figure 3-20 shows the images taken by the camera where the coal was found to be completely consumed leaving the ash inside the concrete tube.

Figure 3-20 Experiment 1: post burn examination from the images captured by mini inspection camera.

After removing the concrete block from the reactor and by breaking the top part, the observation remained same. Figure 3-21 shows the appearance of the concrete tube after gasification.

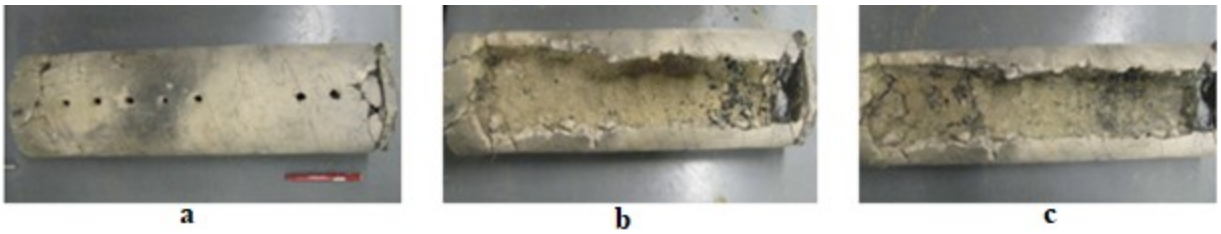

Figure 3-21 Experiment 1: Appearance of the block after gasification at different phases a) full block after gasification, b) presence of ash and coal debris, c) after removing ash and coal debris.

After the completion of this experiment, it can be concluded that the feed rate was too high for the small coal block. Due to the high feed rate, the production of water was high during ignition period and the presence of the excess oxygen that was more than the requirement for complete coal combustion hinders the coal block to have a reducing environment to favor gasification reaction. The presence of the ash signifies that coal combustion was predominant than the gasification reactions.

3.1.5.2 Experiment 2

In the 2nd experiment, coal block type 2 was used where the block was made up with 90% coal particles of 1 cm size and 10% fine coals. Ignition took place with an oxygen flow rate of 600 mL/min and propane flow rate of 116 mL/min. All the thermocouples inside the coal block were placed in the gasification channel. The temperature profile and the locations of thermocouples are shown in Figure 3-22.

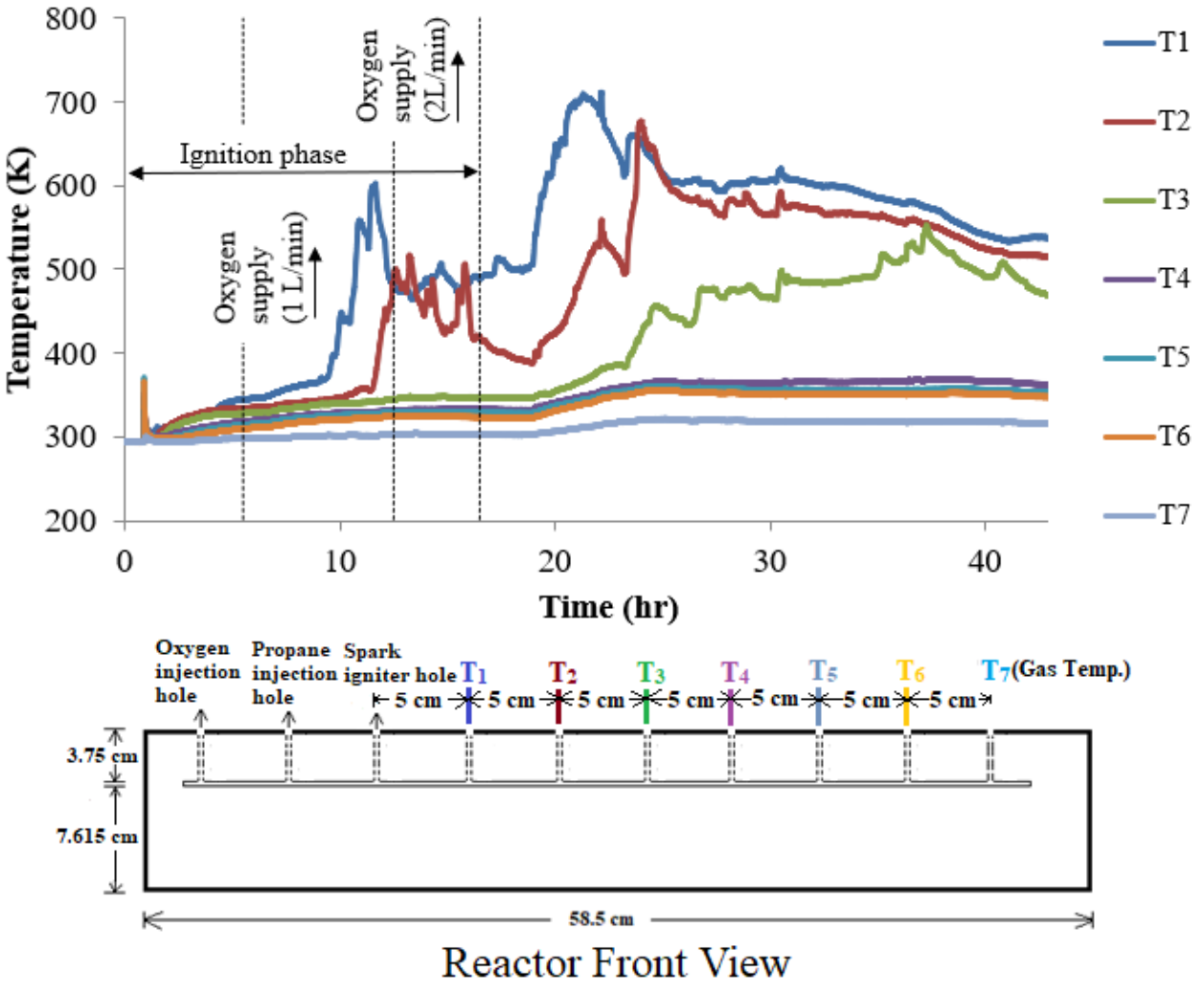

Figure 3-22 Experiment 2: temperature profile in the gasification channel.

The temperature profile for this experiment (Figure 2-22) indicates duration of more than 5 hours of prevailing low temperature after ignition. Due to low temperature observation at low flow rate of oxygen as compared to the first experiment, oxygen flow rate and propane flow rate were increased to a value of 1L/min and 167 mL/min, respectively after 5.5 hours of ignition. Among the thermocouples, the maximum temperature was noticed from thermocouple 1 which was located closest (5 cm) to the igniter. After the increase of the oxygen, the temperature observed on thermocouple 1 was found to rise to a value of 600 K after 12.5 hours of operation. At this

point, oxygen flow rate and propane flow rate were increased once again to a value 2000 mL/min and 333 mL/min for an intention to increase the temperature in the block. However, instead of increasing the temperature, a decline of the temperature was noticed. Due to the declination of the temperature, ignition phase was kept long and continued until 16.5 hours. However, after terminating the supply of propane, the temperature was started to rise to reach a maximum value of 700 K nearly at 21 hours followed by a gradual decline to a value of 530 K at 46.5 hours as observed from the thermocouple no.1. The same trend of temperature was observed by the next two thermocouples (2 and 3).

As the temperature did not to rise to a favorable gasification temperature, a product gas composition of desirable syngas was not expected. Figure 3-23 shows the percentage composition of the gaseous product mixture.

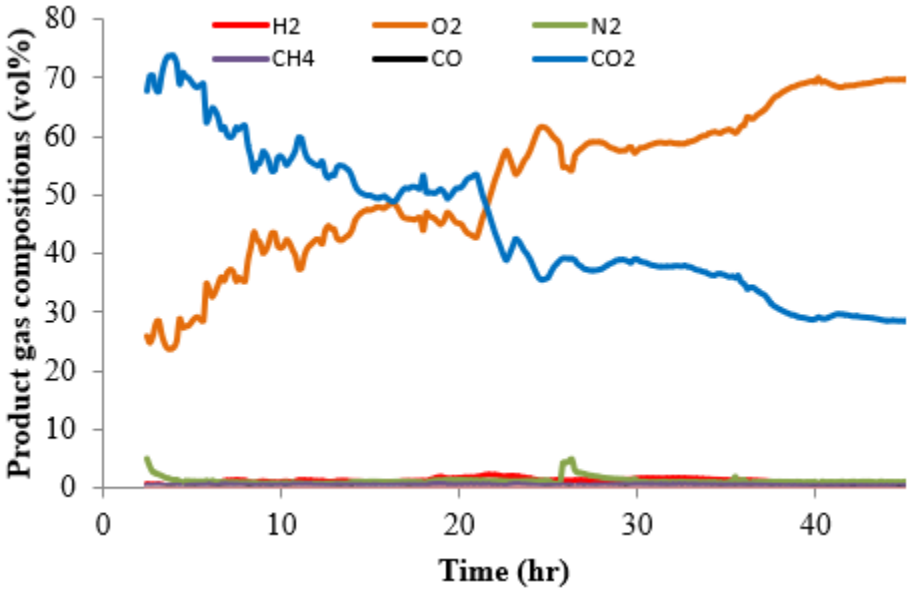

Figure 3-23 Experiment 2: percentage composition of product gas mixture.

Figure 3-23 indicates that there was not any gasification reaction. The continuous increase of oxygen and a decline of carbon dioxide from the initial propane combustion phase raised several speculations. The gradual rise of oxygen could be a result of increasing oxygen supply rate during the ignition phase. It could be a result of improper mixing of ignition gases and bypass of oxygen to some extent. It is also noticed that the increase of oxygen exceeds the concentration of the carbon dioxide followed by the termination of ignition phase. Once the propane was stopped there was no more gas phase combustion; so, carbon dioxide was not produced from gas phase combustion. The source of carbon dioxide after ignition phase could be the oxidation of carbon monoxide evolved due to devolatilization or the combustion of coal.

After removing the concrete and cutting the block, it was observed that only few coal at the top and near the igniter was burnt and the remaining coal was unburned (see Figure 3-24). The link was found to be filled by the small coal particles. So, from the observation of the exposed block, it can be delineated that the gasification channel (link) was collapsed due to the explosion during the ignition. Moreover, due to the location of the channel nearly at the top of the block made it easy for the gas feed to escape through undesirable path, preferably at the top through the empty space between the concrete block and the top coal surface. As a result, a complete combustion reaction was not achieved, and an oxygen bypass was resulted.

Figure 3-24 Experiment 2: Appearance of the block after gasification.

3.1.5.3 Experiment 3

In the 3rd experiment, coal block type 2 was used where the block was prepared by packing coal particles of 1 cm size, fine coals and cement with a ratio of 8: 0.11: 0.9. Ignition was carried out with an oxygen supply rate of 1L/min and a propane supply rate of 167 mL/min. All the thermocouples inside the coal block were placed in the gasification channel to get a temperature profile along the axial direction of the coal block.

Figure 3-25 shows the temperature profile and the thermocouple locations for this experiment. Because of the observation of low initial temperature, oxygen flow rate and propane flow rate were increased to a value of 2 L/min and 333 mL/min, respectively after 11.5 hours. However, as the increase of the temperature was not significant, the flow rates of oxygen and propane were increased further to a value of 3L/min and 500 mL/min, respectively after 25 hours. Because of the low temperature observation, the ignition phase was continued until the end of this experiment. However, the rise of temperature was not satisfactory for combustion/gasification at any time. 440 K was the maximum temperature of the block recorded in thermocouple no 1 after increasing the oxygen flow rate for second time.

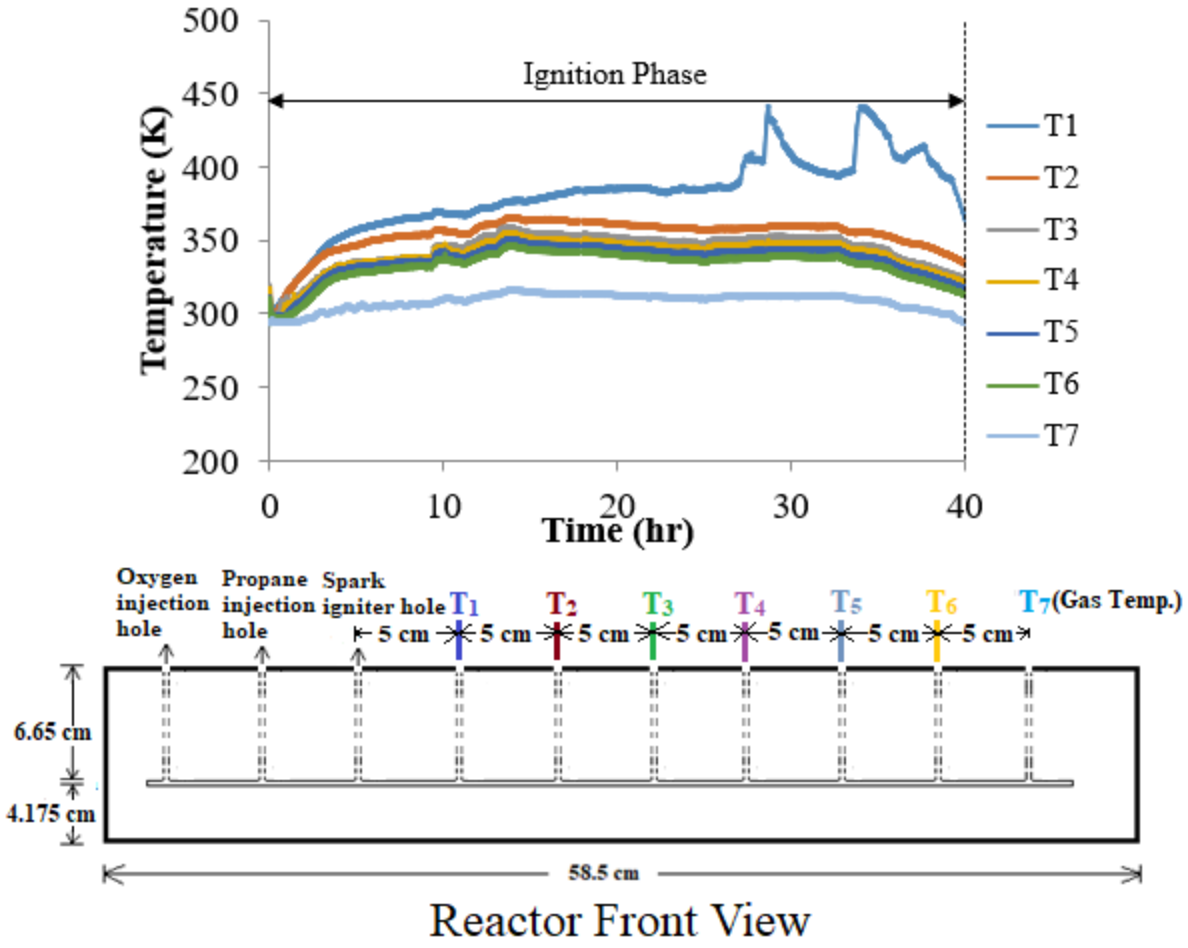

Figure 3-25 Experiment 3: temperature profile in the gasification channel.

The product gas composition shown in Figure 3-26 indicates that the gasification did not take place as the required gasification temperature was not reached. The oxygen composition was observed to increase due to i) increasing flow rate of the oxygen, ii) probably poor gas phase combustion rate and ii) the bypass of the feed gas due to collapse of the link which was detected later. As the propane was supplying until the end of the experiment, from the product gas composition, it was difficult to understand if there was any coal combustion taking place.

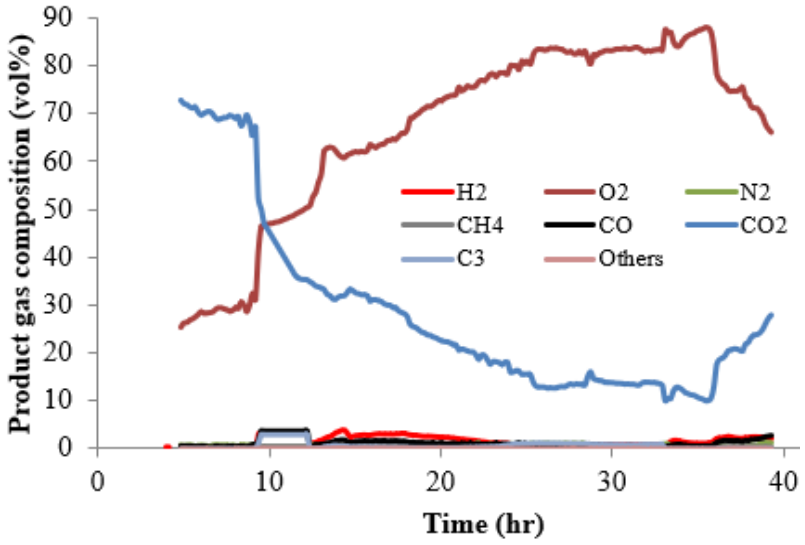

Figure 3-26 Experiment 3: percentage composition of product gas mixture.

After the completion of the experiment, the cavity was examined by taking the images inside the coal block through first three holes (injection, igniter and first thermocouple holes) and compared the images taken before conducting the experiment. The images (see Figure 3-27) provided an impression of coal combustion at the beginning near the injection hole and the igniter hole, however, the combustion did not propagate beyond the location of thermocouple 1.

After removing the concrete tube, it was observed that the tube was cracked to its weaker parts (See Figure 3-28). Beside cracking the tube, the link of the coal block was also found collapsed due to the moderate explosion during the spark of ignition. Some coal of the block was found combusted around the injection and igniter channel and above the location of thermocouple 1. The coal block looked consolidated even after the experience of heavy shacking due to the moderate explosion. From the above observation, the followings can be speculated:

- A bypass of the feed/product gas through the crack of the tube

- The combustion front travelled towards the top of the tube instead the lateral direction due to the direction of the feed/product gas flow towards the top of the tube
- The temperature near the igniter raised to a self-ignition temperature of coal and combustion took place
- The thermocouple could not experience high temperature as the thermal front did not propagate near any of the thermocouple's location.
- The ratio of the ingredients of making the coal block was acceptable to obtain a consolidated coal block.

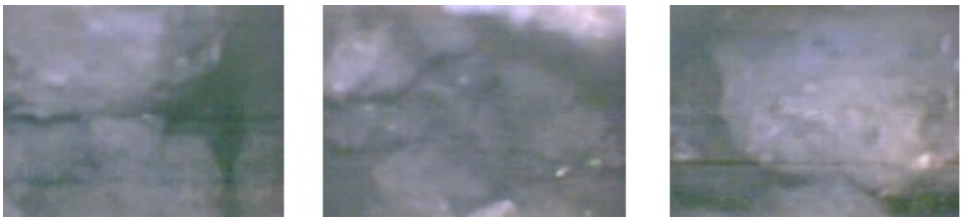

a: pre-burn raw coal images

b: post burn combusted/gasified coal images

Figure 3-27 Experiment 3: a) pre-burn, and b) post burn comparison from the images captured by mini inspection camera.

-

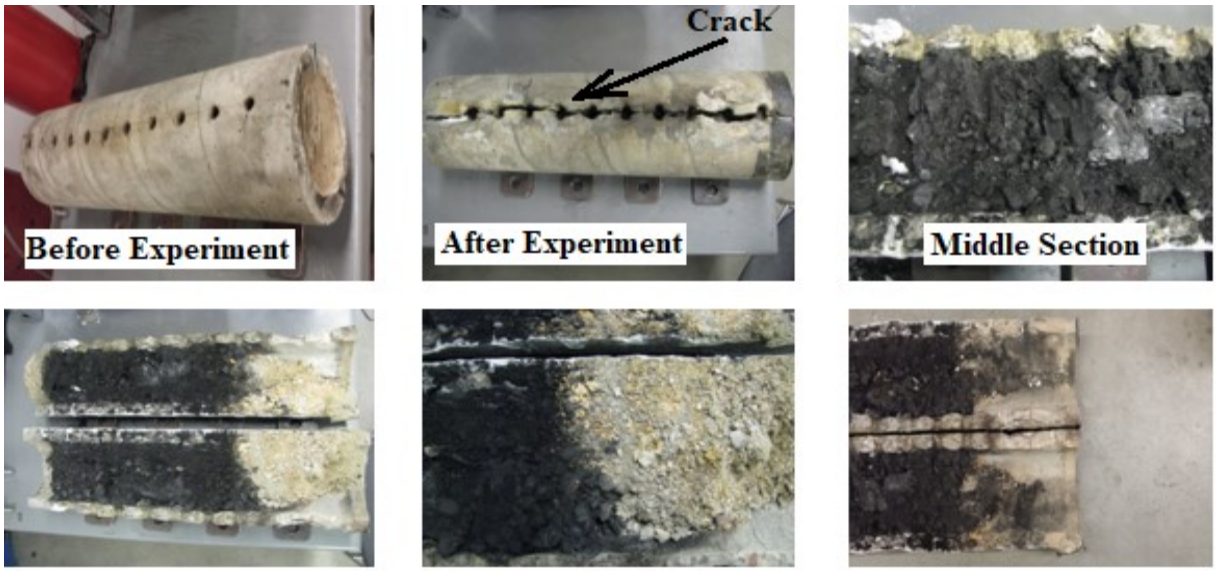

Figure 3-28 Experiment 3: Appearance of the block at the end of the experiment.

From the post burn images near the igniter, it can be concluded that the coal near the igniter was almost completely combusted. During combustion, the moderate high temperature is considered to trigger devolatilization. The presence of syngas is considered the product of the devolatilization.

3.1.5.4 Experiment 4

In the 4th experiment, the coal block was prepared following the composition and the procedure of 3rd experiment. However, a different approach of ignition gas mixing process was adopted in this experiment to avoid poor ignition gas mixing and moderate explosion experienced in the earlier experiments. In this new approach, the ignition gases were injected through a collinear tube along the lateral direction of gasification channel (see Figure 3-12). Ignition was carried out with oxygen flow rate of 750 mL/min through the annular tube and propane flow rate of 125 mL/min through the inner tube. Because of the new approach of ignition gas mixing process, the

explosion during sparking was observed mild as compared to earlier experiments. All the thermocouples inside the coal block were placed in the gasification channel.

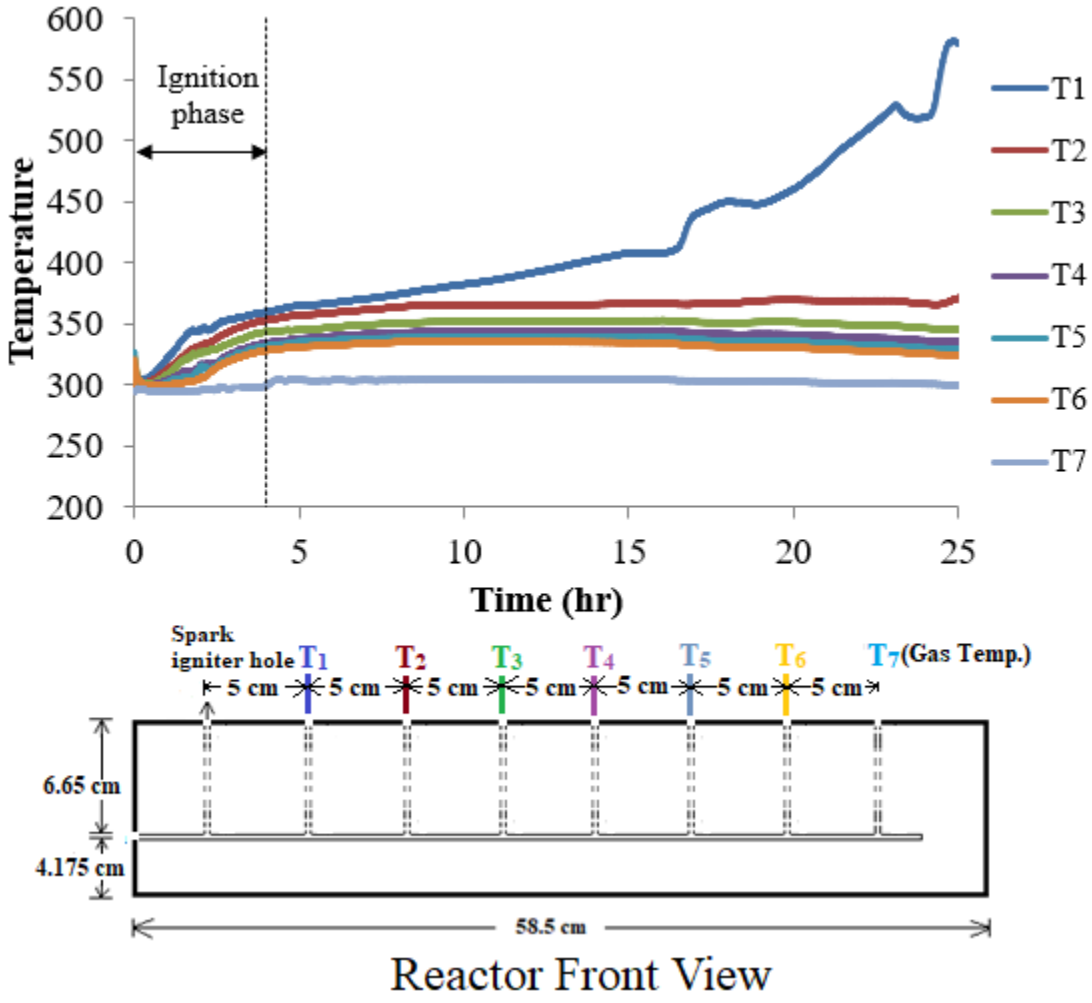

Figure 3-29 Experiment 4: temperature profile in the gasification channel.

The temperature profile and the thermocouple locations for this experiment are shown in Figure 3-29. From the figure (Figure 3-29) it is observed that the temperature did not reach to a desired level for self-ignition of coal; nevertheless, because of previous experimental experience, the flow of propane was terminated after 4 hours. The thermocouple near the igniter showed a temperature of 360 K, however, after terminating the ignition, the temperature continued to increase to a maximum value of 580 K near at 25 hours of operation. The temperatures observed

on all other thermocouples were almost the same throughout the experiment. The temperature was not favorable for gasification reaction.

The production gas mixture composition (see Figure 3-30) shows the same trend of increasing oxygen concentration and decreasing carbon dioxide as observed in the last two experiments. The presence of carbon monoxide and hydrogens was also noticed; however, they cannot be considered as a product of gasification due the low temperature environment as discuss later in this section.

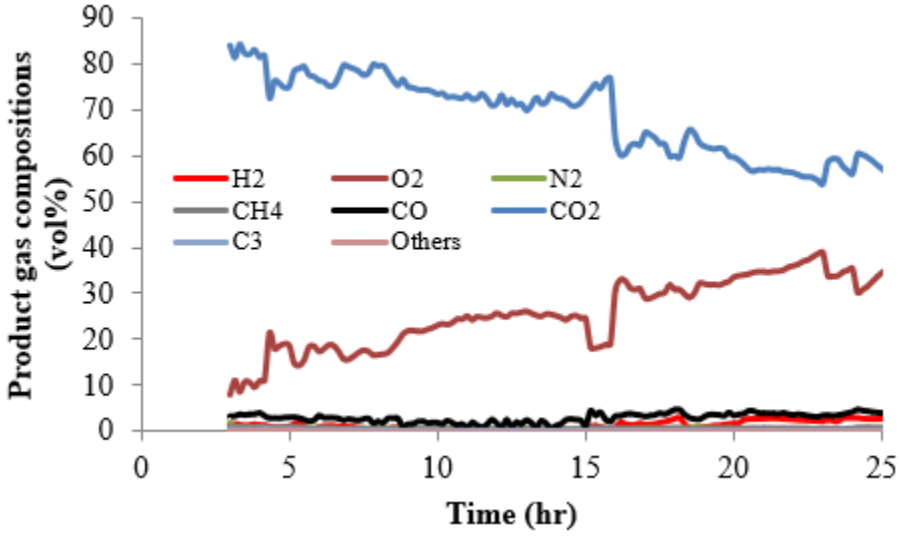

Figure 3-30 Experiment 4: percentage composition of product gas mixture.

After removing the concrete tube, it was observed that the tube was cracked, and the link was collapsed (See Figure 3-31). The scenario was same as observed in the previous experiment (experiment 3). Because of the sign of coal combustion near the igniter, the speculations for this experiment also remain same as discussed in experiment 3.

The scenario of post burn coal block also looks same as the previous coal experiment. From the observation of this post burn block and from the experimental evidences, the presence of syn gas can be explained. The presence of combusted coal and ash in the post burn coal block indicates that the coal block reached to a self-ignition temperature which triggered combustion reaction. The combustion temperature also triggered devolatilization. Carbon monoxide and hydrogen are believed to be the products evolved from devolatilization. However, the presence of carbon monoxide can also be explained from the experimental experience. In the absence of gasification reaction, the presence of carbon monoxide is speculated as a product of oxygen depleted environment which was experienced several times during the experimental operation. During the experiments, the collinear tube was affected several times by the clogging of coal particles or the deposit of water/condensate and seized the oxygen flow rate. This could be due to the bending of collinear tube near the inlet of the coal block (see Figure 3-12). The oxygen flow rate was restored each time by increasing oxygen injection pressure. However, before restoring the oxygen flow rate, there was oxygen depleted environment which could have triggered the partial combustion and produced carbon monoxide. Some of the carbon monoxide might have participated in water-gas shift reaction to produce hydrogen.

Figure 3-31 Experiment 4: Appearance of the block at the end of the experiment.

3.1.5.5 Experiment 5

After experiencing the collapse of the link due to moderate/mild explosion during the ignition, experiment 5 was designed to overcome this problem by changing the mode of the experiment where there was no directional gasification channel. In this run, the whole reactor was filled with coal particles of 1 cm size. Because of loose pack coals, this gasification experiment is closely related to packed bed coal gasification. In this experiment, ignition took place with an oxygen supply rate of 700 mL/min through the annular tube and propane supply rate of 90 mL/min through the inner tube.

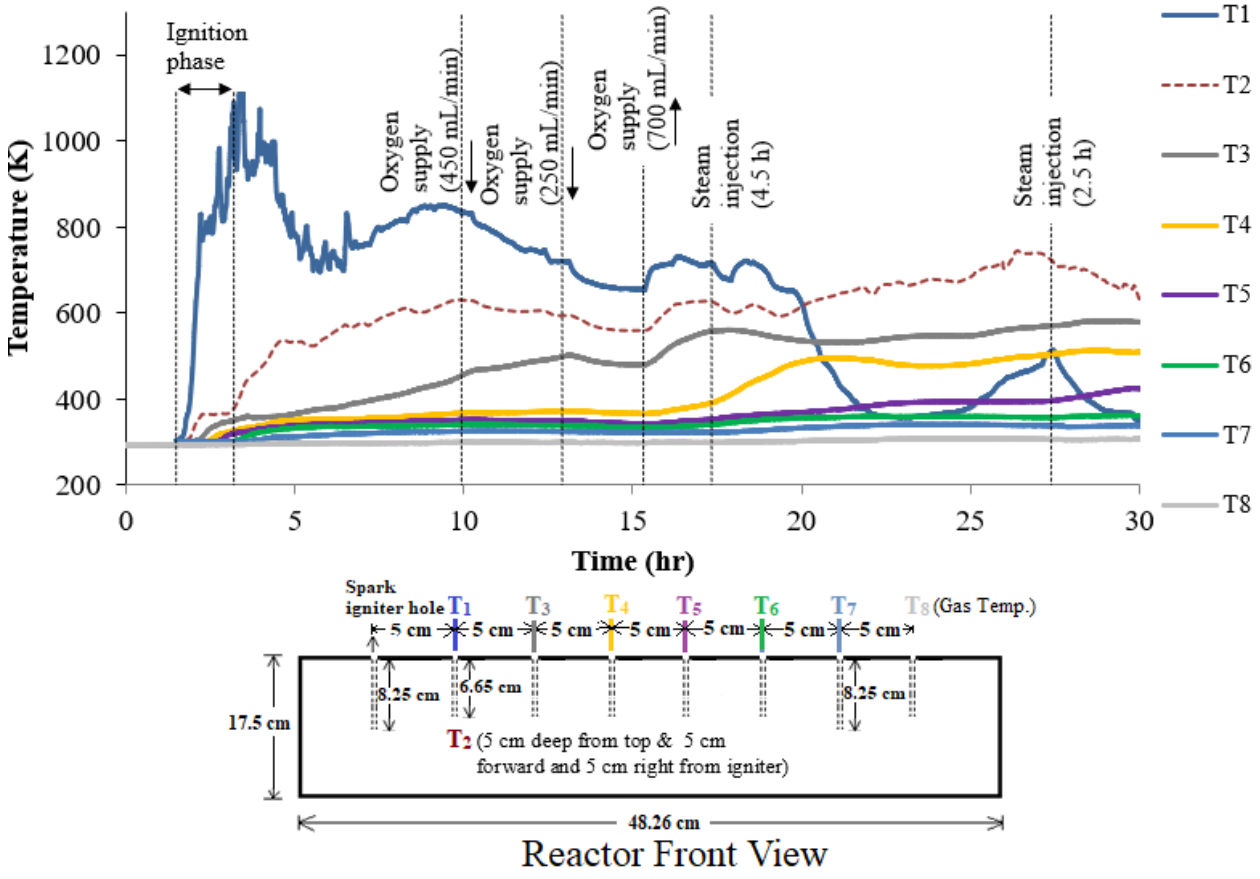

Figure 3-32 Experiment 5: temperature profile inside the packed bed at different locations.

Figure 3-32 shows the temperature profile for this experiment. After one and half hour of ignition as the temperature reached to value of more than 1000 K which was more than a temperature required for a self-ignition temperature of coal, ignition was terminated. However, because of the presence of the residual propane inside the reactor, the temperature was found to increase followed by a decline phase due to depletion of the propane. Later, the gradual increase of the temperature observed on thermocouple 1 indicated the shift of the control of combustion from propane to coal.

As it was observed from previous experiment that the locations of thermocouples are also a factor to capture the actual temperature in a plane. It can be noted that for this experiment, thermocouples 1 and 2 were located at same distance from the igniter along the axial direction of the reactor; however, they are apart from each other in the radial direction. Thermocouple 1 was placed 8.25 cm deep from the top and 5 cam cm from the igniter, whereas thermocouple 2 was placed 5 cm deep from the top and 5 cm right from the line of thermocouple 1 which was in line with other thermocouples (See Figure 3-33).

It is observed that during ignition phase, the maximum difference of the temperature noted from those two thermocouples was nearly 600° C, however, during combustion and gasification phase the maximum difference was nearly 200° C. In general, the difference indicates the role of heat convection and conduction. During ignition phase, propane combustion predominated, so the heat propagated mainly through the convection of hot combusted gaseous products. On the other than, during coal combustion, the adjacent coals also participated in combustion and the conduction of coal beside the convection of gaseous product also took place; as a result, the

temperature difference was found declined in the latter case. From this observation, it can be concluded that even a minimum distance of a thermocouple probe from the actual thermal front might not predict the actual temperature of the thermal front.

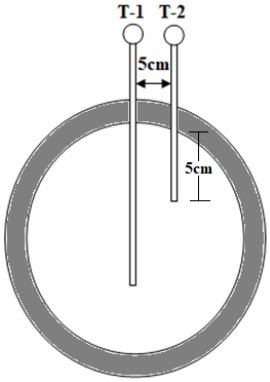

Figure 3-33 Orientation of the thermocouples 1 and 2 side by side in the reactor.

After 9 hours of ignition, oxygen flow rate was reduced to 20% from the initial flow rate and after 12 hours of ignition, oxygen was reduced further to 50% from the initial flow rate. The declination of the oxygen accompanied with a declination of the temperature. Oxygen flow rate was restored to its initial value nearly after 14.5 hours of the ignition. Restoration of oxygen flow rate resulted an increase of the temperature; however, that did not exceed the previously recorded temperature (800 K).

After 16 hours of ignition, steam at 350 °C with a steam to oxygen ratio of 2.5:1 was injected for a period of 4.5 hours to enhance the gasification reaction and observed the effect of steam on the temperature. Injection of steam resulted a sharp declination of the temperature observed in thermocouple 1 due to low steam temperature and depleted coal near that thermocouples. However, the injection of steam did not reduce the temperature observed on other thermocouples. After terminating the supply of steam, the temperature observed in thermocouple

1 was found to increase, however, injection of steam 2nd time after 26 hours of ignition, the temperature was noticed to reduce further. Injection of steam in the latter phase also showed a decline of temperature observed on thermocouple 2. The reason of declining temperature observed on thermocouple 2 is considered the same reason as observed for the case of thermocouple 1 during initial phase of steam injection, i.e., depletion of the coal near the thermocouple. The duration of the 2nd phase steam injection was 2.5 hours.

It is noted that for a packed bed the flow of feed gas and gaseous products cannot be directed to a definite path as it could be done for a coal block with a created channel. As a result, it is very unlikely to capture the actual thermal front by the thermocouples if several thermocouples are not placed at different locations in a plane. So, in the experiment, the temperature at different locations indicated in the figure might not represent the actual temperature in the coal block. The actual temperature is expected to be higher than the observed temperature from the thermocouples. However, the coal temperature distribution along the length in the reactor at different times can provide some hints of the propagation of the reaction and drying/pyrolysis fronts at different speed. Figure 3-34 shows the temperature distribution along the lateral direction of the reactor. The movement of the peak temperature indicates that only one third of the coal was experienced comparatively higher temperature during the time span of the experiment. If the experiment were in operation longer, the consumption of coal would be much higher. Some variation of the temperature can be explained as the effect of steam injection and change in oxygen supply rate.

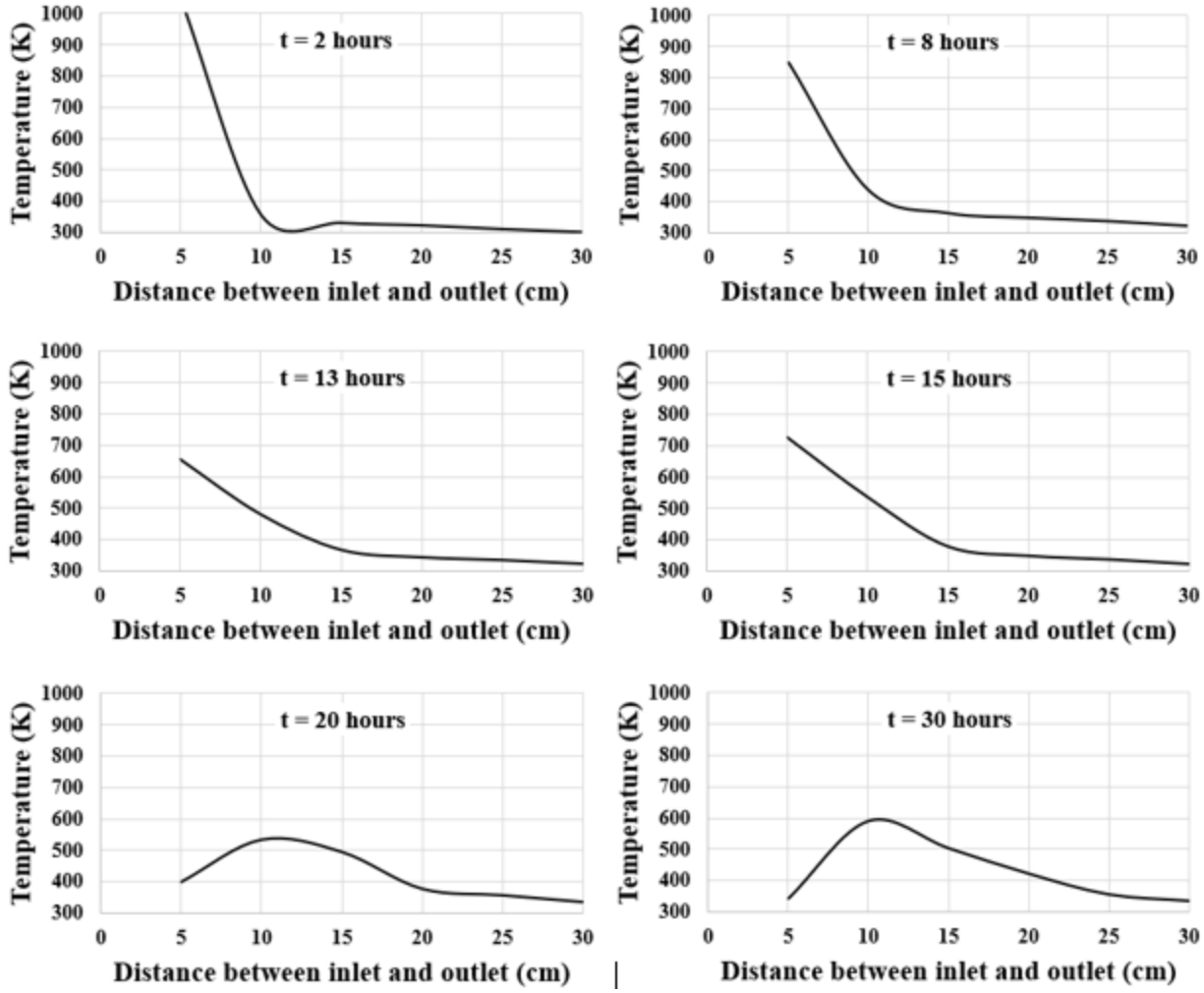

Figure 3-34 Experiment 5: temperature measurement at different times during the experiment.

The product gas composition shown in Figure 3-35 indicates some sign of gasification reactions even the ideal gasification temperature was not always observed from the thermocouples. Oxygen and propane were found to decline sharply right after the ignition. This indicates that ignition phase was successful. After termination of propane, oxygen did not rise. This is an indication of continuous consumption of oxygen which could be due to the oxidation reaction of the pyrolysis gases or due to the coal combustion.

The presence of oxygen in the GC data long after the termination of ignition phase indicates that some unreacted oxygen existed throughout the process. Reducing the oxygen flow rate did not affect the content of oxygen in the product gas. Because of the packed coal particles, feed gas was not directed to go through a definite path; as a result, some of the feed gas escaped the oxidation zone before exiting through the production line of the reactor.

The injection of steam for both times was found to increase the oxygen and decrease the carbon dioxide. This could be due to the drop in the reactor temperature and decreasing coal combustion rate. Hydrogen production was found to be increased, however, carbon monoxide was found to be nearly unresponsive due to steam injection.

From Figure 3-35, it is also observed that right after the ignition, the initial production of carbon monoxide and hydrogen was found very high as compared to the production observed from the rest of the experimental duration. Because of the explosion during ignition, oxygen was readily consumed, and a reducing environment created for a short period and some carbon monoxide production took place due to partial oxidation; however, the increase of hydrogen and methane was due to the release of pyrolysis gas during the initial phase high temperature. After the ignition phase, the production of hydrogen and carbon monoxide is considered to be the products of devolatilization as well as the gasification reactions as the temperature inside the reactor is speculated to be merely favorable for gasification.

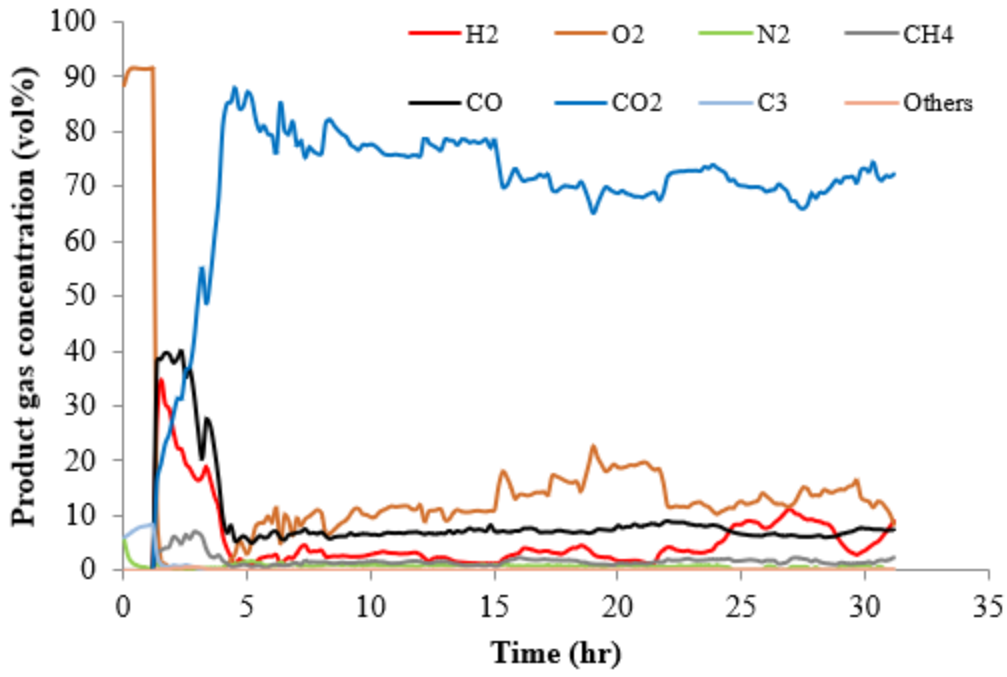

Figure 3-35 Experiment 5: percentage composition of product gas mixture.

Figure 3-36 shows the variation of the gross calorific value of exhaust gas, on dry basis, with time where the gross calorific value was calculated using the formula obtained from Harker and Backhurst [109] as follows:

$$Calorific\ Value\ \left(\frac{KJ}{mole}\right) = \sum_i^N H_i \times y_i \qquad (Eq.\ 3.1)$$

Where; H_i is the heat of combustion and y_i are the mole fractions of the gas species 'i', respectively. However, the calculation was based on the exit concentration of CO, H_2 and CH_4 only. It is noticed that the calorific value was highest at the beginning followed by more uniform value throughout the experiment. The higher production of syngas, as explained earlier, attributed higher calorific value shown in the ignition phase. The uniform calorific value indicates almost a stable syngas production throughout the experiment.

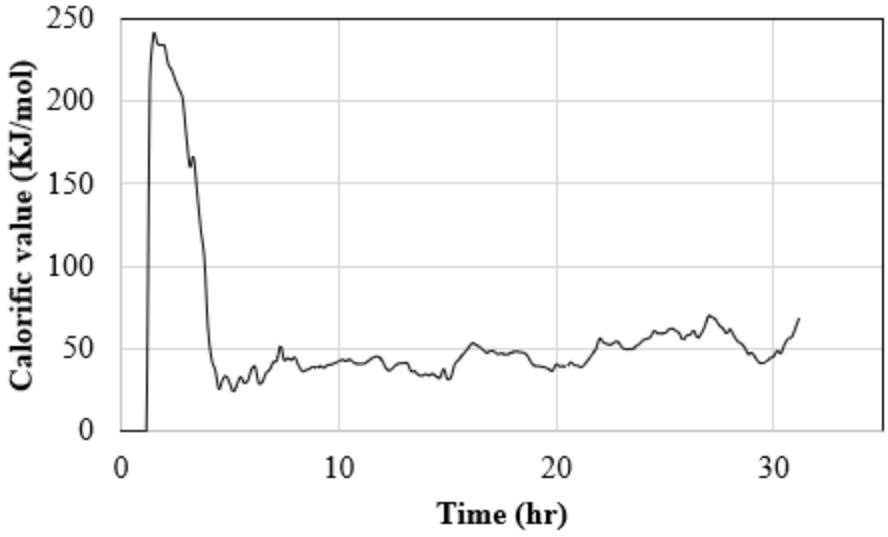

Figure 3-36 Experiment 5: calorific value of gas with time.

In this experiment, the mild explosion was also experienced during the ignition. Because of the explosion, there was a possibility to have an open channel near the top of the coal surface underneath the steel vessel where light gases could reside and travel through the empty space towards the end and finally through the coal to escape from the reactor through the exit channel which was 8.25 cm deep from the top.

Figure 3-37 Experiment 5: post burn images from all the available holes captured by mini inspection camera.

Figure 3-37 shows the gasified coal captured from the top holes of the reactor after the completion of the experiment. It shows that coal was consumed from most of the parts. However, near the exhaust channel there are some unburnt coal and ungasified char.

Figure 3-38 shows the gasified char and unburnt coal inside the reactor. The last image confirms the unburnt coal which could be gasified if the experiment would have continued longer. After calculating the unburnt coal, it was found that even with low temperature almost 52% coal was consumed.

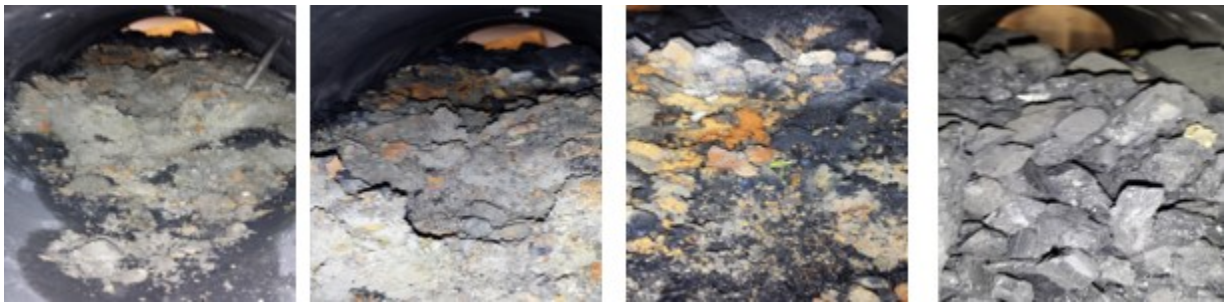

Figure 3-38 Experiment 5: Appearance of the coal bed at the end of the experiment.

3.1.5.6 Experiment 6

The last experiment followed the experimental procedure of experiment 5. However, due to the possibility of the formation of empty space between the top of the coal surface and the steel vessel, the packed bed of coals was made tighter than the earlier experiment. It was expected that there would not generate an empty channel even after mild explosion during the ignition. However, the tight packed bed created another problem which has been discussed later in this section. In this experiment, ignition took place with an oxygen supply rate of 750 mL/min through the annular tube and propane supply rate of 95 mL/min through the inner tube. However,

obtaining a sustainable ignition was difficult. For each trial of ignition, the feed gas was seized to follow because of the clogging of the exit channel due to coal debris after the mild explosion. The pressure inside the reactor continued to build up due to the clogging of the exit tube which forced to terminate the experiment to clean the exit channel. Once a successful ignition was achieved, it took 11 hours to reach a reasonable high temperature (450 °C) which was more than a self-ignition temperature of coal before terminating the ignition phase (see Figure 3-39). The delay of increasing the temperature was due to the reduction of feeding rate of ignition gas mixture (oxygen and propane), which was detected after one hour of the ignition. As a result, the exit line was required to be cleaned while running the experiment by using an alternative channel to pass the combusted gas to the vent directly.

The orientation of the locations of thermocouple 1 and 2 in the radial direction followed the orientation observed in experiment 5 (see Figure 3-33). It is also noted from Figure 3.36 that the difference of the temperature observed between thermocouple 1 and 2 after ignition phase was nearly 200 °C which is same as observed in the previous packed bed experiment.

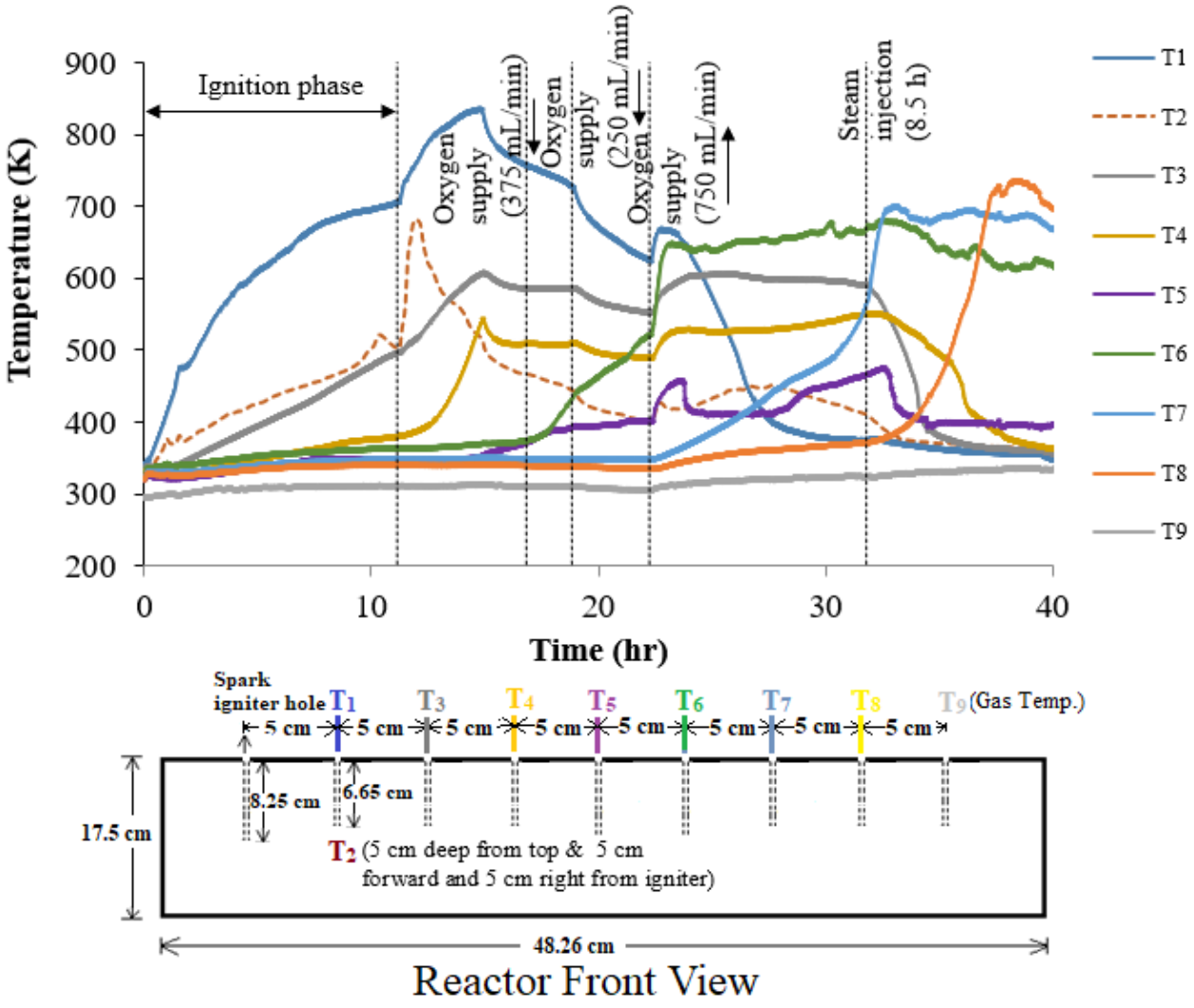

Figure 3-39 Experiment 6: temperature profile inside the packed bed at different locations.

Because of the presence of excess oxygen in the product gas (see Figure 3-42), oxygen flow rate was reduced to 50% from the initial rate after 15 hours and further reduced to 35% from the initial rate after 19 hours of ignition. Further reduction of oxygen supply rate did not reduce the oxygen concentration in the product gas but decreased the temperature significantly. To increase the temperature, oxygen was restored to its initial flow rate after 22.5 hours. The restoration of oxygen flow rate was reflected by the increasing temperature observed in most of

thermocouples; however, it did not change the declining trend of the temperature observed on thermocouples 1 and 2 which were possibly affected by the depletion of the coal near the thermocouple probes.

The temperature recorded on thermocouple 5 after 20 hours of operation was observed very low as compared to the temperature observed on adjacent thermocouples 4 and 6. It is noted that thermocouple 5 was located 1.6 cm lower than the position of the other two thermocouples. The peak temperature observed on thermocouples 6, 7 and 8 shows an increase in the lateral direction. Considering the locations of all the thermocouples, igniter and production channel, it can be speculated that the thermal front followed an incline direction from the point of ignition to the production line (see Figure 3-40). From the peak temperature recorded on thermocouple 7 and 8, the movement of the thermal front can be calculated. It took five hours to move 5 cm along the reactor length. Because of high porosity, consumption of coal and the possible empty space in between the coal surface and the steel vessel, the product gas may rise to the top of the coal surface due to convection; however, that product gas must return to the exit channel to maintain a continuous flow of production to the outlet. Figure 3-40 also shows the anticipated direction of the product gas composition.

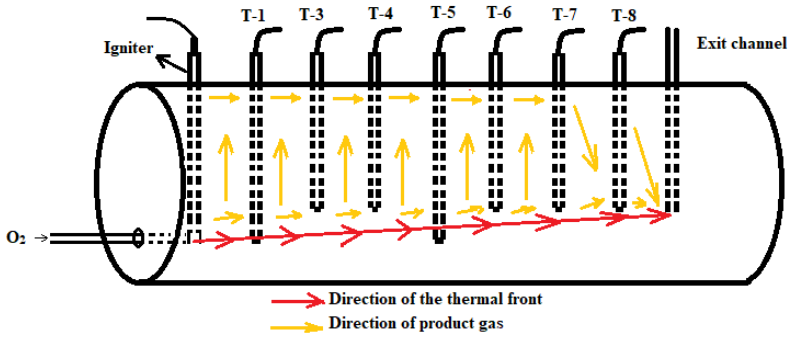

Figure 3-40 Direction of thermal front and the product gas in the reactor.

Steam at 350°C with a steam and oxygen ratio of 2.5:1 was injected after 32 hours for a period of 8 hours. However, steam injection affected the temperature of first four thermocouple which showed a decline in temperature after steam injection; however, the rest of the thermocouples were not found to be affected. Based on previous experimental evidences, it can be concluded that steam injection predominantly affects the space where coal is already depleted or nearly depleted due to the consumption by the surface reactions.

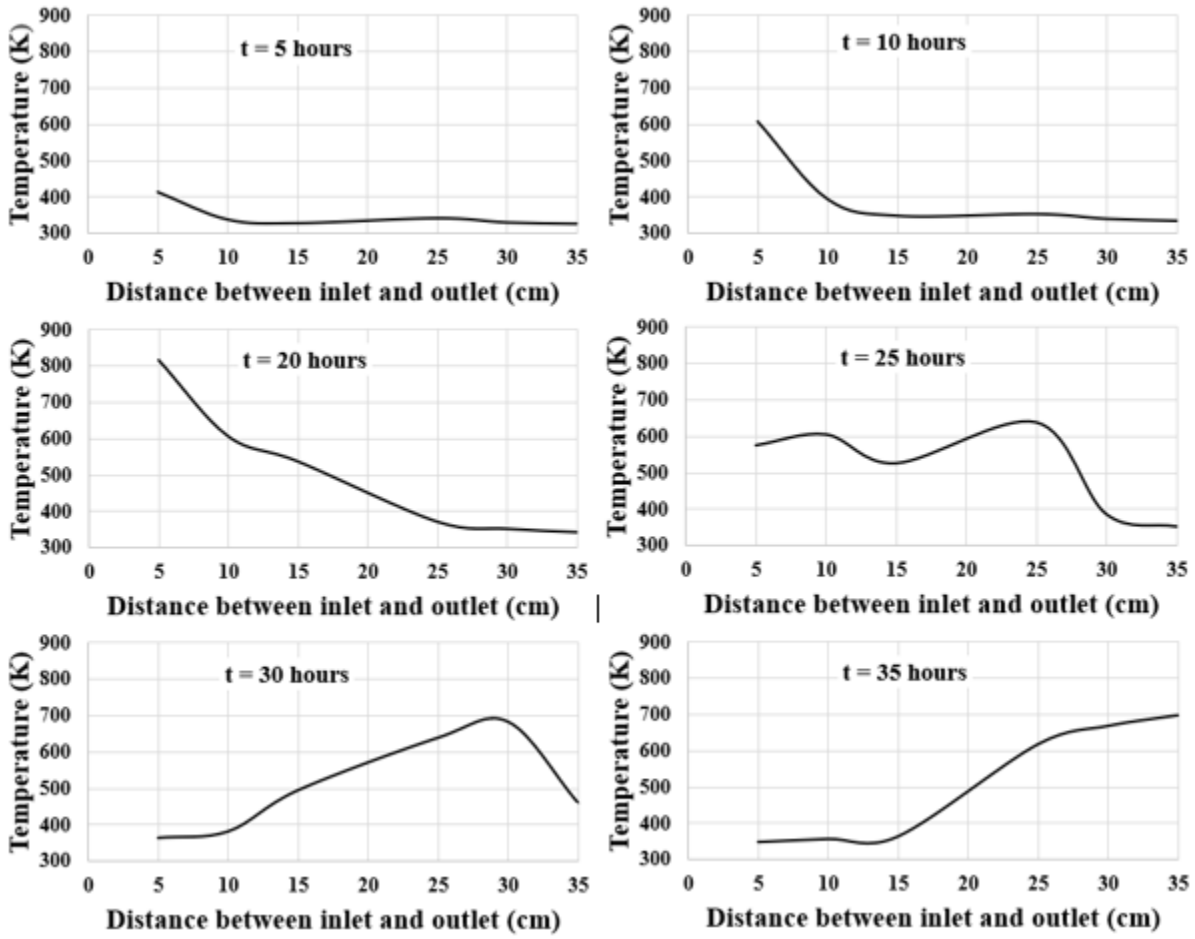

Figure 3-41 Experiment 6: temperature measurement at different times during the experiment.

Figure 3-41 shows the temperature distribution along the lateral direction of the reactor at different times. The rate of progress of peak temperature along the axial distance can be observed from this figure. However, due to the different location, the temperature data obtained from thermocouple 5 was discarded. As a result, the temperature showing at 20 cm distant from the inlet is an average value of its adjacent places. Beside this, some variation of the temperature can be explained as the effect of steam injection and change of oxygen supply rate, as mentioned before. In this experiment, the rate of peak temperature movement is observed faster than the peak movement observed in experiment 5. It can be speculated that because of long ignition phase, more coal came into contact to the hot combusted gas and more surface area was involved in combustion reaction after the ignition phase. As a result, the movement of the thermal front was faster in this experiment.

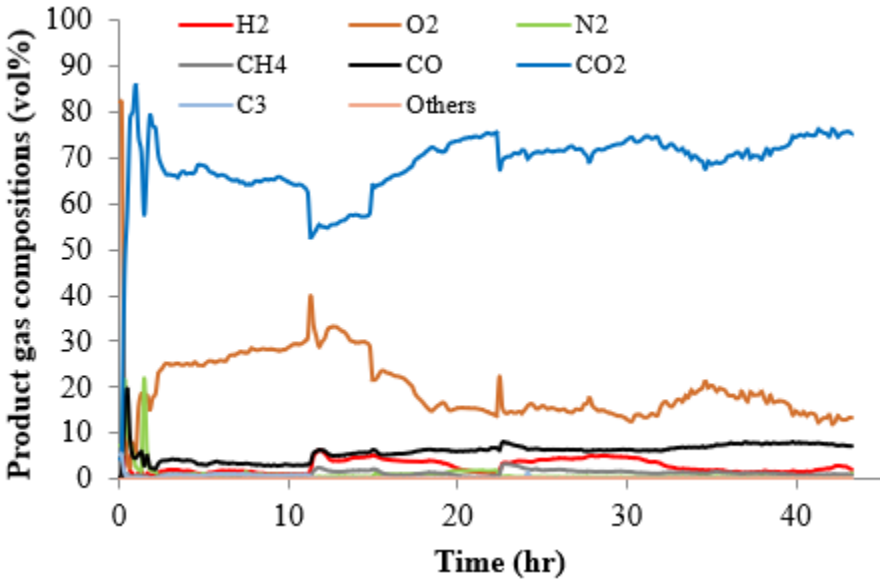

Figure 3-42 Experiment 6: percentage composition of product gas mixture.

From Figure 3-42, it is observed that some syngas at lower concentration was existed throughout the experiment as it was observed in experiment 5. The reason of these products is already mention in the previous experiment.

The calorific value observed in this experiment (see Figure 3-43) is not similar as observed in the previous experiment. Because of lower temperature observation in the ignition phase, the production of the syngas was low, which has a decline effect on the calorific value. However, a stable value was not observed until a latter phase of the experiment. This indicates that the product of the syngas was not uniform, which in turn indicated the instability of the process. This is not abnormal for this experiment as a number of times, the exit line was blocked and needed to be cleaned which in turns had an effect on GC gas analysis as the product gas in the GC was disturbed several times. The calorific value also shows the zigzag trend because of this anomaly.

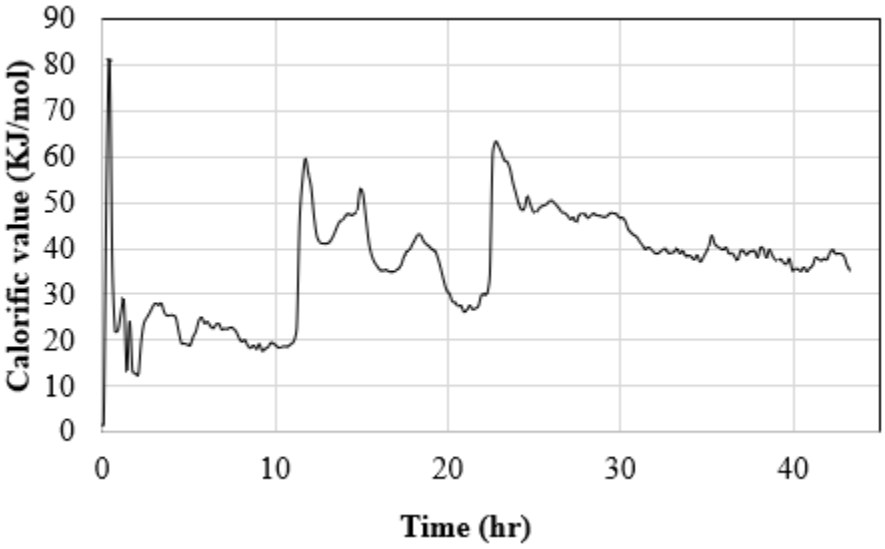

Figure 3-43 Experiment 6: calorific value of gas with respect to time.

The following figure (Figure 3-44) shows the coal consumption after the gasification experiment. After calculating the unburnt coal, it was found that even with low temperature almost 47% coal

was consumed. The coal consumption was less than the previous experiments despite of longer experimental time. It could be due to the low initial temperature during ignition phase.

Figure 3-44 Experiment 6: Appearance of the coal bed at the end of the experiment.

All the experiments described above had one common feature of producing lots of carbon dioxide as compared to carbon monoxide. It can be seen from Figure 3-45 that the production of carbon monoxide is favored at a temperature more than 1000 °K and the concentration is very low at a temperature of 700 °K. As the experiments were carried out in an atmospheric pressure and the temperature merely exceeded 1000 °K, the production of carbon dioxide was preferred.

In all the experiments, methane concentration was observed almost similar throughout the experiment. It can be speculated from this nearly constant value that the methanation did not take place; methane was only the product of devolatilization. Gregg and Edgar [14] reported from the evidence of Soviet field operation at Podmoskovia that the reaction rate for the formation of methane is not appreciable at low temperature and pressure. As the experiments were carried out at atmospheric pressure, the production of methane observed in all the experiments can be justified.

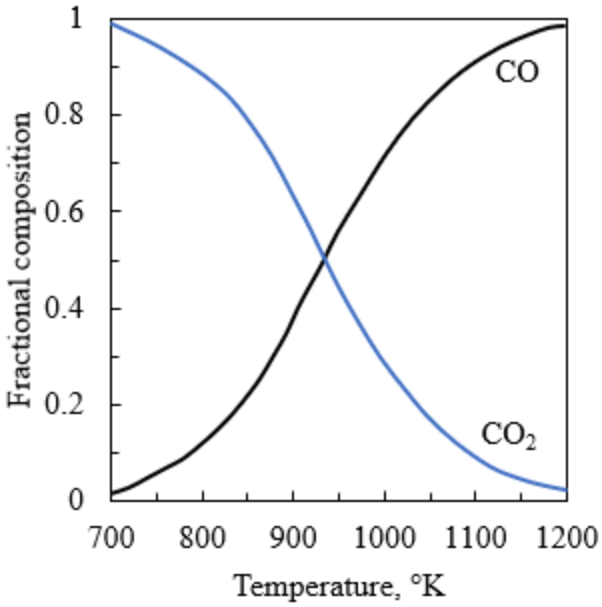

Figure 3-45 Fractional composition of CO and CO_2 in equilibrium with β-graphite at one atmosphere as a function of temperature (redrawn from Gregg and Edgar [14]).

3.1.6 Problems experienced in lab-scale experiments

During performing the Ex-situ UCG experiment several difficulties were encountered. The followings are the main difficulties that were experienced:

- Explosion during ignition.
- Bypass of feed gas
- Measurement of the temperature by thermocouples

3.1.6.1 Explosion during ignition

Ignition is one of the vital steps of gasification process to initiate combustion followed by gasification reactions. However, in each experiment an explosion was observed during ignition. It is mentioned that ignition did not occur until the gasification channel was heated by passing hot air at 180°C to drive away some moisture near the ignition probe. To ensure a complete gas

phase combustion 20% excess oxygen was used with propane as an ignition mixture, however, the explosion could not be eliminated. This could be due to the improper mixing of oxygen and propane near the ignition probe. For the first three experiments, oxygen and propane were supplied from two different channels which were 5 cm apart from each other. Ignition probe was 5 cm apart from propane injection channel (see Figure 3-46). After reaching the ignition gases towards the gasification channel, it was difficult to maintain a constant mixing ratio as the gas can follow other path than the gasification channel. To facilitate injection line, production line, igniter and the thermocouples, several holes were drilled through the concrete tube into the coal block until the drill bit reached the gasification channel. However, after placing injection line, production line, igniter and several thermocouples following the alignment of each hole from steel reactor to coal block, it was not possible to fill the gaps inside each hole (See the gaps in Figure 3-46). Only the holes of the steel reactors were plugged using Swagelok tube fittings. As a result, the feed gas was free to flow through those gaps and travelled between the steel reactor and the concrete coal block. This could lead an improper mixing of oxygen and propane followed by a formation of explosive mixture in some places inside the reactor.

To reduce the mixing problem, collinear tubes were used for the last three experiments. The igniter probe was placed 1cm away from the exit line of the collinear tubes. By this method, the intensity of the explosion was reduced but not eliminated. As the collinear tubes were very near to the ignition probe, oxygen and propane flowing out from annular and inner tubes, respectively might not get enough space to mix properly. Further, the explosion could be due to the explosive mixture that might reach in some place inside the reactor as mentioned earlier.

The explosion caused collapse of the link and blockage of the collinear tubes due to the deposit of coal debris and condensate.

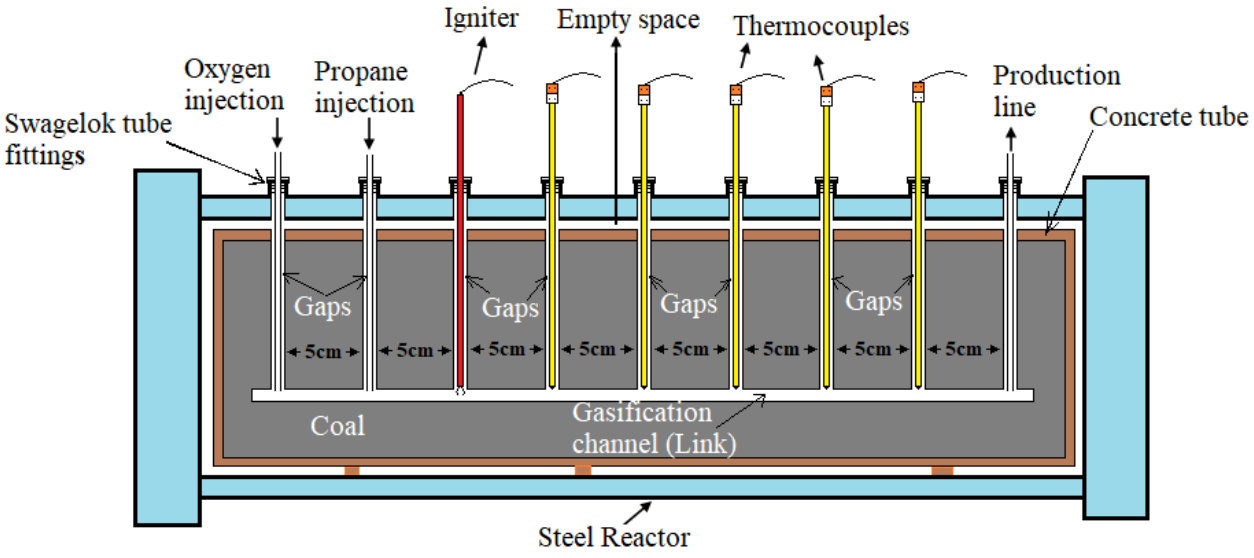

Figure 3-46 Front view of steel reactor and coal block arrangement with necessary fittings.

3.1.6.2 Bypass of feed gas

The bypass of feed gas is related to the explosion of the ignition. Because of the explosion, the link was collapsed. As a result, a significant portion of feed gas could bypass through the gaps of the drilled holes near the ignition probes. The production gas could also follow the same path as the link was blocked. Because of this problem, it was difficult to maintain an oxygen deficient gasification condition and a signification amount of oxygen was present in the product gas. Even without the ignition problem, this problem could not be eliminated completely because of the existence of gaps inside the holes of each feed line, igniter and thermocouple.

3.1.6.3 Measurement of the temperature by thermocouples

Experiments 2 and 4 showed a progress of coal combustion after termination of propane flow. However, the recorded temperature by the thermocouples was less than a self-ignition temperature (~350°C) of coal during the ignition phase. It indicates that the coal reached to a self-ignition temperature of coal, however, the temperature was not captured through the thermocouples. These could be due to the following reasons:

- Locations of the thermocouples
- Physical conditions of the thermocouples

Maximum 8 thermocouples were located in the lateral direction from injection to production lines. The thermocouples were apart from each by 5 cm. In the Ex-situ reactor thermal or combustion front is considered to have highest temperature. However, the propagation of the thermal front was not always in the lateral direction due to other problems as discussed earlier. It could be assumed that the thermocouples were not always located in the thermal front. The thermocouples might be few centimetres apart from the thermal front. However, from experiment 5, 200 to 600°C of temperature difference was observed from thermocouple 1 and 2 which were only 5 cm apart from each other in the same place as seen in Figure 3-33.

Thermocouples located in the gasification channel provided the temperature of the hot gas that were thermally equilibrium with coal particle surface temperature. However, the thermocouples could not read the coal particle surface temperature, as the thermocouples were not directly inserted into the coal particles. Because of the bigger hole compared to the diameter of the thermocouples, the thermocouples were considered suspended in the holes (see Figure 3-46).

That is why, most of the thermocouples were only able to record the temperature of the gas temperature near each location. The coal particle temperature is considered very high in the thermal front. Heat is conducted through conduction on coal surface. Due to high heat release the radiation heat transfer also takes place in the case of a tubular combustion chamber [110]. However, large errors could be resulted when using thermocouples due to both radiative and conductive heat loss [111, 112].

Thermocouples consists of two dissimilar conductors that contact each other to the temperature measuring end. So, the purity of metal and the wire are one of the issues to hold the accuracy of the thermocouples. From the appearance the thermocouples, it was understood that the physical condition of the thermocouples got deteriorated upon exposing to high temperature for long. Due to repeated use, the fouling might occur which could reduce the accuracy of the thermocouples. Further, the conduction through the wires and supports of the probe are other sources of error of temperature measurement with thermocouples [110].

[111]

3.1.7 Ex-situ experiment: conclusions

The ‘syngas’ production observed was very low as compared to the data available in the literature. However, this is expected as the favorable gasification temperature was not reached in these experiments. The gasification channel of the coal block made up of coal particles and fine coals was prone to collapse during the spark ignition due to explosion. Because of the collapse, no directional path for feed/product gas existed; the feed/product gas was leaked through every possible area around the coal block before using the exit channel. This phenomenon caused a

loss of feed gas during ignition and resulted a lower temperature. During ignition phase, the use of propane produced lots of steam because of gas phase combustion. All the experiments needed periodic removal of water even before the steam injection. This simply indicates that if propane is used as a gas for ignition mixture and ignition phase is reasonably long, steam injection is not necessary as the gas phase reaction produce enough steam for subsequent steam gasification reaction. Steam injection was only found to be affected by the places where the temperature was either very low or where the coal was depleted due to surface reactions. The mixing procedure of ignition gases is important to reduce or nullify the explosion during ignition. The reactor with packed bed showed better result due to the avoidance of the link collapse. However, heavy pack can result clogging of the exit line. This issue may not be a vital if the UCG is operated at elevated pressure and if the exit line diameter is larger than the coal particles and a high pressure. As the exit line was with a nominal diameter of 0.653 cm, it was prone to be clogged with coal debris.

3.2 Adsorption Experiment

From Figure 1-1, it can be assumed that the post-UCG site consists of several layers of highly porous residuals and adjacent coal seams, in addition to the cavity voids. These layers can be broadly classified as the partially gasified char layer, the pyrolyzed char layer and the raw coal layer. After cooling down and necessary treatment, these highly permeable layers can be used for storing CO_2 released from the combustion of syngas produced from the same UCG site [28, 87, 102, 113]. Moreover, the existing injection hole can facilitate the injection of CO_2 to access the abandoned cavity.

The implementation of CCS at a UCG site requires careful consideration of other factors such as site-selection criteria to minimize environmental impacts after CO_2 injection and economic feasibility of injecting CO_2 [87, 113]. However, this study has focused mainly CO_2 storage through adsorption in the left-over seam and the char residues in addition to the storage capability of the void. To improve the accuracy of CO_2 estimate in the residual layers, it is essential to gain fundamental insight of the various strata as function of coal properties and char formation conditions. Hitherto, there have been several investigations on the influence of coal properties, such as rank, volatile matters and maceral composition on the CO_2 adsorption on raw coals [114-117]. However, the investigations are very scarce on the adsorption capacity of char particles. This study provides fundamental insight on the storage capacity of virgin coals, pyrolyzed and gasified char samples as a function of the coal rank and char formation temperature. Such data would assist in coal seam selection and improve storage capacity estimation for the development of the CCS system, in a post-UCG site. It is noted that the chars analyzed in this study were prepared at atmospheric pressure under low heating rates. Further,

preparation of the chars under elevated pressures, closer to the UCG conditions, would consider the effect of pressure on the char structure.

In this study, carbon/CO_2 storage potential on different ranks of raw coal, devolatilized coal and gasified coal was investigated. Four sets of experiments were conducted. The author was a co-researcher in each of the experimental set. The sets of experiments are as follows:

The first set of experiments was a preliminary test to assess the CO_2 adsorption and storage capacity of a single coking coal and a single non-coking coal and their respective pyrolyzed coal chars at 800°C and 1000°C. Measurements were performed at a pressure of 41 bar for all the studied samples. Experiments were carried out at an isothermal temperature of 45.5°C. The details of the experiments can be found in a paper published in Proceedings of the 2nd Underground Coal Gasification Network Workshop, 2012 [118].

The second set of experiments was a detailed study to assess the CO_2 adsorption and storage capacity of the above samples including two more non-coking coal/char samples. The influence of coal properties on adsorption was also studied and compared with the literature data. Measurements were performed up to a pressure of 65 bar for all the studied samples. Experiments were carried out at an isothermal temperature of 45.5°C. The details of the experiments can be found in a paper published in Energy & Fuels, 2014 [15].

The third set of experiments was a detailed study of four coals of diverse ranks varying from lignite to bituminous and their respective gasified (at atmospheric pressure) chars at 800, 900,

and 1000°C. Measurements were performed at pressure up to 90 bar for all the studied samples. Experiments were carried out at an isothermal temperature of 45.5°C. The details of the experiments can be found in a paper published in Energy Science & Engineering, 2018 [119].

The fourth set of experiments was conducted using the gasified coal sample collected from the ex-situ experiment 2. Measurements were performed up to a pressure up to 100 bar. Experiments were carried out at an isothermal temperature of 45.5°C. The details of the experiments can be found in recent reference [120].

3.2.1 Experimental set-up

The adsorption capacities of the raw coal and the char samples were determined using custom-designed volumetric adsorption setup to handle large samples weighing nearly 20 g. Figure 3-47 shows the schematic representation of the volumetric adsorption apparatus.

The equipment consists of four segments namely the gas injection, isothermal section, evacuation section, and data acquisition system. The gas injection system consists of a high-pressure syringe pump (Teledyne ISCO 500D) with a rated delivery pressure of 258 bar. To ensure safety, a pressure release valve was installed at the output of the syringe pump. In the isothermal segment the components like reference cell, sample cell, pressure transducers, thermocouples, and valves were placed in a water bath with high precision temperature controller (Thermo scientific Model 253). In addition, the inline thermocouples were integrated next to each cell (i.e., reference cell & sample cell) for measuring the gas temperature, which plays a vital role in determining the gas compressibility factor. Further, the reference and sample cells

were incorporated with an in-line filter to avoid fine solid particles entering the tubing and valves. The evacuation segment consists of a vacuum pump and vent. During the experiment, the excess gases were removed through a vent which was directed to the fume hood. The data acquisition system includes both pressure (Omega PX409-2.5KGUSB) and temperature (NIDAQ 9211) monitoring devices.

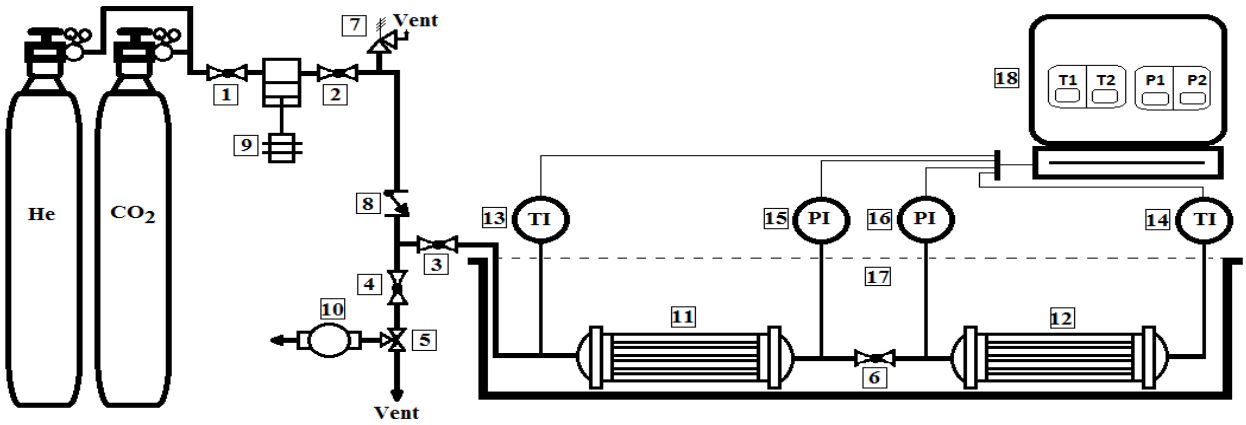

Figure 3-47 Schematic of the volumetric adsorption apparatus (1-6: Valves; 7: Pressure relief valve; 8: Check valve; 9: High pressure syringe pump; 10: Vacuum Pump; 11: Reference cell; 12: Sample cell; 13 & 14: Temperature sensor; 15 & 16: Pressure transducer; 17: Water bath; 18: Data acquisition system) [15].

In a volumetric adsorption apparatus, the variation in the pressure of the system before and after adsorption was used to determine the amount of gas adsorbed by the sample. To obtain a higher accuracy, the earlier pressure transducers were replaced by a Rosemount 3051S inline pressure transducer with an accuracy of 0.025% of span 27-206bar (absolute) in the following set-up. To

reach higher pressure, the volume of the reference cell was also reduced. The latter set-up (see Figure 3-48) was used in determining the adsorption capacity of gasified coal char samples.

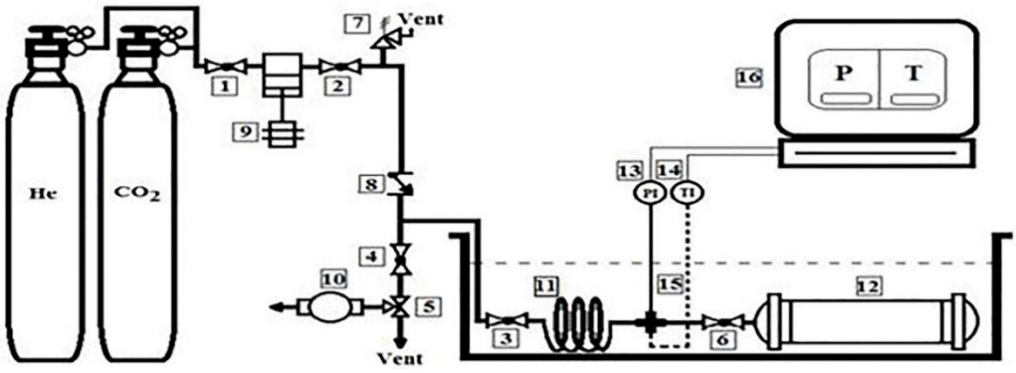

Figure 3-48 Schematic of the volumetric adsorption apparatus (1-6: Valves; 7: Pressure relief valve; 8: Check valve; 9: High pressure syringe pump; 10: Vacuum Pump; 11: Reference cell; 12: Sample cell; 13: Pressure transducer; 14: Temperature sensors; 15: Water bath; 16: Data acquisition system) [119].

3.2.2 Operating procedure

Figure 3-49 schematically shows the steps involved in the gas adsorption measurement. Experiments were carried out at an isothermal environment for single injection pressure only. At first, the desired coal/char sample was weighed and placed in the sample cell. Prior to any adsorption measurement, the trace gases were evacuated from the experimental setup through a vacuum pump. Subsequently, the gas was injected into the reference cell for a desired pressure with the help of gas injection system. Further, the injected gas was retained in the reference cell till isothermal conditions were attained. Later, the gas was allowed to enter into the sample cell for the adsorption process and the pressure was monitored for a prolong period (i.e., approx. 5 hours at moderate pressure and 24 hours at higher pressure) until pressure constancy of 0.07bar was attained.

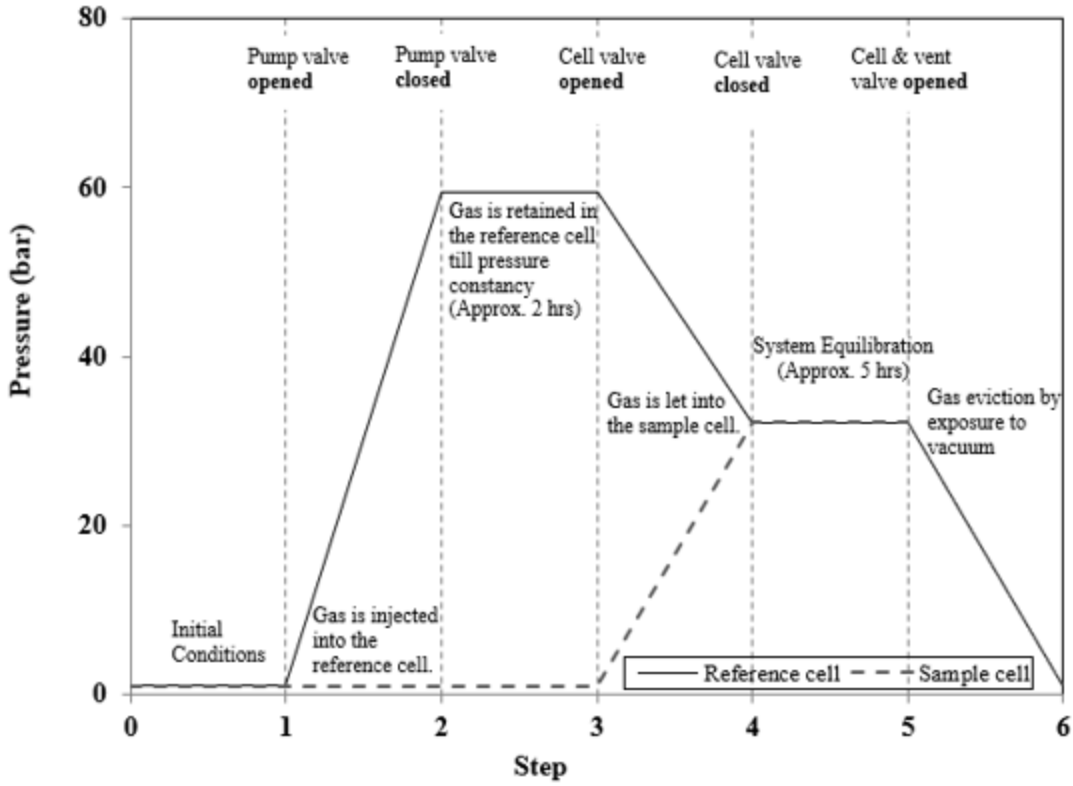

Figure 3-49 Procedure for gas adsorption measurement [15].

The above procedure was repeated to obtain the adsorption amounts at the subsequent pressure points. The reported adsorption amounts for the samples have been obtained after subtraction with the adsorption results with an inert material (glass beads) to correct for the systemic errors. The error analysis procedure is detailed elsewhere [15].

In the volumetric adsorption method, it is essential to predetermine the void volume in the sample cell for measuring the sorption capacity of a sample. Void volume is defined as the space available in the sample cell for the gas to occupy. For instance, if a porous sample is considered, void volume is the volume occupied by the gas apart from the solid surface. In this study, the void volume was determined through helium expansion method. To obtain the porosity of the

coal samples and the bulk density measurements were also carried out using glass beads displacement technique adopted by Ramasamy et al.[118].

3.2.3 Adsorption amount calculation

The mass balance for the system operated after gas equilibration into the sample cell is given by:

$$\rho_1 \times V_R = \rho_1^* \times V_R + \rho_1^* \times (V_{cell} - V_{solid} - V_a) + \rho_a \times V_a \quad \textit{(Eq. 3.2)}$$

where V_R, V_{cell}, V_{solid} are volumes of the reference cell, sample cell and the skeletal volume of the sample. ρ_1 and ρ_1^* are the molar densities of the injected and the equilibrated gas, respectively. V_a and ρ_a are the volume and density of the adsorbed phase, respectively. The third term on the right-hand side of Equation 3.2 is defined as absolute adsorption- the actual amount of gas adsorption on the solid. However, this term cannot be measured experimentally. Therefore, to avoid this limitation, V_a and ρ_a are lumped together to define Gibbs surface excess (GSE) adsorption or excess adsorption as,

$$n_{excess} = V_a \times (\rho_1 - \rho_1^*) \quad \textit{(Eq. 3.3)}$$

In essence, the GSE model assumes that the adsorption occurs at the bulk gas phase density rather than the actual adsorbed phase density.

The mass balance in Equation 3.2 can be rearranged as,

$$n_{excess} = V_R \times (\rho_1 - \rho_1^*) - \rho_1^* \times (V_{cell} - V_{solid}) \quad \textit{(Eq. 3.4)}$$

The excess adsorption isotherms were used to analyze the difference between the various samples. In all studies, the Span and Wagner [121] equation is used to calculate the Z factor of CO_2. The details of the operating procedure for each experimental sets can be found in recent

references: Ramasamy et al. [118], Ramasamy et al. [15], Sripada et al. [119], Zabihi [120], respectively.

3.2.4 Coal/char samples

The virgin coal samples considered for the adsorption measurements include coal A (low volatile subbituminous), coal B (low volatile bituminous), coal C (medium volatile subbituminous), coal D (high volatile subbituminous) and coal E (lignite). Among the samples, coal B is only the coking coal. The size of the coal sample ranged from 22 mm to 32 mm, respectively. The proximate, ultimate and the petrographic analyses of the coals have been listed in the Table 3-3.

Table 3-3 Proximate, Ultimate and Petrographic analysis of raw coals [15, 119, 122].

Parameter	Coal A	Coal B	Coal C	Coal D	Coal E
Proximate Analysis					
Moisture (%)ad	4.8	1.3	4.4	2.8	6.9
Ash (%)ad	9.9	14.0	15.4	10.6	19.2
V.M (%)ad	29.6	22.9	29.9	34.3	31.7
F.C (%)ad	55.7	61.8	50.3	52.3	42.2
Ultimate Analysis					
S (%)daf	0.7	0.7	0.6	0.9	1.4
C (%)daf	82.5	88.4	74.8	72.0	67.2
H (%)daf	4.8	5	4.7	4.6	4.8
N (%)daf	1	1.7	1.3	1.0	1.5
O (%)daf	11	4.2	18.6	21.5	25.1
Petrographic Analysis					
Vitrinite(%)	32.2	44.8	65.2	67.8	53.2
Inertinite(%)	52.1	44.9	22.1	17.9	36.4
Liptinite(%)	4.5	5.1	2.1	7.5	7.0
R_{max} (%)	0.57	1.24	0.56	0.69	0.4

ad, as determined; daf, dry ash free; F.C, fixed carbon; *R*max, maximum vitrinite reflectance; V.M, volatile matter.

Proximate analysis of coal was carried out according to ASTM D7582 MVA in coal and the ultimate analyses were carried out by a Vario MICRO cube elemental analyzer. Petrographic analysis was carried out by CSIRO at Brisbane in Australia for coal A and B, and at Pearson

Coal Petrography in British Columbia for other coals. The details of petrographic analysis of these samples can be found elsewhere [122].

For experiment set 1 only coals A and B were used and for experiment set 2 coals A, B, C and D were used. Coal samples were pyrolyzed at 800°C and 1000°C in a nitrogen environment for 20 min under an estimated heating rate of 2.5°C/s using a drop tube furnace [122]. The surface area of the coal and coal char samples was determined by the density functional theory (DFT) model. For pyrolyzed char samples, the surface area was measured for all the samples using nitrogen as the probe gas in Micromeritics ASAP 2020 at 77 K. Initially, samples were heated to 250°C at a ramp rate of 5°C /min until a vacuum level of 0.5 Pa was reached. After reaching the vacuum set point the samples were outgassed for 4 hours. Surface area and micropore analyses were carried out on ~ 400 mg samples using a fixed dose quantity of 0.25 cc per step with a maximum equilibration delay of 1 hour per step.

For experiment set 3, coals B, C, D and E were used. All the gasified chars were obtained by gasifying coals B, C, D and E in a laboratory-built horizontal tube reactor setup [123] at 800, 900, and 1000°C under CO_2 rich (80%CO_2 in N_2) atmosphere for 10 minutes. The surface area was measured for all the samples using CO_2 as the probe gas in Quantachrome Autosorb iQ instrument at 0°C. For this analysis, the samples (originally in size range 3.75-4.5mm) were crushed to a size <250µm to enable faster measurements on the instrument, this however, led to a slight overestimation of the surface areas. Before the surface area measurements, the crushed samples were degassed at 200°C at 2°C/min for 10 hours under vacuum. The analysis was

carried out on samples of mass approximately 500 mg with a fixed dosing of 0.5 cc per step, with maximum equilibration of 10 mins.

For experiment set 4, only coal C was used. However, the gasified samples were collected at different locations of the concrete tube after gasification experiment. Figure 3-50 *and* Table 3-4 *show the details of the sampling map and the position of the samples.*

Table 3-5 summarizes the proximate analysis for gasified coal samples, which were used to adsorb CO_2.

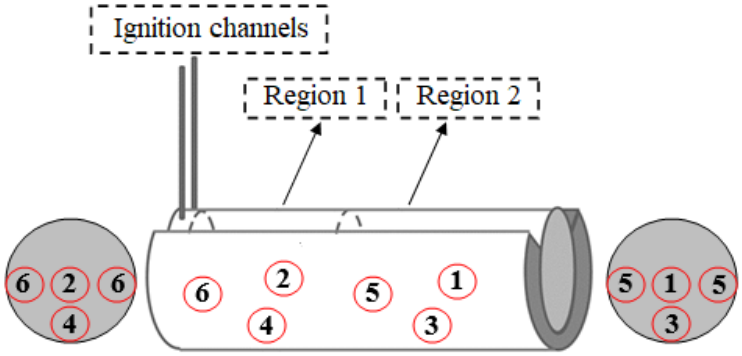

Figure 3-50 Sample position map (modified from Zabihi [120]).

Table 3-4 Coal sample positioning details [120].

Sample Number	Region number	Description
1	Two	Middle of the core
2	One	Middle of the core
3	Two	Bottom layer
4	One	Bottom layer
5	Two	lateral layer
6	One	lateral layer

Table 3-5 Gasified coal sample characterization [120].

Parameter	Gasified coal samples						
	Sample 1	Sample 2	Sample 3	Sample 4	Sample 5	Sample 6	Average
Moisture	2.535	2.96	2.895	3.355	3.18	3.44	3.1
Volatile	23.23	28.4	27.04	30.5	27.875	31.57	28.1
Ash	15.125	14.43	13.195	10.24	12.895	12.185	13
Fixed C	60.645	55.86	58.56	57.84	57.89	54.23	57.5

The adsorption data were obtained by maintaining constant test conditions, which allow the comparisons between the various samples in the study.

3.2.5 Results and discussion

3.2.5.1 Experiment set. 1

In this preliminary set of experiments the influence of pore volume of coal/pyrolyzed char samples in addition to adsorption was assessed to determine the total CO_2 storage capacity of raw coals A and B and their respective pyrolyzed char. The pyrolyzed char was prepared at 800°C following the procedure discussed in the experimental section. The estimation of CO_2 storage is dominated by adsorption capacity level [124]. However, coal seams can also store CO_2 by other mechanisms such as free gas trapping [91]. Therefore, this trapping mechanism is prominent when in-situ char is considered due to its large void space. Considering only virgin coal, at very high pressures the free gas content may become comparable to the adsorbed gas content [91]. So, the total CO_2 storage potential in coal/char layers will be an under-estimation of the realistic storage capacity if the free gas content is not included. In this preliminary set of experiments, coal/pyrolyzed char samples of 22 to 32 mm were used.

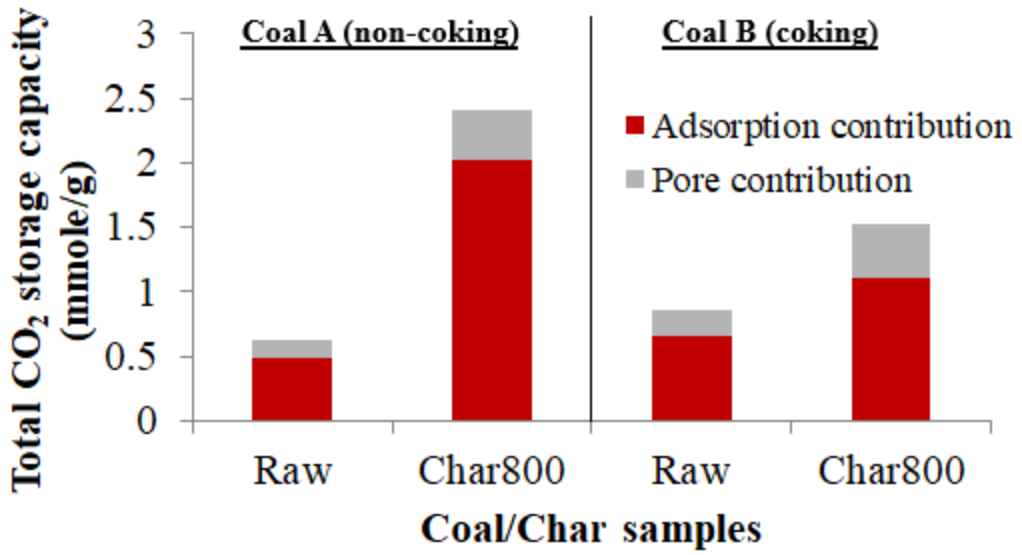

Figure 3-51 Total CO_2 storage potential in virgin coal and coal char samples from coals A & B [118].

Figure 3-51 displays the total CO_2 storage capacity of raw coal and pyrolyzed char samples of non-coking (coal A) and coking (coal B) coals including the contribution from adsorption and pores altogether at a pressure of 41 bar and a temperature of 45.5°C. The impact of pyrolyzed samples on the CO_2 storage capacity was more pronounced in coal A compared to coal B. The total CO_2 storage capacity of the pyrolyzed chars was found to increase by 280% and 77% compared to raw coal A and coal B, respectively. For the same sample size, the CO_2 storage capacity of char of coal A was 58% more compare to char of coal B. Free gas content is considered as the contribution from the void space inside the pores. It is apparent from Figure 3-51 that the contribution of void space increases the total capacity of CO_2 storage. The higher free gas content in the coal/char samples indicates the significance of porosity. Deep coalmine is subjected to very high pressure, so it can be inferred that free gas trapping will be very prominent especially for underground char layers at the prevailing underground pressure.

The total CO_2 storage capacity of the char was dominated by the adsorption capacity compared to the pore contribution. Interestingly, for raw coals, coal B shows higher adsorption capacity compared to coal A. This indicate that coal property of raw coal plays a vital role in determining the adsorption capacity of raw coal which has been further elaborated in the 2nd set of experiments. However, without further investigation, the increase of adsorption capacity can be explained by the increase of the porosity. From the sorption experimental data, Day et al.[114] speculated a general trend of increasing sorption capacity with increasing porosity, presumably because higher porosity provides greater access into the internal microporosity where most of the adsorption takes place. However, this relationship was considered weak and poor indicator of sorption as large number of scatter in the data was observed by Day et al. [114].

3.2.5.2 Experiment set. 2

In the 2nd set of experiments, the influence of coal properties on adsorption was studied using four virgin coal samples, namely, coal A, coal B, coal C and coal D and compared to the literature data. Coals of diverse characteristics have been chosen to provide a better understanding on the influence of various coal properties, such as maceral, volatile matter, and ash contents. This study also provides fundamental insight on CO_2 adsorption capacity of a coal char samples of coal A (non-coking) and coal B (coking) as a function of the coal rank and pyrolyzed temperature of 800°C and 1000°C. UCG residues consist of thermally influenced gasified and pyrolyzed coal layers at different temperatures and virgin coal out side the area influenced by the UCG process. So, such fundamental knowledge is essential for the development of the CCS system, in a post-UCG site.

Figure 3-52a shows a comparison of the adsorption capacity as a function of volatile matter on AR (as received) and AF (ash free) basis in virgin coal for both experimental and literature samples. The experimental data obtained at a pressure of 24 bar and a temperature of 45.5°C. were compared with a literature data [125, 126] obtained at a pressure of 24 bar and temperatures of 45°C and 26°C. Figure 3-52a clearly shows a trend that the excess adsorption decreases with increase in volatile matter for both experimental and literature samples. However, a large difference in the adsorption magnitudes between coals A and C is observed. This difference is presumably due to few properties of coals such as mineral or maceral content that dominate the sorption in coals. The decrease in adsorption with volatile matter can be explained by the fact that the macropore volume increases with increase in volatile matter content [127, 128]. High-volatile coals tend to have higher liptinite content [129], which is mainly composed of macropores [127, 130]. However, adsorption in coal is highly influenced by the micropore structure apart from the surface properties of the matrix [131]. The difference in the excess adsorption magnitudes between the experimental and literature data is attributed mainly to the coal property rather than the minor variations in the test conditions (i.e., temperature). Specifically, for the literature data [125, 126], the excess adsorption magnitudes are similar irrespective of the difference in the test conditions. This suggests that the influence in the coal property is very significant.

In addition, the very similar trends observed in Figure 3-52a between AR and AF basis indicate that the presence of ash does not seem to contribute to the adsorption capacity. However, Figure 3-52b indicates a slightly decrease of excess adsorption with increase in ash content for almost all samples in experiment and literature except for coal C. It can be speculated that the ash

hinders the presence of active sites for adsorption in coal. Thus, implying that the greater the ash content, the lesser the number of active sites per unit volume of coal, resulting in lesser adsorption. Further, the inorganic components such as ash in coal have a negative impact on adsorption [116] and CO_2 adsorption in coal mainly takes place on the organic phase [132]. The higher sorption capacity of Coal C despite higher ash content suggests that the maceral components may have a much more pronounced impact compared to the mineral components.

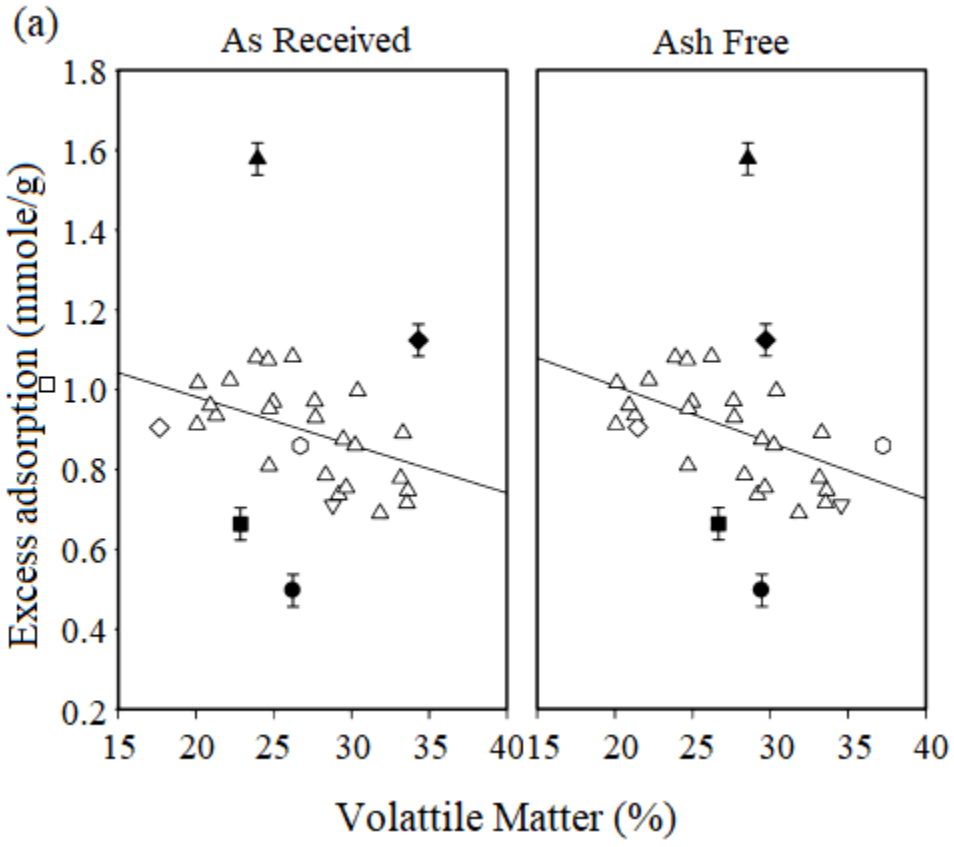

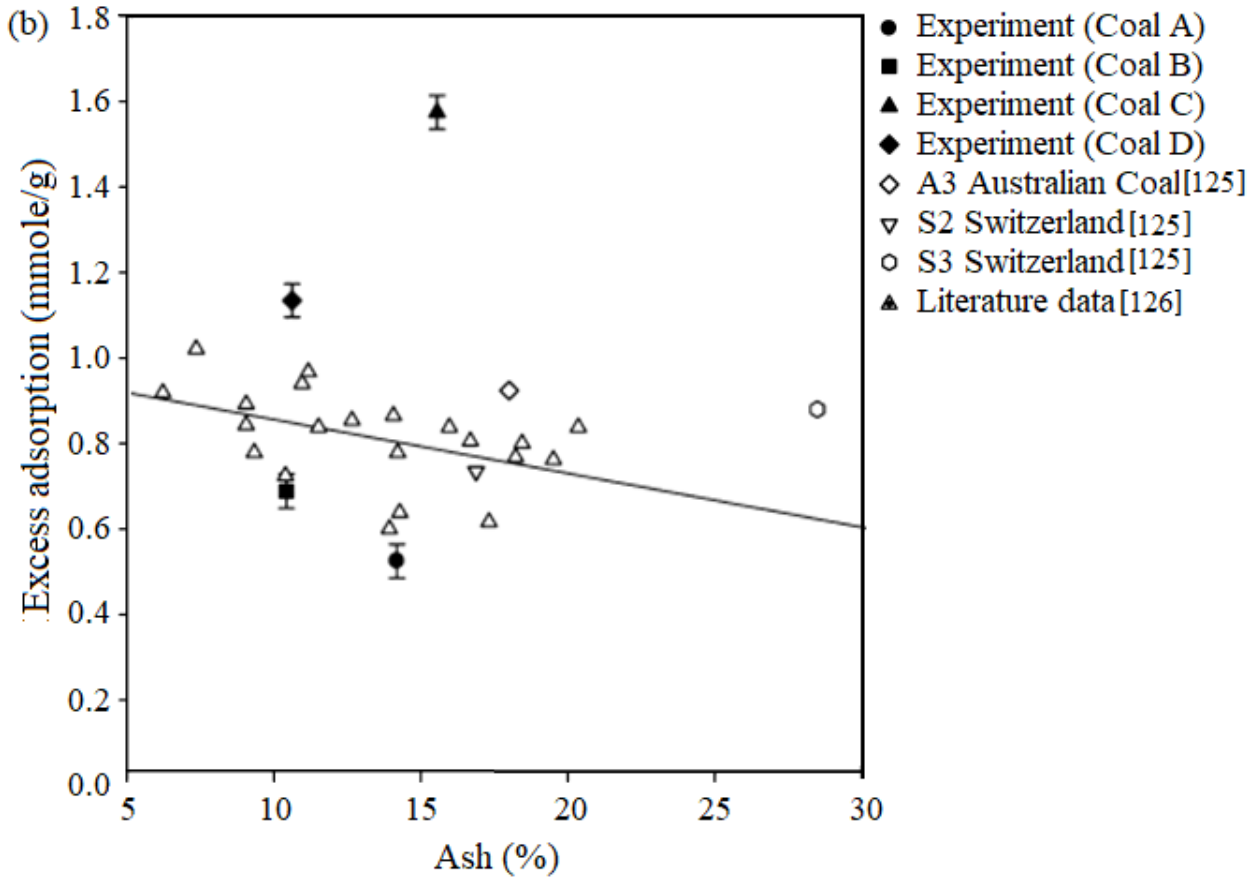

Figure 3-52 Excess adsorption behavior of virgin coal as a function of the (a) volatile matter and (b) ash content [15].

Figure 3-53 shows the relationship between excess adsorption and vitrinite reflectance for virgin coal obtained by the experimental and literature data. Experimental data and literature data from Pini [125] were obtained at 24 bar and temperatures of 45.5 and 45 °C, respectively. On the other hand, literature data from Ryan and Richardson [117] were obtained at a pressure of 20 bar and a temperature of 25 °C. The correlations observed from Figure 3-53 are quite week with considerable scatter in the experimental and literature data that lie in the subbituminous to bituminous region. Coals A and C have almost similar reflectance, but the sorption capacity of coal C is much higher. This large difference in adsorption magnitudes can be attributed to

disparity between the properties of coals A and C. On the other hand, coals D and B have increasingly higher reflectances than that of coal C; however, there is a gradual decrease in the sorption capacity. This could be explained by the fact that the amount of vitrinite is very high in coals C and D, followed by the amount in coal B. It is not only the reflectance but also the amount of vitrinite might have significant influence in determining the amount of CO_2 adsorbed.

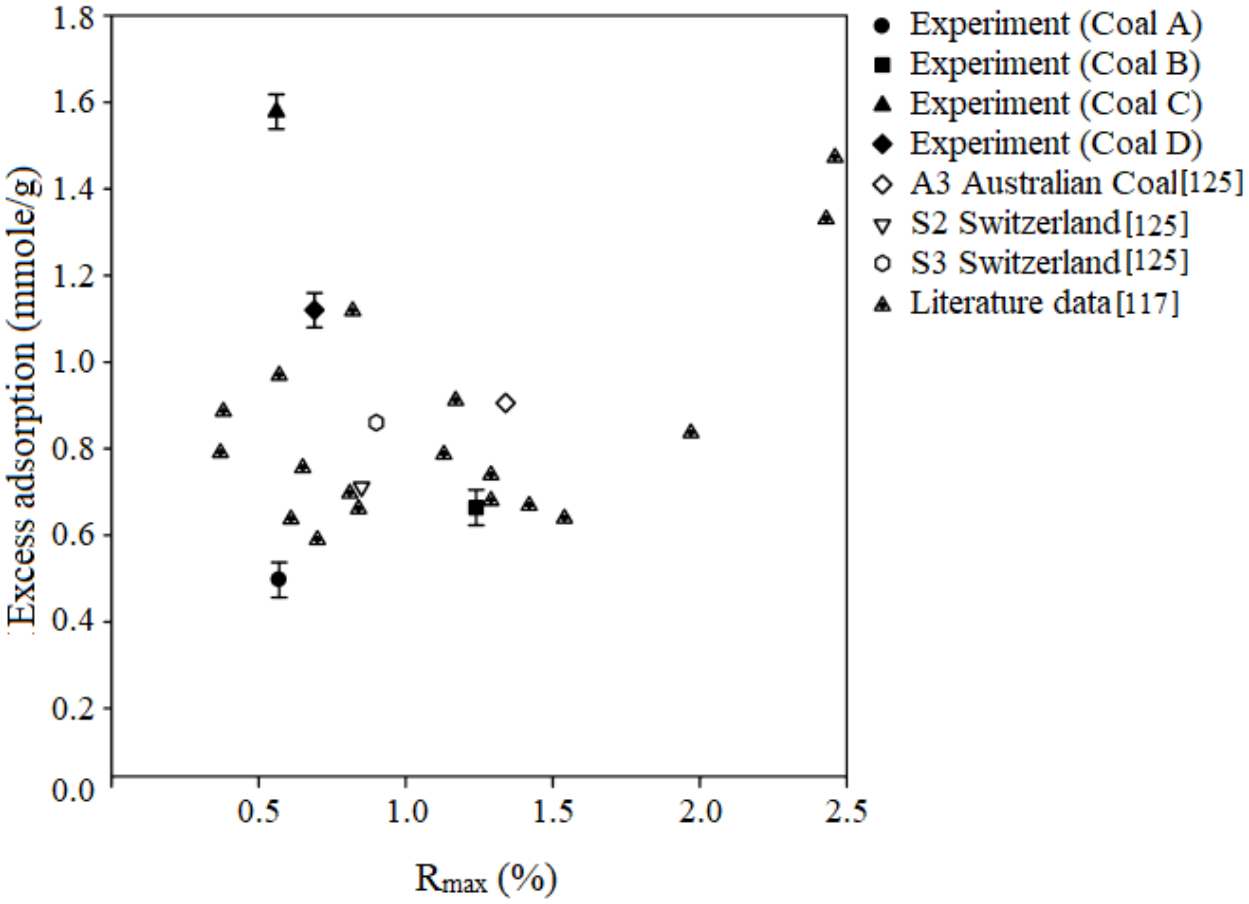

Figure 3-53 Excess adsorption behavior of virgin coal as a function of the coal rank [15].

Figure 3-54 shows the impact of vitrinite content on the excess adsorption of virgin coals obtained from experimental and literature data [132]. The experimental data have been obtained

at a pressure of 24 bar and a temperature of 45.5°C. From Figure 3-54, it can be observed that, the higher the vitrinite content, the greater the adsorption for both experimental and literature data. Within the studied samples, coal C and coal D have much greater vitrinite content than coal A and coal B leading to a larger adsorption capacity. However, although coal D has higher vitrinite content than coal C, the sorption magnitude is lesser. The lower CO_2 adsorption in coal D compared to coal C might be due to the greater presence of the liptinite maceral in coal D. As said earlier that the liptinite maceral is composed of a greater amount of macropores compared to the vitrinite maceral which is principally microporous [127, 130, 131]. However, in general, it may be speculated that the presence of greater vitrinite overpowers the role of other coal properties in determining the adsorption capacity in virgin coals. From the relation between adsorption and vitrinite content it can be speculated that there might exist a correlation between adsorption and micropores.

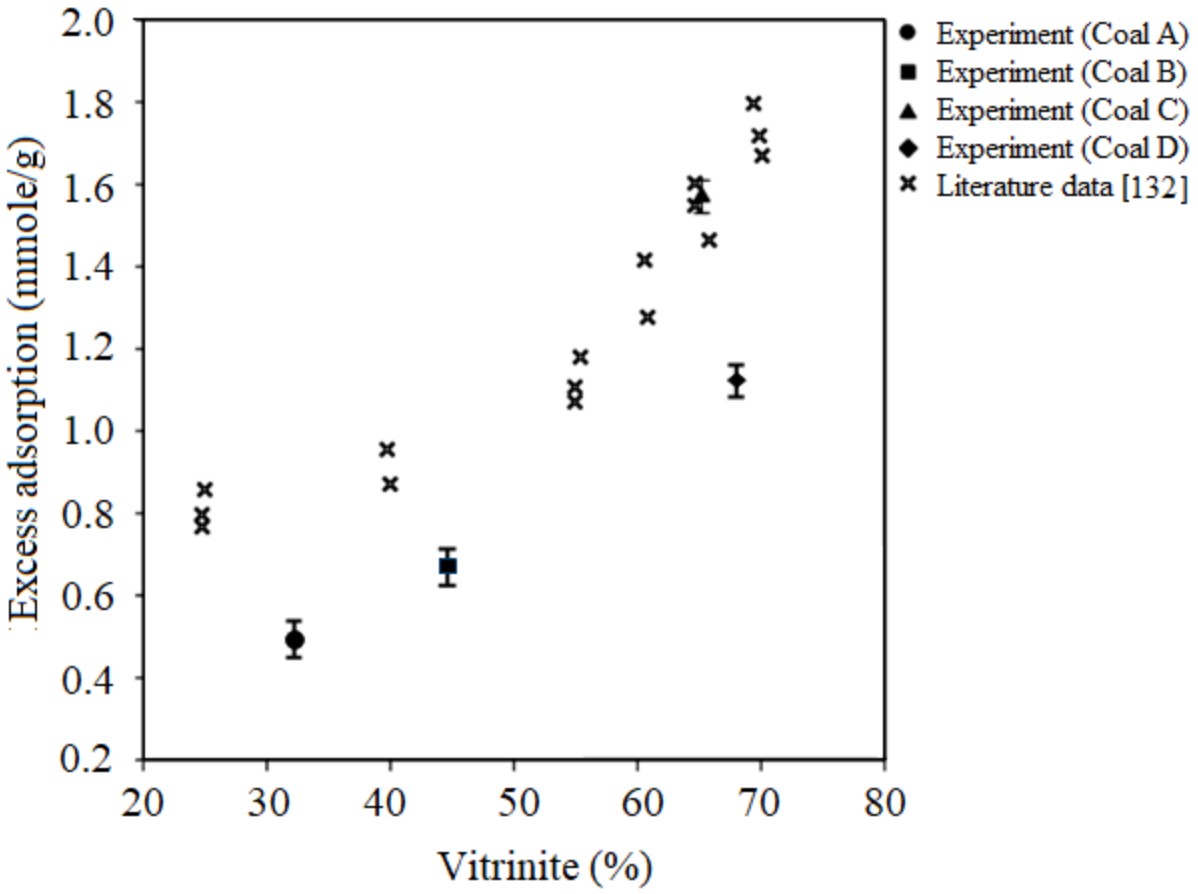

Figure 3-54 Comparison of excess adsorption data for the experiment and literature in the virgin coal sample as a function of the vitrinite content [15].

Figure 3-55 shows the comparison in excess adsorption capacity of coal A and B samples at different pyrolyzed temperatures at a pressure of 24 bar and a temperature of 45.5°C. The trend of adsorption of virgin coal/char800 is very similar as observed in the 1st set of experiments. Slightly less adsorption observation was due to lower pressure operation compared to the preliminary set of experiments. From Figure 3-55, it can be observed that there is no significant change in the adsorption capacities between chars 800 and 1000 for both coals A and B. At higher temperatures, the cross-links between the aromatic rings in the coal matrix undergo

extensive decomposition and the resulting structural rearrangement alters the surface area of the chars. The altered surface area, either a slight increase or decrease (depending upon the coal), leads to only a marginal change in the sorption capacity for char 1000 samples compared to char 800 samples. Within the studied coal samples, the adsorption trend is much higher for coal A char samples than the coal B counterparts. However, in the case of the virgin sample, the adsorption capacity for coal B is higher than that for coal A. In brief, this observation can be partly attributed to the nature of the virgin coals, which dictates the surface area of the produced coal char. In conclusion, it is considered essential to understand the influence of the surface area and the coal nature on adsorption.

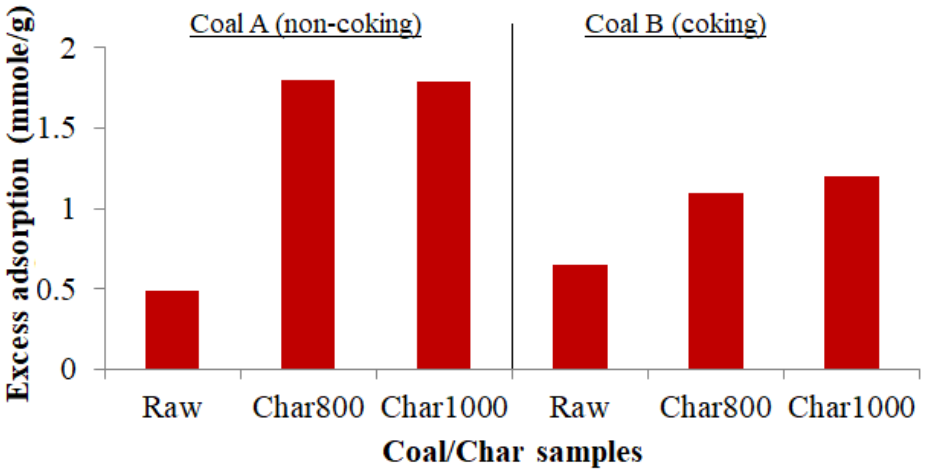

Figure 3-55 Comparison of excess adsorption data for coal and coal char samples (redrawn from Ramasamy et al. [15]).

Figure 3-56 shows the variation of porosity between virgin and char samples obtained at two different pyrolysis temperatures. The most noteworthy feature is that the porosity of char samples was much higher than virgin samples for both coals. It was also found that the rise in porosity is around 4 times for char 800 from the virgin sample. However, it is only 1.2 times

between char 800 and char 1000. The increase in the porosity is due to the development of macropores and the growth of micropores due the pore expansion and new pore formation in char 800 samples. Further, the growth in porosity was affected due to the structural rearrangement at higher temperature for char 1000 samples. Within the studied samples, the porosity is much more pronounced for coal A in comparison to coal B. This can be attributed due the nature of the coal samples. Since, coal B being a coking coal, tends to expel more tar which upon condensation may block the pores. However, it can be seen that the porosity of pyrolyzed chars of coals A and B vary marginally but char of coal A shows a substantial increase in the adsorption capacity. This is because, coal A tends to develop more micropores than coal B which is responsible for the increase in surface area for adsorption. Therefore, it can be concluded that the pore distribution and the nature of the coal has a substantial impact on adsorption behaviour.

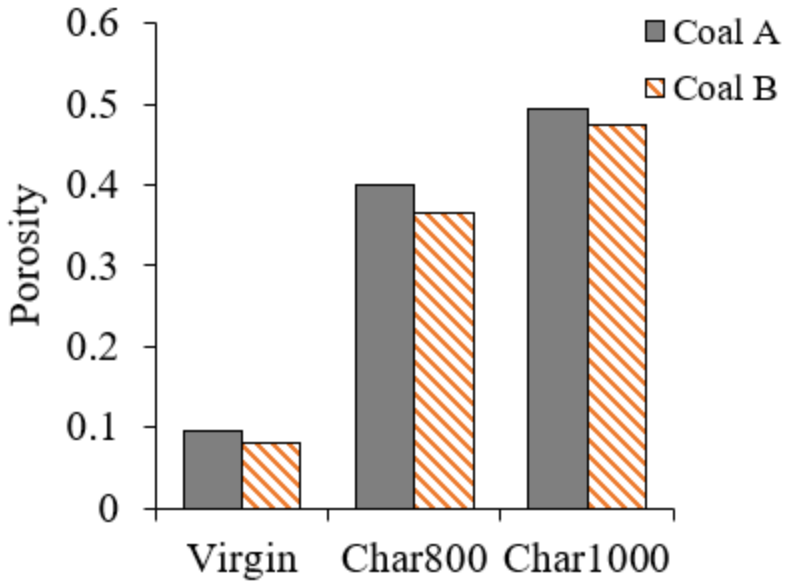

Figure 3-56 Porosity of the char species of coals A and B compared to the respective virgin coal samples (redrawn from Ramasamy et al. [15]).

Figure 3-57 quantifies the percentage of micro (<20Å), meso (20-500Å), and macro (>500Å) pore distribution in virgin and char 800 samples for both coal A and coal B. The observation confirms (see Figure 3-57) that there is a substantial change in the pore size distribution between virgin and char 800 samples particularly for coal A. The rise in the surface area for the char of coal A is more pronounced in micro pores compared to the reduction in the surface area for meso and macro pores. However, a significant rise in the surface area was only observed for mesopores between coal B samples. Within the studied virgin samples, the micro pores in coal B were reasonably higher than coal A. The higher micropores in coal B can be attributed to the greater vitrinite content compared to coal A, since vitrinites are known to be composed of more micropores. It was found from experiment that during pyrolysis at 800°C, the distribution of meso and macro pore was partly transformed into micro pores in coal A. This behaviour can be

attributed to the structural changes like the generation of new pores and coalescence of pores that occur during pyrolysis [127, 133]. Conversely, this behaviour was not observed for coal B, since, being a coking coal, the excess tar produced may condense to form more mesopores [134]. Further, the decomposition of metaplast (a viscous fluid expelled during initial stages of pyrolysis) produces carbon that may plug the pores and cause reduction in the micropore surface area [135]. Therefore, it can be concluded that micropores have the greatest influence on adsorption since they offer a higher surface area compared to other pore sizes. Moreover, the pore size distribution plays a vital role in understanding the impact of coal nature on the adsorption behaviour.

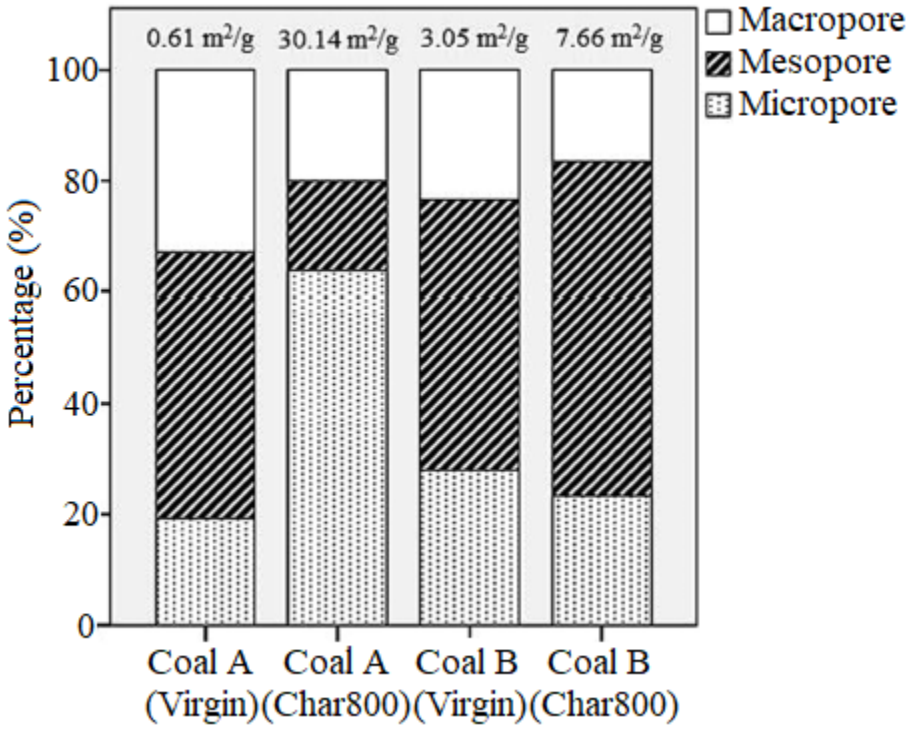

Figure 3-57 Porosity distribution in terms of the surface area for virgin coal and coal char of coals A and B [15].

3.2.5.3 Experiment set. 3

In the 3rd set of experiments, four coals of diverse ranks varying from lignite to bituminous were selected and their respective gasified char at 800, 900, and 1000°C were tested for their adsorption capacity Also, complementary coal and char analysis were carried out for determining the carbon conversion, surface area, pore size distribution, and surface morphology to understand the influence of the coal properties and gasification conditions on adsorption.

The carbon (coal) conversion (χ) of the samples is calculated by using the measured weights m_o (initial weight) and m (final weight) on dry-ash free basis using equation 3.5.

$$\chi(\%) = \frac{m_0 - m}{m_0} * 100 \qquad \textit{(Eq. 3.5)}$$

The coal conversion values during the CO_2 gasification are presented in Figure 3-58. The conversion level among the four coals is considerably different at the three temperatures. The coal E has the highest conversion at all the temperatures followed by the coals C, D, and B. The conversion in coal B is significantly lower compared to the conversions of other coal samples. Particularly for the char800 samples where the conversion of coal E is around 55% followed by the coals C, D, and B at 43, 36, and 17%, respectively.

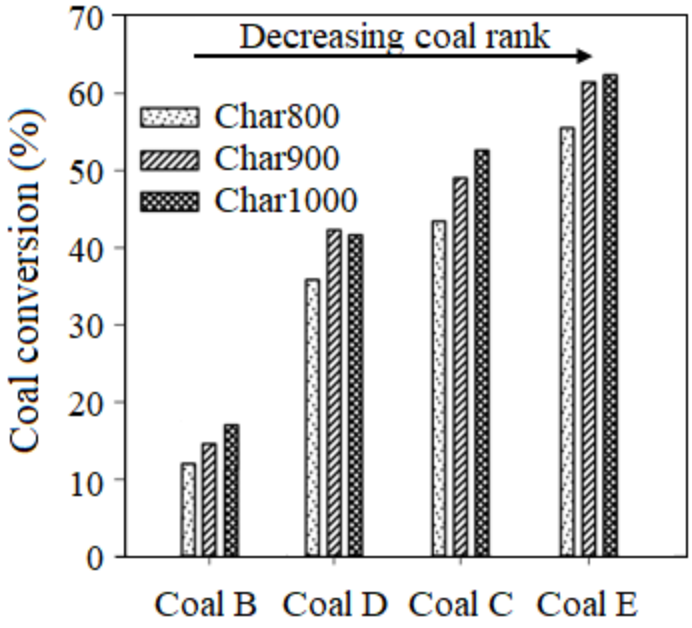

Figure 3-58 Average coal conversion of the four coals after 10 minutes of CO_2 gasification ($80\%CO_2$ in N_2) at 800, 900, and 1000 ℃ (redrawn from Sripada et al.[119]).

The conversion in the char900 samples was higher compared to the char800 samples. For char900 samples of E, C, and D is typically around 10%-points from the respective char800 species; however, for sample B, only an increase of 2%-points was observed. On the other hand, the conversion for char1000 compared to char900 increased marginally for samples B, C and E, and decreased slightly for samples D.

The variation in the conversion trends between the coals at different temperatures are purely a function of the coal properties. The reactivity of the coals during gasification is a function of the nature of pores, inherent minerals and the crystalline structure of the char during the devolatilization stage [116]. The higher gasification reactivity for the lignite coal compared to other higher rank coals is a well-known phenomenon [89, 101, 116]. In other words, carbon conversion is inversely proportional to the coal rank (as observed in Figure 3-58). A study

evaluating the gasification reactivity through chemisorption parameters by Jing et al.[136] demonstrates that for the lower rank coals, such as lignites, the chemisorbed reacting gases would react before desorbing from the surface [116]. However, in the case of higher rank coals, the reacting gases would desorb before reacting on the surface, thus resulting in lower reactivity.

A comparison between the surface areas for the raw coal and the gasified chars at 800, 900, and 1000°C is presented in Figure 3-59. The surface areas have been calculated from the DFT method. The DFT method is a molecular level statistical thermodynamic technique that is effective for determining the pore size distribution from micropore to mesopore size range [137].

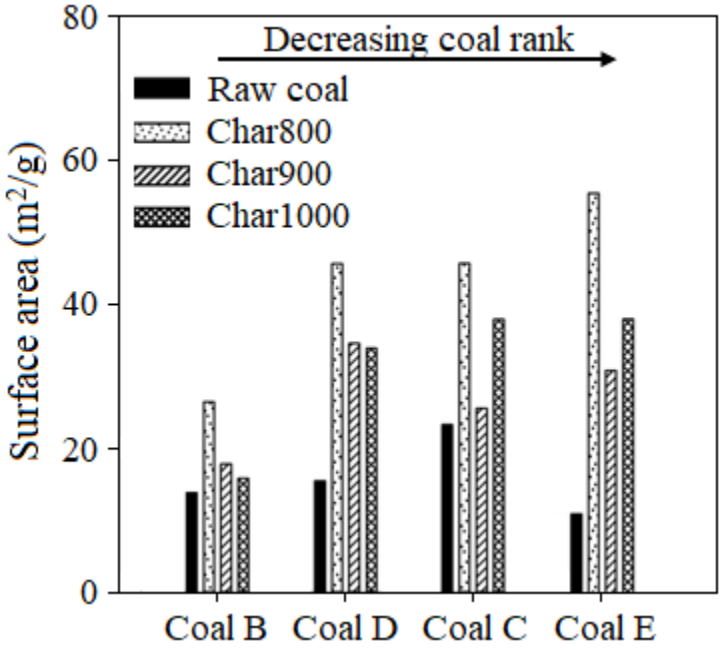

Figure 3-59 Comparison of the surface area (obtained with CO_2 as the probe molecule) of the four raw coals and the respective gasified chars at 800,900 and 1000℃ (redrawn from Sripada et al. [119]).

As expected, the surface area of the gasified chars was higher than the respective raw coals. Among the chars, the char800 species have the highest surface area. Comparatively, the char900 samples have a significantly lower surface area. However, in the case of char1000, two samples C and E have a higher surface area than the respective char900, whereas, the other two samples B and D have a lower surface area. Since the variation of the surface area of char with the gasification temperature is a function of coal properties; it is, therefore, useful to analyze the changes specifically associated with each coal with the rise in temperature. The trends observed in Figure 3-59 can be summarized as follows:

Raw coal: Coal C>Coal D> Coal B>Coal E

Char800: Char E>Char C>Char D>Char B

Char900: Char D>Char E >Char C>Char B

Char1000: Char E>Char C>Char D>Char B.

Among the char species, the trend of the surface area between samples C, D, and E varies with temperature whereas chars of sample A consistently have the least surface area. In general, the char surface areas follow the rank inversely. However, in the case of raw coals, the surface area follows a "U-trend" with rank and is also a strong function of maceral composition as discussed, several reports in the literature [15].

The pore size distributions of coals/chars have been obtained through the application of DFT methods on the low-pressure isotherms of CO_2 adsorption. The pore size distributions have been presented in terms of surface area contribution in Figure 3-60. It is noted that when CO_2 is used as the adsorbate, the adsorption predominantly occurs in the micropores and the mesopores [15].

So, only the distribution of micropores and mesopores are considered in Figure 3-60. The contribution of the micropores towards the total surface area was about 20-40%.

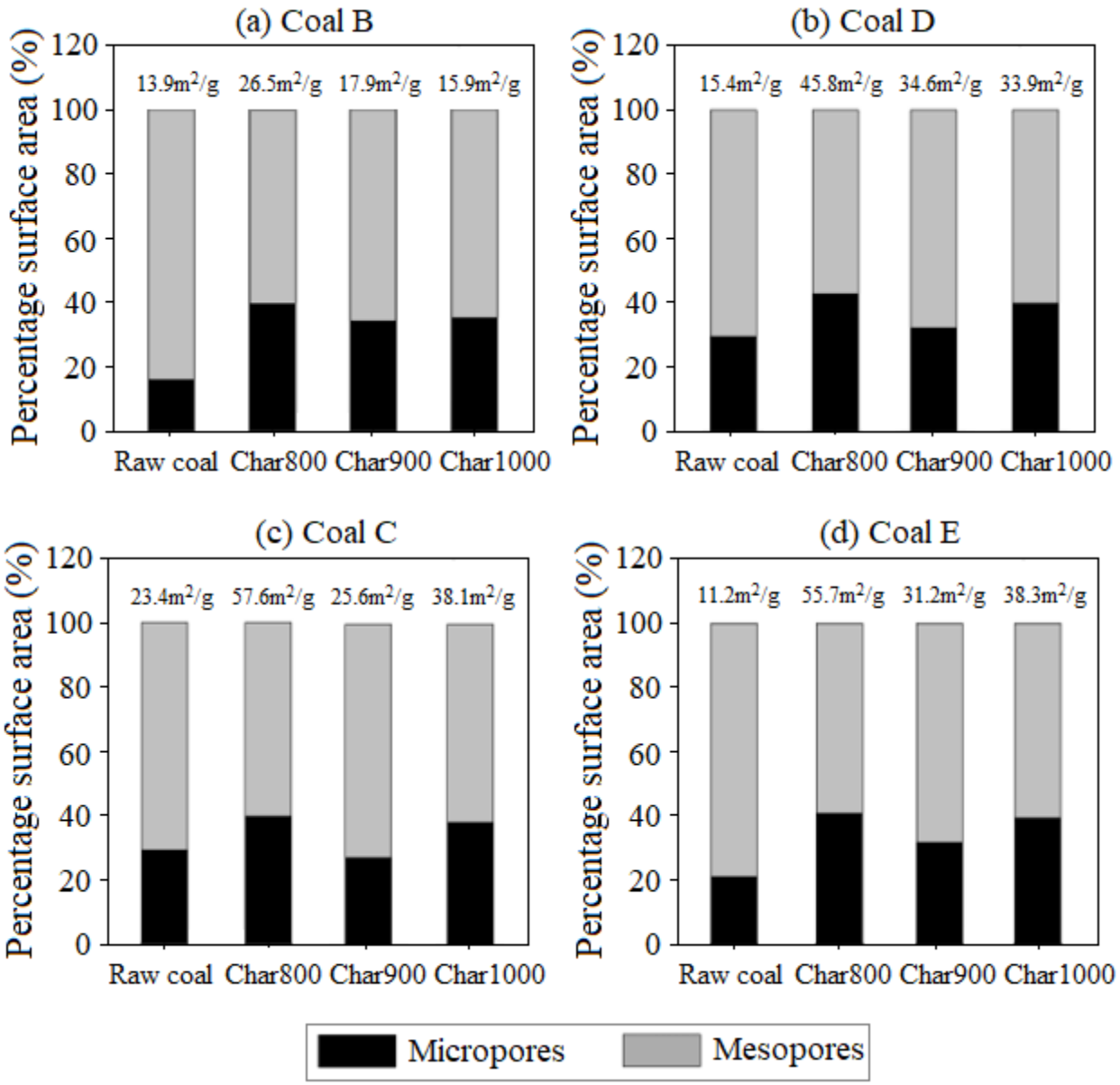

Figure 3-60 (a), (b), (c), and (d). Comparison of the pore size distribution in terms of surface area contribution of the raw coals and chars for coals B, D, C, and E (redrawn from Sripada et al. [119]).

From Figure 3-60, a significant increase in the micropore contribution from the raw coal to the char800 species is observed for all the samples. The increase in the micropore contribution is also reflected in the large increase in the total surface area. Subsequently a slight decrease in the micropore contribution as well as the total surface area for the char900 species. Further, as the temperature is raised to 1000°C an increase in the microporous contribution is observed. The variation in the surface area for the coals can be reasoned through the changes in micro porosity.

For a better visualization of the resultant char surfaces after gasification and to draw inferences on the coking effects on large coal particles (3.35-4.75mm), scanning electron micrographs (SEMs), shown in Figure 3-61, have been obtained on a Zeiss EVO MA 15 microscope stationed at the Department of Earth and Atmospheric Sciences, University of Alberta. The images were obtained in the variable pressure mode to avoid carbon coating. All the images reported were obtained at a relatively lower magnification of 150X to view the surface changes on the large coal particles.

In general, all the raw coals were characteristic of a dense surface. In the case of the gasified chars, considerable changes in the morphology were noted with temperature, particularly with sample B. The char800 of sample B looks considerably different with a ‘frothy’ appearance on the surface. The ‘froth’ is characteristic of a coking coal with clear evidence of the plasticity developed on the surface. However, in the case of char900 of coal B, the frothing reduced significantly. Moreover, for char1000, the char matrix consolidated into a dense mass. The apparent consolidation of the structure with temperature indicates the rearrangement matrix at higher temperatures and may eventually render the char particles being less reactive.

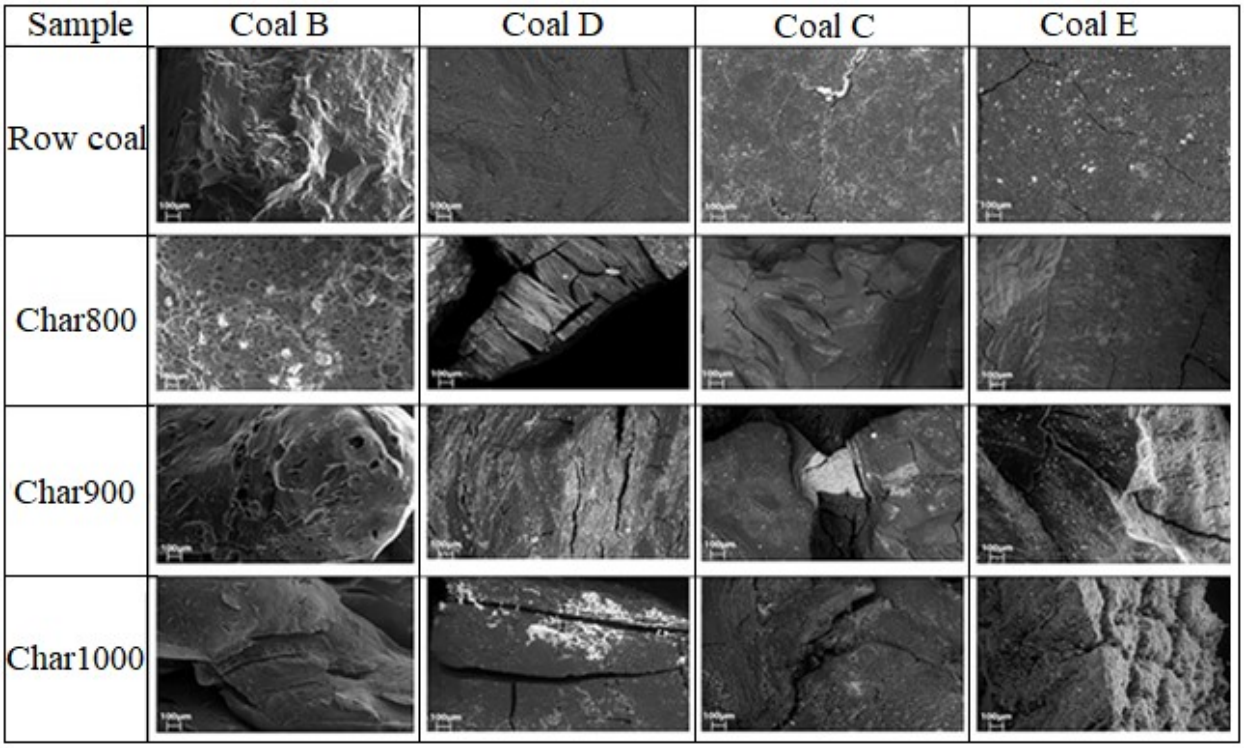

Figure 3-61 Scanning electron micrographs of the raw coals and gasified coal chars at a magnification of 150X [119].

On the other hand, the chars of samples C, D, and E exhibit a behavior different to that of char B. In general, for these chars, a visual observation suggests that the cracks increased in both the size and number as the conversion progresses. For instance, the char1000 of sample E, where the conversion was close to 70%, exhibited a 'flaky' appearance. Interestingly, it was noticed that for many char particles scanned under the microscope, a considerable number of cracks were located at the mineral boundaries. The bright spot in a few images in Figure 3-61 reflects the presence of mineral matter. The energy-dispersive X-ray (EDX) spectra obtained at such locations indicated the major presence of silicon, iron, and even barium in certain cases. However, no consistent trend was observed.

The high-pressure adsorption results of the raw coals and the gasified chars at 45.5°C are summarized and explained in terms of the raw coal/char characterization data (presented earlier) to understand the influence and interplay of various coal properties on the CO_2 adsorption capacities. This would enable in identifying the suitable coal properties such as rank and maceral content for enhanced CO_2 adsorption relevant to the UCG-CCS system.

The isotherms of raw coals are presented in Figure 3-62(a). Among all raw coals, coal C has the highest sorption capacity with a maximum of 2.20mmole/g followed by coal D, coal E, and coal B by 1.42, 1.42 and 0.79mmole/g, respectively at 90 bar. It was noted from a previous study and other reports that the difference in the adsorption amounts in coals is due to their inherent properties [11, 15, 113, 138]. The coal properties such as moisture content, volatile matter, and mineral matter negatively influence the sorption of CO_2 in coals [115]. At low temperature, the mineral matter in coal acts as an inert component, thus effectively decreasing the surface area available for adsorption. Furthermore, maceral components such as vitrinite and inertinite have a positive impact on the CO_2 sorption behavior [116]. For the studied coal samples, the trend of sorption capacity is in good agreement with the vitrinite content. The arrangement of coals in accordance to their sorption capacity (C>D>E>B) and vitrinite content (D>C>E>B) is similar. Interestingly, although coal D has higher vitrinite content than coal C, the sorption magnitude is lesser. The lower CO_2 adsorption in coal D (compared to coal C) might be due to the greater presence of the liptinite maceral as discussed earlier. It has been discussed earlier that the liptinite maceral is composed of a greater amount of macropores compared to the vitrinite maceral which is principally microporous [127, 130]. Thus, for enhanced gas sorption, the contribution of the latter would be critical.

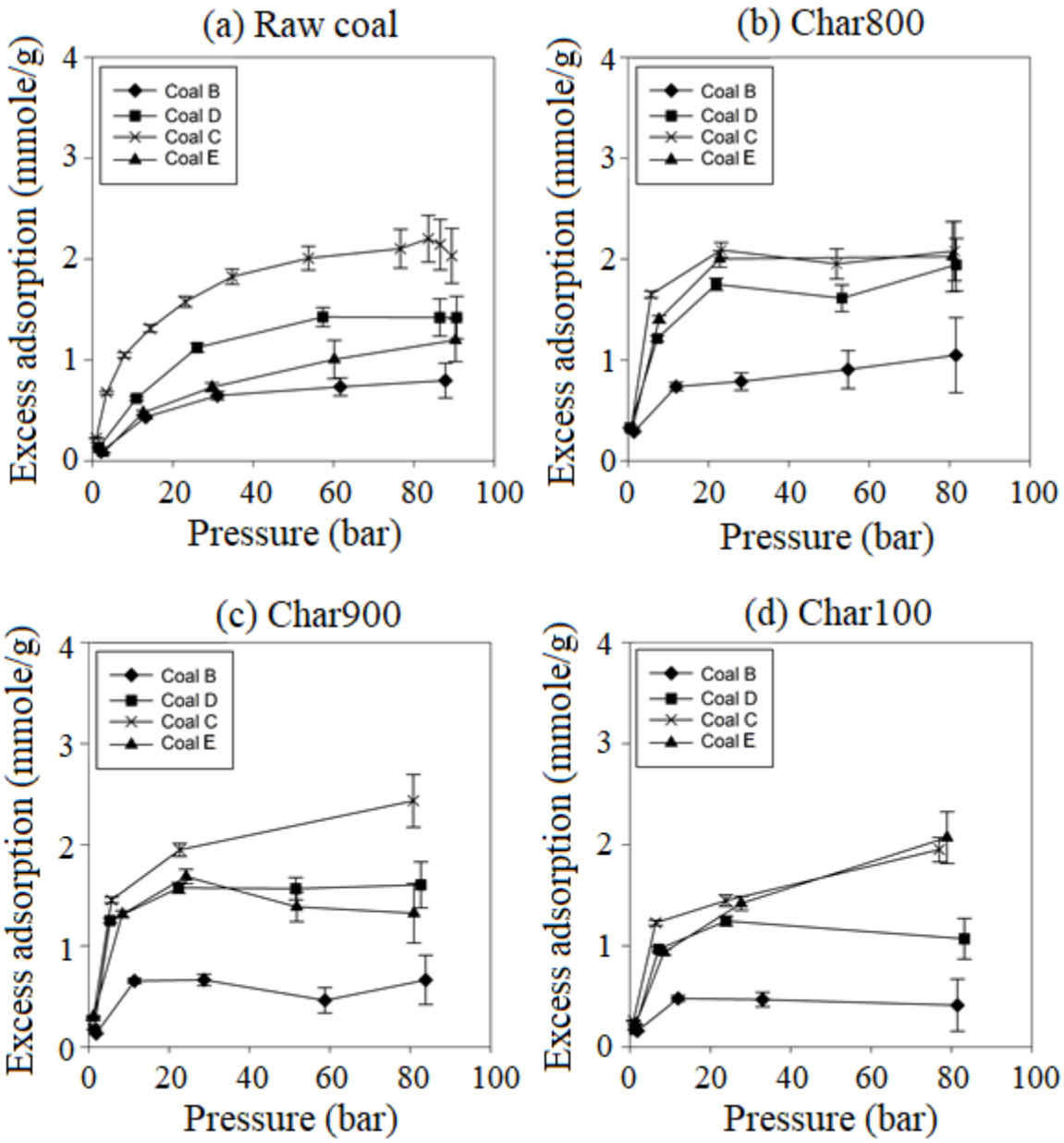

Figure 3-62 (a), (b), (c) and (d). Comparison of the adsorption capacities of raw coal and gasified chars at 800, 900, and 1000℃. Interpolation lines have been indicated between data points [119].

The effect of coal properties on CO_2 adsorption would also extend to the gasified chars as the evolution of the char structure is, in turn, a function of the coal properties. From the isotherms

presented in Figure 3-62(b), it is observed that among the chars at 800°C, sample C char800 has the highest sorption capacity followed by the chars of samples E, D, and B, respectively. Also, compared to the raw coals (shown in Figure 3-62(a)) the sorption capacities are significantly higher for chars B, D, and E derived at 800°C. The adsorption data for gasified char is very scarce in the literature. The sorption capacities obtained for the various chars at 800°C have been compared with the extracted data reported in literature in Table 3-6. The details of the of the coal properties of the literature data can be obtained from the study of Kempka et al. [89]. Their experimental test also exhibited a general increase of CO_2 excess sorption capacity for the char800 from raw coal by 31 - 42% [89].

Table 3-6 Comparison of the adsorption capacities of gasified char at 800℃ of various coal with literature data.

Sample	Adsorption capacity (mmole/g)	Adsorption conditions	Char preparation	Reference
Char B	1.04	45.5°C, 80 bar	CO_2 Gasified 800°C, 1bar	This study
Char D	1.94	45.5°C, 80 bar	CO_2 Gasified 800°C, 1bar	This study
Char C	2.08	45.5°C, 80 bar	CO_2 Gasified 800°C, 1bar	This study
Char E	2.02	45.5°C, 80 bar	CO_2 Gasified 800°C, 1bar	This study
Lippe	1.75	45°C, 80 bar	Air Gasified 800°C, 2bar	Kempka et al.[89]
Prosper-Haniel	1.27	45°C, 80 bar	Air Gasified 800°C, 2bar	Kempka et al.[89]
Ibbenbüren	1.79	45°C, 80 bar	Air Gasified 800°C, 2bar	Kempka et al.[89]

The adsorption isotherms for the char900 species have been presented in Figure 3-62(c). It is noted that the adsorption capacity for the char900 of sample C is the highest at 2.1mmole/g followed by the char900 of D, E, and B. Except for sample A, the adsorption capacity in Char900 was marginally higher compared to char800. From Figure 3-62(d), the char1000 of samples E and C have the highest CO_2 sorption capacity with 2mmole/g. Sample D char1000 has the next highest capacity with 1.1mmole/g followed by sample B. Further, it is observed that the adsorption capacities of all the char1000 species were lower than char800 and char900 species.

It can be seen that for some of the isotherms shown in Figure 3-60, the excess adsorption decreases slightly and increased thereafter (Figure 3-62(b) coal D and Figure 3-62(c) coal B). This behavior is due to the experimental error associated with the adsorption measurements. The major source of errors in a volumetric adsorption apparatus is due to the inaccuracy of the pressure transducer, reference and sample cell volumes, and temperature fluctuations. The error margin is further augmented at higher pressures (in excess of 70 bar) of CO_2 when the molar density is sensitive to slight pressure changes [123].

A comparison between the adsorption capacities of various samples at pressure ~30bar is shown in

Figure 3-63. The experimental point around 30bar was chosen to avoid the critical pressure of CO_2 and also the experimental error bars at this pressure did not overlap between samples, thereby enabling a meaningful interpretation of adsorption capacity as a function of coal properties. It is evident that among the char samples for the various coals, irrespective of the coal type, char800 has the highest sorption capacity. The adsorption capacities of the chars

progressively decrease with increasing temperature. Moreover, the sorption capacities of bituminous coal B and its chars are the least whereas the sorption capacities of sub-bituminous coal C and its chars are the highest. The trends in the adsorption capacities between samples D and E vary between the coal and the chars. Char E has higher adsorption compared to char D. However, this trend is reversed (with only a marginal difference) when the raw coals are considered. The difference in the adsorption capacity between the coals tested in this study can be attributed to the effect of coal properties as the char preparation conditions were maintained identical. Among the raw coals, although there is considerable debate in the literature on the effect of maceral distribution on the sorption capacity, for the coals tested in this study, sorption capacities followed the vitrinite content trend reasonably well [114, 116, 139]. Interestingly, the sorption capacities of the raw coals also follow the vitrinite + liptinite content trend that extends to the chars800 and 900 reasonably well. Although no consistent trend was observed for the tested raw coals in terms of coal rank, the lower ranked chars that of sub-bituminous (C and D) and the lignite (coal E) showed higher sorption capacities compared to the higher rank bituminous coal B.

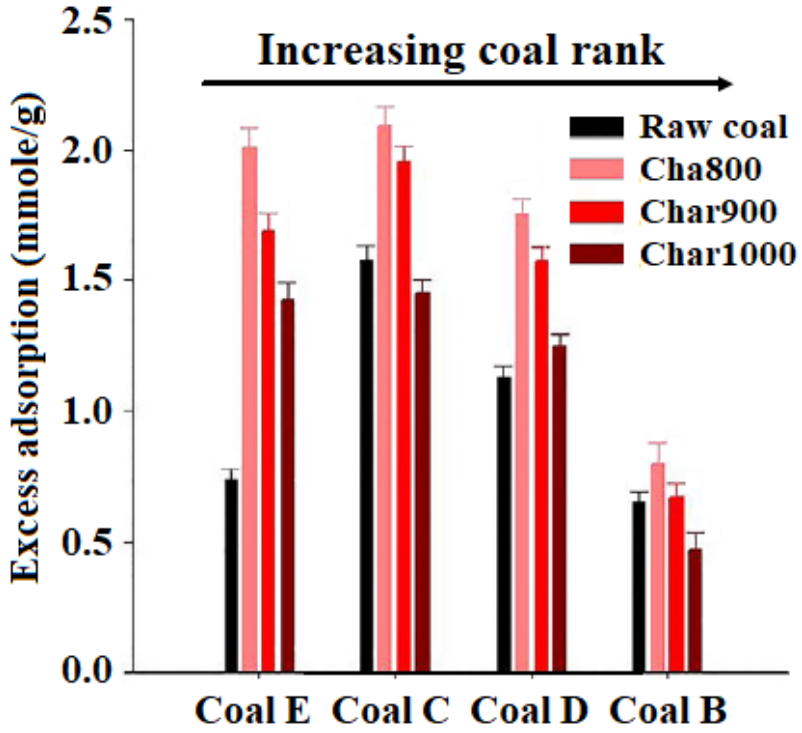

Figure 3-63 Comparison of the adsorption capacities of the raw coals and the coal chars at 30bar pressure [119].

The effect of coal properties on the chars may manifest in two forms, namely, (i) the development of the pores during devolatilization (ii) the reactivity of the chars, thereby consumption of the pores. During the devolatilization phase (before gasification) the increase in the surface area of the char species is because of the enlarged pores that are a consequence of extensive decomposition of the crosslinks in the coal matrix. This phenomenon explains the highest surface area and the adsorption in the char800 species among the examined samples. Subsequently, at high temperatures, typically around 600-800°C, structural realignment of the aromatics takes place resulting in an orderly arrangement of layers and loss in the surface area (as observed in Figure 3-59) [2, 133]. Additionally, during gasification, a part of the carbon is consumed and as the conversion increases more pores are created. Intuitively, with increasing

conversion, the surface area reaches a maximum and decreases thereafter due to merging and coalescence of pores. The decrease in the surface area beyond a critical carbon conversion is an extensively studied phenomenon. Models such as the random pore model (RPM), the partially sintered spheres model (PSSM), and the overlapped grain model (OGM) predict a maximum in the specific surface area due to the enlargement of pore radius with reaction and the subsequent decrease due to pore merging and coalescence [140-142]. The decrease in the surface area for all char900 samples compared to the char800 samples may be due to both the above factors, namely, the structural realignment of the aromatics and the surface consumption due to carbon conversion. However, from the comparison of Figure 3-58 and Figure 3-59 shows that the decrease in surface area from char800 to char900 (30-40%) is much profound as compared to the increase in the conversion (10-15%). This observation suggests that the deteriorating char character at higher temperatures is a dominant factor causing a reduction in surface area. However, with the char1000 species, the matrix may tend to generate more pores after the cross-linking phase, thus resulting in an increase in the surface area [136].

Different coals exhibit different behavior during the devolatilization phase. Particularly in the higher rank coking coal B, the plasticity developed during devolatilization can potentially plug most pores resulting in a deteriorating char quality with temperature. As a consequence, in addition to the drastic reduction in surface area (compared to other coals), the gasification reactivity of the chars also decreased. However, for the other coals, this phenomenon was absent, and the decrease in surface area (hence adsorption capacity) is predominantly because of the surface modification phenomena detailed in the previous paragraph.

Comparing the pore size distributions presented in Figure 3-60 and the sorption capacities in Figure 3-63, it can be observed that the samples with the higher microporous surface area need not always have the highest sorption capacity. For instance, in the case of coal E char 800, the microporous contribution to the surface area is less than 5%. However, the surface area increased tremendously in comparison to the raw coal. This fact leads to suggest that not only the surface area of the individual pores but also their volumetric distribution contributes towards determining the surface area relevant for gas adsorption of the porous material. Compared to the pore size distribution, the DFT surface area trends are in reasonable agreement with the high-pressure adsorption results.

Pressure is known to have a critical impact on the swelling ratio, char structure, and char reactivity during devolatilization [143]. With increasing pressure, the maximum swelling parameter passed through a maximum for several coals investigated by Khan and Jenkins [144]. Also, Gadiou et al. [145] reported an increase in porosity with increase in pyrolysis pressure. In addition to the influence of pressure on the char structure, pore morphology, gas adsorption induced swelling of the coal/char matrix is also to be considered [146, 147].

3.2.5.4 Experiment set. 4

In the 4th set of experiments, the gasified char of coal C was tested for their adsorption capacity to cover both sub and super critical pressure regions of CO_2. However, the gasified char was obtained from the ex-situ experiment 2. Because of the location of the gasified char inside the ex-situ reactor, the char sample of each location experienced different gasification conditions.

The coal (i.e., fixed carbon) conversion values before and after gasification are presented in Figure 3-64. The higher conversions were achieved for sample 1 and 2 as those samples were near the igniter in the gasification channel and above the gasification channel through which the product gas was speculated to travel. However, the conversion of sample 4 was lowest because that sample was collected from the bottom part of the reactor, where it is unlikely to reach the flame front. The conversion is found to be the function of the sample location as the gasification condition is not identical in each location. The CO_2 storage capacity at 45.5°C and 30 bar shows that the storage capacity also depends of the location of the samples. However, because of the same coal rank, it was difficult to draw a conclusion on the relation of storage capacity and the carbon conversion.

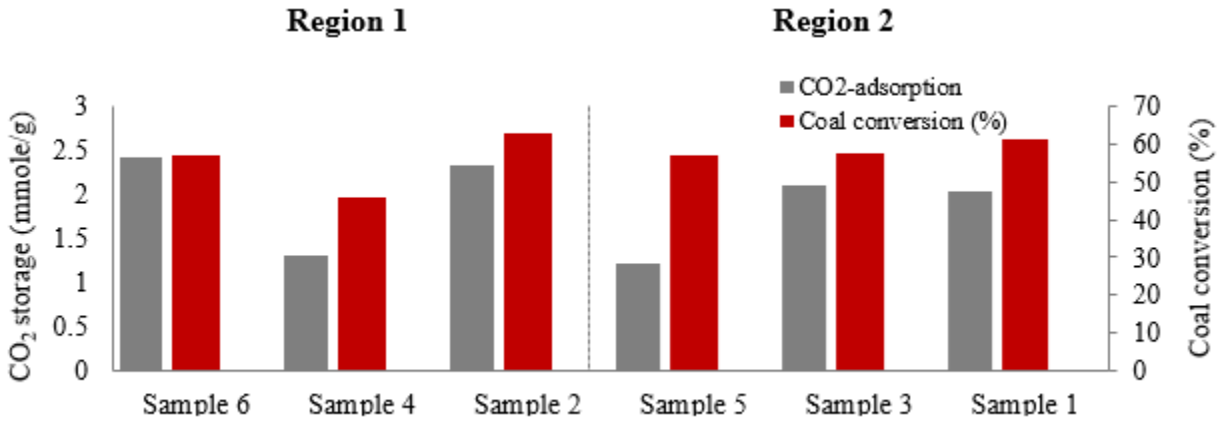

Figure 3-64 Comparison of CO_2 storage capacity and carbon conversion values during the gasification (Produced from the data extracted from Zabihi [120]).

The isotherm graphs of six gasified samples are presented in Figure 3-65. Adsorption of samples at fixed temperature of 45.5°C and pressure range of 30 bar to 70 bar are measured. Among all samples, samples 4 and 5 showed the lowest values for their adsorption capacities. Samples 3, 1,

2, and 6 have higher adsorption capacities. The maximum adsorption capacity was obtained from sample 6 at 62 bar with an amount of 2.58 mmole/g, and the minimum capacity was observed for sample 4 at 35.5 bar with an amount of 0.79 mmole/g. Additionally, all samples showed a steady increase in adsorption with increasing pressure until about 60 bar and continued with a higher slope afterward. The last pressure point for these experiments was chosen below 70 bar to avoid the critical pressure of CO_2. If a comparison is made from the observation of the results from Figure 3-63 and Figure 3-64, it can be speculated that adsorption is not taking place appreciably for the samples of lower carbon conversion.

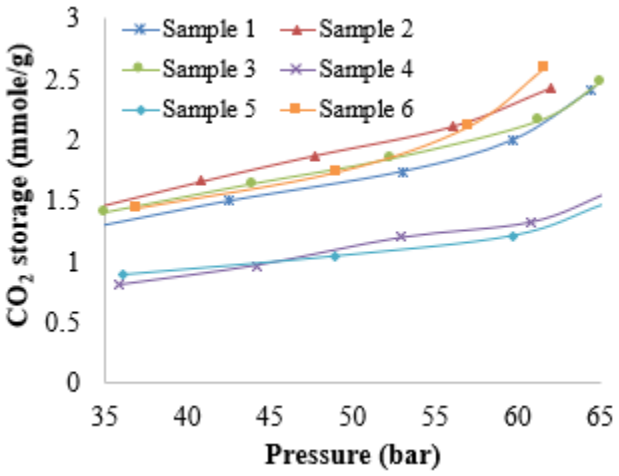

Figure 3-65 Adsorption isotherm of CO_2 on gasified coal at 45.5°C extracted from the volumetric adsorption setup [120].

Adsorption isotherm trends of gasified coal samples at near critical pressure showed a different slope that urged further investigation and experiments. It was also recommended in the literature that for a more specific understanding of UCG-CCS system, the experiments are required to be

conducted at over critical pressures to cover a wide range of pressures [15]. In this regard, two of the gasified samples were randomly chosen to be experimented in volumetric adsorption apparatus under pressures from 35 to 105 bar and at a temperature fixed at 45.5°C as a representation of abandoned underground coal gasification sites. Figure 3-66 shows these results.

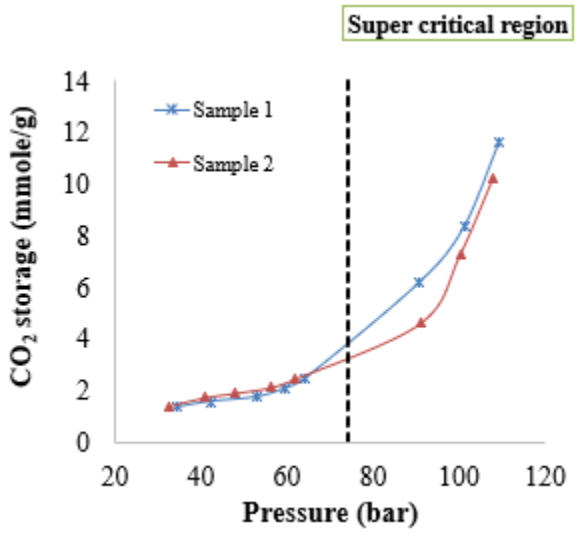

Figure 3-66 Adsorption capacity of gasified coal at super-critical pressures [120].

It can be seen from Figure 3-66 that after the critical pressure, the adsorption capacity of coal increases almost exponentially reaching a maximum of 14 mmole/g at 106 bar for Sample 2 and 13 mmole/g at 108 bar for Sample 1. These results indicate that very deep post UCG site where the pressure is above critical pressure can absorb 5 time more CO_2 compared to subcritical pressure range.

To estimate the duration of the adsorption process until an equilibrium is reached, sorption capacity was calculated in a regular interval of time. Figure 3-67 shows adsorption versus time plot for the randomly chosen data points of the experiments. A sharp increase in adsorption was observed at the beginning followed by a plateau after few hours.

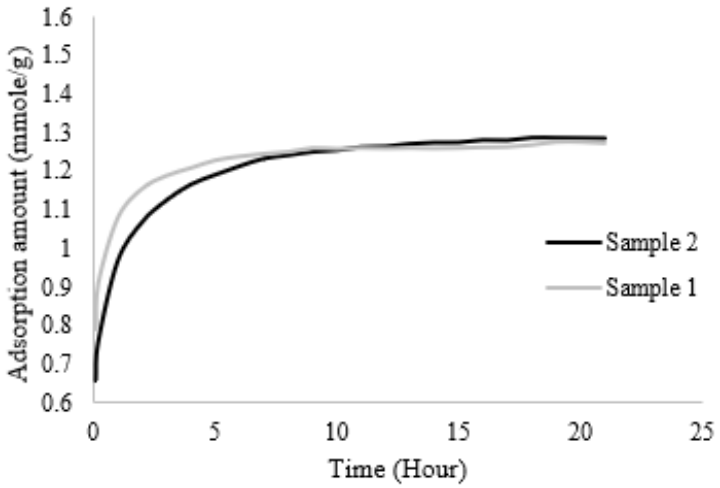

Figure 3-67 Effect of equilibrium time on CO_2 adsorption capacity [120].

At the beginning of the experiment, the pressure was perturbed appreciably; however, with time the pressure tended to attain an acceptable equilibrium at that point the change of adsorption was negligible. To extract specific information, an adsorption values comparison at 10 hours and 20 hours for the different samples at the different pressure points was prepared and represented in Figure 3-68. The linear relationship confirms that adsorption values for all samples at 20 hours are only 0.5 % higher than the value at 10 hours. Therefore, a lot of time can be saved by simply adding 0.5% to adsorption capacity at 10 hours to obtain capacity after 20 hours.

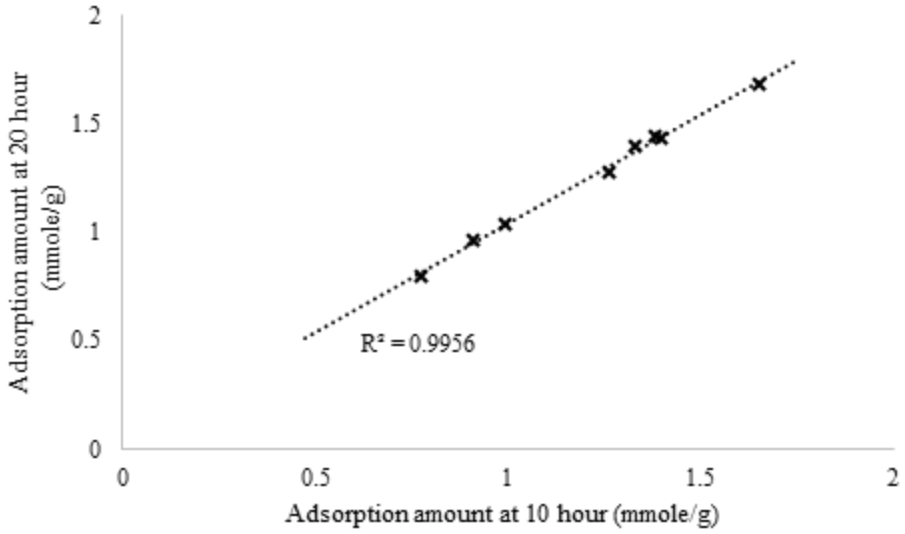

Figure 3-68 Comparison of adsorption values at 10 and 20 hours [120].

3.2.6 Adsorption experiment: conclusions

In general, from all the experiments, it can be concluded that the CO_2 adsorption capacity increases from raw coal to gasified coal in the order of: raw coal < pyrolyzed coal < gasified coal (not following UCG process) < gasified coal (following UCG process). This increase in adsorption in coal chars is because of the enhanced surface area, which is a strong function of coal nature and pyrolysis/gasification temperature. The lower ranked samples exhibited higher adsorption capacity. It was particularly noted that the maceral distribution on the coal samples has a pivotal role in determining the adsorption capacities of virgin coals. Further, it was observed that the sorption capacity of the coals and the chars followed the trend of vitrinite + liptinite content reasonably well. The adsorption capacity also found to increase drastically above the critical pressure.

CHAPTER FOUR: CONCLUSIONS AND RECOMMENDATIONS

4.1 Conclusions

This study described several modes of UCG process under laboratory conditions followed by the CCS studies to assess the feasibility of UCG-CCS option.

4.1.1 Ex-situ experiments

The UCG experiments in the ex-situ reactor suffered several problems as discussed in the chapter conclusion; however, despite those problems, the followings are the finding from the experimental results:

- For the channel gasification, the steam injection was found to lower the temperature near the combustion front; however, the sharp decline of the temperature was observed in the coal deficit area. On the other hand, for the packed bed gasification, the steam injection was not found to lower the temperature near the combustion front; however, as observed in the channel gasification, the steam injection lowered the temperature in coal deficit area.
- For channel gasification, ignition phase was found longer as compared to the ignition phase of packed bed gasification.
- The intensity of the explosion during ignition was found more in case of channel gasification.
- Because of the explosion during ignition, the channel gasification was found to affect more due to the tendency of channel collapse.
- The burnt front propagation rate was found very slow. It implies that the heating rate was very slow.

- The difference of the temperature from a burnt front to a nearby place of 5 cm distant was found to be nearly 200 °C. From this information, it can be concluded that if the thermocouple is not in the right place (at burnt front), it will be difficult to read the highest temperature inside the reactor.
- The product gas was found to have lower calorific value after the initial period of higher value. The initial period indicates the combustion period where the devolatilization took place due to higher temperature. The lower calorific value afterwards indicates that the gasification temperature was merely reached.

Because of the limitation to control the explosion during the ignition phase, packed bed gasification was found better as compared to channel gasification.

4.1.2 Adsorption experiments

To understand the adsorption process, a number of experiments were conducted on virgin coal, pyrolyzed coal and gasified coal samples of coking and non-coking coals of different ranks. Finally, to meet the ultimate objective, a series of adsorption experiments were conducted on gasified coal samples collected from ex-situ UCG reactor to evaluate the storage capability of post-UCG site for CO_2 capturing and storage fulfillment.

The temperature was fixed at 45.5°C to represent the abandoned UCG sites' temperature. For the pressures selection, they were chosen in such a way that could cover both subcritical and supercritical pressures of CO_2.

The followings are the findings from the experimental results:

For raw coal:

- The maceral distribution on the coal samples has a crucial role in determining the adsorption capacities of virgin coals.

Pyrolyzed char:

- The adsorption capacity of coal char samples was significantly higher than virgin coal samples because of the enhanced surface area, which is a strong function of nature of coal and pyrolysis temperature.
- From the pore size distribution studies, it was understood that the char obtained from non-coking coal (coal A) are more microporous than coking coal (coal B), thus leading to the greater adsorption due to enhanced surface area. All the experiments on pyrolyzed chars were conducted below the critical pressure of CO_2.

Gasified char:

- The lower ranked samples exhibited higher adsorption capacity. Specifically, the chars from sub-bituminous coals followed by the lignite and bituminous char, respectively.
- Further, it was observed that the sorption capacity of the chars followed the trend of vitrinite + liptinite content reasonably well.
- A significant increase in the sorption capacity was observed in the gasified char prepared in 800°C compared to the respective raw coals. However, it was observed that compared to the char800 samples, the char900 and 1000 species had a reduced sorption capacity. The decrease in the adsorption capacity was attributed to the structural changes within the coal matrix and the degree of conversion during gasification.

Gasified char from ex-situ UCG experiment:

- Adsorption capacities of the samples increased steadily as the pressure increased in the volumetric adsorption apparatus.
- However, a sharp increase of the adsorption capacities was observed for the supercritical pressure ranges.

In general, from all the experiments, it can be concluded that the CO_2 adsorption capacity increases from raw coal to gasified coal in the order of: raw coal < pyrolyzed coal < gasified coal (not following UCG process) < gasified coal (following UCG process). The high-pressure adsorption experiments also indicated that UCG-CCS is a viable option in terms of CO_2 storage capacity.

4.2 Recommendations for Future Works

The coal block made up of coal particles does not work well for the ex-situ UCG experiment. It is recommended to use big block of coal to simulate the actual coal seam. Recently, researchers are developing methods for indirect measurement of temperatures using laws of non-stationary heat conduction [148, 149]. The use of indirect method of measuring temperature instead of thermocouple would be recommended to obtain a better temperature distribution profile. For small block, instead of propane, other mechanism can be used to initiate the ignition to avoid the explosion; however, after the ignition, propane can be supplied to expedite the combustion phase for reaching high temperature quickly for the gasification process to start. Considering the field

trials, the numbers of small block/lab-scale UCG experiments are very few. However, to evaluate different parameters, a number of experiments are necessary for different types of coal.

The gasified samples collected from the ex-situ reactor cannot be said completely gasified as the temperature of the reactor was not high enough. Field trials showed a higher cavity temperature. So, more experiments on gasified coal samples collected from different places of UCG field trials are necessary to obtain the quantitative adsorption data for complete evaluation of UCG-CCS in terms of adsorption and storage capacity.

REFERENCES

[1] BP Statistical Review of World Energy—June 2007, Egham, Surrey, UK. BP Distribution Services, p. 45. (Accessed: October 20, 2015). Available: http://www.bp.com/content/dam/bp-country/en_ru/documents/publications_PDF_eng/Statistical_review_2007.pdf

[2] G.R. Couch, "Underground Coal Gasification," IEA Clean Coal Centre: London, UK Report No.: Contract No.: CCC/151, 2009.

[3] World Energy Council - 2007 (Accessed: March 20, 2018). *Survey of Energy Resources, World Energy Council: London, UK, 2007*. Available: http://citeseerx.ist.psu.edu/viewdoc/download?doi=10.1.1.478.9340&rep=rep1&type=pdf

[4] Eed A. Abdel-Hadi and T.R. Hsu, "Computer Modeling of Fixed Bed Underground Coal Gasification Using the Permeation Method," *Journal of Energy Resources Technology,* vol. 109, pp. 11-20, 1987.

[5] H. Tsui and C.H. Wu, "Operating Concept of Circulating Fluidized Bed Gasifier from the Kinetic Point of View," *Powder Technology,* vol. 132, pp. 167-183, 2003.

[6] China Labour Bulletin. Deconstructing deadly details from China's coal mine safety statistics, CLB. 2006 (Accessed: October 20, 2015). Available: http://www.clb.org.hk/en/content/deconstructing-deadly-details-chinas-coal-minesafety-statistics

[7] US Mine Safety and Health Administration. Statistics—Coal Mining Fatalities by State—Calendar Year. 2015. (Accessed: October 30, 2015). Available: http://www.msha.gov/stats/charts/coalbystates.pdf

[8] E. Shafirovich and A. Varma, "Underground Coal Gasification: A Brief Review of Current Status," *Industrial and Engineering Chemistry Research,* vol. 48, pp. 7865-7875, 2009.

[9] M. Kariznovi, H. Nourozieh, J. Abedi and Z. Chen, "Simulation Study and Kinetic Parameter Estimation of Underground Coal Gasification in Alberta Reservoirs," *Chemical Engineering Research and Design,* vol. 91, pp. 464-476, 2013.

[10] A.W. Bhutto, A.A. Bazmi and G. Zahedi, "Underground Coal Gasification: From Fundamentals to Applications," *Progress in Energy and Combustion Science,* vol. 39, pp. 189-214, 2013.

[11] E. Burton, J. Friedmann and R. Upadhye, *Best Practices in Underground Coal Gasification; Lawrence Livermore National Laboratory: California, USA, 2006* (Accessed: August 15, 2015). Available:

http://www.purdue.edu/discoverypark/energy/assets/pdfs/cctr/BestPracticesinUCG-draft.pdf

[12] H. Nourozieh, M. Kariznovi, Z. Chen and J. Abedi, "Simulation Study of Underground Coal Gasification in Alberta Reservoirs: Geological Structure and Process Modeling," *Energy & Fuels,* vol. 24, pp. 3540-3550, 2010.

[13] P.V. Skafa, "Underground Gasification of Coal," *Gosudarstvennoe Hauchno-Tekhnicheskoe Izdatel'stvo Literatury Po Gornomu Delu,* 1960.

[14] D.W. Gregg and T. F. Edger, "Underground Coal Gasification," *AIChE Journal,* vol. 24, pp. 753-781, 1978.

[15] S. Ramasamy, P.P. Sripada, M.M. Khan, S. Tian, J. Trivedi and R. Gupta, "Adsorption Behavior of CO_2 in Coal and Coal Char," *Energy & Fuels,* vol. 28, pp. 5241-5251, 2014.

[16] IEA. (2014). *Canada*. Available: https://www.iea.org/ciab/papers/Canada.pdf

[17] G. Perkins, "Mathematical Modelling of Underground Coal Gasification," Ph.D. Thesis, The University of New South Wales, Sydney, Australia, 2005.

[18] M.M. Khan, J.P. Mmbaga, A.S. Shirazi, J. Trivedi, Q. Liu and R. Gupta, "Modelling Underground Coal Gasification—A Review," *Energies,* vol. 8, pp. 12603–12668, 2015.

[19] D.B. Anthony and J.B. Howard, "Coal Devolatilization and Hydrogastification," *AIChE Journal,* vol. 22, pp. 625-656, 1976.

[20] L. Yang, "Numerical Study on the Underground Coal Gasification for Inclined Seams," *AIChE Journal,* vol. 51, pp. 3059-3071, 2005.

[21] A. Klimenko, "Early Ideas in Underground Coal Gasification and Their Evolution," *Energies,* vol. 2, p. 456, 2009.

[22] R.N.H. Kumar, D.L. Udayakumar, A. Stojcevski and A.M. Maung Than Oo, "Underground Coal Gasification: An alternate, Economical, and Viable Solution for future Sustainability," *International journal of engineering science invention,* vol. 3, pp. 57-68, 2014.

[23] F. Su, T. Nakanowataru, K.-i. Itakura, K. Ohga and G. Deguchi, "Evaluation of Structural Changes in the Coal Specimen Heating Process and UCG Model Experiments for Developing Efficient UCG Systems," *Energies,* vol. 6, p. 2386, 2013.F. Su, T. Nakanowataru, K.-i. Itakura, K. Ohga, and G. Deguchi, "Evaluation of Structural Changes in the Coal Specimen Heating Process and UCG Model Experiments for Developing Efficient UCG Systems," *Energies,* vol. 6, p. 2386, 2013.

[24] E.N.J. Biezen, "Modeling Underground Coal Gasification," PhD Thesis, Delft University of Technology, Delft, The Netherlands, 1996.

[25] D.W. Gregg, R.W. Hill and D.U. Olness, "An Overview of the Soviet Effort in Underground Coal Gasification," Lawrence Livermore National Laboratory Report: Livermore, CA, USA, UCRL-52004, 1976.

[26] Y. Derbin, J. Walker, D. Wanatowski and A. Marshall, "Soviet Experience of Underground Coal Gasification Focusing on Surface Subsidence," *Journal of Zhejiang University-SCIENCE A,* vol. 16, pp. 839-850, October 01 2015.

[27] C.B. Thorsness and J.A. Britten, "Underground Coal Gasification Project," Lawrence Livermore National Laboratory Report: Livermore, CA, USA, UCID-21853, 1989.

[28] M. Green, "Recent Developments and Current Position of Underground Coal Gasification," *Proceedings of the Institution of Mechanical Engineers Part A: Journal of Power and Energy* vol. 232, pp. 1-8, 2017.

[29] M.S. Blinderman, D.N. Saulov and A.Y. Klimenko, "Forward and Reverse Combustion Linking in Underground Coal Gasification," *Energy,* vol. 33, pp. 446-454, 2008.

[30] Y. Cui, J. Liang, Z. Wang, X. Zhang, C. Fan, D. Liang*, et al.*, "Forward and Reverse Combustion Gasification of Coal with Production of High-Quality Syngas in a Simulated Pilot System for In Situ Gasification," *Applied Energy,* vol. 131, pp. 9-19, 2014.

[31] P. Bedi, A. Binshtok, A. Blinderman, M. Blinderman and G. Elliott, "Application of the Exergy UCG Technology in CTX Projects," in *2nd Workshop-Underground Coal Gasification Network*, Banff, AB, Canada, 2012.

[32] B. Davis and C. Mallett, "Bloodwood Ck UCG Developments," in *2nd Workshop-Underground Coal Gasification Network*, Banff, AB, Canada, 2012.

[33] A.A. Shirazi, "CFD Simulation of Underground Coal Gasification," Master's Thesis, University of Alberta, Alberta, Canada, 2012.

[34] I.M. Saptikov, "3 - History of UCG development in the USSR," in *Underground Coal Gasification and Combustion*, ed: Woodhead Publishing, 2018, pp. 25-58.

[35] F. Monk, D. Hallowes, K. Moore and L. Ross, *Fuelling the Fire: The Chequered History of Underground Coal Gasification and Coal Chemicals around the World*, 2016, (Accessed: February 14, 2018). Available: www.foei.org/resources/publications/unconventional-coal

[36] D.W. Camp, "A Review of Underground Coal Gasification Research and Development in the United States" Lawrence Livermore National Laboratory LLNL-TR-733952, 2017.

[37] C.B. Thorsness and J.R. Creighton, "Review of Underground Coal Gasification Field Experiments at Hoe Creek," in *AIChE Symposium Series*, 1983, pp. 15-43.

[38] A. Beath and B. Davis, "UCG History," in *Proceedings of the underground coal gasification workshop Kolkata, India*, Kolkata, India, 2006.

[39] M. Sury, M. White, J. Kirton, P. Carr, R. et al. "Review of Environmental Issues of Underground Coal Gasification," Department of Trade and Industry Technology (DTI): London COAL R272; DTI/Pub URN 04/1880, 2004.

[40] R.L. Oliver, G.M. Mason and L.K. Spackman, "Field and Laboratory Results from the Tono I (Crip) Ucg Cavity Excavation Project, Widco Mine Site, Centralia, Washington," *Fuel Science and Technology International,* vol. 7, pp. 1059-1120, 1989.

[41] A. Beath, S. Craig, A. Littleboy, R. Mar and C. Mallett, "Underground Coal Gasification: Evaluating Environmental Barriers," Kenmore, Queensland, Australia CSIRO Exploration and Mining Report P2004/5, 2004.

[42] S.D. Dennis, "Rocky Mountain 1- Underground Coal Gasification test project: Final Technical Report for the period 1986 to 2006," U.S. Department of Energy2006.

[43] G. Perkins, E. du Toit, G. Cochrane and G. Bollaert, "Overview of Underground Coal Gasification Operations at Chinchilla, Australia," *Energ Source Part A Recovery Utilization Environ Effects,* vol. 38, pp. 3639–3646, 2016.

[44] M.J. Shanon, C.B. Thorsness and R.W. Hill, "Early Cavity Growth during forward Burn," Lawrence Livermore National Laboratory Report: Livermore, CA, USA, UCRL-84584, 1980.

[45] R.W. Hill, "Burn Cavity Growth during the Hoe Creek No. 3 Underground Coal Gasification Experiment," Lawrence Livermore National Laboratory Report: Livermore, CA, USA. UCRL-85173-R-1, 1981.

[46] C.B. Thorsness, E.A. Grens and A.A. Sherwood, "One Dimensional Model for in Situ Coal Gasification," Lawrence Livermore National Laboratory Report: Livermore, CA, USA, UCRL-52523, 1978.

[47] D.L. Yeary and J.B. Riggs, "Study of Small-Scale Cavity Growth Mechanisms for UCG," *In Situ,* vol. 11:4, pp. 305–327, 1987.

[48] L.H. Yang, X. Zhang and S. Liu, "Underground Coal Gasification Using Oxygen and Steam," *Energy Sources, Part A,* vol. 31, pp. 1883–1892, 2009.

[49] S. Daggupati, R.N. Mandapati, S.M. Mahajani, A. Ganesh, D.K. Mathur, R.K. Sharma*, et al.*, "Laboratory Studies on Combustion Cavity Growth in Lignite Coal Blocks in the Context of Underground Coal Gasification," *Energy,* vol. 35, pp. 2374-2386, 2010.

[50] S.M. Daggupati, R.N. Mahajani, S.M. Ganesh, A. Sapru, R.K. Sharma and P. Aghalayam, "Laboratory Studies on Cavity Growth and Product Gas Composition in the Context of Underground Coal Gasification," *Energy,* vol. 36, pp. 1776-1784, 2011.

[51] K. Stańczyk, N. Howaniec, A. Smoliński, J. Świadrowski, K. Kapusta, M. Wiatowski*, et al.*, "Gasification of Lignite and Hard Coal with Air and Oxygen Enriched Air in a Pilot Scale Ex Situ Reactor for Underground Gasification," *Fuel,* vol. 90, pp. 1953-1962, 2011.

[52] K. Stańczyk, K. Kapusta, M. Wiatowski, J. Świdrowski, A. Smoliński, J. Rogut*, et al.*, "Experimental Simulation of Hard Coal Underground Gasification for Hydrogen Production," *Fuel,* vol. 91, pp. 40-50, 2012.

[53] C.B. Thorsness and R.W. Hill. Coal Block Gasification: Laboratory Results and Field Plans. Lawrence Livermore National Laboratory Report, Livermore, CA, USA, UCRL-85906, 1981.

[54] R.E. Glass, "Thermal and Structural Properties of Coal in the Big Seam," *In Situ,* vol. 8, p. 193, 1984.

[55] M.C. Mai, T.F. Edgar and K.Y. Park, "Analysis of Early Cavity Growth in Underground Coal Gasification," *In Situ,* vol. 9, pp. 119-147, 1985.

[56] R. Upadhye, E. Burton and J. Friedmann, "Science and Technology Gaps in Underground Coal Gasification," Lawrence Livermore National Laboratory Report, Livermore, CA, USA, UCRL-TR-222523, 2006.

[57] G.H. Higgins, "A New Concept for in-Situ Coal Gasification," Lawrence Livermore National Laboratory Report, Livermore, CA, USA, UCRL-51217, 1972.

[58] C.B. Thorsness and R.B. Rosza, "In-Situ Coal Gasification Program: Model Calculations and Laboratory Experiments," Lawrence Livermore National Laboratory Report, Livermore, CA, USA, UCRL-78302, 1976.

[59] A.A. Uppal, A.I. Bhatti, E. Aamir, R. Samar and S.A. Khan, "Control Oriented Modeling and Optimization of One Dimensional Packed Bed Model of Underground Coal Gasification," *Journal of Process Control,* vol. 24, pp. 269-277, 2014.

[60] B. Dinsmoor, J.M. Galland and T.F. Edgar, "The Modeling of Cavity Formation During Underground Coal Gasification," *Journal of Petroleum Technology,* vol. 30, pp. 695–704, 1978.

[61] R.D. Gunn and D.L. Whitman, "An In-Situ Coal Gasification Model (Forward Mode) for Feasibility Studies and Design," Laramie Energy Research Center: Laramie, WY, LERC/RI-76/2, 1976.

[62] A.N. Khadse, M. Qayyumi, S. Mahajani and P. Aghalayam, "Reactor Model for Underground Coal Gasification Channel," *Int J Rector Eng,* vol. 4, pp. 1-25, 2006.

[63] A.M. Winslow, "Numerical Model of Coal Gasification in a Packed Bed," Livermore National Laboratory (LLNL): Berkeley, CA, USA UCRL-77627, 1976.

[64] C.B. Thorsness and S.W. Kang, "Further Development of a General-Purpose Packed Bed Mode for Analysis of UCG Process," Livermore National Laboratory (LLNL), CA, USA UCRL-92489, 1985.

[65] J.H. Campbell, "Pyrolysis of Subbituminous Coal in Relation to In-Situ Coal Gasification," *Fuel,* vol. 57, pp. 217-224, 1978.

[66] J. Gadsby, C.N. Hinshelwood and K.W. Sykes, "The Kinetics of the Reactions of The Steam-Carbon System," *Proceedings of the Royal Society of London. Series A. Mathematical and Physical Sciences,* vol. 187, p. 129, 1946.

[67] W.K. Lewis, E.R. Gilliland and R.R. Paxton, "Low-Temperature Oxidation of Carbon," *Industrial & Engineering Chemistry,* vol. 46, pp. 1327-1331, 1954.

[68] W.D. Batenburg, N.J. Biezen and J. Bruining, "A New Channel Model for Underground Coal Gasification of Thin, Deep Coal Seams," *In Situ,* vol. 18, pp. 419–451, 1994.

[69] R.A. Kuyper, T.H. van der Meer and J. Bruining, "Simulation of Underground Gasification of Thin Coal Seams," *In Situ,* vol. 20, pp. 311–346, 1996.

[70] R.D. Gunn and W.B. Krantz, "Underground Coal Gasification: Development of Theory, Laboratory Experimentation, Interpretation, & Correlation with the Hanna Field Tests: Final report," DOE/LC/10442-2345, 1987.

[71] T.L. Eddy and S.H. Schwartz, "A Side Wall Burn Model for Cavity Growth in Underground Coal Gasification," *Journal of Energy Resources Technology,* vol. 105, pp. 145-155, 1983.

[72] Y. Luo, M. Coertzen and S. Dumble, "Comparison of UCG Cavity Growth with CFD Model Predictions," in *In Proceedings of the 7th International Conference on CFD in the Minerals and Process Industries CSIRO*, Melbourne, Australia, 2009.

[73] P. Pirlot, J.P. Pirard, A. Coeme and M.A. Mostade, "Coupling of Chemical Processes and Flow in View of the Cavity Growth Simulation of an Underground Coal Gasifier at Great Depth," *In Situ,* vol. 22, pp. 141–156, 1998.

[74] R.A. Kuyper, T.H. Van Der Meer and C.J. Hoogendoorn, "Turbulent Natural Convection Flow due to Combined Buoyancy Forces during Underground Gasification of Thin Coal Layers," *Chemical Engineering Science,* vol. 49, pp. 851-861, 1994.

[75] G. Perkins and V. Sahajwalla, "Modelling of Heat and Mass Transport Phenomena and Chemical Reaction in Underground Coal Gasification," *Chemical Engineering Research and Design,* vol. 85, pp. 329-343, 2007.

[76] S.Y. Schwartz, T.L. Eddy, K.H. Mehta, S.A. Lutz and M.B. Binaie-Kondolojy, "Cavity Growth Mechanisms in UCG with Side Wall Burn Gasification," in *In Proceedings of the SPE Annual Fall Technical Conference and Exhibition*, Houston, TX, USA, 1978.

[77] D.E. Daney, "Turbulent Natural Convection of Liquid Deuterium, Hydrogen and Nitrogen within Enclosed Vessels," *International Journal of Heat and Mass Transfer,* vol. 19, pp. 431-441, 1976.

[78] A.C. Bailey, F. Bartlett, H.H. Boswinkel, J. Bruining, V. Chandelle, G. Del Amor*, et al.*, "The Future Development of Underground Coal Gasification in Europe: a comprehensive report to CEC," Brussels, Belgium 1989.

[79] I.H.C. Wilks, "The Cavity Produced by Gasifying Thin Deep Seams," in *In Proceedings of the 9th Underground Coal Gasification Symposium US*, Washington, DC, USA, 1983, pp. 314–322.

[80] R.J. Cena, J.A. Britten and C.B. Thorsness, "Excavation of the Partial Seam CRIP Underground Coal Gasification Test Site," Lawrence Livermore National Laboratory: Livermore, CA, USA, UCRL-97245, 1987.

[81] J. Bruining, N.M. Herkstroter, A.M. Lankhorst, C.P. Visser and H. Ronde, "Free Convection Enhanced Mass Transfer during Underground Tunnel Gasification of Coal," in *Proceedings of the Thirteenth Annual Underground Coal Gasification Symposium; U.S. Department of Energy*, Washington, DC, USA, 1987, pp. 225–233.

[82] R.W. Hill and C. Thorsness, "Summary Report on Large Block Experiments in Underground Coal Gasification, Tono Basin, Washington: Volume 1. Experimental Description and Data Analysis," Lawrence Livermore National Laboratory (LLNL) Report, Berkeley, CA, USA UCRL-53305, 1982.

[83] B.E. Launder and B.I. Sharma, "Application of the Energy-Dissipation Model of Turbulence to the Calculation ff Flow Near a Spinning Disc," *Letters in Heat and Mass Transfer,* vol. 1, pp. 131-137, 1974.

[84] D.N. Saulov, O.A. Plumb and A.Y. Klimenko, "Flame Propagation In A Gasification Channel," *Energy,* vol. 35, pp. 1264-1273, 2010.

[85] A.B. Chernyshev, *Izbrannye Trudy*. USSR: Izdatel'stvo: Moscow, 1956.

[86] H. Liu, H. Yao, K. Yao, F. Chen and G. Luo, "Characteristics of "Three zones" during Underground Coal Gasification," *Advanced Materials Research,* vol. 524–527, pp. 56-62, 2012.

[87] D.J. Roddy and P.L. Younger, "Underground Coal Gasification with CCS: a Pathway to Decarbonising Industry," *Energy & Environmental Science,* vol. 3, pp. 400-407, 2010.

[88] P. Pei, Z. Zeng and J. He, "Feasibility Study of Underground Coal Gasification Combined with CO2 Capture and Sequestration inWilliston Basin, North Dakota," in *Proceedings of the 44th US Rock Mechanics Symposium and 5th U.S.—Canada Rock Mechanics Symposium*, Salt Lake City, UT, USA, 2010.

[89] T. Kempka, T. Fernández-Steeger, D.Y. Li, M. Schulten, R. Schlüter and B.M. Krooss, "Carbon dioxide Sorption Capacities of Coal Gasification Residues," *Environmental Science and Technology,* vol. 45, pp. 1719-1723, 2011.

[90] P.P. Sripada, M.M. Khan, S. Ramasamy, V.T. Kanneganti, RGupta, "Comparison of CO_2 Storage Potential in Pyrolysed Coal Char of different Coal Ranks," in *Gas Injection for Disposal and Enhanced Recovery*, Y. Wu, , J. J. Carroll, , and Q. Li, Eds., ed: John Wiley & Sons, Inc., 2014, pp. 293-304.

[91] A. Saghafi, M. Faiz and D. Roberts, "CO_2 Storage and Gas Diffusivity Properties of Coals from Sydney Basin, Australia," *International Journal of Coal Geology,* vol. 70, pp. 240-254, 2007.

[92] A.L. Goodman, L.M. Campus and K.T. Schroeder, "Direct Evidence of Carbon Dioxide Sorption on Argonne Premium Coals using Attenuated Total Reflectance−Fourier Transform Infrared Spectroscopy," *Energy & Fuels,* vol. 19, pp. 471-476, 2005.

[93] E.N. Biezen, J. Bruining and J. Molenaar, "An Integrated Model for Underground Coal Gasification," in *Proceedings of the Annual Technical Conference of the Society of Petroleum Engineers*, New Orleans, LA, USA, 1994.

[94] J. Brand, "Progress Feedback on Wildhorse's Hungarian UCG Project," in *Proceedings of the 2nd Underground Coal Gasification NetworkWorkshop*, Banff, Alberta, Canada, 2012.

[95] K.L. Zamzow, *Underground Coal Gasification: History, Environmental Issues, and the Proposed Project at Beluga, Alaska*, (Accessed : October 15, 2015). Available: http://www.groundtruthtrekking.org/Documents/UCG/UCG-KZamzow-2010.pdf

[96] W.D. Batenburg and J. Bruining, "The Efficiency of Filtration Gasification," *In Situ,* vol. 17, pp. 413–437, 1993.

[97] R.D. Gunn, "Problem Solved and Problem not Solved in UCG," *Fuel,* vol. 22, pp. 64–75, 1977.

[98] P.L. Younger, "Hydrogeological and Geomechanical Aspects of Underground Coal Gasification and its Direct Coupling to Carbon Capture and Storage," *Mine Water and the Environment,* vol. 30, pp. 127-140, 2011.

[99] D. Yang, V. Sarhosis and Y. Sheng, "Thermal–Mechanical Modelling around the Cavities of Underground Coal Gasification," *Journal of the Energy Institute,* vol. 87, pp. 321-329, 2014.

[100] Y. Sheng, A. Benderev, D. Bukolska, K. I.-I. Eshiet, C. D. da Gama, T. Gorka*, et al.*, "Interdisciplinary Studies on the Technical and Economic Feasibility of Deep Underground Coal Gasification with CO_2 Storage in Bulgaria," *Mitigation and Adaptation Strategies for Global Change,* vol. 21, pp. 595-627, April 01 2016.

[101] V. Sarhosis, D. Yang, Y. Sheng and T. Kempka, "Coupled Hydro-thermal Analysis of Underground Coal Gasification Reactor Cool Down for Subsequent CO_2 Storage," *Energy Procedia,* vol. 40, pp. 428-436, 2013.

[102] N. Nakaten, R. Schlüter, R. Azzam and T. Kempka, "Development of a Techno-Economic Model for Dynamic Calculation of Cost of Electricity, Energy Demand and CO_2 Emissions of an Integrated UCG–CCS Process," *Energy,* vol. 66, pp. 779-790, 2014.

[103] M. Laciak, K. Kostúr, M. Durdán, J. Kačur and P. Flegner, "The Analysis of the Underground Coal Gasification in Experimental Equipment," *Energy,* vol. 114, pp. 332-343, 2016.

[104] R.R. Glaser and Johnson, L.A., "Physical Simulations of Underground Coal Gasification in an Eastern Bituminous Coal," Wyoming Research Corp., Laramie, Western Research Inst., USA DOE/FE/60177-2249, 1986.

[105] M. Gur, N. Eskin, H. Okutan, A. Arısoy, E. Böke, Ü. Altıntaş*, et al.*, "Experimental results of underground coal gasification of Turkish lignite in an ex-situ reactor," *Fuel,* vol. 203, pp. 997-1006, 2017.

[106] L. Yang, X. Zhang, S. Liu, L. Yu and W. Zhang, "Field Test of Large-Scale Hydrogen Manufacturing from Underground Coal Gasification (UCG)," *Int. J. Hydrogen Energy* vol. 33, pp. 1275-1285, 2008.

[107] M. Wiatowski, K. Kapusta, M. Ludwik-Pardała and K. Stańczyk, "Ex-situ Experimental Simulation of Hard Coal Underground Gasification at Elevated Pressure," *Fuel,* vol. 184, pp. 401-408, 2016.

[108] K. Kostur, M. Laciak, M. Durdan, J. Kacur and P. Flegner, "Low-Calorific Gasification of Underground Coal with a Higher Humidity," *Measurement,* vol. 63, pp. 69–80, 2015.

[109] J.H. Harker and J.R. Backhurst, *Fuel and Energy (Energy Science and Engineering)*. London, UK: Academic Press, 1981.

[110] J.A. Carvalho and W. F. N. dos Santos, "Radiation Errors in Temperature Measurements with Thermocouples in a Cylindrical Combustor," *International Communications in Heat and Mass Transfer,* vol. 17, pp. 663-673, 1990.

[111] D. Bradley and K. J. Matthews, "Measurement of High Gas Temperatures with Fine Wire Thermocouples," *Journal of Mechanical Engineering Science,* vol. 10, pp. 299-305, 1968.

[112] M.V. Heitor and A. L. N. Moreira, "Thermocouples and Sample Probes for Combustion Studies," *Progress in Energy and Combustion Science,* vol. 19, pp. 259-278, 1993.

[113] D. Yang, N. Koukouzas, M. Green and Y. Sheng, "Recent Development on Underground Coal Gasification and Subsequent CO_2 Storage. ," *Journal of the Energy Institute* vol. 89, pp. 469-484, 2016.

[114] S. Day, G. Duffy, R. Sakurovs and S. Weir, "Effect of Coal Properties on CO_2 Sorption Capacity under Supercritical Conditions," *International Journal of Greenhouse Gas Control,* vol. 2, pp. 342-352, 2008.

[115] R.E. Carroll and J.C. Pashin, "Relationship of Sorption Capacity to Coal Quality: CO_2 Sequestration Potential of Coalbed Methane Reservoirs in the Black Warrior Basin.," in *International coalbed methane symposium proceedings*, Alabama, USA, 2003.

[116] M. Mastalerz, H. Gluskoter and J. Rupp, "Carbon dioxide and Methane Sorption in High Volatile Bituminous Coals from Indiana, USA.," *Int. J. Coal Geol.,* vol. 60, p. 43−55, 2004.

[117] B. Ryan and D. Richardson, "The Potential for CO_2 sequestration in British Columbia Coal Seams.," British Columbia Ministry of Energy and Mines2005.

[118] S. Ramasamy, S. Tian, M. M. Khan, J. Trivedi and R. Gupta, "Assessing CO_2 Storage Potential in Coal Chars for UCG-CCS System.," in *Proceedings of the 2nd Underground Coal Gasification NetworkWorkshop*, Banff, AB, Canada, 2012.

[119] P. Sripada, M.M. Khan, S. Ramasamy, J. Trivedi and R. Gupta, "Influence of Coal Properties on the CO_2 Adsorption Capacity of Coal Gasification Residues," *Energy Science & Engineering,* vol. 6, pp. 321-335, 2018.

[120] S. Zabihi, "Subcritical and Supercritical CO_2 Adsorption Capacity of Post-UCG Gasified Coal " Masters, Petroleum Engineering, University of Alberta, 2017.

[121] R. Span and W. Wagner, "A New Equation of State for Carbon Dioxide Covering the Fluid Region from the Triple-Point Temperature to 1100 K at Pressures up to 800 MPa," *Journal of Physical and Chemical Reference Data,* vol. 25, pp. 1509–1596, 1996.

[122] S. Tian, "Fragmentation of Large Coal Particles at High Temperature in a Drop Tube Furnace.," Master's, University of Alberta, Edmonton, Alberta, 2011.

[123] P.P. Sripada, "CO_2 Adsorption Capacities of Gasified Coal Chars," Master's, University of Alberta, Edmonton, Alberta, 2014.

[124] C. White, "Sequestration of Carbon Dioxide in Coal with Enhanced Coalbed Methane Recovery - A Review," *Energy Fuels,* vol. 19, pp. 659-724, 2005.

[125] R. Pini, "Enhanced Coal Bed Methane Recovery Finalized to Carbon dioxide Storage," Ph.D, ETH Zurich, Zurich, Switzerland, 2009.

[126] J.C. Pashin, R.E. Carroll, R.H.J. Groshong, D.E. Raymond, M. McIntyre and J.W. Payton, "Geologic Screening Criteria for Sequestration of CO_2 in Coal: Quantifying Potential of the Black Warrior Coalbed Methane Fairway, Alabama," National Energy Technology Laboratory, U.S. Department of Energy, Washington, D.C. Report No. DE-FC-00NT40927, 2003.

[127] C.R. Clarkson and R.M. Marc Bustin, "Variation in Micropore Capacity and Size Distribution with Composition in Bituminous Coal of the Western Canadian Sedimentary Basin: Implications for Coalbed Methane Potential.," *Fuel,* vol. 75, p. 1483−1498, 1996.

[128] D. Prinz and R. Littke, "Development of the Micro- and Ultramicroporous Structure of Coals with Rank as Deduced from the Accessibility to Water," *Fuel,* vol. 84, p. 1645−1652, 2005.

[129] R.K. Hessley, J.W. Reasoner and J.T. Riley, *Coal science: An Introduction to Chemistry, Technology and Utilization*, 1986.

[130] J. Teng, M. Mastalerz and L. Hampton, "Maceral Controls on Porosity Characteristics of Lithotypes of Pennsylvanian High Volatile Bituminous Coal: Example from the Illinois Basin," *International Journal of Coal Geology,* vol. 172, pp. 80-94, 2017.

[131] Y. Liu and J. Wilcox, "Molecular Simulation of CO_2 Adsorption in Micro- and Mesoporous Carbons with Surface Heterogeneity," *International Journal of Coal Geology,* vol. 104, pp. 83-95, 2012.

[132] M.S.A. Perera, P.G. Ranjith, S.K. Choi, D. Airey, P. Weniger, "Estimation of Gas Desorption Capacity in Coal: A Review and an Analytical Study," *Int. J. Coal Prep. Util.,* vol. 32, pp. 25-55, 2012.

[133] A. de Koranyi and V. Balek, "Structural Changes in Coals During Pyrolysis," *Thermochim. Acta,* vol. 93, p. 737−740, 1985.

[134] E.M. Suuberg, D. Lee and J.W. Larsen, "Dependence of Crosslinking Processes in Pyrolysing Coals," *Fuel,* vol. 64, p. 1668−1671, 1985.

[135] W.D. Jiang, I-C. Lee and R.Y.K. Yang, "Microstructural Variations of Lignite, Subbituminous and Bituminous Coals and their High Temperature chars.," *Fuel Process. Technol,* vol. 18, p. 11−23, 1988.

[136] X. Jing, Z. Wang, Q. Zhang, et al., "Evaluation of CO2 Gasification Reactivity of Different Coal Rank Chars by Physicochemical Properties," *Energy and Fuels* vol. 27, pp. 7287-7293, 2013.

[137] B. Feng and S.K. Bhatia, "Variation of the Pore Structure of Coal Chars during Gasification," *Carbon,* vol. 41, pp. 507-523, 2003.

[138] N. Nankaten, R. Schlüter, R. Azzam and T. Kempka, "Development of a Techno-Economic Model for Dynamic Calculation of Cost of Electricity, Energy Demand and CO2 Emissions of an Integrated UCG-CCS Process. ," *Energy* vol. 66, pp. 779-790, 2014.

[139] G. Gürdal and M.N. Yalçın, "Gas Adsorption Capacity of Carboniferous Coals in the Zonguldak Basin (NW Turkey) and its Controlling Factors," *Fuel,* vol. 79, pp. 1913-1924, 2000.

[140] S.K. Bhatia and D.D. Perlmutter, "A Random Pore Model for Fluid-Solid Reactions: I. Isothermal, Kinetic Control," *AIChE Journal* vol. 26, pp. 379-386, 1980.

[141] T. Adschiri, T. Kojima and T. Furusawa, "Estimation of Dynamic Change in Gasification Rate of Chars—II. Overlapped Grain Model," *Chemical Engineering Science* vol. 42, pp. 1319-1322, 1987.

[142] B. Lindner and D. Simonsson, "Comparison of Structural Models for Gas-Solid Reactions in Porous Solids Undergoing Structural Changes," *Chemical Engineering Science,* vol. 36, pp. 1519-1527, 1981.

[143] J. Yu, J.A. Lucas and T.F. Wall, "Formation of the Structure of Chars during Devolatilization of Pulverized Coal and its Thermoproperties: A Review," *Progress in Energy and Combustion Science,* vol. 33, pp. 135-170, 2007.

[144] M.R. Khan and R.G. Jenkins, "Swelling and Plastic Properties of coal Devolatilized at Elevated Pressures: an Examination of the Influences of Coal Type," *Fuel,* vol. 65, pp. 725-731, 1986.

[145] R. Gadiou, Y. Bouzidi and G. Prado, *The Devolatilisation of Millimetre Sized Coal Particles at High Heating Rate: The Influence of Pressure on the Structure and Reactivity of the Char*, 2002.

[146] K. Zhang, Y. Cheng, K. Jin, H. Guo, Q. Liu, J. Dong*, et al.*, "Effects of Supercritical CO_2 Fluids on Pore Morphology of Coal: Implications for CO_2 Geological Sequestration," *Energy & Fuels,* vol. 31, pp. 4731-4741, 2017.

[147] A.S. Ranathunga, M.S.A. Perera, P.G. Ranjith, T.D. Rathnaweera and X.G. Zhang, "Effect of Coal Rank on CO_2 Adsorption Induced Coal Matrix Swelling with Different CO_2 Properties and Reservoir Depths," *Energy & Fuels,* vol. 31, pp. 5297-5305, 2017.

[148] J. Kačur, M. Laciak and M. Durdán, "Remote Monitoring and Control of the UCG Process," in *2011 12th International Carpathian Control Conference (ICCC)*, 2011, pp. 176-180.

[149] M. Durdán and J. Kačur, "Indirect Temperatures Measurement in the UCG Process," in *Proceedings of the 14th International Carpathian Control Conference (ICCC)*, 2013, pp. 73-78.